CH bond activation of methane and unsaturated molecules by a transient eta2-cyclopropene complex of niobium : synthesis, characterization and mechanistic studies

Chen Li

▶ **To cite this version:**

Chen Li. CH bond activation of methane and unsaturated molecules by a transient eta2-cyclopropene complex of niobium : synthesis, characterization and mechanistic studies. Coordination chemistry. INSA de Toulouse, 2015. English. NNT : 2015ISAT0029 . tel-01244867

HAL Id: tel-01244867

https://theses.hal.science/tel-01244867

Submitted on 16 Dec 2015

HAL is a multi-disciplinary open access archive for the deposit and dissemination of scientific research documents, whether they are published or not. The documents may come from teaching and research institutions in France or abroad, or from public or private research centers.

L'archive ouverte pluridisciplinaire **HAL**, est destinée au dépôt et à la diffusion de documents scientifiques de niveau recherche, publiés ou non, émanant des établissements d'enseignement et de recherche français ou étrangers, des laboratoires publics ou privés.

Université Fédérale
Toulouse Midi-Pyrénées

THÈSE

En vue de l'obtention du

DOCTORAT DE L'UNIVERSITÉ DE TOULOUSE

Délivré par Institut National des Sciences Appliquées de Toulouse (INSA Toulouse)
Discipline ou spécialité : Chimie Organométallique et de Coordination

---

Présentée et soutenue par Chen LI
Le vendredi 20 novembre 2015

Titre :
CH bond activation of methane and unsaturated molecules by a transient eta2-cyclopropene complex of niobium: synthesis, characterization and mechanistic studies

---

JURY
Pr. Parisa MEHRKHODAVANDI, University of British Columbia, Vancouver, Canada
Pr. Blanca MARTIN VACA, LHFA, Université de Toulouse
Dr. Chiara DINOI, LCC, Université de Toulouse (invitée)

Ecole doctorale : Sciences de la Matière (SDM)
Unité de recherche : Laboratoire de Chimie de Coordination du CNRS (LCC) UPR 8241
Directeur(s) de Thèse : Pr. Michel ETIENNE (LCC Toulouse), Pr. Laurent MARON (LPCNO Toulouse)
Rapporteurs : Pr. Robin PERUTZ, University of York, York, Royaume-Uni
Dr. Chloé THIEULEUX, Chargée de Recherche CNRS, Université de Lyon

Remerciements

Ce travail a été réalisé grâce au financement de la Région Midi-Pyrénées et du PRES-de l'Université de Toulouse.

En premier lieu, je tiens à remercier mes encadrants de thèse, le Dr. Chiara Dinoi et le Prof. Michel Etienne. Je vous remercie de m'avoir donné l'opportunité d'étudier en France en tant que doctorante. Au cours de ces trois années d'études, à travers le travail expérimental et les nombreuses discussions scientifiques que nous avons partagé, j'ai pu acquérir beaucoup de connaissances scientifiques ainsi que maîtriser des nombreuses techniques expérimentales précieuses sur la chimie organométallique. Avec votre patience et vos conseils rigoureux sur mon sujet de recherche, je suis parvenu à surmonter les difficultés rencontrées lors de la réalisation des expériences et de la rédaction de la thèse, en obtenant le diplôme de doctorat.

En second lieu, je tiens à remercier le Dr. Chloé Thieuleux et le Prof. Robin Perutz pour avoir accepté de juger ce travail en tant que Rapporteurs et pour leur participation à mon jury de thèse.

Mes remerciements s'adressent également à mon co-supervisor, le Prof. Laurent Maron, au président du jury, le Prof. Blanca Martin Vaca, et au Prof. Parisa Mehrkhodavandi, pour avoir respectivement accepté avec gentillesse de participer à mon jury de thèse.

J'adresse mes remerciements à l'ensemble du personnel des services scientifiques et techniques du LCC qui ont participé à la réalisation de ce travail, et plus particulièrement à: Laure Vendier du service de diffraction des rayons X, Yannick Coppel, Francis Lacassin, Christian Bijani du service RMN, Alain Moreau et Isabelle Borget du service de microanalyse et Alix Sournia-Saquet du service d'électrochimie.

Je remercie les membres de l'équipe E avec qui j'ai partagé ces trois années de thèse: Kane, Christian, Jean-Louis, Nuria, Yimu, Quentin, Natalie, Antoine, Kyle.

Merci à mes amis Guanghua, Yin, Haonan, Qian, Katie, Tugce, Clève, Amelle, Chongwei, Chunxiang et les autres… pour votre affection pendant ces trois années.

Finalement, merci à mes parents et à mon copain, Hongguang.

Table of contents

Table of contents ..... A
List of abbreviations C
General introduction 1
Chapter 1: Methane CH bond activation processes 3
1.1- CH bond activation of methane by late transition metal complexes 8
1.1.1- Electrophilic substitution 8
1.1.2- Oxidative addition 9
1.1.3- Carbene insertion 19
1.1.4- Metalloradical addition 20
1.2- CH bond activation of methane by early transition metal complexes 21
1.2.1- σ-Bond metathesis 21
1.2.2- 1,2-CH addition 24
1.2.3- 1,3-CH addition 26
1.3- Conclusion and perspectives 28
References 30
Chapter 2: CH bond activation of methane by a transient η^2-cyclopropene niobium complex 37
2.1- Introduction 39
2.2- Objectives of this work 41
2.3- Degenerate reaction of 1 with $^{13}CH_4$ and CD_4 42
2.4- CH bond activation of $^{12}CH_4$ by 1 (SST) 47
2.5- Kinetic study of the reaction between 3 and CH_4 53
2.6- Discussion 58
2.7 Conclusion 62
Experimental Section 63
References 72
Chapter 3: CH bond activation of unsaturated hydrocarbons by a niobium methyl cyclopropyl precursor 75
3.1- Introduction 77
3.2- Objectives of this work 80
3.3- CH bond activation of furan and thiophene 80

3.4- CH bond activation of 1-alkyne and alkene 84
3.5- CH bond activation of ferrocene 88
3.6- CH bond activation of pentafluorobenzene 92
3.7- Electrochemistry 100
3.8- Discussion 103
3.9- Conclusion 108
Experimental Section 110
References 120
Appendix 123
Conclusion and perspectives 141
Résumé 143

List of abbreviations

$B(Ar^F)_4$	$B[3,5\text{-}(CF_3)_2C_6H_3]_4$
BCP	Bond Critical Point
BDI	N, N-Diisopro-Pylphenyl-β-Diketiminate
BDE	Bond Dissociation Energy
$Cp^{\neq}$	η^5-1,2-$C_5H_3(^tBu)_2$
HEB	η^6-Hexaethylbenzene
HOESY	Heteronuclear Overhauser Effect Spectroscopy
Me_3tacn	1,4,7-Trimethyl-l,4,7-Triazacyclononane
Op*	$C_5Me_4SiMe_2C_5Me_4$
PNP	$N[2\text{-}P(CHMe_2)_2\text{-}4\text{-}Methylphenyl]_2$
PONOP	$2,6\text{-}(^tBu_2PO)_2C_5H_3N$
ROESY	Rotational Rrame Nuclear Overhauser Effect Spectroscopy
RCP	Ring Dritical Point
RDS	Rate-Determining Step
SST	Spin Saturation Transfer
TOF	Turnover Frequency
TON	Turnover Number
Tp^{Me2}	Hydrotris(3,5-Dimethyl-Pyrazolyl)Borate

D

General introduction

Despite the fact that the reserves of methane, CH_4, the simplest hydrocarbon and the main component of natural gas and other fossil fuels such as shale gas, are huge, there is an ever growing pressure to use these reserves in a more sensible way on economic and environmental grounds. Actually, methane is a potent green-house gas and its current uses in industry, although very useful and valuable, lead to a considerable degradation of its energetic and chemical quality. Many of them are high energy, poorly selective transformations. The main reason for this is that its CH bonds are strong and inert. Thus there is also a scientific challenge behind the so-called problem of "CH bond activation" of methane. Finding ways to functionalize the CH bond(s) of methane selectively to high value-added chemicals using low energy processes is a difficult but exciting problem.

This manuscript is divided in two parts. Results focusing on a mechanistic study of the CH bond activation of methane by a transient η^2-cyclopropene complex of niobium are presented in the first part, which includes Chapter 1 (bibliographic introduction) and Chapter 2. The second part (Chapter 3) presents CH bond activation of heteraromatic and unsaturated hydrocarbons by the same reactive intermediate.

The work presented has been carried out in the "Laboratoire de Chimie de Coordination" (CNRS, Toulouse) in the framework of a joint project with the "Laboratoire de Physique et Chimie des Nano-Objets" (INSA Toulouse, CNRS) funded by the Région Midi-Pyrénées and the PRES-Université de Toulouse. It revolves around the mechanistic investigations of the activation of the C–H bond of methane by early transition metal complexes with the aim of designing, ultimately, new catalysts able to functionalize methane under mild conditions through new mechanistic pathways.

Chapter 1 summarizes the different ways by which transition metal complexes activate the CH bond of methane. Late transition metal complexes usually activate the CH bond of methane by oxidative addition, electrophilic activation and metalloradical addition, while high valent, early transition-metal complexes cleave the CH bond of methane via two main mechanisms: σ-bond metathesis or 1,2-addition across M=N, M=C, M≡C bonds. There is only one case where the CH bond of methane is cleaved by a 1,3-addition across an unsaturated η^2-1,3-butadiene tungsten complex. For the last two reactions, the reactive intermediates are generated through the mechanistic reverse, namely intramolecular α-H or β-H abstraction of a hydrocarbon, respectively. Capitalizing on previous studies in the group, we suggest that the transient η^2-cyclopropene niobium complex [$Tp^{Me2}Nb(\eta^2$-*c*-

C_3H_4)(MeCCMe)] (**A**) could be a good candidate for the activation of CH_4 via a 1,3-addition pathway.

In Chapter 2, we show that it is indeed the case. The niobium bound methyl group in [$Tp^{Me2}NbCH_3$(*c*-C_3H_5)(MeCCMe)] (**1**) abstracts a β-H of the cyclopropyl group intramolecularly, generating **A** under very mild conditions. Degenerate exchange reactions of methane isotopomers (**$^{13}CH_4$** and **CD_4**) with **1** are reported. A kinetic study of the degenerated exchange between **1** and **CH_4** through spin saturation transfer experiments is provided. Productive methane activation of methane giving **1** from the mesitylene complex [$Tp^{Me2}Nb(CH_2$-3,5-$C_6H_3Me_2$)(*c*-C_3H_5)(MeCCMe)] (**3**) is then realized together with a detailed kinetic analysis of the reaction. DFT studies of key intermediates and transition state for the methane CH bond elimination/activation are presented.

In Chapter 3 we show how complex **A** is able to selectively activate the CH bond of heteroaromatics like furan and thiophene, unsaturated hydrocarbons like phenylacetylene, 1-cyclopentene, pentafluorobenzene and ferrocene (FcH) to afford [$Tp^{Me2}NbX$(*c*-C_3H_5)(MeCCMe)] (X =2-C_4H_3O (**4a**), 2-C_4H_3S (**4b**), PhC≡C(**5**), 1-C_5H_7 (**6**), Fc(**7**), and C_6F_5 (**8**)) complexes under mild conditions. Selectivity issues based on thermodynamic properties of CH versus NbC bond strengths are discussed. Electrochemical studies of complexes **1**, **5, 6,** and **7** have been carried out to study the influence of the hydrocarbyl groups on the redox properties of the complexes. An unexpected product arising from cyclopropyl ring opening followed by alkyne coupling from **8** is also presented and DFT studies aimed at understanding the mechanism of this reaction are discussed.

The manuscript ends up with a general conclusion where some perspectives are put forward.

Chapter 1

Methane CH bond activation processes

Chapter 1: Methane CH bond activation processes

Methane is an highly abundant energy and chemical source found as the main component of natural gas (80–90%) and shale gas.[1,2] Current uses of methane include its full oxidation to CO_2 and H_2O to provide heat (and electricity) and the production of *syngas* (a mixture of CO and H_2) by steam reforming ($CH_4 + H_2O = CO + 3H_2$), a high energy demanding endergonic process catalyzed by nickel-based catalysts at high temperatures (*ca* 700 – 1000 °C) and moderate pressure (< 25 bar), which is used for the synthesis of a whole range of commodity chemicals.

Efficient catalytic functionalization of methane directly into easily transportable and high value-added chemicals in a potentially clean and sustainable way remains a long term goal on scientific, environmental, and economic grounds.[3–6] Methane is indeed highly inert, showing an ionization potential of ~12.5 eV,[7,8] with Pauling electronegativities $\chi_C = 2.55$ and $\chi_H = 2.20$, an estimated pK_a value of ~50–51 and a C–H homolytic bond dissociation enthalpy of 440 kJ.mol^{-1} at 25 °C.[9] Therefore, it is very difficult to activate the strong CH bond of methane directly, in either a heterolytic or homolytic way.

Nature has provided enzymes, the so-called methane monoxygenases (MMO) ,[10] which are able to oxidize the C-H bond of methane and other alkanes. Methane monoxygenases (MMO) include two sorts of forms: the soluble form (sMMO) and the particulate form (pMMO). The proposed catalytic cycle for the transformation of methane to methanol catalyzed by sMMO is shown in Scheme 1.1.[11] The diiron centers in the $MMOH_{red}$ form react with the O_2 to generate the peroxide intermediate P. P then converts to intermediate Q, which was proposed to consist of two antiferromagnetically coupled high-spin Fe^{IV} centers with a diamond core structure. It is this species that oxidizes CH_4 to CH_3OH, regenerating the MMOHox form. The intermediate Q oxidizes methane to methanol through either a radical or a nonradical pathway.

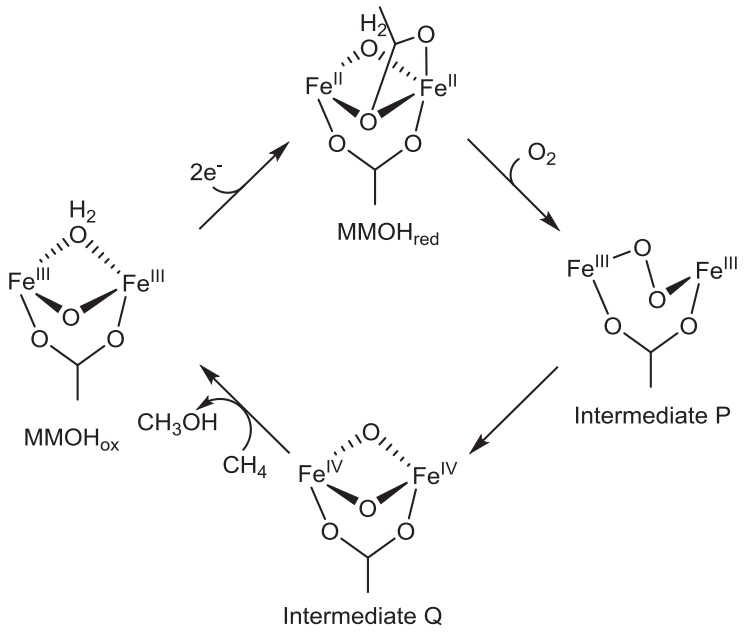

Scheme 1.1. *Transformation of methane into methanol by MMO.*

At the industrial level, transformation of methane into high value-added products is realized through either partial oxidation or alkane metathesis mechanisms catalyzed by heterogeneous catalysts. The attractive oxidative coupling of methane to ethylene and water ($2\ CH_4 + O_2 = C_2H_4 + 2\ H_2O$) has not reached levels of industrial relevance due to the limiting global yield, the lack of stability and selectivity of the catalysts under the harsh reaction conditions (> 700 °C).[12] Methanol CH_3OH, a highly desirable large scale intermediate for fuel and chemical industry, is currently made from *syngas* (see above). The alternative selective oxidation of methane to methanol ($CH_4 + ½\ O_2 = CH_3OH$) pauses the recurrent problem of having a product, CH_3OH, more prone to oxidation than the reactant CH_4 itself (CH bond dissociation energies for methane 440 $kJ.mol^{-1}$; for methanol 374 $kJ.mol^{-1}$) yielding first formaldehyde CH_2O then formic acid HCO_2H and ultimately carbon dioxide CO_2.[3–6] Remarkable selectivities (> 80%), turnover numbers (TON > 3000) and turnover frequencies (TOF > 6000 h^{-1}) have been obtained recently in various Cu or Fe doped zeolites under an international competition scheme, "the Methane Challenge" funded by the Dow Chemical Company.[13]

A promising approach to catalytic methane conversion is realized under the general scheme of alkane metathesis, a reaction that occurs at early transition metal sites (*e.g.* well-defined hydrides TaH and WH supported on silica or alumina;surface organometallic chemistry).[14] The equilibrating cross metathesis of methane and propane yields ethane ($CH_4 + C_3H_8 = 2\ C_2H_6$), a reaction that can be extended to higher alkanes.[15] A most remarkable

reaction is the non-oxidative coupling of methane to give ethane and dihydrogen (2 CH_4 = C_2H_6 + H_2). Despite an unfavorable Gibbs free energy thus low conversions, high selectivity (98%) could be obtained in continuous flow reactors at moderate pressure (P_{CH4} = 50 bar) and temperature (T = 250 °C). The mechanism is shown in Scheme 1.2.[16]

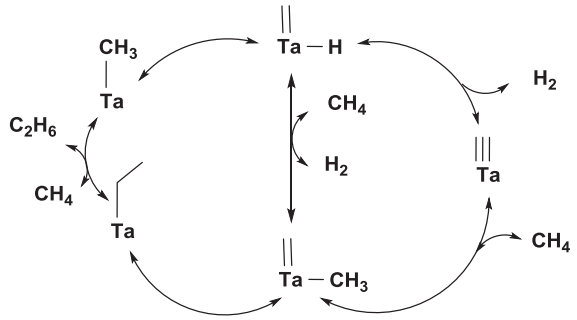

Scheme 1.2. *Proposed mechanism for the non-oxidative coupling reaction of methane catalyzed by the silica-supported tantalum hydride* $(\equiv SiO)_2Ta–H$

The reaction is speculated to begin with the CH bond activation of methane by the silica-supported tantalum hydride $(\equiv SiO)_2Ta–H$ to generate a surface tantalum–methyl species and molecular hydrogen. This tantalum–methyl, upon dehydrogenation, is transformed to a carbene–hydride and a carbyne species and dihydrogen. Both species are able to activate methane through a σ-bond metathesis mechanism, yielding a methyl–methylidene key intermediate. Then, the methyl group in $(\equiv SiO)_2Ta(=CH_2)CH_3$, migratory inserts onto the carbene ligand to yield the tantalum–ethyl bond. Finally, in the presence of large excess of methane, the ethyl ligand can be exchanged with methane via σ-bond metathesis, to generate ethane and return to a tantalum–methyl species.

With the hope of benefiting of the flexibility ascribed to homogeneous systems, catalysis with discrete transition metal complexes has emerged as an important strategy. Furthermore it potentially allows precise tuning of various factors so that the molecular design of catalysts and the detailed understanding of the intimate mechanism of the reactions are possible. A summary of the different ways of cleaving a CH bond by transition metal complexes are shown in Scheme 1.3. Early and late transition metal complexes activate methane by different mechanistic pathways, but only a few of them have led to catalytic applications. In the following sections we will make a general overview of the CH bond activation schemes by which late and early transition metal complexes may activate methane in homogeneous conditions.

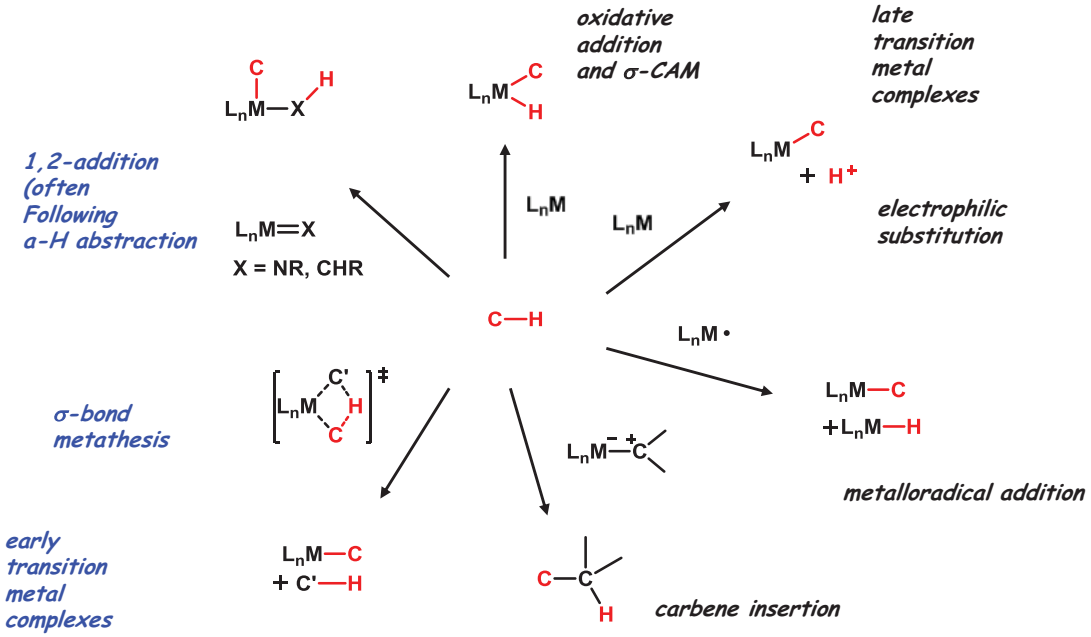

Scheme 1.3. *CH bond activation pathways at transition metal centers.*

1.1- CH bond activation of methane by late transition metal complexes

Late transition metal complexes activate the CH bond of methane by different pathways such as the electrophilic substitution, oxidative addition, carbene insertion and metalloradical addition. In the following section the main features of each type of CH bond activation mechanism is discussed.

1.1.1- Electrophilic substitution

Late- or post-transition metals act as Lewis acids, reacting with methane by electrophilic substitution in polar medium (Equation 1.1).

(1.1)

Systems working through electrophilic substitution are described in Scheme 1.4. They are remarkable since they constitute rare examples of catalytic methane functionalization with homogeneous metal complexes, although with low TOF and TON. As developed by Catalytica (Periana),[17–19] routes C and D in Scheme 1.4 show the synthesis of methanol (or some of its derivatives) by oxidation of methane avoiding the *syngas* route. These ways use

Hg or Pt catalysts and operate under harsh acidic conditions (H_2SO_4) at high temperatures (180 to 220°C) ([Pt] = [(bpym)$PtCl_2$], bpym = 2,2'-bipyrimidine). They give methylbisulphate in 70% yield albeit with a very modest TOF (10^{-3} s^{-1}). These studies all rely on the initial fundamental studies of Shilov conducted in the late 1960's (routes A and B).[20] The conversion of methane to acetic acid has also been achieved. It is performed either with V-based catalysts (complex radical mechanism, trifluoroacetic acid, peroxodisulfate as oxidant, 50% yield route E),[21] or with a Pd(II) catalysts under Catalytica-like conditions with a TON of 4 (route F).[22] Note that in these methane functionalization reactions, CH bond activation does not occur through a conventional CH oxidative addition but rather via an electrophilic mechanism where H^+ is expelled directly.

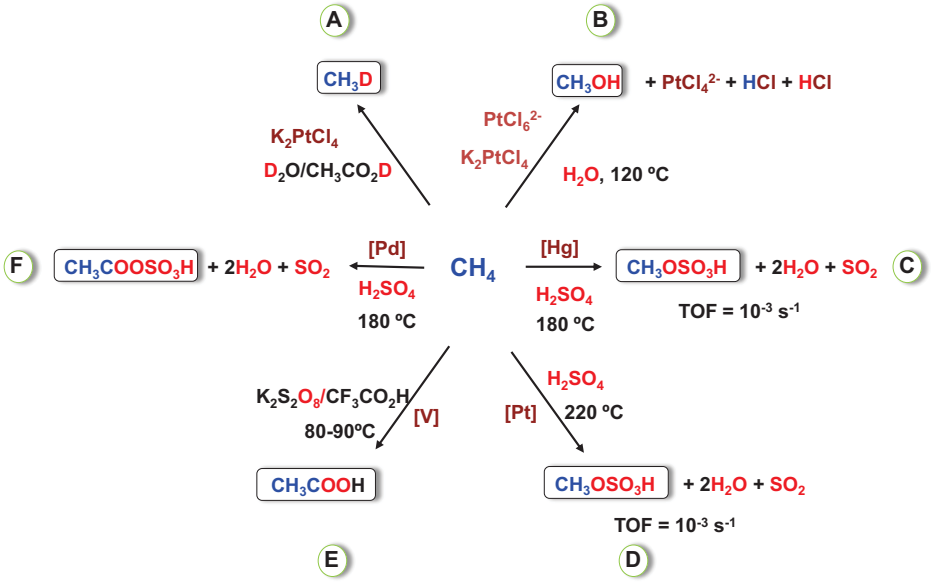

Scheme 1.4. *Catalytic methane CH bond functionalization by electrophilic substitution.*

1.1.2- Oxidative addition

The most common mechanism of oxidative addition of the CH bond of methane is a concerted 3-center addition in which the reducing equivalent from the metal must be high enough in energy to locate at the C–H σ* orbital and generate two new bonds (M–C and M–H). According to equation 1.2, therefore, the increasing of the metal oxidation state by two units is accompanied by the formation of two new metal–methyl and metal–hydride bonds.

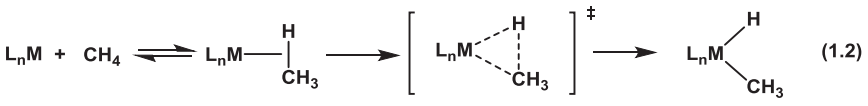

(1.2)

In the 1980s, Janowicz and Bergman[23] and Graham[24,25] discovered that electron-rich, low-oxidation-state cyclopentadienyliridium(I) transients activate the CH bond of methane. Graham et *al.* found that [Cp*Ir(CO)] and [CpIr(CO)], photogenerated from [Cp*Ir(CO)$_2$] and [CpIr(CO)$_2$] added methane (20 bar) at room temperature in cyclohexane yielding the respective iridum(III)hydridomethyl complex in 20% yield (Scheme 1.5).[23]

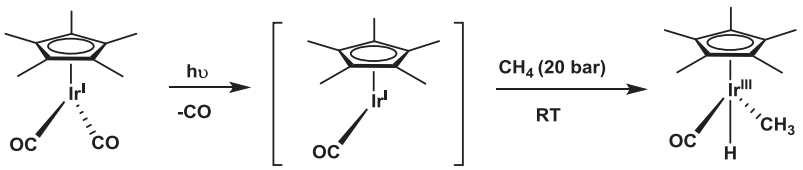

Scheme 1.5. *Oxidative addition of methane by a photogenerated unsaturated Ir(I) complex.*

Bergman reported that [Cp*Ir(PMe$_3$)], produced by thermolysis (140–150°C for several hours) of [Cp*Ir(PMe$_3$)(*c*-C$_6$H$_{11}$)H] via reductive elimination, was able to cleave the C–H bond of methane (20 bar) to give [Cp*Ir(PMe$_3$)(CH$_3$)H] in 58% yield (Scheme 1.6).[23,26]

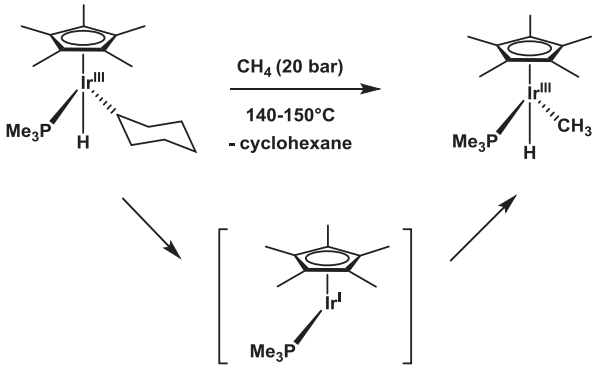

Scheme 1.6. *Oxidative addition of methane by a thermolytically generated unsaturated Ir(I) complex.*

The same authors discovered 10 years later that a cationic iridium(III) complex [Cp*Ir(PMe$_3$)(CH$_3$)(CH$_2$Cl$_2$)][BArF$_4$][27,28] was even more reactive toward methane. By exchange reaction in the presence of ^{13}CH$_4$, it was shown that this extremely electrophilic Ir(III) cation could activate methane even at 10°C, yielding [Cp*Ir(PMe$_3$)(^{13}CH$_3$)(CH$_2$Cl$_2$)][BArF$_4$] (Scheme 1.7). Hall *et al*. has computed an oxidative addition-reductive elimination pathway involving an Ir(V) intermediate.[29]

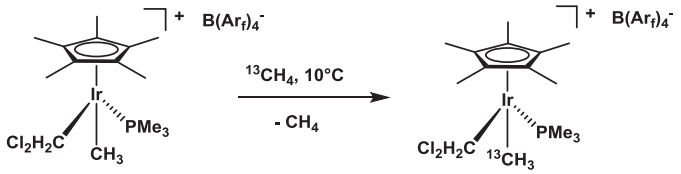

Scheme 1.7. *C–H bond activation of $^{13}CH_4$ by [Cp*Ir(PMe$_3$)(CH$_3$)(CH$_2$Cl$_2$)][BArF$_4$]*

Jones and Maguire have taken advantage of the Re(III)/(V) couple, showing that [CpRe(PPh$_3$)$_2$H$_2$] could catalyze the H/D exchange between C_6D_6 and CH_4, with 68 turnovers over 3 h, representing one of the few catalytic methane-activating systems based on this mechanism (Scheme 1.8).[30]

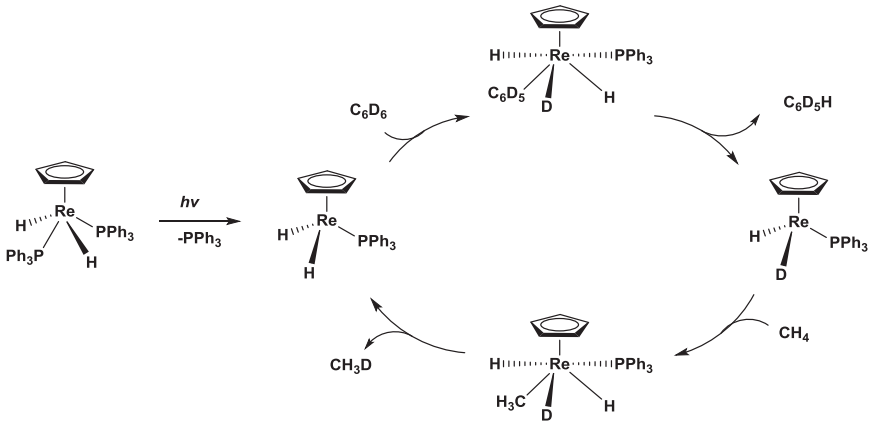

Scheme 1.8. *Mechanism for the H/D exchange between CH_4 and C_6D_6, catalyzed by a cyclopentadienylrhenium(I) complex.*

Other low valent complexes can also promote oxidative addition of methane. The complex [(dmpe)$_2$FeH$_2$] is the only first-row transition metal complex shown to cleave a CH bond of methane by oxidative addition. At –100°C, the transient [(dmpe)$_2$Fe] species, generated photolytically, activates methane (in liquid xenon) to form [*cis*-(dmpe)$_2$Fe(CH$_3$)H].[31] Another group 8 complex, [(PMe$_3$)$_4$Os(CH$_2$tBu)H], eliminates neopentane at elevated temperatures and pressures to generate [Os(PMe$_3$)$_4$] which adds methane in poor yields (16%).[32]

In the presence of Re, Rh and Ir precursors, oxidative addition, coupled to borylation reactions, has shown great potential for the functionalization of alkanes and arenes toward the formation of extended C–C bonds.[33] However none of these transformations have been expanded to CH_4, possibly due to difficulties in manipulating this gas as well as to potential competition between CH_4 and the solvent itself.

1.1.2.1- σ-CH_4 intermediates along the oxidative addition pathway

In the oxidative addition pathway, the cleavage of the methane CH bond by the transition metal complexes likely starts by the coordination of the CH bond of methane to the metal center. Four possible methane binding modes have been proposed for the σ-coordinated complexes, including the η^1-H, η^2-H,H, η^2-C,H, and η^3-H,H,H interactions (Scheme 1.9).[34]

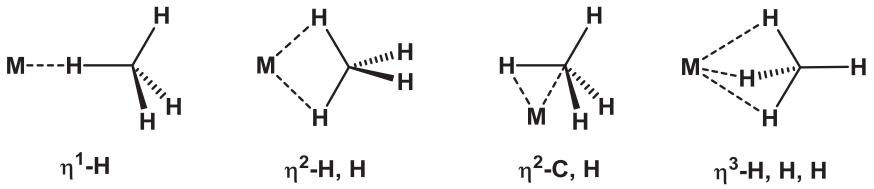

Scheme 1.9. *Possible coordination modes of methane to a transition metal center.*

Evidence for the existence of these σ-complexes comes from sources such as matrix and gas phase IR and UV/vis photolysis and, more recently, NMR spectroscopy; however the actual coordination mode of methane is often unknown. Evidence of methane coordination was initially suggested through UV/vis photolysis experiments in which a ligand dissociated from the metal center generating a coordinately unsaturated complex, which was then trapped by methane (Equation 1.3).

$$[L_{n+1}M] \overset{-L}{\rightleftharpoons} [L_nM] \overset{CH_4}{\rightleftharpoons} [L_nM(CH_3\text{-}H)] \rightleftharpoons L_nM\begin{matrix}CH_3\\H\end{matrix} \qquad (1.3)$$

Unsaturated d^6 metal complexes such as $[M(CO)_5]$ (M = Cr, W) and $[CpML_2]$ (M = Mn, Re) have been found to trap methane to form σ-methane complexes. In the classic work of Perutz and Turner, for instance, a methane complex was inferred by changes in the UV/vis photolysis experiments where $[Cr(CO)_5]$ was photogenerated from $[Cr(CO)_6]$ in methane matrix at 12 K.[35] The detection of σ-methane complexes has also been carried out by using time-resolved infrared spectroscopy studies (TRIR). George and coworkers have recently used TRIR to detect transient metal carbonyl σ-methane and σ-ethane complexes generated in the supercritical alkane at room temperature from their IR spectra in the region of the CO stretching frequencies.[36] In *sc*CH_4, in particular, transient methane adducts such as $[W(CO)_5(CH_4)]$, $[CpM(CO)_2(CH_4)]$ (M = Mn, Re), and $[Cp^*Re(CO)_2(CH_4)]$ could be generated and the CH_4 binding enthalpies to the metal center have been obtained: W–CH_4 (30

kJ.mol^{-1}), Mn–CH_4 (39 kJ.mol^{-1}), and Re–CH_4 (51 kJ.mol^{-1}) in [$W(CO)_5(CH_4)$], [$CpMn(CO)_2(CH_4)$], and [$CpRe(CO)_2(CH_4)$], respectively.[37] Theoretical calculations have also established the plausibility of methane adducts especially as intermediates on the pathway to oxidative addition. Methane complexation to 14 and 16 electron fragments, sometimes derived from hypothetical complexes, has been studied by a variety of computational methods. Depending on the computed system, the authors proposed either a η^2-C,H,[38] or η^1-H,[39] or η^2-H,H[40] or η^3-H,H,H,[41] coordination mode, showing how all of the structures reported in Scheme 1.9 may be envisaged.

Evidence for σ-methane complex intermediates can be inferred from isotopic labeling experiments: specifically, i) the observation of deuterium exchange between hydride and methyl sites (such as between [$L_nM(CH_3)D$] and [$L_nM(CH_2D)H$]), and ii) the measurement of kinetic isotope effects (KIEs). A series of kinetic and thermodynamic deuterium isotope effects have been described in the literature by the groups of Norton,[42] Bercaw,[43] Green,[44] Parkin[45] and Jones[46] (Scheme 1.10).

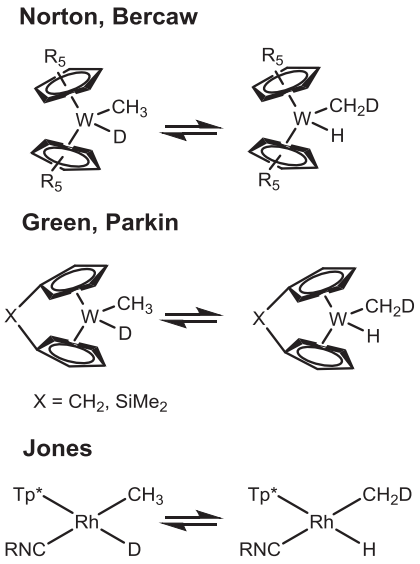

Scheme 1.10. *Interconversion of [$L_nM(CH_3)D$] and [$L_nM(CH_2D)H$].*

In the interconversion of [W{(η-C_5H_4)CMe_2(η-C_5H_4)}$(CH_3)D$] to [W{(η-C_5H_4)CMe_2(η-C_5H_4)}$(CH_2D)H$] by ^2H NMR (Figure 1.1), for instance, the disappearance of the deuteride signal is associated to the appearance and growth of the new CH_2D signal .

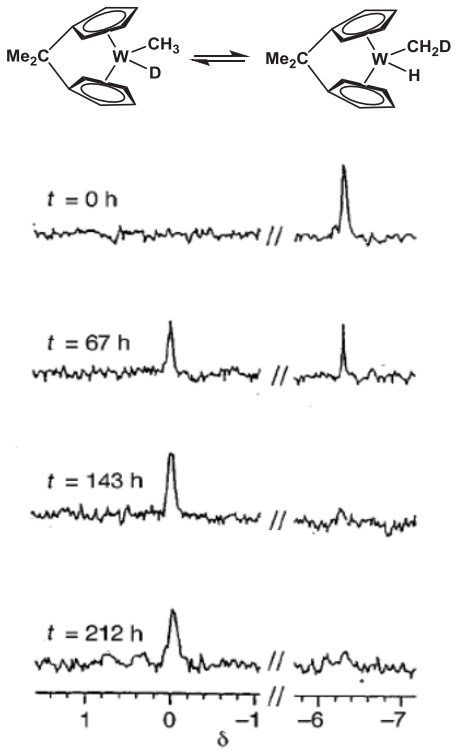

Figure 1.1. *The ^2H NMR spectra of [W{(η-C_5H_4)CMe_2(η-C_5H_4)}(CH_3)D] in benzene as a function of time (high field extension).*

The measurement of the kinetic isotope effect is realized by the study of rate constants using ^1H NMR spectroscopy. Norton[42] has shown that comparison of the rate of CH_4 elimination from [$Cp_2W(CH_3)H$] with that of CD_4 from [$Cp_2W(CD_3)D$] occurred with an inverse isotope effect of 0.7 at 72.6 °C (Scheme 1.11).

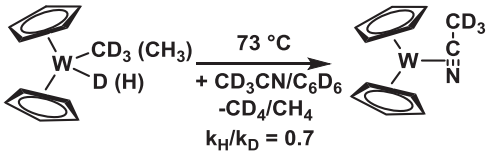

Scheme 1.11. *Kinetics of CH_4/CD_4 elimination from [$Cp_2W(CH_3)H$]/[$Cp_2W(CD_3)D$].*

Other complexes that exhibit inverse KIE include [$Cp^*_2W(CH_3)H$] (0.70),[43] [$Cp_2Re(CH_3)H$]$^+$ (0.8),[47] [(Me_3tacn)Rh(PMe_3)(CH_3)H]$^+$ (0.74),[48] and [(tmeda)Pt(CH_3)H(Cl)] (0.29).[49] Jones has analyzed this inverse isotope effect systematically.[50] As shown in Scheme 1.12, the proposed reaction steps are similar for all these examples and the formation of the methyl hydride product is reversible. The intermediacy of a σ-methane complex is often demonstrated by preparation of a methyl deuteride complex, which then reversibly scrambles

the deuterium into the α-hydrogen of the methyl ligand, presumably via the unseen σ-methane complex. Dissociation of methane from the σ-complex, followed by irreversible trapping of the reactive fragment [L_nM] with an external ligand, is typically observed as a slower process. The [$L_nM(CH_3)D$] compound slowly transforms into the unseen η^2-C,D intermediate through reductive coupling, which interconverts first into the η^2-H,D, and then into the η^2-C,H σ-methane intermediates by the fast exchange of deuterium with hydrogen. Then the η^2-C,H bond of methane recoordinates with the metal center and is cleaved by the metal to form [$L_nM(CH_2D)H$] (Scheme 1.12).

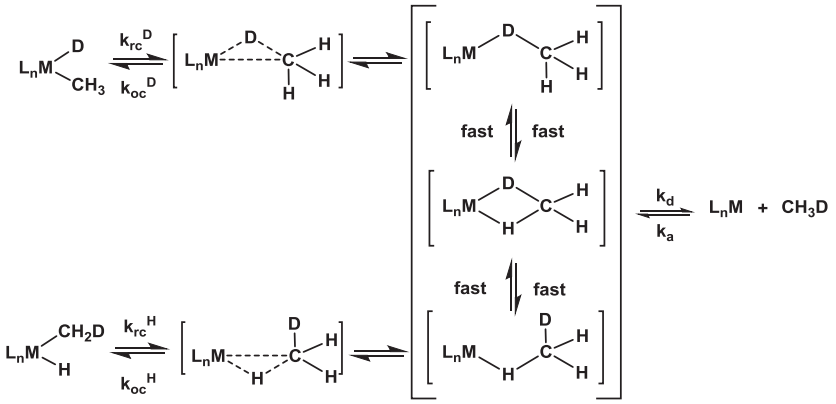

Scheme 1.12. *Deuterium scrambling in the interconversion of [$L_nM(CH_3)(D)$] with [$L_nM(CH_2D)(H)$].*

The reductive elimination, thus, consists of reductive coupling (rc) followed by dissociation (d), while the microscopic reverse, oxidative addition, consists of ligand association (a) followed by oxidative cleavage (oc). The rate constant for irreversible reductive elimination is a composite of the rate constants for reductive coupling (k_{rc}), oxidative cleavage (k_{oc}), and dissociation (k_d), namely, $k_{obs} = k_{rc}k_d/(k_{oc}+k_d)$. For $k_d << k_{oc}$, $k_{obs} = k_{rc}k_d/k_{oc}$, if the isotope effect for dissociation of CH_3D is considered to be close to unity (i.e. $[k_d^H/k_d^D] = 1$), the isotope effect on reductive elimination is dominated by the ratio of the isotope effect on reductive coupling to that of oxidative addition, i.e. $[k_{rc}^H/k_{rc}^D]/[k_{oc}^H/k_{oc}^D]$. This ratio is identical to the equilibrium isotope effect (EIE) for interconversion of [$L_nM(CH_3)D$] and [$L_nM(CH_2D)H$] which would be predicted to be inverse because the zero-point energy difference between M–H and M–D bonds in the methyl hydride complex is smaller than the zero-point energy difference between C–H and C–D bonds in the σ-methane complex. In most of the examples the inverse kinetic isotope effect is due to an inverse equilibrium isotope effect (i.e. $K_{eq}^{H/D} < 1$). Two possibilities have to be used to illustrate this

phenomenon. In one case, shown in Scheme 1.13(a), besides the zero point energy difference in the reactant and product, there are also zero point energy differences in the transition state. In this case there is an inverse kinetic isotope effect ($k_{rc}^{H}/k_{rc}^{D} < 1$) for the reduction coupling step and a normal kinetic isotope effect ($k_{oc}^{H}/k_{oc}^{D} > 1$) for the reverse oxidative cleavage step. In the second case, shown in Scheme 1.13(b), there is no zero point energy difference between C–H and C–D bonds in the transition state. Normal kinetic isotope effects are assumed on both directions. However, kinetic isotope effect in the oxidative cleavage step is much larger than kinetic isotope effect in the reductive coupling step, which results in an inverse isotope effect for the global reaction.

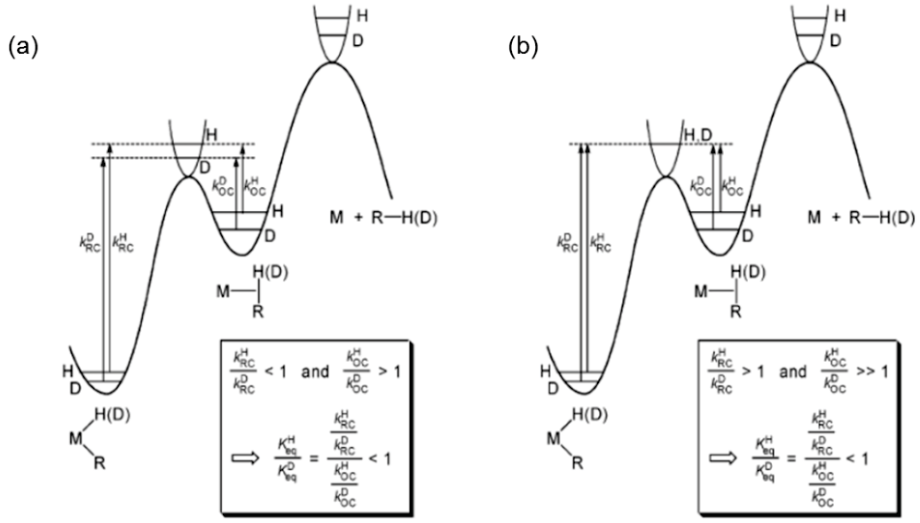

Scheme 1.13. *Inverse isotope effect.*

Two important points can be noted. First, both situations are consistent with an inverse equilibrium isotope effect separating the methyl hydride complex from the σ-methane complex, since the transition state does not affect the equilibrium. Second, the observation of an inverse kinetic isotope effect for the loss of methane from a methyl hydride/deuteride complex cannot, in itself, distinguish between these two cases. The examples reported until now for the $D(H)/CH_3(CH_2D)$ scrambling[45–46] show a normal kinetic isotope effect for reductive coupling and oxidative cleavage, the latter being larger than the former. These systems, therefore, are best described by Scheme 1.13(b), by which the inverse equilibrium isotope effect arises as a result of two normal isotope effects of different magnitudes that oppose each other. Scheme 1.13(a) has been never observed for the $D(H)/CH_3(CH_2D)$ scrambling, but it has been observed for the $D(H)/C_6D_2H_3(C_6H_2D_3)$ scrambling in the coordinatively unsaturated fragment $[Cp^*Rh(PMe_3)]$.[51]

NMR experiments have also been used to characterize σ-alkane complexes. The alkane complexes [Cp'ReL(Cp)(alkane)] (L = CO, PF_3; alkane = *n*-C_5H_{12}, *n*-C_7H_{16}, *c*-C_5H_{10}, *c*-C_6H_{12}, *i*-C_4H_{10}),[52] (HEB)$W(CO)_2$(pentane),[53] $CpRe(CO)_2$(alkane) (alkane = *c*-C_5H_{12}, 2,2-dimethyl-butane) and $Cp^{\neq}Re(CO)_2$(alkane) (alkane = *c*-C_5H_{10}, *n*-C_7H_{16}),[54] $CpMn(CO)_2$(alkane)[55] (alkane = C_2H_6 and *i*-C_5H_{12}) have been generated by low-temperature photodissociation experiments in pure alkane solvents. Although these thermally unstable species are produced in modest yields, the σ-alkane complexes are well characterized by low temperature ^1H and ^{13}C NMR spectroscopy. However, this method is not applicable to methane due to its very low boiling point. The only full NMR characterization of a transition metal σ-methane complex in solution has been reported by Bernskoetter, Brookhart and coworkers in a rhodium(I) compound.[56] Protonation of the rhodium(I) methyl complex, [(PONOP)Rh(CH_3)] with H[BAr^F_4](Et_2O)$_2$ in $CDFCl_2$ solvent at –110°C yields the rhodium(I) σ-methane complex, [(PONOP)Rh(CH_4)][BAr^F_4] (Scheme 1.14), which was characterized by a series of low-temperature ^1H, ^2H, ^{13}C NMR experiments.

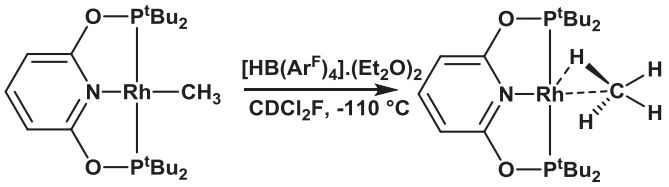

Scheme 1.14. *Synthesis of the [(PONOP)Rh(CH_4)][BAr^F_4] σ-methane complex*

As shown in Figure 1.2, the ^1H and ^{13}C NMR spectra of the [(PONOP)Rh($^{13}CH_4$)][BAr^F_4] compound at –110 °C exhibit a doublet of doublets at δ –0.86 ppm ($J_{C–H}$ = 124 Hz, $J_{Rh–H}$ = 6.3 Hz) and a quintet at δ –41.7 ppm ($J_{C–H}$ = 124 Hz), respectively.

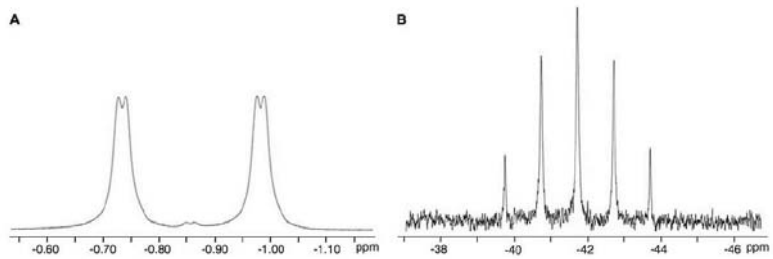

Figure 1.2. *The ^1H and ^{13}C NMR spectra of [(PONOP)Rh($^{13}CH_4$)][$B(Ar^F)_4$] at –110 °C*

Even at –110 °C, methane rapidly tumbles in the coordination sphere of rhodium, exchanging free and bound hydrogens. Kinetic studies reveal a half-life of about 83 minutes at –87°C for the dissociation of methane. Remarkably, the σ-methane complex, $[(PONOP)Rh(CH_4)][BAr^F{}_4]$ is shown to be more stable than the corresponding rhodium(III) methyl hydride complex. DFT calculations showed an unsymmetrical interaction between rhodium and the methane ligand, with only one C–H bond coordinated to the metal according to a η^2-C,H coordination mode in Scheme 1.9.

1.1.2.2- σ-complex-assisted metathesis (σ-CAM) mechanism

Different from the familiar oxidative-reductive elimination mechanisms and σ-bond metathesis (see below), CH bond activation of methane could also happen without changing the oxidation state of the late transition metal in the σ-complex through the so-called σ-CAM mechanism.[57]

Hartwig first has proposed that borylation of methane at $[CpM(CO)_n(boryl)]$ complexes (M = Fe, W) could occur through the σ-CAM mechanism via DFT calculation.[58] The mechanism is shown in Scheme 1.15. A σ-CH_4 complex A is first transformed to σ-borane B via a σ-CAM step. Then B undergoes σ-rotation to form σ-borane B'. B' is converted to σ-alkylborane C with B–C bond coupling via a second σ-CAM step. $[CpRhH\{B(OR)_2\}]$ or $[CpRh\{B(OR)_2\}_2]$ complexes also follows this mechanism.

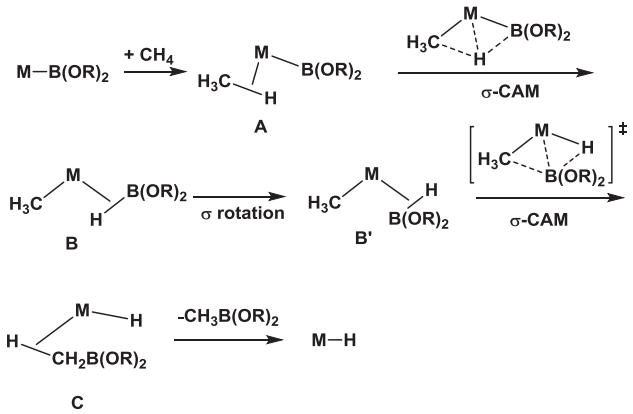

Scheme 1.15. *Borylation of methane at $[CpM(CO)_n(boryl)]$ complexes (M = Fe, W) via σ-CAM mechanism*

Ng *et al.* has also reported that $[TpRuH(MeCN)(PPh_3)]$ catalyzes H/D exchange between methane and C_6D_6 at 100 °C. The σ-CAM mechanism has been analyzed by DFT calculations. η^2-H_2, η^2-CH_4, and η^2-benzene ligands are involved in this mechanism (Scheme

1.16).[59] The bonds between the nonmetal atoms connected to the metal center could be cleaved in the transition states of the σ-CAM step.

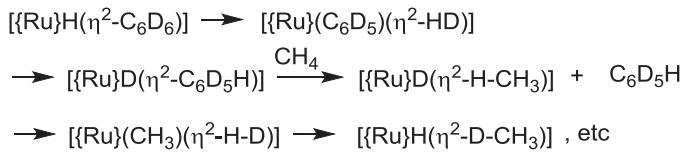

Scheme 1.16. *H/D exchange between methane and C_6D_6 at 100 °C through σ-CAM mechanism.*

Lam *et al.* has compared the behavior of Fe, Ru, and Os in the reaction of [MH] (M = [TpFe(PH_3)], [TpRu(PH_3)], [TpOs(PH_3)]) with methane to form [MH(η^2-CH_4)], which is then transformed to [MCH_3(η^2-H_2)] and then to [M(CH_3)] and dihydrogen via DFT calculations.[60] In contrast to the oxidative cleavage mechanism for Os, Fe and Ru complexes follow the σ-CAM mechanism.

1.1.3- Carbene insertion

A different approach to selective alkane CH activation and functionalization involves the insertion of electrophilic carbon into CH bonds. This strategy has been realized recently by the Perez, Etienne and Asensio groups via the catalytic insertion of a carbene into the C–H bond of methane.[61,62] By using a perfluorinated tris(indazolyl)borate ligand on Ag(I), high pressures of methane (160 atm), supercritical CO_2 conditions (250 atm), and ethyldiazoacetate (EDA) as the carbene source, methane has been converted into ethylpropionate by carbene :$CHCO_2Et$ insertion into a CH bond of methane (Scheme 1.17(a)). TON and TOF of 734 and 1.4×10^{-2} s^{-1}, respectively, have been achieved, the latter being, to the best of our knowledge, the highest conversion rate reported to date for methane functionalization under homogenous conditions. A plausible mechanism for CH functionalization of methane (and other hydrocarbons) involves metal-catalyzed N_2 elimination from the diazo substrate followed by carbene transfer mediated by a highly electrophilic metal carbene intermediate (Scheme 1.17(b)). In this chemistry, therefore, the metal complex does not break directly the CH bond of methane but rather a very electrophilic silver carbene complex polarizes the inert CH bond to induce insertion.

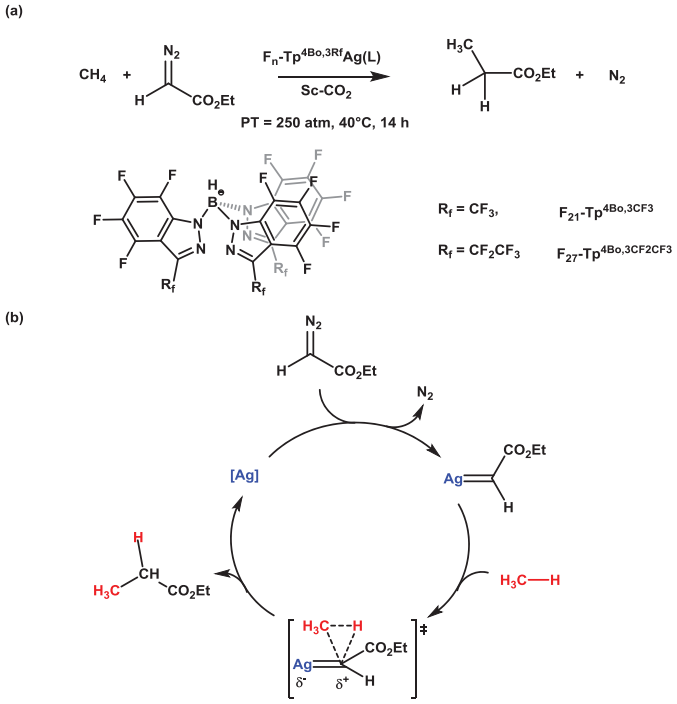

Scheme 1.17. *Catalytic functionalization of methane by carbene insertion.*

1.1.4- Metalloradical addition

In the early 1990s Wayland *et al*. discovered that (tetramesitylporphyrin)Rh(II) compounds activated the CH bond of methane by a metalloradical pathway to form a Rh–H and a Rh–Me bond under mild conditions.[63–65] Kinetic studies showed that the reaction rate was second order in the (tetramesitylporphyrin)Rh(II) radical system and first order in CH_4. The rate determining step was proposed to be the CH cleavage of methane with the formation of a linear 4-center Rh…H…C…Rh transition state featuring a trigonal pyramidal methane (Scheme 1.18). When CD_4 was employed, a large, temperature dependent, KIE was measured (8 at 23°C and 5 at 80 °C), consistent with methane CH bond cleavage being the rate-determining step. Wayland *et al.* also reported that complexes containing porphyrin ligands joined by a *m*-xylene tether could activate CH_4.[66–68] DiMagno *et al.* has found that a perfluoro and perfluoroaryl substituted porphyrin of Rh(II) activated and ultimately functionalized methane by delivering the methyl carbonium moiety to PPh_3 to give $[PPh_3CH_3]^+$.[69]

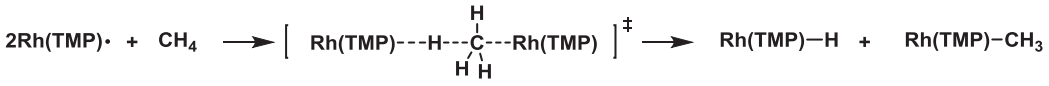

Scheme 1.18. *CH bond activation of methane by Rh(TMP) radical*

1.2- CH bond activation of methane by early transition metal complexes.

High oxidation state early transition metal complexes (and related electropositive metals such as lanthanides or actinides) have been also shown to activate the CH bond of methane (and more generally hydrocarbons). In these cases, the mechanistic pathways involved are σ-bond metathesis, 1,2-addition (often following α-H abstraction) and 1,3-addition (often following β-H abstraction).

1.2.1- σ-Bond metathesis.

Electron poor d^0 and d^0f^n transition metal alkyl and hydride complexes are able to activate saturated C–H bonds by σ-bond metathesis.[70–72] The σ-bond metathesis mechanism involves the formation of a polar four-center, four-electron transition state in which the metal–alkyl bond of the original complex is broken to form a new metal–alkyl bond and free alkane (Scheme 1.19). The σ-bond metathesis differs from the other mechanisms discussed herein in that the CH activation is the rate-determining step.

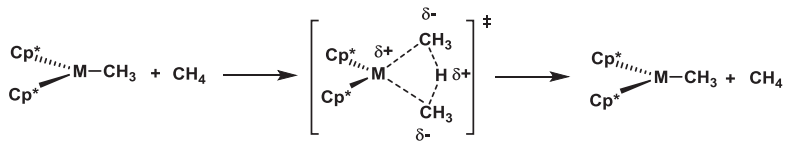

Scheme 1.19. *σ-bond metathesis of methane.*

Watson found that yttrium and lutetium metallocenes methyl complexes activate the CH bond of methane through a four-center transition state, where the hydrogen atom being transferred is located at the midway point between the two methyl groups. $^{13}CH_4$ reacts with $[Cp^*_2M(CH_3)]$ (M = Lu, Y) through a degenerate exchange process to form $[Cp^*_2M(^{13}CH_3)]$ and CH_4 at 70°C (Scheme 1.20).[70] The decrease of the intensity of the $^{13}CH_4$ and $Lu^{13}CH_3$ signals is accompanied by the concomitant growth of the $^{12}CH_4$ resonance, as observed by both ^1H and ^{13}C NMR (Figure 1.3). In addition, $[Cp^*_2Lu(CH_3)]$ reacts with CD_4 to give $[Cp^*_2Lu(CD_3)]$, which is characterized by ^2H NMR spectroscopy (Scheme 1.20). Kinetic studies show that the reaction rate is first order in $[Cp^*_2Lu(CH_3)]$ and first order in CH_4, implying a four-center transition state.

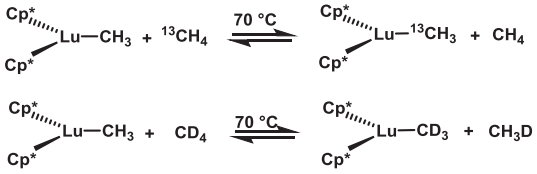

Scheme 1.20. *Degenerate reactions of [Cp$_2$Lu(CH$_3$)] with $^{13}CH_4$ and CD_4*

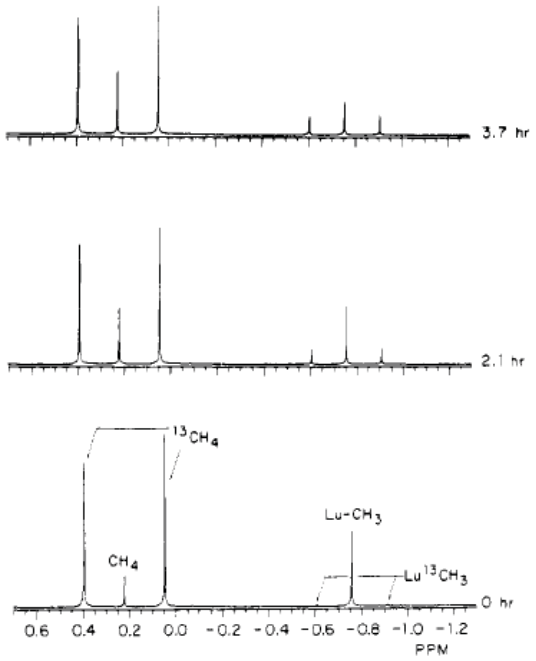

Figure 1.3. *^{1}H NMR spectra of reaction of [Cp*$_2$Lu(CH$_3$)] with $^{13}CH_4$ as a function of time at 70 °C.*

Bercaw's group has undertaken an in-depth investigation of the reaction of permethylscandocene hydride or alkyl derivatives for the activation of sp^3, sp^2 and sp CH bonds of various hydrocarbons.[71] $^{13}CH_4$ reacts with [Cp*$_2$Sc(CH$_3$)] through a degenerate exchange process to form [Cp*$_2$Sc(^{13}CH$_3$)] and CH_4 at 70°C. The reaction with the Sc derivative is approximately 50 times slower than that with [Cp*$_2$Lu(CH$_3$)] and 250 times slower than that with [Cp*$_2$Y(CH$_3$)]. DFT calculations by Maron and Eisenstein showed that the relative rates of reactions for Sc, Y, Lu are influenced by the ionic radius of the metal.[73]

According to experimental and computational papers,[73–76] the reaction coordinate proceeds to the transition state (TS) with no intermediate. The TS for the CH bond cleavage has a distinctive kite shape with an almost linear CH$_3$…H…CH$_3$ disposition and the C–H bond distance is much longer in the transition state (1.33 Å) than in free methane (1.09 Å).[74] The alternation of charge is reminiscent of a proton transfer between two negatively charged methyl groups (Scheme 1.19). Bond critical points (BCP) are located along the M–C and C–H

coordinates, and ring critical points (RCP) are located inside the *c*-M–C–H–C, which suggests the four-center geometry of the σ-bond metathesis transition state. The fact that no BCP can be located along M–H coordinate suggests no direct interaction between the hydrogen and the metal center during H transfer.[77,78]

Marks has found that the thoracyclobutane [$Cp^*_2Th(^cCH_2C(CH_3)_2CH_2)$] activates methane in a similar manner affording [$Cp^*_2Th(CH_3)(CH_2C(CH_3)_3)$] in 50% yield (Scheme 1.21).[72] An intermolecular KIE of 6(2) has been measured when CD_4 is used, demonstrating that cleavage of the methane C–H bond is involved in the rate-determining step.

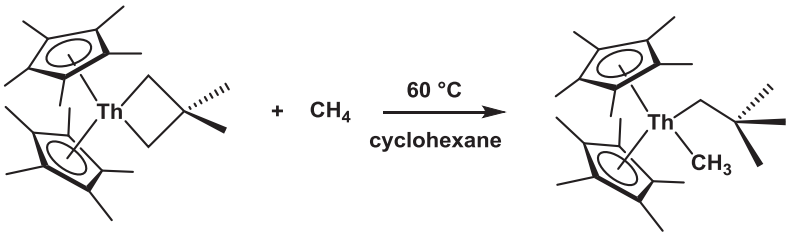

Scheme 1.21. *CH bond activation of methane by [$Cp^*_2Th(^cCH_2C(CH_3)_2CH_2)$]*

In 2003, Sadow and Tilley demonstrated that metallocene-alkyl complexes of scandium could activate methane preferentially over benzene at room temperature. By coupling σ-bond metathesis and migratory insertion reactions, they have realized the catalytic coupling of methane and propene to give 2-methylpropane. As shown in Scheme 1.22(a), [$Cp^*_2ScCH_3$] inserts propene to give [$Cp^*_2Sc(CH_2CH(CH_3)_2)$]. This complex reacts with CH_4 to give 2-methylpropane and regenerate the methyl complex with a low TON of 4.[79] Attempts to improve the TON met with limited success since the *ansa*-bridged complex [$Op^*_2Sc(CH_2CH(CH_3)_2)$] is more active towards methane activation than [$Cp^*_2Sc(CH_2CH(CH_3)_2)$] but is less selective for olefin insertion.[80] [$Cp^*_2Sc(CH_3)$] is also a catalyst for the dehydrocoupling reaction of methane and diphenylsilane by which Ph_2SiH_2 and CH_4 are converted into Ph_2MeSiH and H_2 via two consecutive σ-bond metathesis reactions (Scheme 1.22(b)).[81,82]

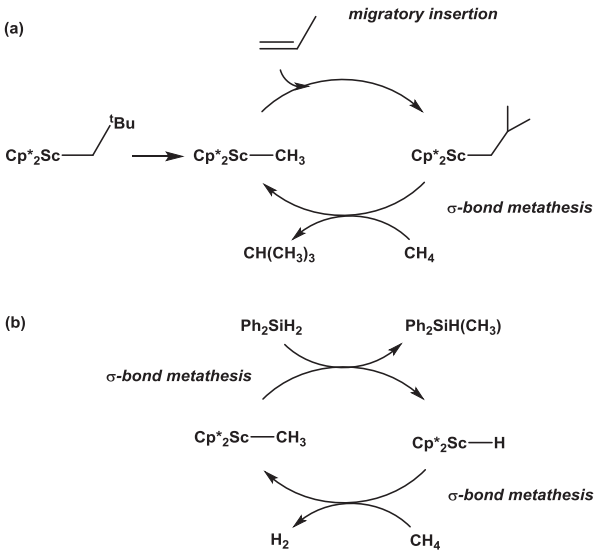

Scheme 1.22. *Productive σ-bond metathesis of methane.*

1.2.2- 1,2-CH addition.

Addition of a CH bond across a metal–ligand multiple bond has been referred to as 1,2-CH bond addition. Although this process resembles σ-bond metathesis, since it involves a 4-center transition state, the outcome is significantly different. The 1,2-CH bond addition, indeed, involves the generation of a high energy, metal–ligand multiply bonded intermediate, which performs the CH cleavage step. A remarkable system based on four-coordinate group 4, 5 and 6 metals has been developed by Wolczanski and coworkers. The first example of methane activation (among many hydrocarbons) is exemplified by tris(amido)alkyl zirconium complexes of the type $[(^{t}Bu_3SiNH)_3ZrR]$. [83,84] With R = Cy, cyclohexane is eliminated above 80°C by an intramolecular α-CH abstraction of an amido hydrogen to give the transient, unobserved, diamido imido complex $[(^{t}Bu_3SiNH)_2Zr{=}NSi^{t}Bu_3]$ (Scheme 1.23). After methane coordination, this reactive unsaturated complex cleaves the C–H bond of methane to give the methyl complex $[(^{t}Bu_3SiNH)_3Zr(CH_3)]$ via 1,2-CH addition. The experimental study of the microscopic reverse, methane elimination from $[(^{t}Bu_3SiNH)_3Zr(CH_3)]$, reveals large intramolecular kinetic isotope effects and a negative entropy of activation pointing to an ordered transition state not dissimilar to that of the σ-bond metathesis with a characteristic alternation of charges as corroborated by computational studies.[85] Intricate kinetic and thermodynamic studies on this and related systems (*i.e.* $[(^{t}Bu_3SiO)_2Ti(NHSi^{t}Bu_3)R]$)[86,87] indicate that an unobserved methane adduct precedes the CH bond activation process. The stability of the alkane adduct is central to the understanding of selectivity issues. Related amido imido vanadium[88] and tungsten[89] complexes also activate methane via this α-CH

abstraction / 1,2-CH bond addition scheme.

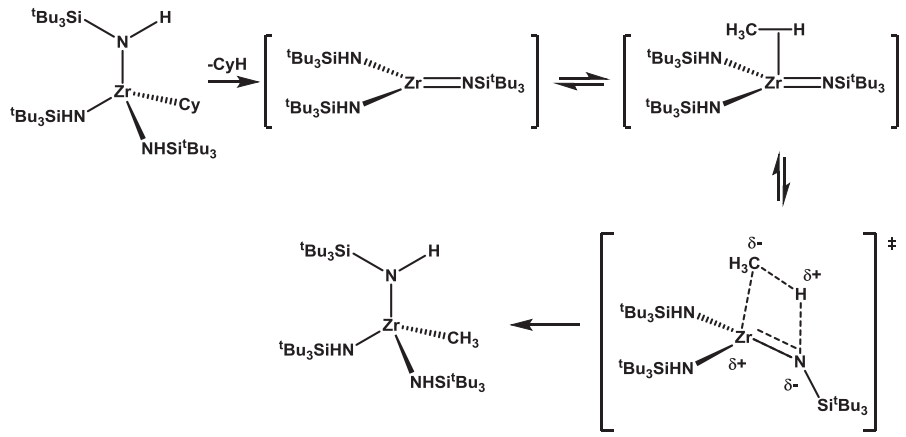

Scheme 1.23. *CH bond activation of methane by a zirconium imido intermediate.*

More recently, the α-CH abstraction / 1,2-CH bond addition has been extended to metal carbon triple bonds by Mindiola (Scheme 1.24).[90] A transient titanium alkylidyne compound [(PNP)Ti≡CR], generated by α-H abstraction of an alkane from an alkyl alkylidene complex [(PNP)Ti(=CH^{t}Bu)(CH$_2$^{t}Bu)], cleaves a CH bond of methane following a similar pathway. Remarkably [(PNP)Ti(=CH^{t}Bu)(CH$_3$)] extrudes methane very slowly at room temperature ($t_{1/2}$ = 62 h at 25°C). Just like in the zirconium case, there is a strong polarization of the Ti≡C bond involving a proton-like transfer in the TS.

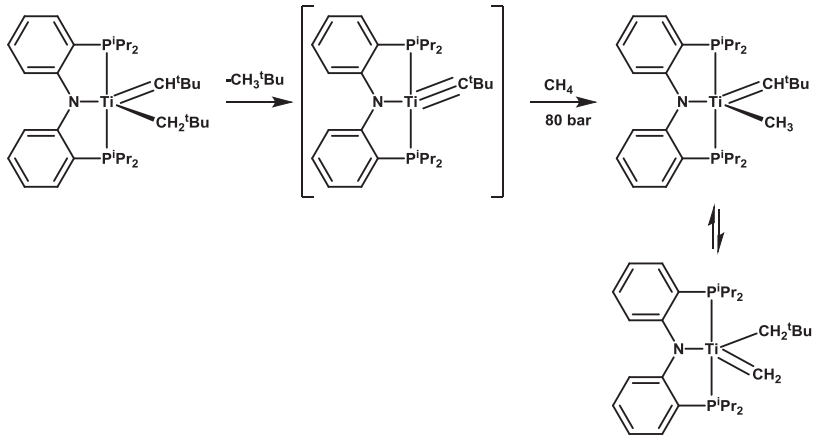

Scheme 1.24. *C–H bond activation of methane by a titanium alkylidyne intermediate.*

Isotopic labeling studies, including KIE experiments, show H/D exchange between the Ti–CH$_3$ and Ti=CH^{t}Bu positions. The dehydrogenation of CH$_4$ to methylidene is especially important because it could allow for the conversion of methane to an industrially important

reagent such as ethylene, via intermolecular "CH_2" coupling routes. As suggested in this study, therefore, 1,2-CH bond addition and tautomerization may constitute a plausible pathway for the dehydrogenation of methane, forming in the process a terminal titanium methylidene. Unsaturated metal alkylidenes had been known previously to activate CH bonds of other hydrocarbons[91–94] but this was the first example for methane activation.

1.2.3- 1,3-CH addition.

Compared to the numerous examples of reversible α-CH abstraction / 1,2-CH bond addition reactions, there are few examples of reversible β-CH abstraction / 1,3-CH bond addition from dialkyl complexes and only one describing the activation of methane. Erker first demonstrated that a relative stable [$Cp_2Zr(\eta^2$-benzyne)] intermediate, generated by reversible intramolecular β-H abstraction from diaryl zirconocenes, was able to cleave the CH bond of benzene by 1,3-addition.[95] However, activation of an alkane from a dialkyl precursor for example is less favorable. In most cases the intermediate η^2-alkene complex is not stable enough to allow CH bond activation in a subsequent step (Scheme 1.25). It is well known that [$Cp_2Zr(n\text{-}Bu)_2$] readily eliminates butane by β-H abstraction to yield the transient η^2-1-butene [$Cp_2Zr(\eta^2\text{-}CH{=}CHCH_2CH_3)$] for which a rich organic chemistry but no CH bond activation was developed.[96] Also alkyl groups bearing β-hydrogens may undergo the competitive deleterious β-H elimination yielding an alkene hydride complex (microscopic reverse of the migratory insertion) (Scheme 1.25).

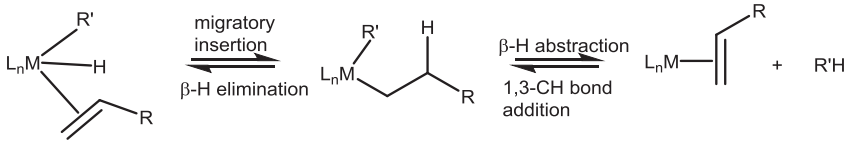

Scheme 1.25. *β-H abstraction and β-H elimination in alkyl complexes.*

The unique case of methane activation following this 1,3-CH bond addition pathway has been realized at a tungsten center in the group of Legzdins (Scheme 1.26).[97,98] The transient unsaturated (unobserved but trapped) η^2-diene d^2 complex [Cp*W(NO)(η^2-*trans*-1,3-butadiene)] was generated via CMe_4 elimination from the allyl neopentyl precursor [Cp*W(NO)(CH_2CMe_3)(η^3-$CH_2CHCHMe$)]. This complex could cleave the C–H bond of methane (70 bars), ethane (27 bars) and *n*-pentane at room temperature to afford the corresponding alkyl allyl complexes. The transient species was trapped with PMe_3 to form

[Cp*W(NO)(η^2-*trans*-1,3-butadiene)(PMe_3)]. Calculations suggested that CH bond activation involves an alkane σ-complex, followed by a metal-mediated H atom transfer to the diene.[98] Deuteration studies using *n*-C_5D_{12} ruled out the involvement of an η^2-allene [Cp*W(NO)(η^2-H_2C=C=CHMe)] as a possible intermediate for the C–H activation step (Scheme 1.26).[97]

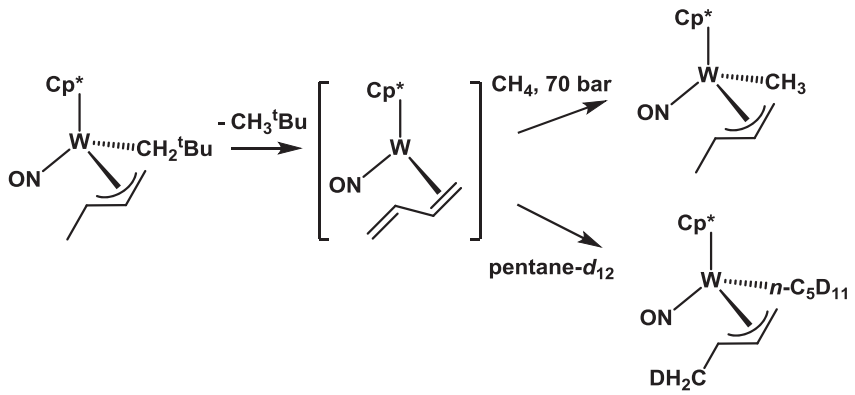

Scheme 1.26. *CH bond activation by the [Cp*W(NO)(η^2-butadiene)] intermediate.*

Our group has also proposed a similar 1,3-addition pathway for the CH bond activation of benzene and different alkylaromatics at a transient niobium η^2-cyclopropene intermediate [Tp^{Me2}Nb(*c*-C_3H_4)(MeCCMe)] (**A**), generated by β-H abstraction of methane from a methyl cyclopropyl Nb complex [Tp^{Me2}NbCH_3(*c*-C_3H_5) (MeCCMe)] (**1**) (Scheme 1.27).[99–101] This chemistry as well as our efforts to activate the CH bond of methane with the same intermediate that constitute the core of this PhD studies will be discussed in the next chapter.

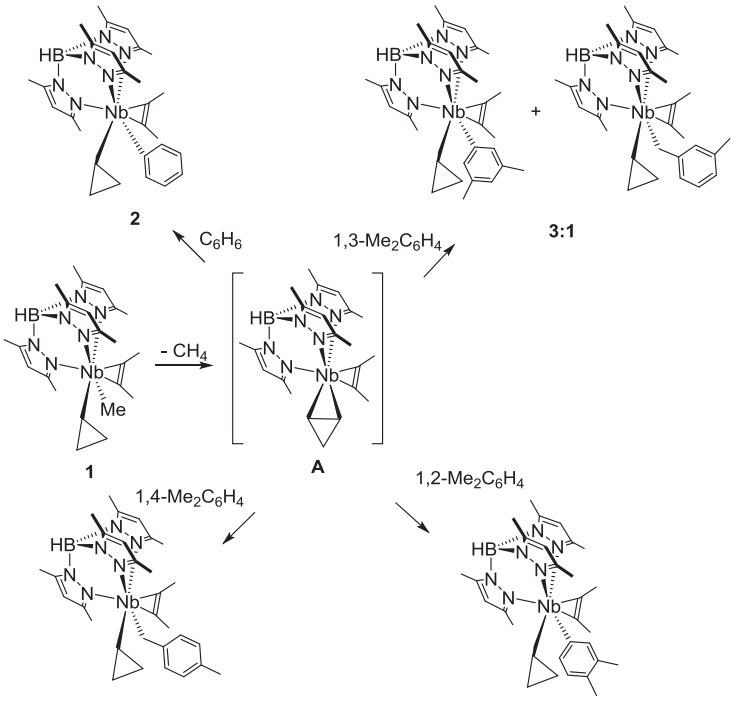

Scheme 1.25. *CH bond activation of benzene and different alkylaromatics by the transient intermediate [Tp^{Me2}Nb(c-C$_3$H$_4$)(MeCCMe)] (**A**).*

1.3- Conclusion and perspectives

Scientifically methane functionalization by soluble transition metal complexes remains a major challenge because of the need to combine two independent steps in one reaction: i) the cleavage of the CH bond and ii) the functionalization of the activated methane. Among all pathways discussed in the present chapter, only three has led to catalytic methane functionalization: i) the electrophilic route which involves homogeneous electrophilic complexes mainly based on Hg, Pt, Pd and V; ii) the carbene insertion, which involves highly electron poor perfluorinated scorpionate silver complexes and iii) the σ-bond metathesis at metallocene-alkyl complexes of scandium, by which the catalytic hydromethylation of propene and dehydrocoupling of diphenylsilane with methane were developed. The other pathways, on the other hand, namely i) the oxidative addition and metalloradical addition (ideally at low valent late transition metal centers), ii) the 1,2-CH bond addition across a M=X bond (M = High valent early transition metals complexes; X = C, NR, etc) and iii) the 1,3-CH bond addition across a M-η^2-alkene (M = high valent early transition metal complexes) have never been incorporated into a catalytic scheme for the functionalization of methane. Although these processes do not provide a catalytic functionalization, they realize the methane C–H bond cleavage, a central step toward the design of catalytic reactions.

In the following chapters, we will focus on the CH bond cleavage of methane and different unsaturated molecules by a transient η^2-cyclopropene complex of niobium by using a methodology based on the synergy between synthesis, characterization and mechanistic studies.

References

(1) NaturalGas.org. Overview of Natural Gas. http://www.naturalgas.org.

(2) Shale-gas europe. http://www.shalegas-europe.eu/en/index.php/resources.

(3) Caballero, A.; Pérez, P. J. *Chem. Soc. Rev.* **2013**, *42*, 8809.

(4) Schwarz, H. *Angew. Chem. Int. Ed.* **2011**, *50*, 10096–10115.

(5) Crabtree, R. H. *Chem. Rev.* **1995**, *95*, 987–1007.

(6) Cavaliere, V. N.; Mindiola, D. J. *Chem. Sci.* **2012**, *3*, 3356-3365.

(7) Berkowitz, J.; Greene, J. P.; Cho, H.; Ruscić, B. *J. Chem. Phys.* **1987**, *86*, 674–676.

(8) Chupka, W. A.; Berkowitz, J. *J. Chem. Phys.* **1971**, *54*, 4256–4259.

(9) Blanksby, S. J.; Ellison, G. B. *Acc. Chem. Res.* **2003**, *36*, 255–263.

(10) Merkx, M.; Kopp, D. A.; Sazinsky, M. H.; Blazyk, J. L.; Muller, J.; Lippard, S. J. *Angew. Chem. Int. Ed.* **2001**, *40*, 2782–2807.

(11) Basch, H.; Mogi, K.; Musaev, D. G.; Morokuma, K. J. Am. Chem. Soc. **1999**, *121*, 7249-7256.

(12) Hammond, C.; Conrad, S.; Hermans, I. *ChemSusChem* **2012**, *5*, 1668–1686.

(13) Hammond, C.; Forde, M. M.; Ab Rahim, M. H.; Thetford, A.; He, Q.; Jenkins, R. L.; Dimitratos, N.; Lopez-Sanchez, J. A.; Dummer, N. F.; Murphy, D. M.; Carley, A. F.; Taylor, S. H.; Willock, D. J.; Stangland, E. E.; Kang, J.; Hagen, H.; Kiely, C. J.; Hutchings, G. J. *Angew. Chem. Int. Ed.* **2012**, *51*, 5129–5133.

(14) Basset, J.; Coperet, C.; Soulivong, D.; Taoufik, M.; Cazat, J. T. *Acc. Chem. Res.* **2010**, *43*, 323–334.

(15) Soulivong, D.; Copéret, C.; Thivolle-Cazat, J.; Basset, J.-M.; Maunders, B. M.; Pardy, R. B. A.; Sunley, G. J. *Angew. Chem. Int. Ed.* **2004**, *116*, 5480–5483.

(16) Soulivong, D.; Norsic, S.; Taoufik, M.; Copéret, C.; Thivolle-Cazat, J.; Chakka, S.; Basset, J. M. *J. Am. Chem. Soc.* **2008**, *130*, 5044–5045.

(17) Hashiguchi, B. G.; Bischof, S. M.; Konnick, M. M.; Periana, R. A. *Acc. Chem. Res.* **2012**, *45*, 885–898.

(18) Periana, R. A.; Taube, D. J.; Gamble, S.; Taube, H.; Satoh, T.; Fujii, H. *Science* **1998**, *280*, 560–564.

(19) Webb, J. R.; Bolaño, T.; Gunnoe, T. B. *ChemSusChem* **2011**, *4*, 37–49.

(20) Shilov, A. E.; Shul'pin, G. B. *Chem. Rev.* **1997**, *97*, 2879–2932.

(21) Kirillova, M. V.; Kuznetsov, M. L.; Reis, P. M.; Da Silva, J. A. L.; Fraústo Da Silva, J. J. R.; Pombeiro, A. J. L. *J. Am. Chem. Soc.* **2007**, *129*, 10531–10545.

(22) Periana, R. A.; Mironov, O.; Taube, D.; Bhalla, G.; Jones, C. J. *Science* **2003**, *301*, 814–818.

(23) Janowicz, A. H.; Bergman, R. G. *J. Am. Chem. Soc.* **1982**, *104*, 352–354.

(24) Hoyano, J. K.; McMaster, A. D.; Graham, W. A. G. *J. Am. Chem. Soc.* **1983**, *105*, 7190–7191.

(25) Tilley, T. D.; Andersen, R. A.; Zalkin, A. *J. Am. Chem. Soc.* **1982**, *104*, 3723–3725.

(26) Bergman, R. G. *Science* **1984**, *223*, 902–908.

(27) Burger, P.; Bergman, R. G. *J. Am. Chem. Soc.* **1993**, *115*, 10462–10463.

(28) Bruce A. Arndtsen; Robert G. Bergman. Science **1995**, *270*, 1970–1973.

(29) Strout, D. L.; S., Z.; Niu, S.; Hall, M. B. *J. Am. Chem. Soc.* **1996**, *118*, 6068–6069.

(30) Jones, W. D.; Maguire, J. A. *Organometallics* **1986**, *5*, 590–591.

(31) Field, L.; George, A. V; Messerle, B. A. *J. Chem. Soc., Chem. Comm.* **1991**, 1339–1341.

(32) Harper, T. G. P.; Shinomoto, R. S.; Deming, M. A.; Flood, T. C. *J. Am. Chem. Soc.* **1988**, *110*, 7915–7916.

(33) Hartwig, J. F. *Chem. Soc. Rev.* **2011**, *40*, 1992–2002.

(34) Hall, C.; Perutz, R. N. *Chem. Rev.* **1996**, *96*, 3125–3146.

(35) Perutz, R. N.; Turner, J. J. *J. Am. Chem. Soc.* **1975**, *97*, 4791–4800.

(36) Cowan, A. J.; Portius, P.; Kawanami, H. K.; Jina, O. S.; Grills, D. C.; Sun, X. Z.; McMaster, J.; George, M. W. *Proc. Natl. Acad. Sci.* **2007**, *104*, 6933–6938.

(37) George, M. W.; Hall, M. B.; Jina, O. S.; Portius, P.; Sun, X. Z.; Towrie, M.; Wu, H.; Yang, X. Z.; D., Z. S. *Proc. Natl. Acad. Sci.* **2010**, *107*, 20178–20183.

(38) Song, J.; Hall, M. B. *Organometallics* **1993**, *12*, 3118–3126.

(39) Saillard, Y. I.; Hoffmann, R. *J. Am. Chem. Soc.* **1984**, *106*, 2006–2026.

(40) Koga, N.; Morokuma, K. *J. Phys. Chem.* **1990**, *94*, 5454–5462.

(41) Siegbahn, P. E. M.; Svensson, M. *J. Am. Chem. Soc.* **1994**, *116*, 10124–10128.

(42) Bullock, R. M.; Headford, C. E. L.; Hennessy, K. M.; Kegley, S. E.; Norton, J. R. *J. Am. Chem. Soc.* **1989**, *111*, 3897–3908.

(43) Parkin, G.; Bercaw, J. E. *Organometallics* **1989**, *8*, 1172–1179.

(44) Chernega, A.; Cook, J.; Green, M. L. H.; Labella, L.; Simpson, S. J.; Souter, J.; Stephens, A. H. H. *J. Chem. Soc., Dalton Trans.* **1997**, *4*, 3225–3244.

(45) Churchill, D. G.; Janak, K. E.; Wittenberg, J. S.; Parkin, G. *J. Am. Chem. Soc.* **2003**, *125*, 1403–1420.

(46) Northcutt, T. O.; Wick, D. D.; Vetter, A. J.; Jones, W. D. *J. Am. Chem. Soc.* **2001**, *123*, 7257–7270.

(47) Gould, G. L.; Heinekey, D. M. *J. Am. Chem. Soc.* **1989**, *111*, 5502–5504.

(48) Wang, C.; Ziller, J. W.; Flood, T. C.; Soc, T. C. J. A. C. *J. Am. Chem. Soc.* **1995**, *117*, 1647–1648.

(49) Stahl, S. S.; Labinger, J. A.; Bercaw, J. E. *J. Am. Chem. Soc.* **1996**, *118*, 5961–5976.

(50) Jones, W. D. *Acc. Chem. Res.* **2003**, *36*, 140–146.

(51) Jones, W. D.; Feher, F. J. *J. Am. Chem. Soc.* **1986**, *108*, 4814–4819.

(52) Ball, G. E.; Brookes, C. M.; Cowan, A. J.; Darwish, T. A.; George, M. W.; Kawanami, H. K.; Portius, P.; Rourke, J. P. *Proc. Natl. Acad. Sci.* **2007**, *104*, 6927–6932.

(53) Young, R. D.; Lawes, D. J.; Hill, A. F.; Ball, G. E. *J. Am. Chem. Soc.* **2012**, *134*, 8294–8297.

(54) Calladine, J. A.; Torres, O.; Anstey, M.; Ball, G. E.; Bergman, R. G.; Curley, J.; Duckett, S. B.; George, M. W.; Gilson, A. I.; Lawes, D. J.; Perutz, R. N.; Sun, X. Z.; Vollhardt, K. P. C. *Chem. Sci.* **2010**, *1*, 622-630.

(55) Torres, O.; Calladine, J. A.; Duckett, S. B.; George, M. W.; Perutz, R. N. *Chem. Sci.* **2014**, *6*, 418–424.

(56) Bernskoetter, W. H.; Schauer, C. K.; Goldberg, K. I.; Brookhart, M. *Science* **2009**, *326*, 553–556.

(57) Perutz, R. N.; Sabo-Etienne, S. *Angew. Chem. Int. Ed.* **2007**, *46*, 2578–2592.

(58) Webster, C. E.; Fan, Y.; Hall, M. B.; Kunz, D.; Hartwig, J. F. *J. Am. Chem. Soc.* **2003**, *125*, 858–859.

(59) Ng, S. M.; Lam, W. H.; Mak, C. C.; Tsang, C. W.; Jia, G.; Lin, Z.; Lau, C. P. *Organometallics* **2003**, *22*, 641–651.

(60) Lam, W. H.; Jia, G.; Lin, Z.; Lau, C. P.; Eisenstein, O. *Chem. - Eur. J.* **2003**, *9*, 2775–2782.

(61) Fuentes, M. Á.; Olmos, A.; Muñoz, B. K.; Jacob, K.; González-Núñez, M. E.; Mello, R.; Asensio, G.; Caballero, A.; Etienne, M.; Pérez, P. J. *Chem. - Eur. J.* **2014**, *20*, 11013–11018.

(62) Caballero, A.; Despagnet-Ayoub, E.; Díaz-Requejo, M. M.; Díaz-Rodríguez, A.; González-Núñez, M. E.; Mello, R.; Muñoz, B. K.; Ojo, W.-S.; Asensio, G.; Etienne, M.; Pérez, P. J. *Science* **2011**, *332*, 835–838.

(63) Sherry, A. E.; Wayland, B. B. *J. Am. Chem. Soc.* **1990**, *112*, 1259–1261.

(64) Wayland, B. B.; Ba, S.; Sherry, A. E. *J. Am. Chem. Soc.* **1991**, *113*, 5305–5311.

(65) Zhang, X.; Wayland, B. B. *J. Am. Chem. Soc.* **1994**, *116*, 7897–7898.

(66) Nelson, A. P.; DiMagno, S. G. *J. Am. Chem. Soc.* **2000**, *122*, 8569–8570.

(67) Cui, W.; Zhang, X. P.; Wayland, B. B. *J. Am. Chem. Soc.* **2003**, *125*, 4994–4995.

(68) Cui, W.; Wayland, B. B. *J. Am. Chem. Soc.* **2004**, *126*, 8266–8274.

(69) Zhang, X. X.; Wayland, B. B. *Inorg. Chem.* **2000**, *39*, 5318–5325.

(70) Watson, P. L. *J. Am. Chem. Soc.* **1983**, *105*, 6491–6493.

(71) Thompson, M. E.; Baxter, S. M.; Bulls, A. R.; Burger, B. J.; Nolan, M. C.; Santarsiero, B. D.; Schaefer, W. P.; Bercaw, J. E. *J. Am. Chem. Soc.* **1987**, *109*, 203–219.

(72) Fendrick, C. M.; Marks, T. J. *J. Am. Chem. Soc.* **1984**, *106*, 2214–2216.

(73) Barros, N.; Eisenstein, O.; Maron, L. *Dalton trans.* **2006**, 3052–3057.

(74) Lin, Z. *Coord. Chem. Rev.* **2007**, *251*, 2280–2291.

(75) Watson, L. A.; Yandulov, D. V; Caulton, K. G. *J. Am. Chem. Soc.* **2001**, *123*, 603–611.

(76) Lewin, J. L.; Woodrum, N. L.; Cramer, C. J. *Organometallics* **2003**, *22*, 1682–1689.

(77) Vastine, B. A.; Hall, M. B. *Coord. Chem. Rev.* **2009**, *253*, 1202–1218.

(78) Vastine, B. A.; Hall, M. B. *J. Am. Chem. Soc.* **2007**, *129*, 12068–12069.

(79) Sadow, A. D.; Tilley, T. D. *J. Am. Chem. Soc.* **2003**, *125*, 7971–7977.

(80) Fontaine, F. G.; Tilley, T. D. *Organometallics* **2005**, *24*, 4340–4342.

(81) Sadow, A. D.; Tilley, T. D. *Angew. Chem. Int. Ed.* **2003**, *42*, 803–805.

(82) Sadow, A. D.; Tilley, T. D. *J. Am. Chem. Soc.* **2005**, *127*, 643–656.

(83) Schaller, C. P.; Cummins, C. C.; Wolczanski, P. T. *J. Am. Chem. Soc.* **1996**, *118*, 591–611.

(84) Walsh, P. J.; Hollander, F. J.; Bergman, R. G. *J. Am. Chem. Soc.* **1988**, *110*, 8729–8731.

(85) Cundari, T. R.; Klinckman, T. R.; Wolczanski, P. T. *J. Am. Chem. Soc.* **2002**, *124*, 1481–1487.

(86) Schaller, C. P.; Bonanno, J. B.; Wolczanski, P. T. *J. Am. Chem. Soc.* **1994**, *116*, 4133–4134.

(87) Bennett, J. L.; Wolczanski, P. T. *J. Am. Chem. Soc.* **1997**, *119*, 10696–10719.

(88) With, J. D.; Horton, A. D. *Angew. Chem. Int. Ed.* **1993**, *32*, 903–905.

(89) Schafer, D. F. I.; Wolczanski, P. T. *J. Am. Chem. Soc.* **1998**, *120*, 4881–4882.

(90) Flores, J. A.; Cavaliere, V. N.; Buck, D.; Pintér, B.; Chen, G.; Crestani, M. G.; Baik, M. H.; Mindiola, D. J. *Chem. Sci.* **2011**, *2*, 1457–1462.

(91) Hickey, A. K.; Crestani, M. G.; Fout, A. R.; Gao, X.; Chen, C.H.; Mindiola, D. J. *Dalton Trans.* **2014**, *43*, 9834–9837.

(92) Bailey, B. C.; Fan, H.; Baum, E. W.; Huffman, J. C.; Baik, M. H.; Mindiola, D. J. *J. Am. Chem. Soc.* **2005**, *127*, 16016–16017.

(93) Cavaliere, V. N.; Crestani, M. G.; Pinter, B.; Pink, M.; Chen, C. H.; Baik, M. H.; Mindiola, D. J. *J. Am. Chem. Soc.* **2011**, *133*, 10700–10703.

(94) Crestani, M. G.; Hickey, A. K.; Gao, X.; Pinter, B.; Cavaliere, V. N.; Ito, J. I.; Chen, C. H.; Mindiola, D. J. *J. Am. Chem. Soc.* **2013**, *135*, 14754–14767.

(95) Erker, G. *J. Organometal. Chem.* **1977**, *134*, 189–202.

(96) Negishi, E.; Takahashi, T. *Acc. Chem. Res.* **1994**, *27*, 124–130.

(97) Tsang, J. Y. K.; Buschhaus, M. S. A.; Graham, P. M.; Semiao, C. J.; Semproni, S. P.; Kim, S. J.; Legzdins, P. *J. Am. Chem. Soc.* **2008**, *130*, 3652–3663.

(98) Baillie, R. A.; Man, R. W. Y.; Shree, M. V; Chow, C.; Thibault, M. E.; McNeil, W. S.; Legzdins, P. *Organometallics* **2011**, *30*, 6201–6217.

(99) Oulié, P.; Boulho, C.; Vendier, L.; Coppel, Y.; Etienne, M. *J. Am. Chem. Soc.* **2006**, *128*, 15962–15963.

(100) Boulho, C.; Oulie, P.; Vendier, L.; Etienne, M.; Pimienta, V.; Locati, A.; Bessac, F.; Maseras, F.; Pantazis, D. A.; McGrady, J. E. *J. Am. Chem. Soc.* **2010**, *132*, 14239–14250.

(101) Boulho, C.; Vendier, L.; Etienne, M.; Locati, A.; Maseras, F.; McGrady, J. E. *Organometallics* **2011**, *30*, 3999–4007.

Chapter 2

CH bond activation of methane by a transient η^2-cyclopropene niobium complex

Chapter 2: CH bond activation of methane by a transient η^2-cyclopropene niobium complex

2.1- Introduction

Previous studies performed in our group indicate that the niobium cyclopropyl complex [Tp^{Me2}NbMe(*c*-C_3H_5)(MeCCMe)] (**1**) is able to activate the CH bond of benzene by β-H abstraction /1,3-addition pathways (Scheme 2.1).[1,2] Complex **1** reacts smoothly at room temperature with benzene ($t_{1/2}$ *ca.* 7 h) to give [Tp^{Me2}NbPh(*c*-C_3H_5)(MeCCMe)] (**2**) and methane. Kinetic studies in cyclohexane-d_{12} shows that the reaction converting **1** to **2** is first order in **1** and zeroth order in benzene with a rate constant k_{obs} at 303 K of 2.93 ± 0.05 × 10^{-5} s^{-1}. Temperature-dependent studies (303-323 K) lead to activation parameters $\Delta H^{\ddagger}$= 99 ± 5 kJ/mol and $\Delta S^{\ddagger}$=-6 ± 10 J/K.mol. Reaction of **1** with C_6D_6 instead of C_6H_6 gives an insignificant isotope effect providing a ratio k_H/k_D of 1.0 at 303 K. These data support that the rate-determining step is an intramolecular abstraction of a β-H of the cyclopropyl group to form methane, yielding the transient unsaturated η^2-cyclopropene / metallacyclobutane intermediate [Tp^{Me2}Nb(η^2-*c*-C_3H_4)(MeCCMe)] **A**. This is followed by the 1,3-CH bond addition of benzene to afford **2**. DFT computational studies confirm that the formation of **A** passes through a four-center transition state (**1-TS**) exhibiting an almost linear C…H…C arrangement (CHC angles > 166°) with the hydrogen positioned symmetrically between the two carbon centers (Scheme 2.1). This structural rearrangement is very similar to those described by Legzdins[3] and is reminiscent of σ-bond metathesis processes.[4]

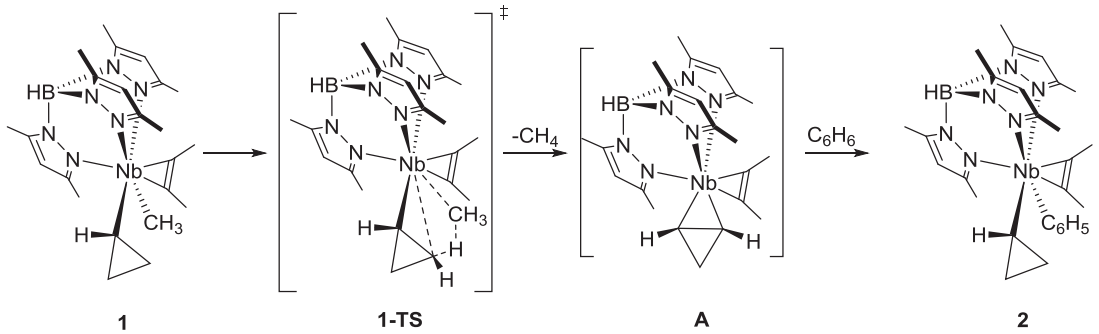

Scheme 2.1. *CH bond activation of benzene by a transient η^2-cyclopropene niobium/niobiacyclobutane complex [Tp^{Me2}Nb(η^2-c-C_3H_4)(MeCCMe)] (**A**).*

Kinetic experimental data for the activation of benzene by **1** (**1**→**2** via intermediate **A**) have been acquired by ^{1}H NMR and analyzed by numerical simulation. Three separate experiments adding 2, 6, and 31 equiv of benzene to solutions of **1** in cyclohexane-d_{12} at 323 K were carried out. The concentrations of **1** and **2** as determined by integration of key ^{1}H NMR signals were plotted as a function of time. The kinetic model shown in Scheme 2.2 was used to simultaneously fit the data. It involves four distinct processes and it indicates that the 1,3-CH bond activation of methane or benzene by the intermediate **A** are bimolecular reactions with first order in **A** and first order in methane or benzene, respectively. At 323 K, the rate constant k_2 for the reaction of **A** with benzene is shown to be *ca* 3 times that for the reaction of **A** with methane (k_{-1}) (Scheme 2.2). Therefore, **A** reacts ca 3 times faster with benzene than with methane itself at 323 K, which implies the possibility of the activation of methane by the intermediate **A**.

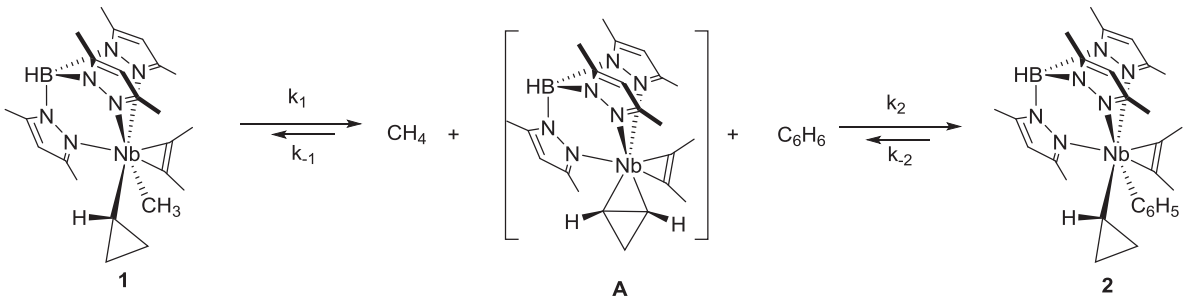

Scheme 2.2. *Reaction of **A** with methane and benzene.*

As shown by ^{1}H, ^{2}H, and ^{13}C NMR spectroscopy, reaction of **1** with C_6D_6 gives two diastereomers with a selective insertion of a single deuterium at either of the two Cβ positions on the same enantioface of the cyclopropyl ring as niobium, in a *ca* 2:1 ratio. This conclusively establishes that **A** is an unsaturated η^2-cyclopropene complex generated from **1** by a β-H or 1,3-abstraction of CH_4. A CH/CD bond of C_6H_6/C_6D_6 then rapidly adds the Nb–C bond of **A** in a stereospecific 1,3-fashion (Scheme 2.3) to give two diastereomers in 2:1 ratio. Competition reaction of **1** with an excess of a 1:1 molar mixture of benzene and benzene-d_6 at 310 K to form **2** and **2-*d*$_6$** affords an isotope effect (k_H/k_D) of 4.0, reflecting a C–H/C–D bond cleavage event, with significant weakening of the bonds in the transition state from **A** to **2**.

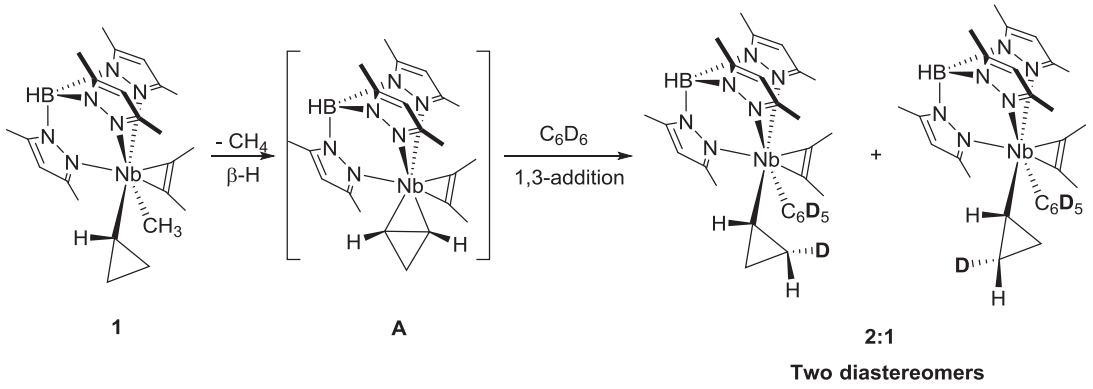

Scheme2.3. *C–D bond activation of benzene-d_6 by **A**.*

The η^2-cyclopropene species **A**, [Tp^{Me2}Nb(η^2-*c*-C_3H_4)(MeCCMe)] is trapped by mixing **1** with an excess of pyridine, resulting in the air-sensitive η^2-cyclopropene pyridine complex [Tp^{Me2}Nb(*c*-C_3H_4)(NC_5H_5)(MeCCMe)] (Scheme 2.4).[1] This species is a formally $18e^-$ niobium(I) complex. It is significant that no C–H bond of heteroaromatic pyridine is activated under these conditions.

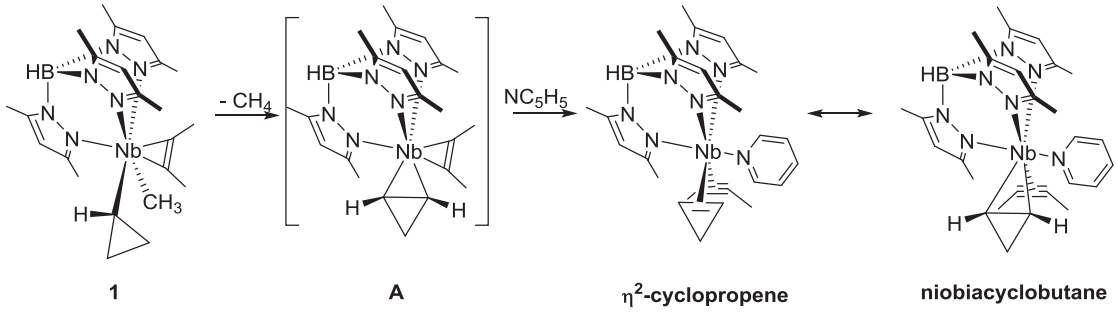

Scheme 2.4. *Trapping of the η^2-cyclopropene species **A**, [Tp^{Me2}Nb(η^2-c-C_3H_4)(MeCCMe)], with pyridine.*

2.2- Objectives of this work

Inspired by the work cited above, we aimed to see whether **1** was capable to activate the inert CH bond of methane in a similar way as benzene. The mechanistic pathway was first detected by isotopic labelling experiments using $^{13}CH_4$ and CD_4 to see whether **1** could react with $^{13}CH_4$ and CD_4 to form **1-$^{13}CH_3$** and **1-d_4**, respectively (Scheme 2.5). A kinetic study of the degenerate exchange between **1** and $^{12}CH_4$ through spin saturation transfer experiments (SST) was carried out to study the elementary steps. Kinetic studies of the reaction between [Tp^{Me2}Nb(CH_2-3,5-$Me_2C_6H_3$)(*c*-C_3H_5)(MeCCMe)] (**3**) and $^{12}CH_4$ revealed that the β-H

abstraction is the rate-determining step (RDS), providing rate constants and activation parameters which reflect the structure of the transition state in the RDS.DFT calculations, carried out by professor Michel Etienne, were used to compute the energy of key intermediates and transition states for the CH bond elimination/activation of methane. The mechanism was compared with the σ-bond metathesis and the α-H abstraction/1,2-addition mechanisms.

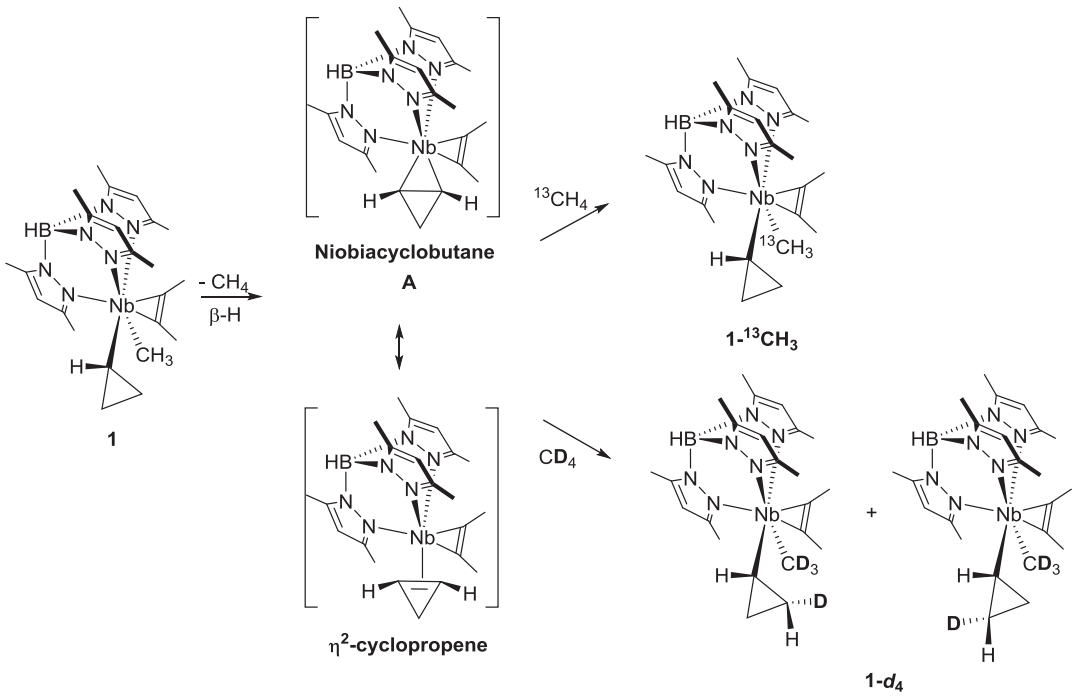

Scheme 2.5. *CH bond activation of methane by a transient η^2-cyclopropene Nb intermediate **A**.*

2.3-Degenerate reaction of 1 with $^{13}CH_4$ and CD_4

2.3.1-Degenerate reaction of 1 with $^{13}CH_4$

Initially a medium pressure J-Young NMR tube was charged with compound **1** (0.030 g, 0.060 mmol) in cyclohexane-d_{12} (0.5 mL) and was pressurized with $^{13}CH_4$ to *ca* 3 bar at 173 K (ethanol/liquid N_2 bath) for 1 min. The tube was then placed in the ^{1}H NMR spectrometer with the probe set at 313 K. 1.2 equivalents of $^{13}CH_4$ could be quantified in solution by integration of the $^{13}CH_4$ signal (δ 0.19 (d, $^1J_{CH}$ = 125.0 Hz)) compared to the $Tp^{Me2}CH$ signal of complex **1**. The reaction was subsequently monitored by ^{1}H NMR over 19 hours, displaying the activation of $^{13}CH_4$ by **1** to form [$Tp^{Me2}Nb^{13}CH_3$(*c*-C_3H_5)(MeCCMe)] **1-$^{13}CH_3$**. Within 5 hours the ^{1}H NMR spectrum showed the appearance and the growth of the

Nb^{13}CH_3 resonance as a doublet centered at δ 0.766 ppm with $^1J_{CH}$ = 119.6 Hz (Figure 2.2(a)). This signal was superimposed with the singlet at δ 0.779 ppm corresponding to the Nb^{12}CH_3 group in **1** (Figure 2.2(a)). The ^{13}C NMR spectrum showed the appearance and the growth of the Nb^{13}CH_3 resonance at δ 48.90 ppm (Figure 2.2(b)).

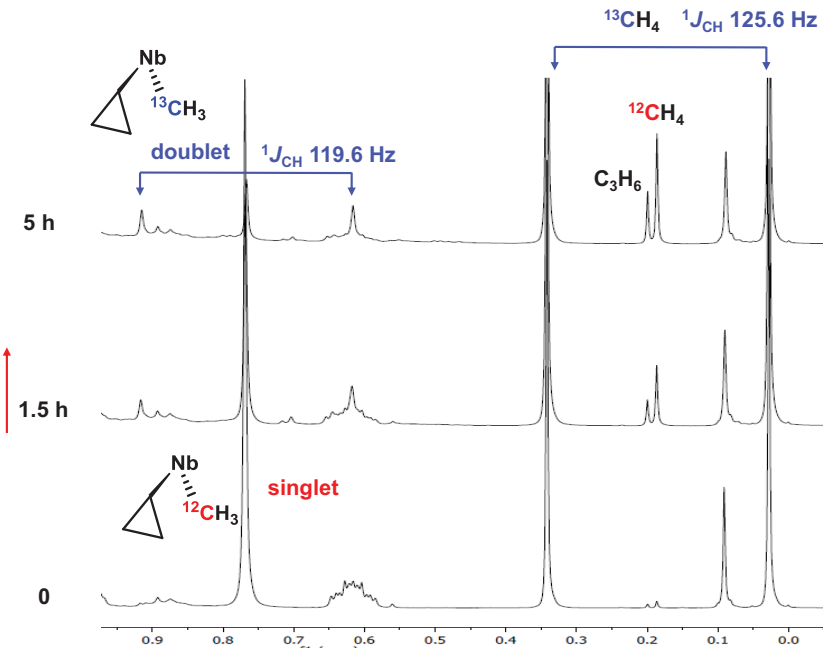

Figure 2.2(a). *^{1}H NMR spectrum of the reaction of **1** with $^{13}CH_4$ to give **1-$^{13}CH_3$**.*

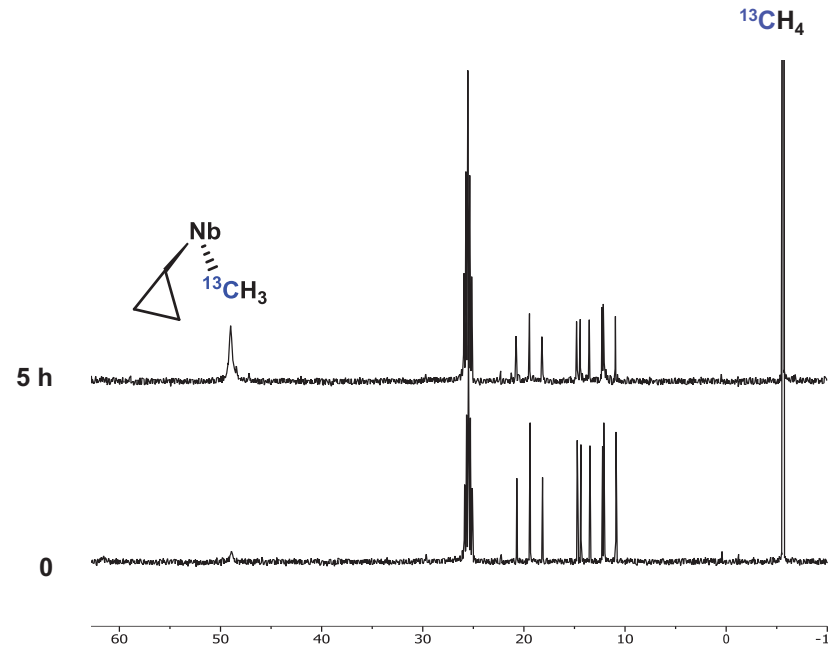

Figure 2.2(b). *^{13}C NMR spectrum of the reaction of **1** with $^{13}CH_4$ to give **1-$^{13}CH_3$**.*

This preliminary experiment establishes the presence of an equilibrium between **1** and **1-^{13}CH$_3$** (Scheme 2.6), confirming that intermediate **A** readily reacts with methane.

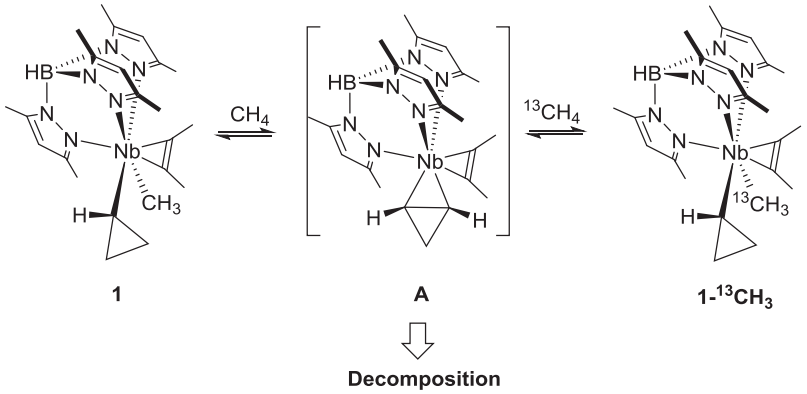

Scheme 2.6. *Reaction of* ***1*** *with* $^{13}CH_4$ *to give* ***1-^{13}CH$_3$****.*

For longer reaction times, however, decomposition of **1** and **1-^{13}CH$_3$** was observed from the decrease of the Nb^{12}C*H*$_3$ and Nb^{13}CH$_3$ signals. The pressure of $^{13}CH_4$ is not high enough to prevent the decomposition of the intermediate **A**,[1] precluding a kinetic analysis of the reaction.

2.3.2-Degenerate reaction of 1 with CD_4

2.3.2.1- Characterization of [Tp^{Me2}NbMe(c-C$_3$H$_5$)(MeCCMe)] by ^{1}H ROESY NMR

In order to assess the stereochemical outcome of the formation of **1-d$_4$** (Scheme 2.5), we carried out a ^{1}H ROESY NMR experiment of **1**, allowing the assignment of all diastereotopic protons of the cyclopropyl group in **1** (Chart 2.1). The interpretation of the ^{1}H ROESY NMR spectrum of **1** follows that of [Tp^{Me2}NbPh(*c*-C$_3$H$_5$)(MeC≡CMe)],[2] where the 2-butyne stays in the pseudo-symmetry plane of the complex, virtually parallel to the *trans* 3,5-dimethylpyrazolyl ring, a structural characteristic of all [Tp^{Me2}NbXX'(MeC≡CMe)] complexes. The methyl protons of the 2-butyne ligand that are distal to Tp^{Me2} are deshielded (δ 2.92), whereas those proximal to Tp^{Me2} are shielded (δ 2.24). At 283 K, they exchange very slowly in cyclohexane-d_{12} (Chart 2.1, Figure 2.3 (a)). In the ROESY spectrum, correlation between the distal methyl protons and H$_7$, one of β-hydrogen of the cyclopropyl group, is clearly observed and serves to build the other ROESY correlations (Chart 2.1, Figure 2.3(b)).

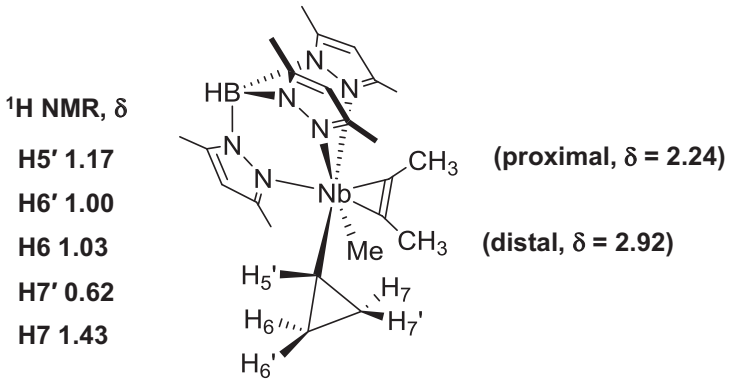

Chart 2.1. *Diastereotopic protons of the cyclopropyl group in* ***1****.*

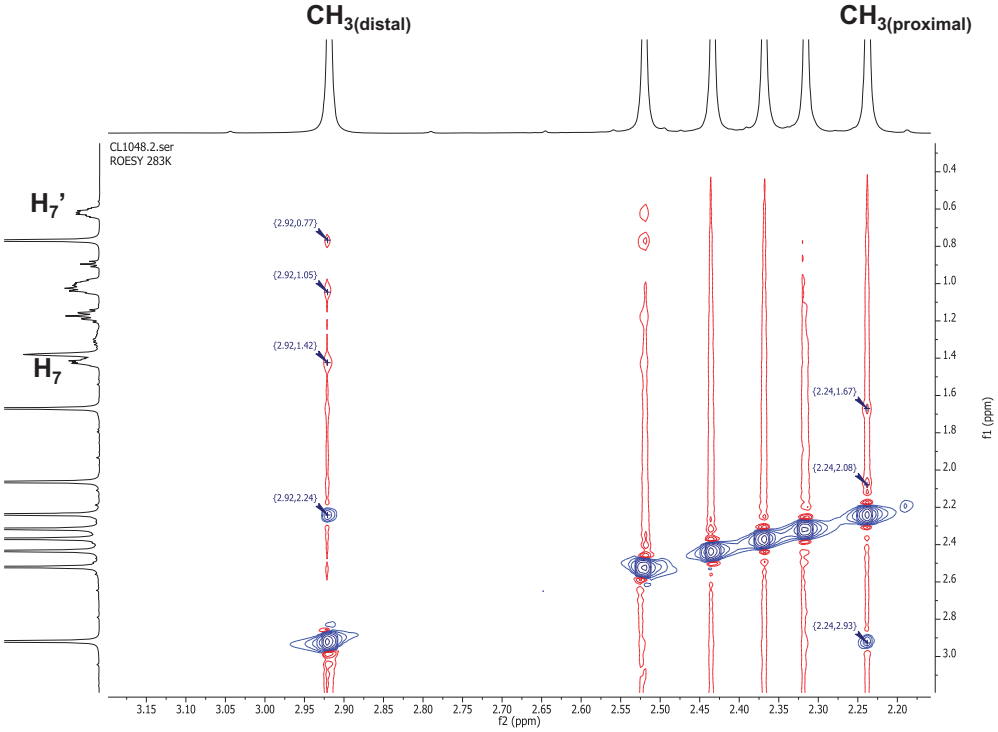

Figure 2.3(a). *^{1}H ROESY NMR spectrum of* ***1****, showing the ROESY correlation for distal and proximal protons.*

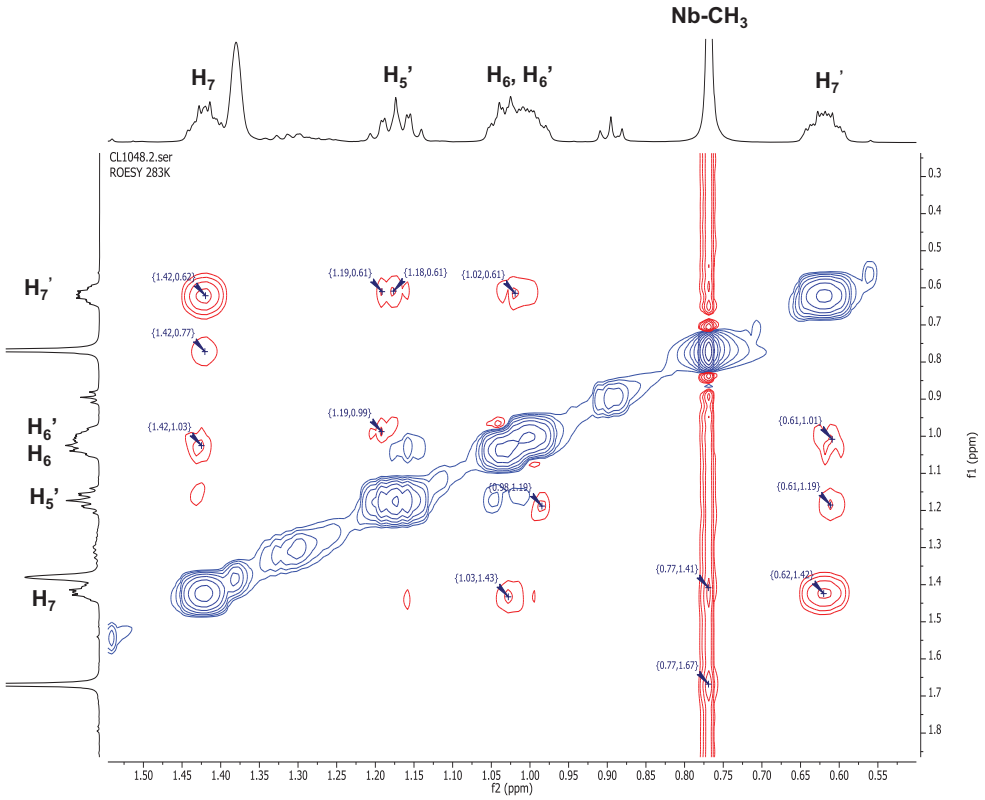

Figure 2.3(b). *^{1}H ROESY NMR spectrum of **1** (expansion plot).*

2.3.2.2-C–D Bond Activation of CD_4 by 1.

A medium pressure J-Young NMR tube was charged with compound **1** (0.030 g, 0.060 mmol) in perfluorobenzene (0.5 mL) and was pressurized with CD_4 to *ca* 8 bar at 157 K (ethanol/liquid N_2 bath) for 3 mins. The tube was then placed in the ^{1}H NMR spectrometer with the probe set at 303 K. At this temperature the pressure of CD_4 in the tube was ca. 16 bar. The reaction was subsequently monitored by ^{1}H NMR and ^{2}H{^{1}H} NMR for 4 hours at 303 K in a 600 MHz NMR spectrometer equipped with a cryoprobe. Comparison of ^{1}H and ^{2}H{^{1}H} NMR spectra showed the formation of two diastereomers of [Tp^{Me2}NbCD$_3$(c-C$_3$H$_4$D)(MeCCMe)] **1-d$_4$** in a 3:1 ratio, displaying, in addition to a Nb–CD$_3$ group, the D atom either in position 7 or 6 of the cyclopropyl ring, respectively. Interestingly, the β-positions D6 and D7 are on the same enantioface of the cyclopropyl group as the niobium (Figure 2.4). No deuterated solvent (*i.e.* cyclohexane-d_{12}) was added to the sample to lock the spectrometer, in order to avoid (i) overlap of the cyclopropyl deuterated signals by the deuterated solvent, (ii) saturating the ^{2}H NMR spectrum or (iii) reaction with adventitious CH/D bonds (ie benzene-d_6). Therefore the chemical shifts of the signals in Figure 2.4 had no formal reference and the CD_4 resonance was arbitrarily set at δ – 0.13. The C_6F_6 is a suitable solvent to follow the reaction: it is inert to complex **1** and to intermediate **A** as there is no C–F

bond activation when monitoring the thermolysis of **1** in C_6F_6. These results confirm that **A** is generated by a rate-determining intramolecular abstraction of a β-H of the cyclopropyl group by the niobium bound methyl group to form methane from **1**, which is followed by its microscopic reverse, a stereospecific 1,3-CH/D bond addition of CH_4/CD_4 across a Nb–C bond of the Nb(η^2-*c*-C_3H_4) compound (Figure 2.4). **A** is known to activate benzene/benzene-d_6 in a similar manner but the ratio of the two phenyl cyclopropyl diastereomers was *ca* 2:1 in similar experimental circumstances.[1]

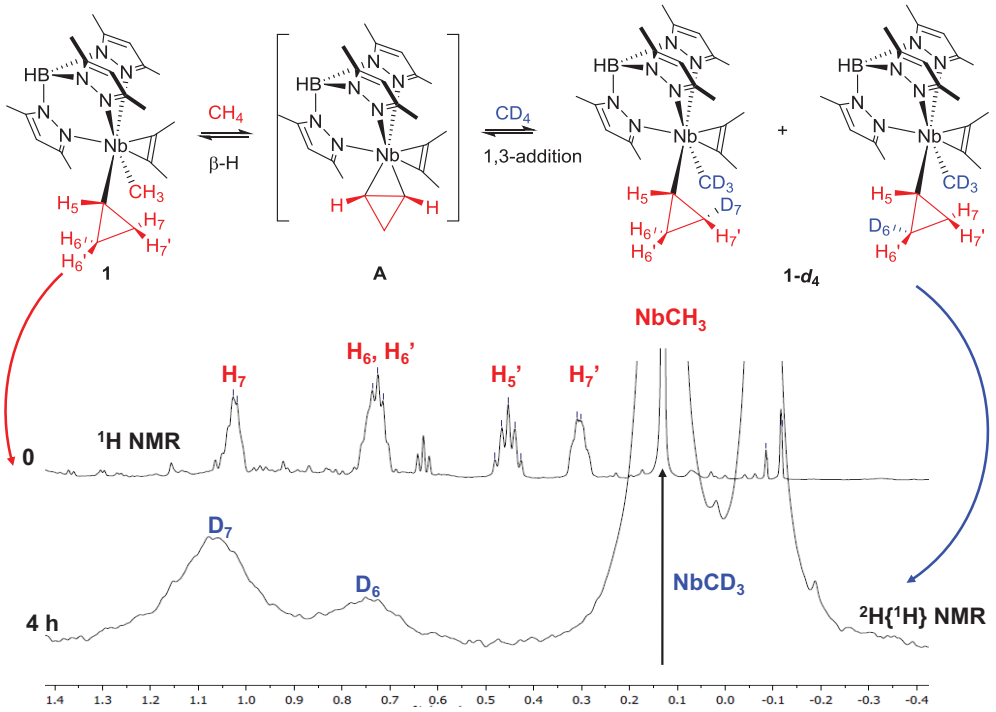

Figure 2.4. *Superimposed ^1H and $^2H\{^1H\}$ NMR spectra for the reaction of **1** with CD_4 to form **1-d$_4$**.*

2.4- CH bond activation of $^{12}CH_4$ by 1 (SST)

In order to investigate how methane undergoes elimination/addition more quantitatively, we next focused on the reaction of **1** with methane ($^{12}CH_4$) by spin saturation transfer (SST) experiments.

Scheme 2.7(a) shows the degenerate reaction of **1** with methane, whereas Scheme 2.7(b) shows the elementary steps. The forward reaction (rate constant k_1) is the unimolecular methane elimination that yields **A** and methane as shown previously. The reverse reaction (rate constant k_{-1}) is the bimolecular reaction of **A** with methane that yields **1**, the CH bond activation of methane.

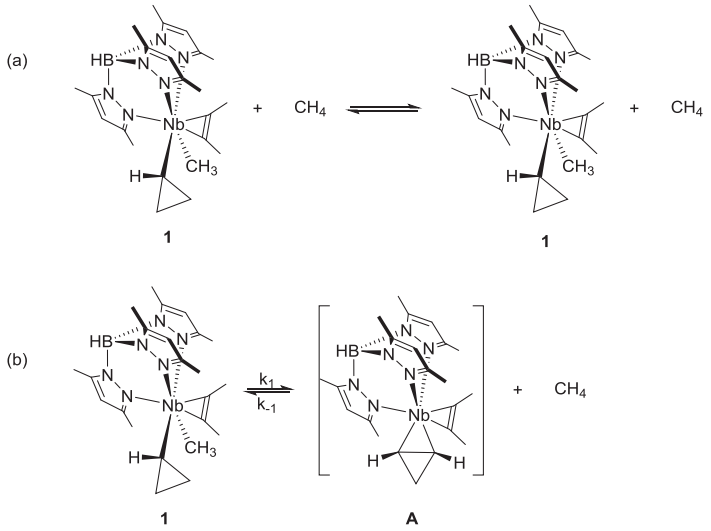

Scheme 2.7. *Degenerate reaction of **1** with methane (a) and its elementary steps (b).*

2.4.1- Mechanism of spin saturation transfer (SST) experiments

A summary of the SST experiments including data acquisition and kinetic treatment could be found in the literature.[5] The two sites exchange kinetics for the reaction of **1** with methane ($^{12}CH_4$) is shown in Scheme 2.8, where [NbMe], [NbMe*], [CH_4] and [CH_4*] are the lower and upper nuclear spin-state populations of the methyl group of **1** and of methane, respectively. $M_{(NbMe)}$ = [NbMe] – [NbMe*] and M_{CH4} = [CH_4] – [CH_4*] are the net magnetizations of the methyl group of **1** and methane, respectively. **A** is the η^2-cyclopropene intermediate and C_A is its concentration. $T_{1[NbMe]}$ and $T_{1[CH4]}$ are the spin-lattice relaxation times for the methyl group of **1** and methane, respectively. k_1 is the first order rate constant for the transformation of **1** to **A** and methane, assuming a dissociative mechanism as shown previously.[1] k_{-1} is the second order rate constant for the reverse bimolecular reaction.

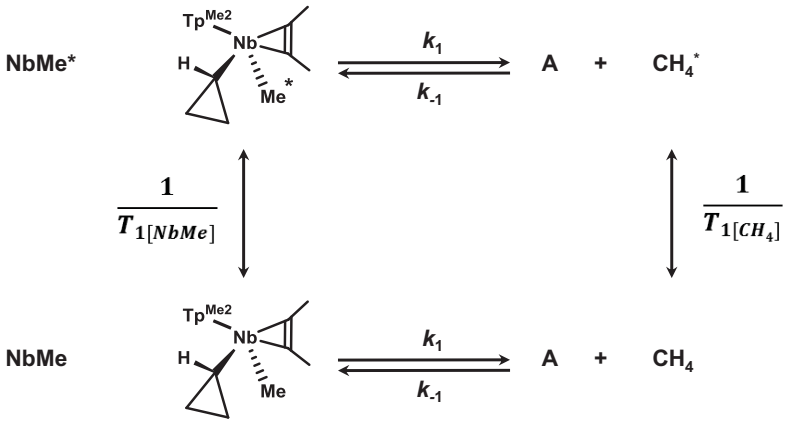

Scheme 2.8. *The two sites exchange kinetics for the reaction of **1** with methane.*

The rate equations for the lower and upper spin-state populations are considered first in the absence of spin-lattice relaxations as given in equations 2.1 and 2.2.

$$\frac{d[\mathrm{NbMe}]}{dt} = -k_1[\mathrm{NbMe}] + k_{-1}\mathrm{C_A}[\mathrm{CH_4}] = -\frac{d[\mathrm{CH_4}]}{dt} \quad (2.1)$$

$$\frac{d[\mathrm{NbMe^*}]}{dt} = -k_1[\mathrm{NbMe^*}] + k_{-1}\mathrm{C_A}[\mathrm{CH_4}^*] = -\frac{d[\mathrm{CH_4}^*]}{dt} \quad (2.2)$$

Moreover, spin-lattice relaxation processes that keep spin-state populations in thermal equilibrium are considered in the absence of chemical exchange as expressed in equations 2.3 and 2.4.

$$\frac{dM_{(\mathrm{NbMe})}}{dt} = \frac{M_{0(\mathrm{NbMe})} - M_{(\mathrm{NbMe})}}{T_{1(\mathrm{NbMe})}} \quad (2.3)$$

$$\frac{dM_{(\mathrm{CH4})}}{dt} = \frac{M_{0(\mathrm{CH4})} - M_{(\mathrm{CH4})}}{T_{1(\mathrm{CH4})}} \quad (2.4)$$

The rate equations for the net magnetization in the presence of both the chemical exchange and spin-lattice relaxation are given in equations 2.5 and 2.6.

$$\frac{dM_{(\mathrm{NbMe})}}{dt} = -k_1 M_{(\mathrm{NbMe})} + k_{-1}\mathrm{C_A} M_{(\mathrm{CH4})} + \frac{M_{0(\mathrm{NbMe})} - M_{(\mathrm{NbMe})}}{T_{1(\mathrm{NbMe})}} \quad (2.5)$$

$$\frac{dM_{(\mathrm{CH4})}}{dt} = k_1 M_{(\mathrm{NbMe})} - k_{-1}\mathrm{C_A} M_{(\mathrm{CH4})} + \frac{M_{0(\mathrm{CH4})} - M_{(\mathrm{CH4})}}{T_{1(\mathrm{CH4})}} \quad (2.6)$$

When the peak of methane is saturated by a low power CW irradiation during a time $\tau_{sat} \geq 5T_{1(CH4)}$ making the upper and lower spin state populations of methane equal, that is $M_{sat(CH4)} = [CH_4] - [CH_4^*] = 0$, the saturated spin population is transferred to the methyl group of **1** via chemical exchange, resulting in partial loss of the net magnetization of the methyl group of **1** from its thermal equilibrium value, $M_{0(NbMe)}$, observed in the absence of saturation. The exchange between the saturated signal of CH_4 and the methyl group of **1** is therefore characterized by a decrease of the signal of the methyl group of **1**. If CH_4 is irradiated in such a way that $M_{sat(CH4)} = 0$ and that a steady state is reached for $M_{sat(NbMe)}$ ($dM_{sat(NbMe)}/dt = 0$) , applying these conditions to equation 2.5 gives equation 2.7, from which the value of k_1 can be derived from equation 2.8:

$$-k_1 M_{\mathrm{sat(NbMe)}} + \frac{M_{0(\mathrm{NbMe})} - M_{\mathrm{sat(NbMe)}}}{T_{1(\mathrm{NbMe})}} = 0 \quad (2.7)$$

$$k_1 = \frac{1}{T_{1(\mathrm{NbMe})}} \left(\frac{M_{0(\mathrm{NbMe})}}{M_{\mathrm{sat(NbMe)}}} - 1\right) \quad (2.8)$$

Vice versa, when the peak of the methyl group of **1** is saturated by a low power CW irradiation during a time $\tau_{sat} \geq 5T_{1(\mathrm{NbMe})}$ making the upper and lower spin state populations of the methyl group of **1** equal, that is $M_{sat(NbMe)}$= [NbMe] – [NbMe*] = 0, the saturated spin population is transferred to methane via chemical exchange, resulting in partial loss of the net magnetization of methane from its thermal equilibrium value, $M_{0(CH4)}$, observed in the absence of saturation. Once again, if NbMe is irradiated in such a way that $M_{sat(NbMe)} = 0$ and that a steady state is reached for $M_{sat(CH4)}$ ($dM_{sat(CH4)}/dt = 0$) applying these conditions to equation 2.6 gives equation 2.9, from which the value of k_1 can be derived from equation 2.10:

$$-k_{-1} C_A M_{\mathrm{sat(CH4)}} + \frac{M_{0(\mathrm{CH4})} - M_{\mathrm{sat(CH4)}}}{T_{1(\mathrm{CH4})}} = 0 \quad (2.9)$$

$$k_{-1obs} = k_{-1} C_A = \frac{1}{T_{1(\mathrm{CH4})}} \left(\frac{M_{0(\mathrm{CH4})}}{M_{\mathrm{sat(CH4)}}} - 1\right) \quad (2.10)$$

It must be noted here that this requires the assumption that C_A is constant. This is fully reasonable since **A** is a very reactive intermediate implying that a steady state approximation can be applied.

The SST experiments were carried out at high and medium CH_4 pressure, on Bruker Avance 400 and 500 spectrometers, respectively.

2.4.2- SST experiments of 1 with medium pressure $^{12}CH_4$

A medium pressure J-Young NMR tube was charged with compound **1** (0.030 g, 0.060 mmol) in C_6F_6 (0.5 mL, with one drop of cyclohexane-d_{12} for the lock of the spectrometer) and was pressurized with $^{12}CH_4$ to *ca* 6 bar at 213 K for 3 mins. The tube was then placed in the ^{1}H NMR spectrometer with the probe set at 341 K. The reaction was subsequently monitored by ^{1}H NMR in a 500 MHz NMR spectrometer. 4 equivalents of $^{12}CH_4$ could be quantified in solution by integration of the $^{12}CH_4$ signal at δ 0.14 compared to the $Tp^{Me2}CH$

signal of complex **1**. Saturation of the $NbCH_3$ resonance at δ 0.59 was followed by observation of the CH_4 resonance at δ 0.14 after the probe pulse. Integration of the CH_4 resonance before and after the saturation revealed a *ca* 10% decrease (Figure 2.5). However, a closer look at the ^1H NMR spectrum revealed significant decomposition of **1** at the temperature and CH_4 pressure used. Under these conditions, the decomposition process precluded the accurate measurement of the corresponding rate constant because decomposition of **A** is competitive with its reaction with CH_4.

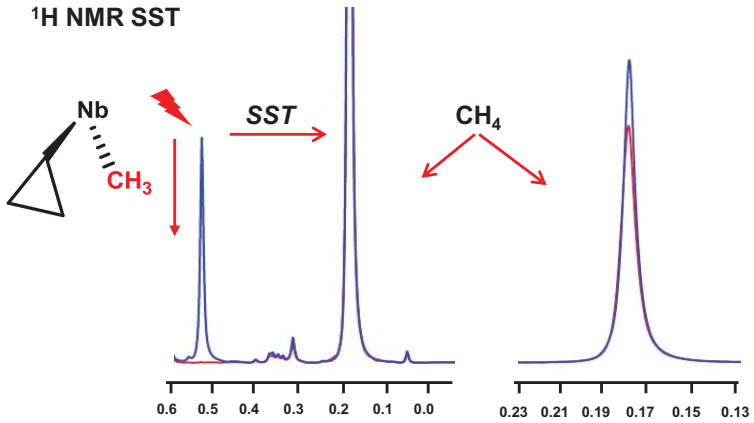

Figure 2.5. *Irradiation of the Nb-CH_3 signal and decrease of the CH_4 peak intensity (10%) after Spin Saturation Transfer.*

2.4.3- SST experiments of 1 with high pressure of $^{12}CH_4$

In order to favor the bimolecular reaction of methane with **A** with respect to its decomposition and to get quantitative results, we resorted to high pressure HP NMR techniques (400 MHz instrument). **1** (0.100 g, 0.200 mmol) was charged in a 1 cm (outside diameter) sapphire HP NMR tube and dissolved in a 1:1 mixture of C_6F_6/cyclohexane-d_{12} (2 mL). The HP NMR tube was then pressurized with methane at *ca* 60 bar at room temperature and carefully shaken to ensure homogeneous methane dissolution. The SST study was carried out in a 400 MHz NMR spectrometer at 351 K with a $[CH_4]$:[**1**] ratio of 29. Saturation of the $NbCH_3$ resonance at δ 0.59 was followed by observation of the CH_4 resonance at δ 0.14 (Figure 2.6). Integration of the CH_4 resonance before and after the saturation revealed a 12% decrease which translated to a rate constant $k_{-1obs} = k_{-1}C_A = (2.67 \pm 0.23) \times 10^{-2}$ s^{-1}, using equation 2.10.

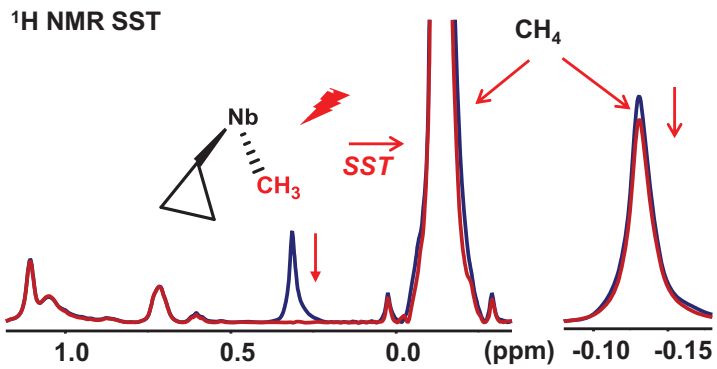

Figure 2.6. *Irradiation of the Nb-CH_3 signal and decrease of the CH_4 peak intensity (11%), after Spin Saturation Transfer.*

However, when the methane signal at δ 0.14 was saturated, insignificant changes in the intensity of the niobium bound methyl signal at δ 0.59 in **1** were noted (Figure 2.7).

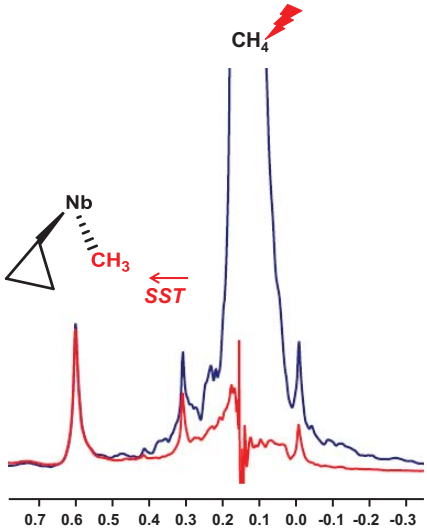

Figure 2.7. *Irradiation of the CH_4 (δ 0.18 ppm) signal and barely decrease of the Nb-CH_3 peak intensity after Spin Saturation Transfer.*

These SST experiments could best be accounted for with the help of the kinetic scheme described in Scheme 2.7(b). The reverse reaction (rate constant k_{-1}) is the bimolecular reaction of **A** with methane that yields **1**, the CH bond activation of methane, and k_{-1obs} equals to $k_{-1}C_A$, assuming that the reactive intermediate **A** is in a steady-state concentration. Unfortunately, this does not allow us to discuss the ability of **A** to activate methane since we cannot determine k_{-1} here, simply knowing k_{-1obs}. The failure to observe an intensity change of the $NbCH_3$ resonance when saturating the methane resonance unfortunately precluded the

measurement of k_1 through the SST experiment. This can be ascribed to the difference in relaxation times T_1 for the protons of the niobium bound methyl group [$T_1(NbCH_3)$ =1.34 s] and those of methane [$T_1(CH_4)$ =4.95 s] with respect to the actual rate constant k_1. From the activation parameters previously determined for the β-H intramolecular abstraction of methane from **1** ($\Delta H^{\dagger}$= 99 ± 5 kJ/mol and $\Delta S^{\dagger}$= -6 ±10 J/K·mol),[1] we can calculate a $\Delta G^{\dagger}$ value of 101 kJ·mol^{-1}at 351 K which corresponds to a k_1 value of 6.6×10^{-3} s^{-1}. In that case, only a variation of less than 1 % of the $NbCH_3$ signal intensity would be expected upon saturation of the CH_4 signal. Considering equation 2.8 and introducing k_1 at 351 K previously determined for the β-H intramolecular abstraction of methane from **1**[2] and $T_{1(NbMe)}$, one calculates the expected $M_{0(NbMe)}/M_{sat(NbMe)}$ ratio, that is $M_{0(NbMe)}/M_{sat(NbMe)}= k_{1(351)}\times T_{1(NbMe)} + 1 = (6.6\times 10^{-3}\times 1.34) + 1 = 1.009$. In other words, there is a factor of 4 in T_1 and another factor of 4 in k_{obs} and since the magnesation effect on $NbCH_3$ is 12%, one can calculate the magnesation effect on CH_4, which equals to

$$12\% \times \frac{T_{1NbMe}}{T_{1CH4}} \times \frac{k_{1obs}}{k_{-1obs}} = 12\% \times \frac{1.34}{4.95} \times \frac{6.6 \times 10^{-3}}{2.67 \times 10^{-2}} = 0.8\%$$

2.5- Kinetic study of the reaction between [Tp^{Me2}Nb(CH$_2$-3,5-C$_6$H$_3$Me$_2$)(c-C$_3$H$_5$)(MeCCMe)] (3) and CH$_4$

We have nevertheless realized a productive activation of methane. Along the lines established by Jones[6–9] and Wolczanski,[10] we surmised that the reaction of a weak Nb-1-mesityl bond with a strong CH bond in methane would yield a stronger Nb-methyl bond and a weaker CH bond in mesitylene. An excess of methane should make the reaction even more favorable thermodynamically. Here, we investigated how the CH bond of methane is activated by the mesityl complex [Tp^{Me2}Nb(CH$_2$-3,5-C$_6$H$_3$Me$_2$)(c-C$_3$H$_5$)(MeCCMe)] (**3**).

Compound **3** (0.072 g, 0.12 mmol) was dissolved in a mixture of cyclohexane-d_{12} (1 mL) and perfluorobenzene (1 mL), and then transferred into a high pressure (HP) single-crystal 10 mm sapphire NMR tube by syringe. The HP NMR tube was pressurized with 40 bar of methane and the reaction process was monitored by ^{1}H NMR spectroscopy.

From the ^{1}H NMR spectrum, it was found that **3** reacted with CH_4 to give **1** and mesitylene (Figure 2.8). To carry out a complete kinetic study, the course of the reaction was monitored at 290, 303, 314 and 321 K for more than 5 half-lives but for practical reasons was treated within 1.8, 2.3, 2.3 and 3.2 half-lives, respectively. Integration of the CH_4 signal compared to the Tp^{Me2}CH signal of **3** indicated that *ca.* 12-33 equivalents of methane vs **3**

were present in solution. Under these pseudo-first order conditions, the disappearance of **3** was monitored. To determine the rate constant, *k*, the peak of the *p*-C_6H_3 of **3** (δ 6.10) of each ^{1}H NMR spectrum acquired during the run was integrated and normalized with respect to the sum of the peaks of the C_6H_3 of free mesitylene (δ 6.56), the *p*-C_6H_3 of **3** (δ 6.10), the *o*-C_6H_3 of **3** (δ 5.87), the $Tp^{Me2}CH$ of **3** (δ 5.80, 5.71, 5.66) and the $Tp^{Me2}CH$ of **1** (δ 5.87, 5.73, 5.59), as an internal reference (Figure 2.8). Although adamantane was added to the sample as an internal reference, we were not able to confidently integrate its signals due to their proximity to the Tp^{Me2} Me signals of **1** and **3**. Figure 2.9 and Table 2.1 showed the kinetic constants at different temperatures.

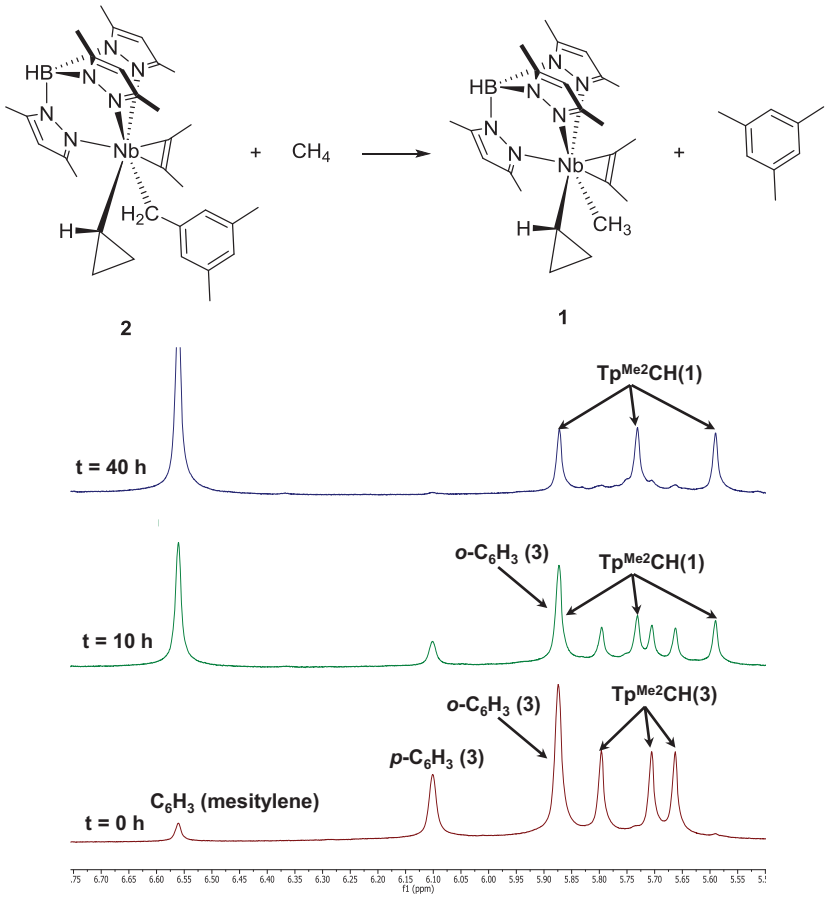

Figure 2.8. *Low-field expansions of stacked ^{1}H NMR spectra obtained from reaction of **3** with methane to give **1** in cyclohexane-d_{12} (1 mL) and perfluorobenzene (1 mL) at 314 K.*

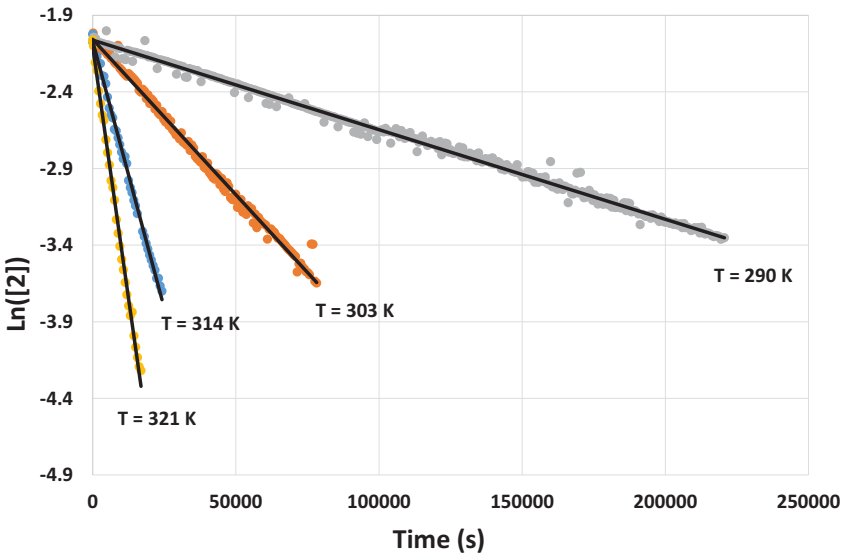

***Figure 2.9**. First-order kinetic plot for the β-H abstraction of mesitylene in **3** as a function of temperature.*

Table 2.1**. First order rate constants for β-H abstraction of mesitylene from **3

T (K)	k ($s^{-1} \times 10^{-6}$)	CH_4 equiv.
290	5.85 ± 0.02	12
303	20.3 ± 0.2	29
314	70.2 ± 0.3	27
314	71.9 ± 0.4	33
321	132 ± 2	27

The reaction of **3** with different concentrations of methane (27 and 33 equivalents) at 314 K gave the same rate constants (Table 2.1), indicating that the reaction is first order in **3** and zero order in methane (equation 2.11).

$$-\frac{d[2]}{dt} = k_{obs}[2] \quad (2.11)$$

From the rate constants at different temperatures (Figure 2.9 and Table 2.1), the activation parameters can be obtained from the Arrhenius and Eyring equations.

The Arrhenius equation has the form:

$$\ln(k) = \frac{-E_a}{R}\frac{1}{T} + \ln(A)$$

The plot of ln*k* with $\frac{1}{T}$ is linear with the slope representing $\frac{-E_a}{R}$ (Figure 2.10) which yields activation energy: E_a = 78 ± 5 kJ/mol.

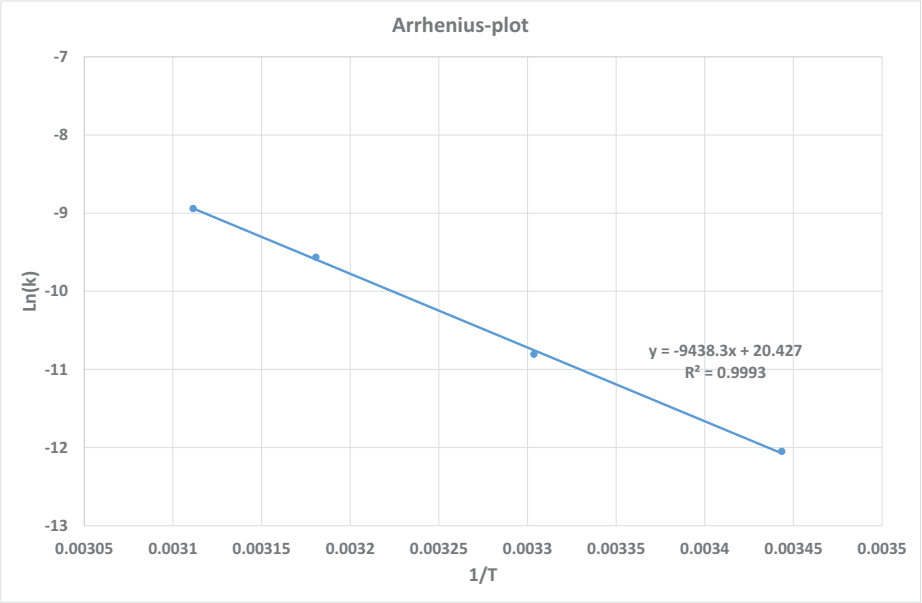

***Figure 2.10**. Arrhenius plot of the β-H abstraction of mesitylene in **3**.*

Similiarly, the Eyring equation has the form:

$$\ln\frac{k}{T} = \frac{-\Delta H^{\dagger}}{R}\frac{1}{T} + \ln\frac{k_B}{h} + \frac{\Delta S^{\dagger}}{R}$$

The linear plot of $\ln\frac{k}{T}$ with $\frac{1}{T}$ gives the slope of $\frac{-\Delta H^{\dagger}}{R}$, while the intercept is $\ln\frac{k_B}{h} + \frac{\Delta S^{\dagger}}{R}$ (Figure 2.12). Therefore, the enthalpy and entropy of activation, $\Delta H^{\dagger}$= 76 ± 5 kJ/mol and $\Delta S^{\dagger}$= – 84 ± 10 J/K.mol, respectively, were obtained.

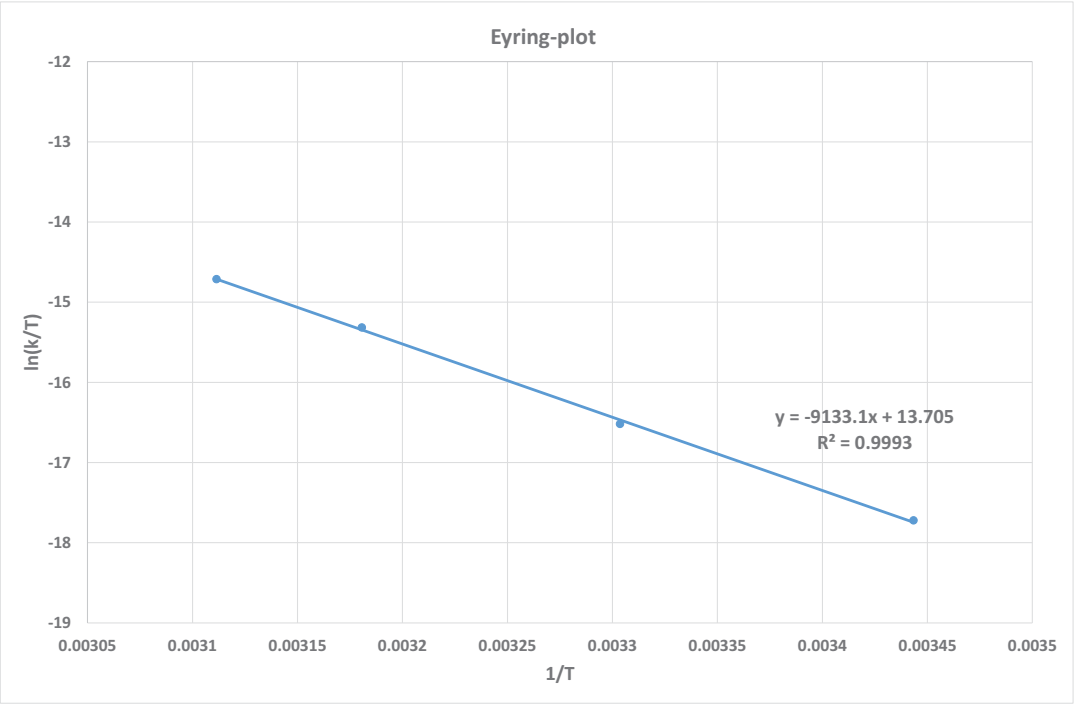

Figure 2.11. *Eyring plot of the β-H abstraction of mesitylene in* ***3****.*

This kinetic analysis for the disappearance of **3** in the T = 290 – 321 K range (Figure 2.9) revealed a first-order dependence in **3** and a zeroth order in methane which, together with a highly ordered transition state, are consistent with a rate-determining intramolecular loss of mesitylene forming **A** followed by fast reaction with CH_4 yielding **1** as expected (Scheme 2.9). The activation enthalpy for the elimination of mesitylene from **3** ($\Delta H^{\dagger}$= 76 ± 5 kJ/mol) is smaller than that for the elimination of methane from **1** ($\Delta H^{\dagger}$= 99 ± 5 kJ/mol)[2] because the Nb-mesityl bond is weaker than the Nb-methyl bond. The activation entropy for the elimination of mesitylene from **3** ($\Delta S^{\dagger}$= – 84 ± 10 J/K.mol) is significantly more negative than that for the elimination of methane from **1** ($\Delta S^{\dagger}$= – 6 ± 10 J/K.mol)[2] (Scheme 2.9). We suggest that this is the result of the elimination of the sterically demanding mesitylene from **3** as compared to that of methane from **1** which involves more substantial conformational changes to reach the ordered four-center transition state.

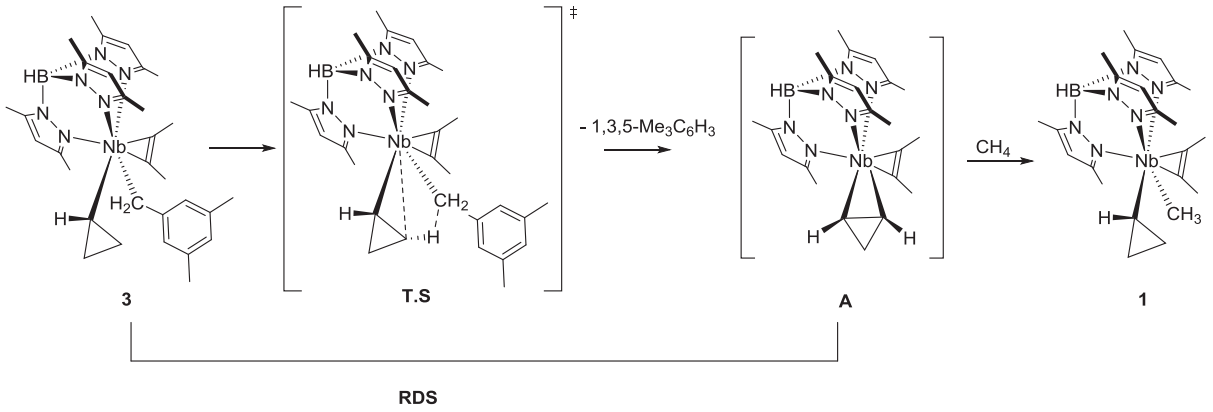

Scheme 2.9. *CH bond activation of methane by* ***3*** *to give* ***1****.*

2.6- Discussion

2.6.1- β-H abstraction versus α-H abstraction

As detailed in chapter 1, the activation of methane by the σ-bond metathesis mechanism[11,12] is a bimolecular process. In the activation of methane by β-H abstraction/1,3-addition and α-H abstraction/1,2-addition,[13] on the other hand, the rate determining step is the β-H abstraction and the α-H abstraction respectively, resulting in a first order rate constant for the overall process. While we cannot compare the rate constant of the σ-bond metathesis with the rate constants of the β-H abstraction/1,3-addition and the α-H abstraction/1,2-addition processes since they have a second order and a first order rate constant respectively, we may nevertheless compare the rate constants of the β-H abstraction/1,3-addition and the α-H abstraction/1,2-addition mechanism. Legzdins et *al*. has reported that the rate constant for the β-H abstraction of CMe_4 from [Cp*W(NO)(CH_2CMe_3)(η^3-$CH_2CHCHMe$)] is 7.1(5) × 10^{-5} s^{-1} at 20°C.[14] Mindiola et *al*. has found that the rate constant for the α-H abstraction of $CH_3{}^tBu$ from the alkylidyne precursor [(PNP)Ti=$CH^tBu(CH_2{}^tBu)$] is 5.86 × 10^{-5} s^{-1} at 31°C.[15] For the β-H abstraction of CH_4 and mesitylene from the cyclopropyl precursors **1** and **3**, our group has obtained the rate constants 2.93 × 10^{-5} s^{-1} and 2.03 × 10^{-5} s^{-1}, respectively,[1] at 30°C. Therefore, the rate constants corresponding to the CH bond activation of methane have the same order of magnitude for the β-H abstraction/1,3-addition and the α-H abstraction/1,2-addition processes.

2.6.2-Thermodynamics of the reaction of 2 with CH_4 to form 1 and mesitylene.

During the reaction, a C–H bond and a M–C bond are broken and a C–H bond and a M–C bond are formed. We must therefore take into account these four factors to study the reaction. Jones et *al*.[6–9] and Wolczanski et *al*.[10] have shown that the correlation between the strengths of the M–C bonds in titanium and rhodium complexes, respectively, and the bond dissociation energy (BDE) of the C–H bond of the corresponding hydrocarbon lead to approximately linear slopes, which are larger than 1. This reflects the fact that the differences between the bond strengths of two M–C bonds is always larger than the differences between the bond strengths of the two C–H bonds of the corresponding hydrocarbons. Figure 2.12, for instance, shows that linear correlation between relative Ti–C bond strengths ($D(TiR)_{rel}$, kcal/mol) in [$(silox)_2(^tBu_3SiNH)TiR$] and the C–H bond strengths (D(RH) (BDE), kcal/mol) of the corresponding hydrocarbon gives a slope of 1.1.[10] For the reaction between a weaker Nb–mesityl bond and a stronger CH_3–H bond to form a stronger Nb–CH_3 and a weaker mesityl–H bond, the enthalpy of the reaction $\Delta H_{reaction}$, which can be derived from the differences of the relative Nb–C and C–H bond strengths according to equation 2.10, should be larger than zero. Therefore, the C–H bond activation of methane by **3** to form **1** and mesitylene is thermodynamically preferred.

$$\Delta H_{reaction} = (D(Nb–CH_3) – D(M–mesityl)) – (D(CH_3–H) - D(mesityl–H)) \quad (2.10)$$

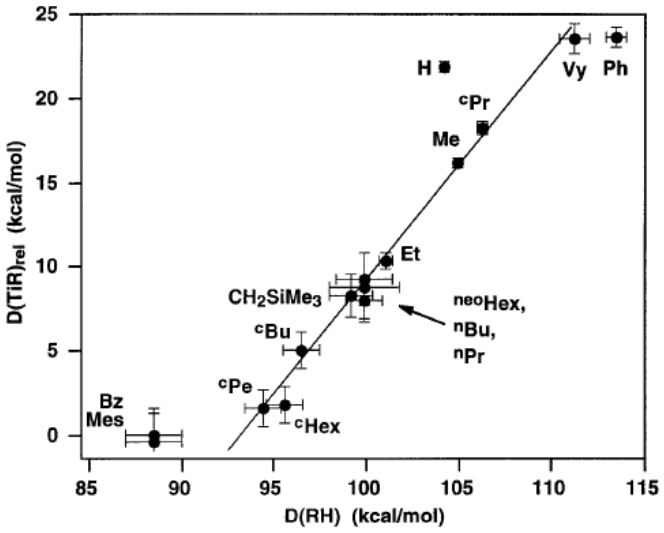

***Figure 2.12**. Relative Ti–C bond strengths (kcal/mol) in [(silox)$_2$(^{t}Bu$_3$SiNH)TiR] versus the C–H bond strength of the corresponding hydrocarbon. D(TiR)$_{rel}$ = D(TiR) –D(TiBz). The line (slope =1.1, r=0.95) is a least-squares fit to all points.*

2.6.3-Involvement of a σ-CH$_4$ complex and transition state structure for the elimination/activation of CH$_4$

Whereas the generation of intermediate **A** and its ability to activate methane via a rare 1,3-CH bond addition pathway constitute a remarkable result, the intermediacy of a methane adduct along the reaction coordinate remained an open question. In several low-valent late-transition metal systems, methane complexes have been inferred from kinetic analyses,[16] directly observed by time-resolved spectroscopy[17] or matrix trapping experiments[18] and even characterized by NMR in solution more recently.[19] In high oxidation state early transition metal systems however, methane adducts have eluded direct characterization.[13] DFT modelling has yielded structures and energetic data suggesting little thermodynamic stability and high kinetic lability of these adducts (barely elongation of the CH bond length of the coordinated methane compared to free methane and small binding energy (4 kJ/mol) in the σ-CH$_4$ complexes).[13] These values are significantly smaller than those for a directly observed rhodium complex (significant elongation of the CH bond distance of the coordinated methane (1.14 Å) compared to free methane (1.09 Å) and large binding energy (61 kJ.mol^{-1}) in the σ-CH$_4$ complexes).[19] In order to compare the Nb case with these systems, professor Michel Etienne carried out a series of DFT calculations performed to explore the origin of the elimination/activation of CH$_4$. The computed electronic and free energy surface for the conversion of **A** + **CH$_4$→ A-CH$_4$→ 1-TS→1** is shown in Figure 2.13.

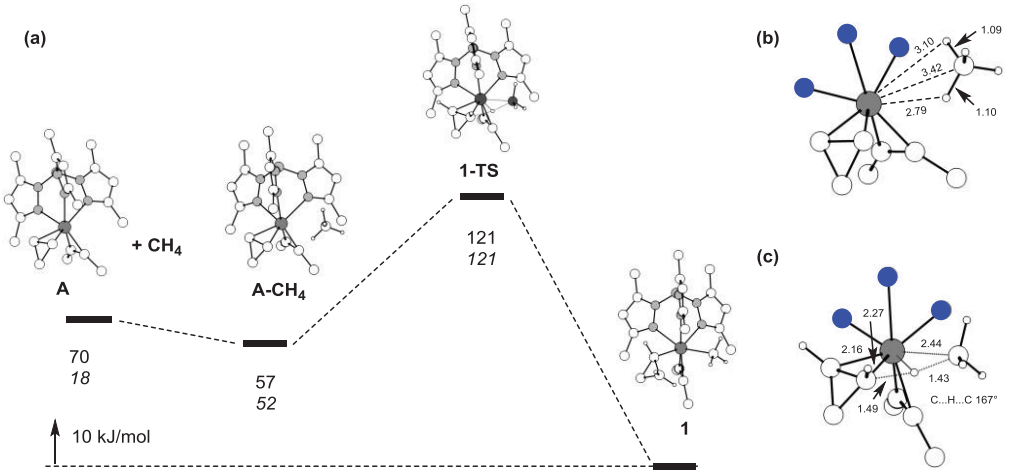

Figure 2.13. *(a) Potential energy surface (wB97XD functional) for the activation of methane by [Tp^{Me2}Nb(η^2-c-C$_3$H$_4$)(MeCCMe)]* ***(A)*** *(electronic energy with ZPE, top; free energy, below italicized) (b)* ***A-CH$_4$*** *and (c)* ***1-TS*** *(distances in Å). Color code: Nb, gray, N; blue; C, large white; H, small white. Only atoms of ancillary ligands bound to Nb are shown for clarity.*

It is confirmed here that **A**–**CH$_4$** is only a loose van der Waals complex, the binding energy between **A** and **CH$_4$**, which is derived from the electronic energy difference between **A**–**CH$_4$** and **A** + **CH$_4$**, is 13 kJ/mol (Figure 2.13 (a)). Barely elongation of the CH bond distance of methane (1.10 Å) compared to free methane (1.09 Å) is noted in the σ-CH$_4$ (Figure 2.13(b)). The optimized transition state **1-TS** for the CH bond activation of CH$_4$ (Figure 2.13(c)) exhibits a relatively symmetrical situation with an almost linear C…H…C arrangement (167°).

Figure 2.14 presents an analysis of the electron density of **1-TS** following the NPA NBO approach.[20] There is a slight excess of positive charge on the hydrogen being transferred between the two Nb bound carbons. The methyl carbon bears a strong negative charge; whereas the negative charge on the incipient cyclopropene ligand is shared equally between the two carbon atoms. The NLMO describing the interaction in the transition state is mainly delocalized on the niobium and the β-CH but some tails on the α-C and the methyl carbon are also seen. Overall the bonding picture is that of a σ-bond metathesis[21–23] but with a distinctive involvement of both niobium-bound carbons of the η^2-cyclopropene ligand engaged in the hydrogen transfer. This highlights the structural and electronic differences with the more common α-abstraction/1,2-CH addition mechanism.[13]

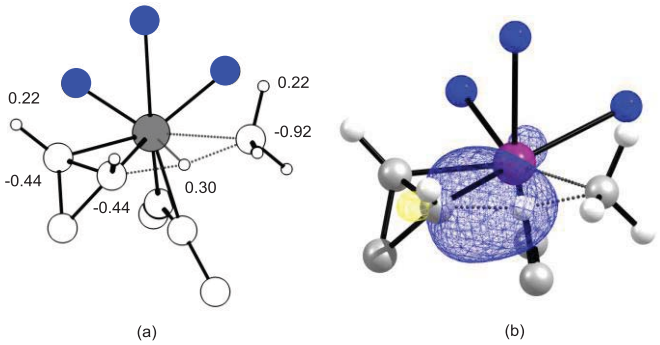

Figure 2.14. *(a) Natural Charges and (b) NLMO for* ***1-TS****.*

2.7- Conclusion

We have shown that a transient unsaturated η^2-cyclopropene complex of niobium (**A**) was able to cleave a CH bond of methane via a 1,3-CH bond addition pathway under mild conditions. Degenerate reaction of **1** with $^{13}CH_4$ formed the isotopologue product **1-^{13}CH$_3$**. In the presence of CD_4, the formation of two diastereoisomers in a 3:1 ratio indicates the involvement of a stereospecific 1,3-addition process to the transient η^2-cyclopropene intermediate **A**. Spin saturation transfer experiments demonstrate that [Tp^{Me2}NbMe(c-C_3H_5)(MeCCMe)] (**1**) activates the CH bond of methane by a reversible β-H abstraction/1,3-addition pathway. Kinetic study on the reaction of [Tp^{Me2}Nb(Mesityl)(c-C_3H_5)(MeCCMe)] (**3**) with high pressure CH_4 shows that the reaction is 1st order in **3** and zeroth order in CH_4, indicating that the formation of the transient η^2-cyclopropene intermediate **A** is rate-determining. A very negative activation entropy, finally, suggests an ordered transition state in the β-H abstraction step. The optimized transition state for the methane CH bond elimination/activation is in a four-center σ-bond metathesis mode with a distinctive involvement of both carbons of the η^2-cyclopropene ligand engaged in the hydrogen transfer.

Experimental Section

All operations were performed with rigorous exclusion of air and moisture, using standard Schlenk, high-vacuum, and glovebox techniques under Ar (O_2 < 3 ppm, H_2O < 1 ppm). Perfluorobenzene and cyclohexane-d_{12} were dried over molecular sieves, filtered, degassed by several freeze-pump-thaw cycles and stored in sealed ampules in the glovebox. ^1H and ^{13}C NMR spectra were recorded using Bruker Avance 400 (^1H, 400.13 MHz) and Bruker Avance 500 (^1H, 500.33 MHz) spectrometers. ^2H NMR spectra were recorded using a Bruker Avance 600 spectrometer (^1H, 600.13; ^2H, 92.12 MHz) equipped with a cryoprobe. For the kinetic and SST studies, the temperature of the probes was calibrated with 80% ethylene glycol (DMSO-d_6). For the SST and kinetic experiments ^1H NMR signals of adamantane were used as internal standards.

Methane, (C_2H_6 < 100 ppb, CO_2 < 100 ppb, total C_nH_m < 50 ppb, O_2 < 500 ppb, N_2 < 2 ppm, H_2O < 2 ppm, H_2 < 2 ppb) was purchased from Alpha Gaz and used as received. CD_4 (isotope enrichment 99.93%) and $^{13}CH_4$ (isotope enrichment 99.9%) were purchased from Euriso-top and used as received. [Tp^{Me2}NbMe(*c*-C_3H_5)(MeC≡CMe)] (**1**) and [Tp^{Me2}Nb(CH_2-3,5-$Me_2C_6H_3$)(*c*-C_3H_5)(MeC≡CMe)] (**2**) were prepared according to published procedures.[1,2]

Medium pressure J-Young NMR tubes (5 mm diameter, thin wall precision, quick pressure valve, 7 inch length, max pressure *ca* 10 bar) were purchased from WilmadLabGlass. For the high pressure (HP) NMR experiments, a single-crystal 10 mm sapphire (aluminulm oxide) NMR tube was used. The tube is quite chemically inert and it can withstand pressures up to 100 bar and temperatures up to 90 °C, which allows a sufficiently large sample volume (2 ml) for observation of nuclei such as ^1H, ^{13}C and all measurements were carried out under the limits of the tube. While the tube surface is not perfectly concentric, the loss of resolution that this entails was deemed to be less important. The high pressure measurements were carried out on a Bruker Avance 400 spectrometer equipped with a 10mm TBO probe.

Chart 2.2 shows a schematic view of the *Ti*-alloy valve connected to the sapphire NMR tube.[31] The valve is designed to put gases under pressure (6, in Chart 2.2) and to seal the tube (8, in Chart 2.2). All metal parts are made of a 6A1, 4V titanium alloy. The sample tube (12, in Chart 2.2) is connected to the titanium-alloy flange (9, in Chart 2.2) by a single component epoxy adhesive (10, in Chart 2.2). The valve body is connected to the flange through four threaded bolts (7, in Chart 2.2). In a typical operation, the sapphire tube is filled in a glove box with the sample solution by syringe. The valve body is then connected to the

sapphire tube through the four bolts and sealed by closing the Viton O ring seal (8, in Chart 2.2). The tube is then filled with high pressure methane through the gas inlet port (6, in Chart 2.2) at room temperature. The assembly is protected by a polymethylmethacrylate safety shield which allows the lowering of the tube into the probe avoiding the direct exposure of the operator to the pressurized tube. The pneumatic air system has to be controlled manually to allow the lower of the tube into the probe safely. The tube valve assembly has a light weight, which allows the tube to spin symmetrically using only a slight increase of the normal spinner nitrogen pressure usually employed.

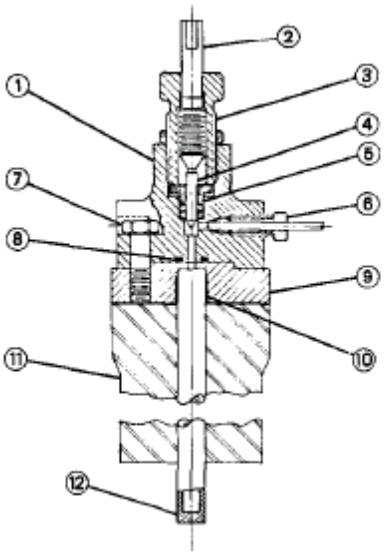

Chart 2.2. *Schematic drawing of the Ti-alloy valve sapphire tube assembly. Numbered details are 1, valve body; 2, handle of the stem drive of the valve; 3, stem drive and packing gland; 4, nonrotating stem; 5, packing assembly; 6, gas inlet port; 7, assembly screw (total of 4); 8, Viton O-ring seal, 9, flange to which the tube is mounted; 10, epoxy sealant; 11, spinner turbine; 12, sapphire tube.*

CH Bond Activation of $^{13}CH_4$ by 1.

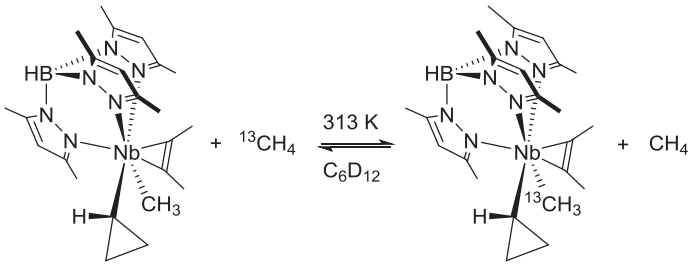

1 **1-$^{13}CH_3$**

A medium pressure J-Young NMR tube was charged with compound **1** (0.030 g, 0.060 mmol) in cyclohexane-d_{12} (0.5 mL) and was pressurized with $^{13}CH_4$ to *ca* 3 bar at 173 K (ethanol/liquid N_2 bath) for 1 min. The tube was then placed in the ^{1}H NMR spectrometer with the probe set at 313 K. 1.2 equivalents of $^{13}CH_4$ could be quantified by integration of the $^{13}C\mathit{H}_4$ signal [δ 0.19 (d, $^1J_{CH}$ = 125.0 Hz)] compared to the $Tp^{Me2}C\mathit{H}$ signal of complex **1**. The reaction was subsequently monitored by ^{1}HNMR over 19 hours at 313 K.

CD Bond Activation of CD_4 by 1.

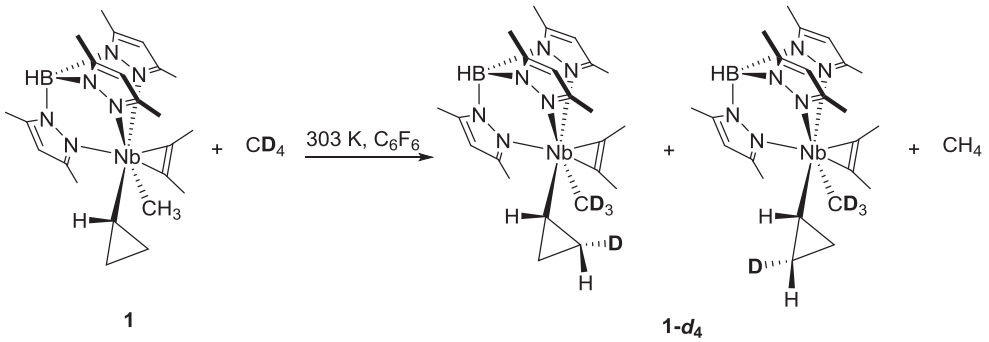

1 **1-d_4**

A medium pressure J-Young NMR tube was charged with compound **1** (0.030 g, 0.060 mmol) in perfluorobenzene (0.5 mL) and was pressurized with CD_4 to ca 8 bar at 157 K (ethanol/liquid N_2 bath) for 3 mins. The tube was then placed in the ^{1}H NMR spectrometer with the probe set at 303 K. The reaction was subsequently monitored by ^{1}H NMR and ^{2}H{^{1}H} NMR for 4 hours at 303 K.

Spin saturation transfer (SST) experiments.

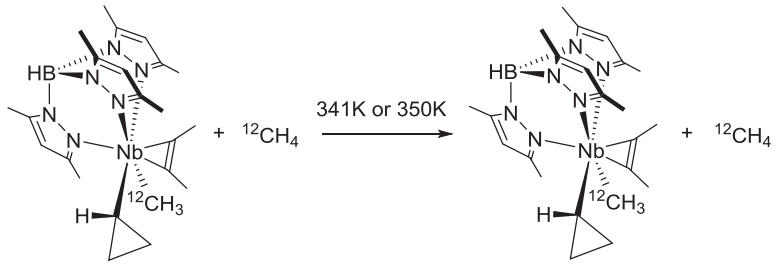

1 **1**

Samples preparation

Medium pressure NMR tube reaction: In the glovebox, a medium pressure J-Young NMR tube was charged with compound **1** (0.030 g, 0.06 mmol), C_6F_6 (0.5 ml), a drop of cyclohexane-d_{12} (0.01ml) as the lock solvent and adamantane (7.6 mg, 0.0565 mmol) as internal standard. The tube was then frozen at 213 K, charged with CH_4 (6 bar) for 3 minutes, and sealed. It was then placed in a Bruker Avance 500 NMR spectrometer with the probe set at 341 K. 4 equivalents of CH_4 could be quantified by integration of the C*H*$_4$ signal (δ 0.14) compared to the Tp^{Me2}C*H* signal of complex **1**.

High pressure NMR tube reaction: In the glovebox, compound **1** (0.100 g, 0.200 mmol) and adamantane (8 mg, 0.06 mmol) as internal standard were dissolved in a mixture of cyclohexane-d_{12} (1 mL) and C_6F_6 (1 mL) and then transferred into a single-crystal 10 mm sapphire HP NMR tube. The tube was then protected by a polycarbonate casing and equipped with a high-pressure manifold. It was then pressurized with 60 bar of methane at RT and carefully shaken to ensure the dissolution of methane. The tube was then placed in a Bruker Avance 400 NMR spectrometer with the probe set at 351 K. 29 equivalents of CH_4 in solution could be quantified by integration of the C*H*$_4$ signal (δ 0.14) compared to the Tp^{Me2}C*H* signal of complex **1**.

SST Acquisition procedure

The High Pressure or Medium Pressure NMR tube was set into the NMR spectrometer for 15 min to establish thermal equilibrium and the magnet was shimmed as necessary. The saturation pulses were carefully set up for obtaining a complete saturation of the irradiated signal with a minimum power value in order to limit as much as possible partial saturation of side signals. A reference experiment was run with exactly the same parameters than the

saturation experiment but with a saturation offset frequency set to a part of the NMR spectrum devoid of signals. The reference offset frequency (O_{ref}) was chosen such that its difference with the frequency of the measured signal (O_{mes}) was exactly the same as the difference between the measured and the irradiated (O_{irr}) frequencies: $O_{ref}–O_{mes} = O_{mes}– O_{irr}$. The saturation and reference experiments were repeated at least five times for error evaluations. The spectra were processed with a special attention to phase and baseline corrections. The integration of the measured signals used for the rate constant calculations was then extracted from the reference and the saturation spectra.

T_1 measurements

The spin-lattice relaxation times T_1 were measured by the inversion recovery method. On the 500 MHz spectrometer, at 341 K, the spin-lattice relaxation times for NbMe and C*H*$_4$ were $T_{1(NbMe)}$ 1.00 s and $T_{1(CH4)}$ 4.90 s, respectively. On the 400 MHz spectrometer, at 351 K, the spin-lattice relaxation times for NbMe and C*H*$_4$ were $T_{1(NbMe)}$ 1.34 s and $T_{1(CH4)}$ 4.95 s, respectively. The corresponding T1 curves are shown below (Figure 2.15).

(a)

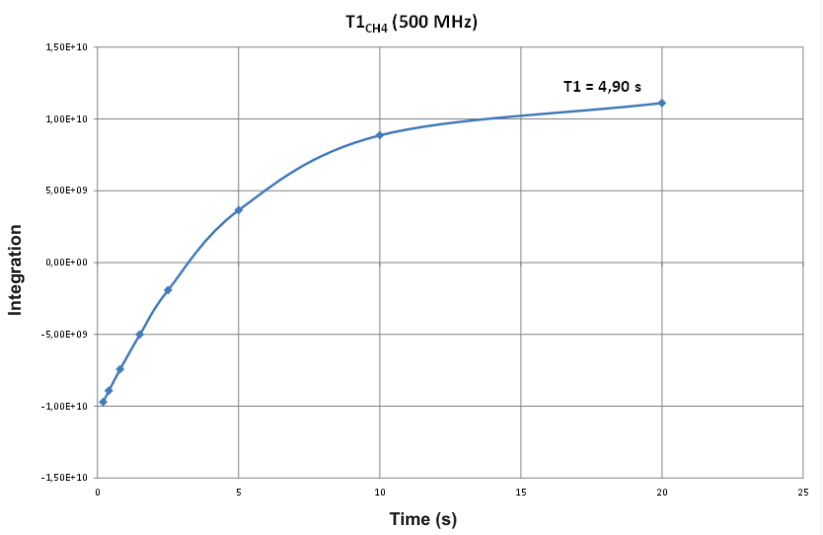

(b)

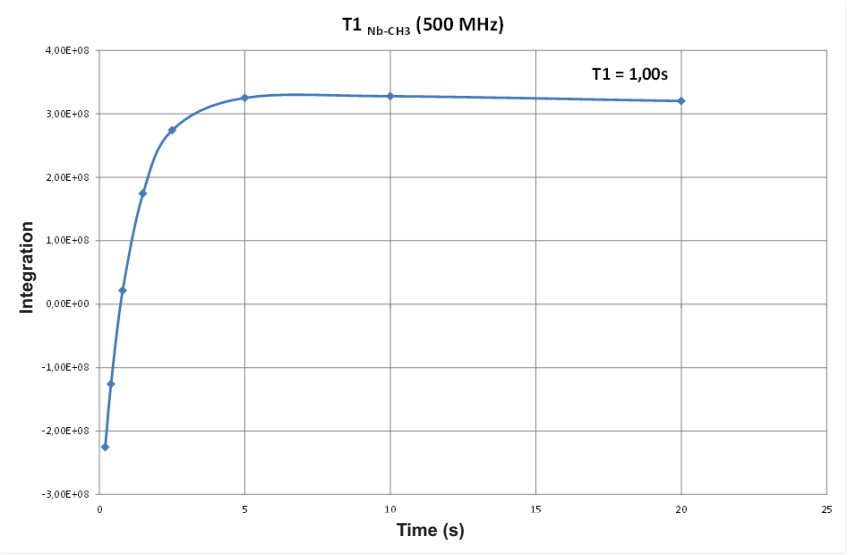
T1 Nb-CH3 (500 MHz)
T1 = 1,00s
Integration
Time (s)
4,00E+08
3,00E+08
2,00E+08
1,00E+08
0,00E+00
-1,00E+08
-2,00E+08
-3,00E+08
0
5
10
15
20
25

(c)

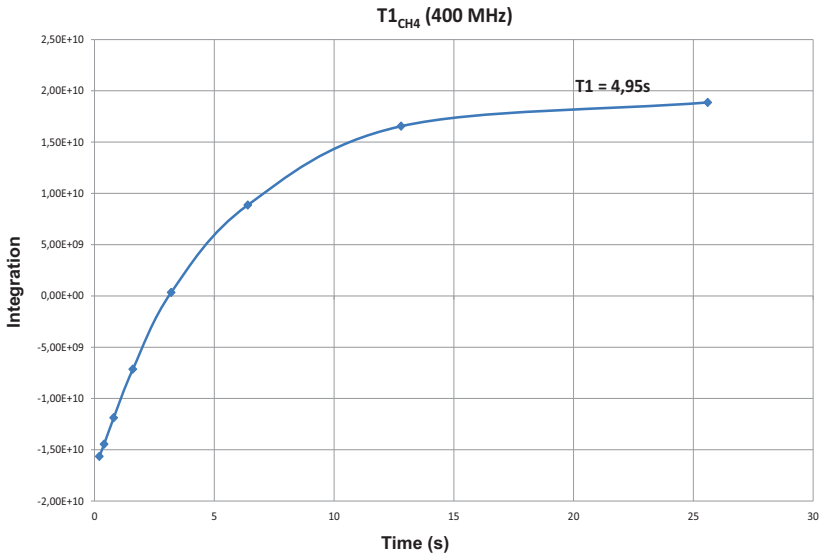
T1CH4 (400 MHz)
T1 = 4,95s
Integration
Time (s)
2,50E+10
2,00E+10
1,50E+10
1,00E+10
5,00E+09
0,00E+00
-5,00E+09
-1,00E+10
-1,50E+10
-2,00E+10
0
5
10
15
20
25
30

(d)

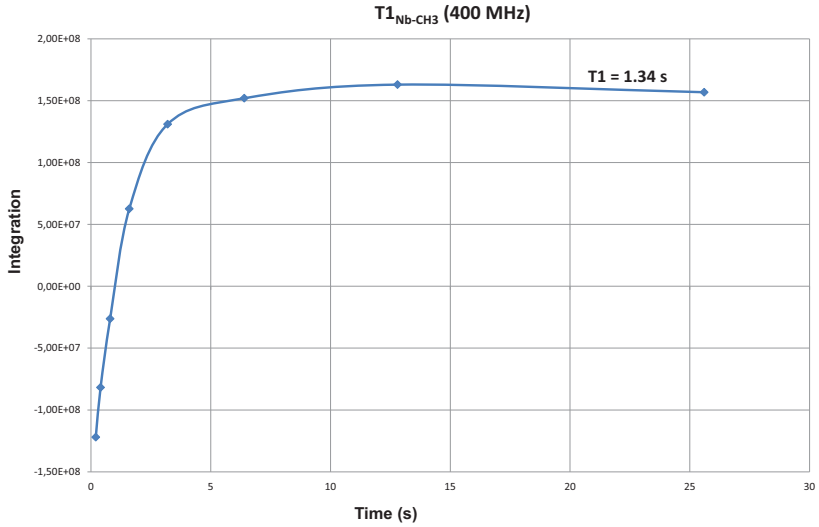

***Figure 2.15**. Plots of the area of the NMR signal vs. delay time, after the inversion recovery sequence, allowing determination of the spin-lattice relaxation times for CH_4 and NbMe on the 500 MHz spectrometer at 341 K (a) and b) and on the 400 MHz spectrometer at 351 K (c) and d)).*

SST by irradiation of the NbMe peak

The saturation pulses were carefully set up to obtain a complete saturation of the irradiated NbMe signal (δ 0.59) without affecting the other signals. The reference experiment was run with exactly the same parameters than the saturation experiment but with a saturation offset frequency set to δ -0.31 [the reference offset frequency (O_{ref}) is located 0.45 ppm upfield from CH_4 (δ 0.14)]. The irradiation of the NbMe signal (δ 0.59) gave rise to a significant decrease of the CH_4 peak intensity (11%), compared to the reference CH_4 value. The SST experiment was carried out at 341 and 351 K for medium (4 equivalents) and high (29 equivalents) CH_4 pressures respectively. The saturation delays (t_{sat}) were chosen so that $t_{sat} \geq 5T_1$ of the irradiated signal (5 and 30 seconds respectively for medium (500 MHz) and high (400 MHz) CH_4 pressures). For the medium CH_4 pressure experiment, shorter saturation delays were employed, since the decomposition process of **A** competes with the C–H bond activation of methane by **A** during the SST irradiation.

The CH_4 signals were then integrated for the reference and the irradiated spectra, respectively, in order to obtain the M_{0CH4} and M_{satCH4} values for the calculation of the rate constant k_{-1obs}. The reported k_{-1obs} value, obtained from the high pressure SST experiment, is the average of several experiments carried out under identical conditions.

SST by irradiation of the CH_4 peak

For the irradiation of the CH_4 peak, a similar procedure to that described above for the irradiation of the NbMe peak was followed. After finding the suitable saturation pulses for obtaining complete saturation of the irradiated CH_4 (δ 0.14) signal, the reference experiment was run by setting the saturation off-set frequency not to δ 1.04 (ca. 0.45 ppm downfield of the NbMe peak at δ 0.59) as usually done for a symmetrical reference, but to δ -0.44 (ca. 1.03 ppm upfield from the NbMe peak at δ 0.59 to avoid irradiation of the β *c*-C_3H_5 peak at δ1.15. The irradiation of the CH_4 (δ 0.14) signal gave rise to a poorly reproducible, very small decrease of the NbMe peak intensity (between 0 and 5%), compared to the reference NbMe value. This small variation of the NbMe signal is likely due to the low $T_{1(NbMe)}$ value. The saturation delays (t_{sat}) were chosen so that $t_{sat} \geq 5T_1$of the irradiated signal (60 seconds for high CH_4 pressures (400 MHz spectrometer)).

Kinetic Experiments

Reaction of 3 with methane to give 1.

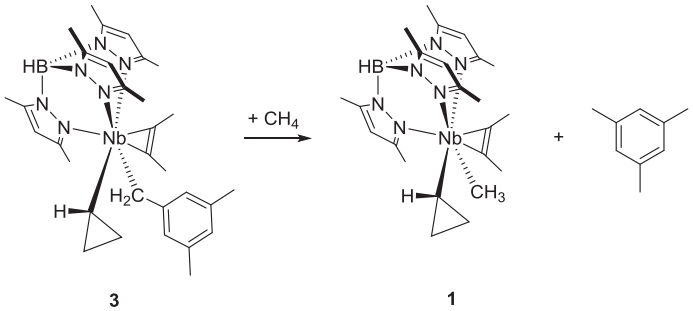

3 1

In a glove box, compound **3** (0.072 g, 0.12 mmol) was dissolved in a mixture of cyclohexane-d_{12} (1 mL) and perfluorobenzene (1 mL) and then transferred into a high pressure (HP) single-crystal 10 mm sapphire NMR tube, which was then protected by a polycarbonate casing and equipped with a high-pressure manifold. The HP NMR tube was pressurized with 40 bars of methane and carefully shaken to ensure the dissolution of methane. To carry out a complete kinetic study, the course of the reaction was monitored at 290, 303, 314 and 321 K for more than 5 half-lives but for practical reasons was treated within 1.8, 2.3, 2.3 and 3.2 half-lives, respectively. Integration of the CH_4 signal compared to

the Tp^{Me2}C*H* signal of **3** indicated that *ca* 12-33 equivalents of methane vs **3** were present in solution.

Computational studies

Calculations were performed at the DFT level with the different functionals as implemented in Gaussian09, revision D.01.[24] Nb was described using the Stuttgart/Dresden RECP (SDD) pseudo-potential and its associated basis set.[25] For N, C, B and H, the TZVP basis set was used.[26] Structure optimizations were carried out without symmetry constraints. The nature of the stationary points was ascertained by a vibrational analysis within the harmonic approximation (1 atm and 298 K). Minima were identified by a full set of real frequencies and transitions states by the presence of a single imaginary frequency. Transitions states were relaxed on both reactant and product sides. Electronic energies are reported with zero-point energy correction as hartree in the text. Since reactions were carried out either in non-polar cyclohexane or in cyclohexane/hexafluorobenzene mixtures with similar results, solvent corrections were not included. NBO calculations were carried out with NBO 6.0 as implemented in Gaussian09.[27]

Three types of functionals were tested in addition to the one used originally (M06/SDD/6-31G(d), CMD correction).[1] They either contain different types of dispersion corrections or no correction (wB97XD, PBE0-GD3BJ, PBE0).[28-30] While energies vary slightly, the geometries of stationary points do not vary significantly except for the methane adduct. In the absence of dispersion correction (*ie* PBE0), the interaction of methane with the η^2-cyclopropene niobium complex [$Tp^{Me2}Nb(\eta^2$-*c*-$C_3H_4)$(MeCCMe)] appears much weaker with a long niobium…methane distance.

References

(1) Boulho, C.; Oulie, P.; Vendier, L.; Etienne, M.; Pimienta, V.; Locati, A.; Bessac, F.; Maseras, F.; Pantazis, D. A.; McGrady, J. E. *J. Am. Chem. Soc.* **2010**, *132*, 14239–14250.

(2) Oulié, P.; Boulho, C.; Vendier, L.; Coppel, Y.; Etienne, M. *J. Am. Chem. Soc.* **2006**, *128*, 15962–15963.

(3) Wada, K.; Pamplin, C. B.; Legzdins, P.; Patrick, B. O.; Tsyba, I.; Bau, R. *J. Am. Chem. Soc.* **2003**, *125*, 7035–7048.

(4) Vastine, B. A.; Hall, M. B. *Coord. Chem. Rev.* **2009**, *253*, 1202–1218.

(5) (a) Jarek, R. L.; Flesher, R. J.; Shin, S. K. *J. Chem. Edu.* **1997**, *74*, 978–982; (b) Uğurbil, K. *J. Magn. Reson.* **1985**, *64*, 207-219.

(6) Clot, E.; Megret, C.; Eisenstein, O.; Perutz, R. N. *J. Am. Chem. Soc.* **2006**, *128*, 8350–8357.

(7) Evans, M. E.; Li, T.; Vetter, A. J.; Rieth, R. D.; Jones, W. D. *J. Org. Chem.* **2009**, *74*, 6907–6914.

(8) Jiao, Y.; Brennessel, W. W.; Jones, W. D. *Chem. Sci.* **2014**, *5*, 804–812.

(9) Schock, L. E.; Marks, T. J. *J. Am. Chem. Soc.* **1988**, *110*, 7701–7715.

(10) Bennett, J. L.; Wolczanski, P. T. *J. Am. Chem. Soc.* **1997**, *119*, 10696.

(11) Watson, P. L. *J. Am. Chem. Soc.* **1983**, *105*, 6491–6493.

(12) Thompson, M. E.; Baxter, S. M.; Bulls, A. R.; Burger, B. J.; Nolan, M. C.; Santarsiero, B. D.; Schaefer, W. P.; Bercaw, J. E. *J. Am. Chem. Soc.* **1987**, *109*, 203–219.

(13) Flores, J. A.; Cavaliere, V. N.; Buck, D.; Pintér, B.; Chen, G.; Crestani, M. G.; Baik, M.-H.; Mindiola, D. J. *Chem. Sci.* **2011**, *2*, 1457–1462.

(14) Tsang, J. Y. K.; Buschhaus, M. S. A.; Graham, P. M.; Semiao, C. J.; Semproni, S. P.; Kim, S. J.; Legzdins, P. *J. Am. Chem. Soc.* **2008**, *130*, 3652–3663.

(15) Andino, J. G.; Kilgore, U. J.; Pink, M.; Ozarowski, A.; Krzystek, J.; Telser, J.; Baik, M.-H.; Mindiola, D. J. *Chem. Sci.* **2010**, *1*, 351–356.

(16) Jones, W. D. *Acc. Chem. Res.* **2003**, *36*, 140–146.

(17) Cowan, A. J.; Portius, P.; Kawanami, H. K.; Jina, O. S.; Grills, D. C.; Sun, X.-Z.; McMaster, J.; George, M. W. *Proc. Natl. Acad. Sci.* **2007**, *104*, 6933–6938.

(18) Hall, C.; Perutz, R. N. *Chem. Rev.* **1996**, *96*, 3125–3146.

(19) Bernskoetter, W. H.; Schauer, C. K.; Goldberg, K. I.; Brookhart, M. *Science.* **2009**, *326*, 553–556.

(20) Reed, A. E.; Curtiss, L. A.; Weinhold, F. *Chem. Rev.* **1988**, *88*, 899–926.

(21) Watson, L. A.; Yandulov, D. V; Caulton, K. G. *J. Am. Chem. Soc.* **2001**, *123*, 603–611.

(22) Maron, L.; Perrin, L.; Eisenstein, O. *J. Chem. Soc., Dalton Trans.* **2002**, 534–539.

(23) Barros, N.; Eisenstein, O.; Maron, L. *Dalton Trans.* **2006**, 3052–3057.

(24) Gaussian09, revision D.01. Frisch, M. J.; Trucks, G. W.; Schlegel, H. B.; Scuseria, G. E.; Robb, M. A.; Cheeseman, J. R.; Scalmani, G.; Barone, V.; Mennucci, B.; Petersson, G. A.; Nakatsuji, H.; Caricato, M.; Li, X.; Hratchian, H. P.; Izmaylov, A. F.; Bloino, J.; Zheng, G.; Sonnenberg, J. L.; Hada, M.; Ehara, M.; Toyota, K.; Fukuda, R.; Hasegawa, J.; Ishida, M.; Nakajima, T.; Honda, Y.; Kitao, O.; Nakai, H.; Vreven, T.; Montgomery, Jr., J. A.; Peralta, J. E.; Ogliaro, F.; Bearpark, M.; Heyd, J. J.; Brothers, E.; Kudin, K. N.; Staroverov, V. N.; Keith, T.; Kobayashi, R.; Normand, J.; Raghavachari, K.; Rendell, A.; Burant, J. C.; Iyengar, S. S.; Tomasi, J.; Cossi, M.; Rega, N.; Millam, J. M.; Klene, M.; Knox, J. E.; Cross, J. B.; Bakken, V.; Adamo, C.; Jaramillo, J.; Gomperts, R.; Stratmann, R. E.; Yazyev, O.; Austin, A. J.; Cammi, R.; Pomelli, C.; Ochterski, J. W.; Martin, R. L.; Morokuma, K.; Zakrzewski, V. G.; Voth, G. A.; Salvador, P.; Dannenberg, J. J.; Dapprich, S.; Daniels, A. D.; Farkas, O.; Foresman, J. B.; Ortiz, J. V.; Cioslowski, J.; Fox, D. J.; Gaussian, Inc., Wallingford CT, 2013.

(25) Andrae, D.; Haeussermann, U.; Dolg, M.; Stoll, H.; Preuss, H. *Theor. Chem. Acc.* **1990,** *77*, 123-141.

(26) Schaefer, A.; Huber, C.; Ahlrichs, R. *J. Chem. Phys.* **1994**, *100*, 5829-5835.

(27) ***NBO 6.0.*** Glendening, E. D.; Badenhoop, J. K.; Reed, A. E.; Carpenter, J. E.; Bohmann, J. A.; Morales, C. M.; Landis, C. R.; Weinhold, F. Theoretical Chemistry Institute, University of Wisconsin, Madison (2013).

(28) Chai, J.D.; Head-Gordon, M. *Phys. Chem. Chem. Phys.* **2008**, *10*, 6615-6620.

(29) Adamo C.; Barone, V. *J. Chem. Phys.* **1999**, *110*, 6158-6169.

(30) Grimme, S., Ehrlich, S.; Goerigk, L. *J. Comp. Chem.* **2011**, *32*, 1456-1465.

(31) Roe, D. C. *J. Magn. Reson.* **1985***, 63*, 388-391.

Chapter 3

CH bond activation of heteraromatic and unsaturated hydrocarbons by a niobium methyl cyclopropyl precursor

Chapter 3: CH bond activation of heteraromatic and unsaturated hydrocarbons by a niobium methyl cyclopropyl precursor

3.1- Introduction

Besides σ-bond metathesis and 1,2-CH bond activation (often following α-H abstraction), 1,3-CH bond activation (often following β-H abstraction) has been reported to be an important mechanism for the activation of C–H bonds of simple hydrocarbons at early transition metals. To date, a number of transient early transition metal complexes with benzyne, alkyne, allene, diene and alkene ligands are competent to cleave the strong and inert C–H bonds of hydrocarbons via this mechanism. Erker first reported that [$Cp_2Zr(\eta^2$-aryne)], generated by reversible intramolecular β-H abstraction of diaryl zirconocenes, could cleave the CH bond of benzene by 1,3-addition.[1] The reactions of other early transition metal η^2-benzyne (Mo,[2,3] W,[2] V,[4,5] Nb[6]) and η^2-alkyne (W[7,8]) complexes are now well-documented (Scheme 3.1(a)). Early transition metal η^2-allene and η^2-diene intermediates generated from alkyl allyl complexes of the type [Cp*M(NO)(R)(η^3-CH_2CHCHR)] (M = Mo, W) also activate the CH bond of hydrocarbons via 1,3-addition mechanism (Scheme 3.1(b)).[9–12] Although a number of early transition metal η^2-alkene complexes (M = Ti,[13,14] Zr,[15] Hf,[16] Nb, Ta,[17] and W[18]) could be generated from β-H abstraction of relevant alkyl compounds, only a few of them activate the CH bond of benzene[16] and terminal alkynes[14,15] via intermolecular 1,3-CH addition (Scheme 3.1 (c)).

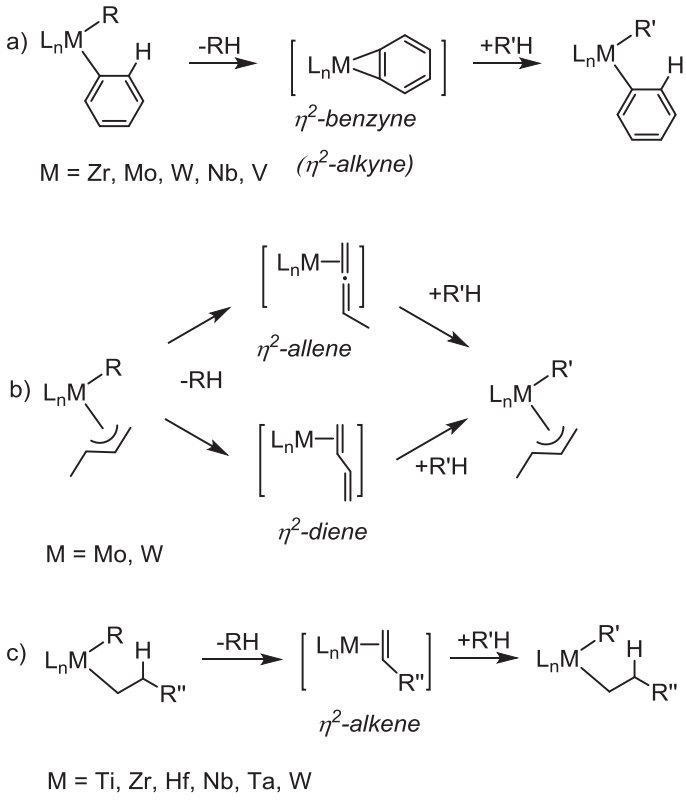

Scheme 3.1. *β-H abstraction/1,3-CH bond addition by different intermediates.*

Previously our group has reported that a transient η^2-cyclopropene niobium complex **A** generated by intramolecular β-H abstraction of methane from the methyl cyclopropyl complex [Tp^{Me2}NbMe(*c*-C_3H_5)(MeCCMe)] (**1**) is able to activate the aromatic and benzylic C–H bonds of alkyl aromatics under mild conditions.[6,19,20] For instance, **A** reacts with 1,3-dimethylbenzene to give a 3:1 mixture of arene and benzylic CH activated products, translating to a 18:1 preference for aromatic versus benzylic CH bond activation on a per CH bond basis (Scheme 3.2). Computational studies have shown that the aryl complex is preferred over the benzylic complex by ca. 20 kJ·mol^{-1}.

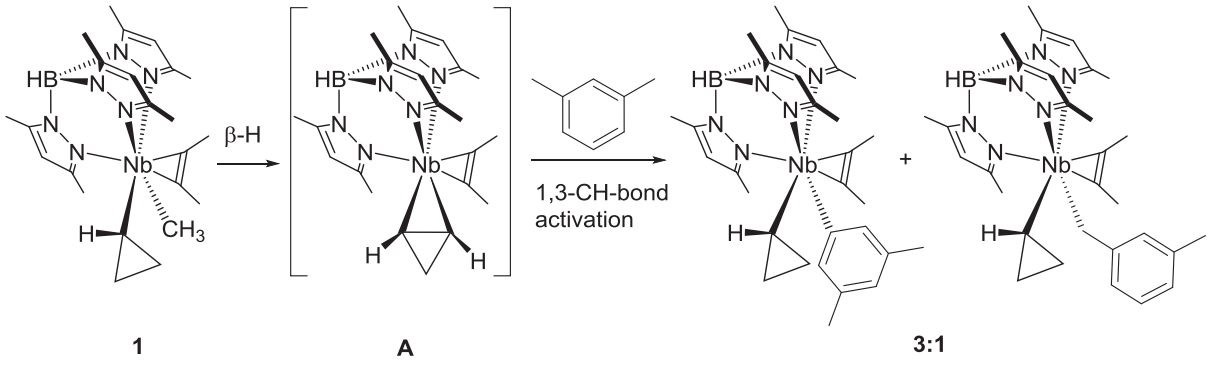

Scheme 3.2. *Aromatic and benzylic CH bond addition of 1,3-dimethylbenzene by **A**.*

Different from other η^2-alkene complexes, the cyclopropene niobium system is able to activate the CH bond of various hydrocarbons, including methane (Chapter 2), due to the unique interaction mode of cyclopropene with an early transition metal fragment. The strained C_3 ring, indeed, changes the properties of the alkene-based orbitals. Parallel computational study shows that the energy for β-H abstraction of methane from [Tp^{Me2}Nb(Me)(Et)(MeCCMe)] to form [Tp^{Me2}Nb(η^2-C_2H_4)(MeCCMe)] (**A_{et}**) (ΔG = –28 kJ·mol^{-1}) is more exergonic than β-H abstraction of methane from **1** to form **A** (ΔG = –1 kJ·mol^{-1}). This highlights the importance of the C_3 ring in decreasing the thermodynamic driving force for the initial β-H abstraction step, stabilizing the alkyl complex. Moreover, alkene complexes of early transition metals generally decompose rapidly via alkene loss, which is an obstacle for them to activate the CH bond of hydrocarbons. The fact that the ligand exchange reaction **A** + C_2H_4 →**A_{et}** + C_3H_4 is strongly endergonic (ΔG = +64 kJ/mol), clearly reflects that the interaction between the niobium center and the C=C π bond of cyclopropene is actually considerably stronger than that with ethylene, which allows **A** to have a lifetime long enough to activate the CH bond of hydrocarbons. In agreement with the energetic data, the Nb–C bond lengths in **A** (2.15 Å) are shorter than **A_{et}** (2.23 Å), while the Mulliken populations of +0.9 (Nb) and –0.31 (C) in **A** vs +0.72 and –0.22 in **A_{et}** indicate the greater charge transfer for the formation of the Nb–(cyclopropene) bond. Therefore, the unique geometric strain of **A** allows it to activate the C–H bond of hydrocarbons rather than to decompose via ligand loss.

Moreover, our group recently reported that a zirconium analogue of **A**, [$Cp_2Zr(\eta^2$-*c*-$C_3H_4)$], generated from the intramolecular β-H abstraction of Cp_2Zr(*c*-$C_3H_5)_2$, could selectively activate the CH bond of the more reactive furan or thiophene via 1,3-CH-bond activation (Scheme 3.3).[21]

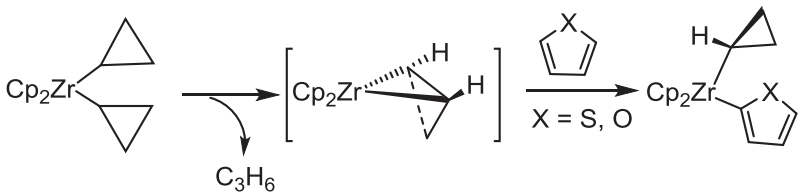

Scheme 3.3. *CH bond activation of furan and thiophene via β-H abstraction/1,3-addition pathway*

3.2- Objectives of this work

Here, we aimed to demonstrate that **A**, formed by β-H abstraction from **1**, was able to regioselectively activate the CH bond of a variety of unsaturated hydrocarbons including 1-alkene, 1-alkyne and heteroaromatics but also ferrocene and pentafluorobenzene via 1,3-CH-bond activation pathway to generate [Tp^{Me2}NbX(*c*-C_3H_5)(MeCCMe)] (X = 2-C_4H_3O (**4a**), 2-C_4H_3S(**4b**), 1-C_5H_7(**5**), PhC≡C(**6**), Fc(**7**), C_6F_5(**8**)) under mild conditions. These complexes were characterized by ^{1}H NMR, ^{13}C NMR, ^{19}F NMR spectroscopy, X-ray crystallography, elementary analysis. Moreover, thermolysis of **8** provided two unexpected isomeric products (**9a**,**b**) arising from cyclopropyl ring opening followed by alkyne coupling. The mechanism involved was investigated by computational analysis in collaboration with Dr. Abel Locati and Prof. Feliu Maseras (ICIQ, Tarragona, Spain). Electrochemical studies of **1**, **5**, **6**, and **7** were carried out to compare the electronic effect of the different unsaturated substituents to the metal center. This research was carried out in collaboration with Dr. Pascal Oulié, a former post-doctoral associate in our group.

3.3- CH bond activation of furan and thiophene

3.3.1- Synthesis of [Tp^{Me2}Nb(c-C_3H_5)(2-C_4H_3X)(MeCCMe)] (4a, X = O; 4b, X = S)

[Tp^{Me2}NbMe(*c*-C_3H_5)(MeCCMe)] (**1**) reacted with an excess of furan (4.7 equivalents) or thiophene (5.1 equivalents) to afford [Tp^{Me2}Nb(*c*-C_3H_5)(2-C_4H_3O)(MeCCMe)] **4a** and [Tp^{Me2}Nb(*c*-C_3H_5)(2-C_4H_3S)(MeCCMe)] **4b** as yellow powders in 62 % and 53 % yield, respectively (Scheme 3.4). Complexes **4a** and **4b** are stable at room temperature under Ar and they do not react with benzene even under mild heating (318 K).

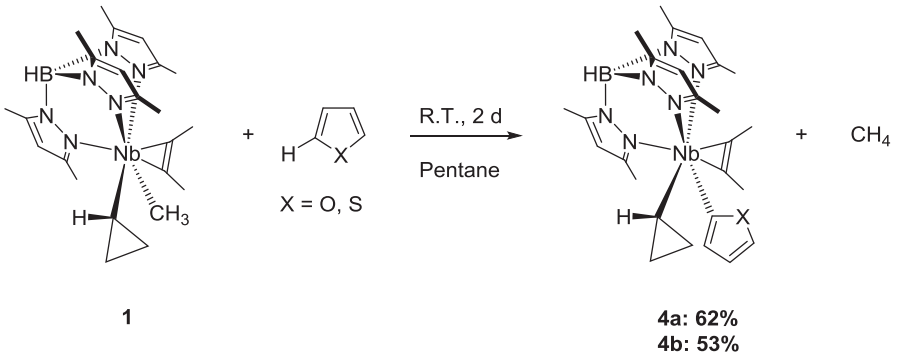

Scheme 3.4. *CH bond activation of furan and thiophene by **1**.*

3.3.2- ^{1}H NMR and ^{13}C NMR spectroscopy characterization of 4a and 4b

Complexes **4a** and **4b** were characterized by ^{1}H NMR and ^{13}C NMR in benzene-d_6 at 298 K. The ^{1}H NMR spectrum of **4a** confirms that the compound obtained is chiral (Figure 3.1). Like complex **1**,[6] the resonances of the C*H* and CH_3 protons of the pyrazoles show three singlets, integrating for one proton each, and six singlets, integrating for three protons each, respectively. The methyl protons of the alkyne resonate as singlets at δ 3.16 and 2.27 ppm. The five protons of the cyclopropyl group resonate as five multiplets. Interestingly, the 4-*H* (δ 6.21 ppm) resonates as a doublet of doublets and couples with both 5-*H* (δ 7.35 ppm) and 3-*H* (δ 6.50 ppm) ($J_{H–H}$ = 1.5 Hz and 3.0 Hz), indicating that CH bond activation occurs selectively at the α position (Scheme 3.4). The 3-*C* at δ 108.2 ppm (ddd, J_{CH} 169, 14, 6 Hz), 4-*C* at δ 120.5 ppm (dt, J_{CH} 168, 6 Hz) and 5-*C* at δ 142.3 ppm (ddd, J_{CH} 195, 11, 7 Hz, 5-*C*-furyl) give characteristic signals by ^{13}C NMR. A strongly niobium-broadened C2 resonance appears at δ 210.4 ppm. According to the 2D ROESY spectrum of [Tp^{Me2}NbPh(*c*-C_3H_5)(MeCCMe)], the protons at the β'-position (Hβ'), on the same enantioface of the cyclopropyl group as the niobium, are more deshielded than those at the β-position (Hβ) on the same face as Hα. Based on this assignment, we could distinguish in complex **4a** the Hβ and Hβ' in the cyclopropyl group at δ 1.36, 0.76 and δ 2.27, 1.51 ppm, respectively. The α proton Hα resonates at δ 2.03 ppm as a triplet of triplets. In the ^{13}C NMR spectra, the signals of the Cα, Cβ and Cβ carbons of the cyclopropyl group are observed at δ 72.2, 22.3, and 10.3 ppm.

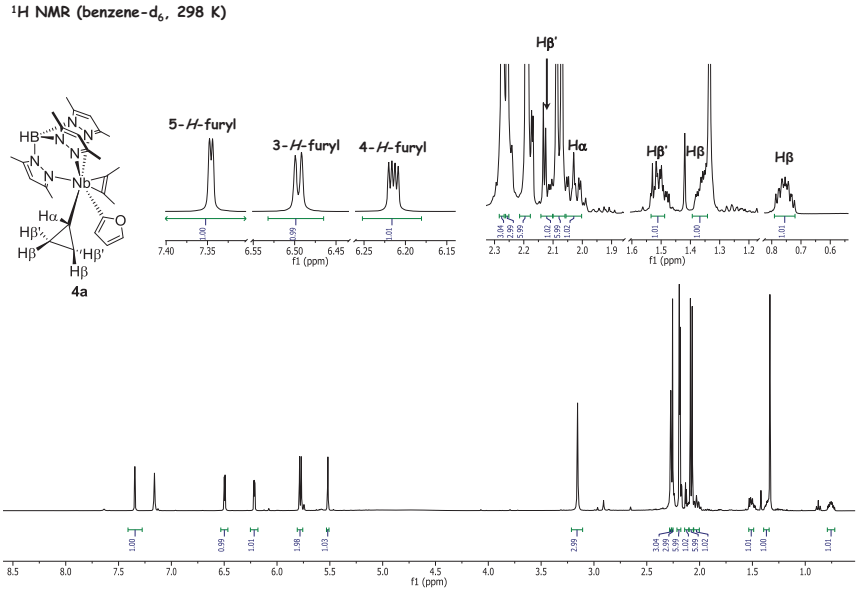

Figure 3.1. *^{1}H NMR of **4a** in benzene-d_6 at 298 K.*

The NMR characterization of **4b** is similar to that described above for complex **4a**. In the ^{1}H NMR, three thienyl signals at δ 7.57, 7.01, 6.85 ppm correspond to the protons 5-*H*, 4-*H*, and 3-*H,* respectively. The multiplets characteristic of the cyclopropyl group resonate at δ 2.52 (*c*-C$_3$*H*$_5$ β'), 2.25 (*c*-C$_3$*H*$_5$ α), 1.73(*c*-C$_3$*H*$_5$ β'), 1.50 (*c*-C$_3$*H*$_5$ β) and 0.96 (*c*-C$_3$*H*$_5$ β) ppm. In the ^{13}C NMR spectra, the signals of the Cα, Cβ and Cβ carbons of the cyclopropyl group are observed at δ 74.6, 22.4, and 12.3 ppm, respectively. There is no evidence for C–H agostic interactions with the Nb center. Signals for the thienyl group were observed at δ 136.0 (3-*C*), 129.0 (4-*C*), and 126.0 (5-*C*) ppm. However, the resonance for Nb-C2 was so broadened that it could not be observed. This is due to the coupling between ^{13}C (I = 1/2) and the quadrupolar ^{93}Nb (I=9/2).

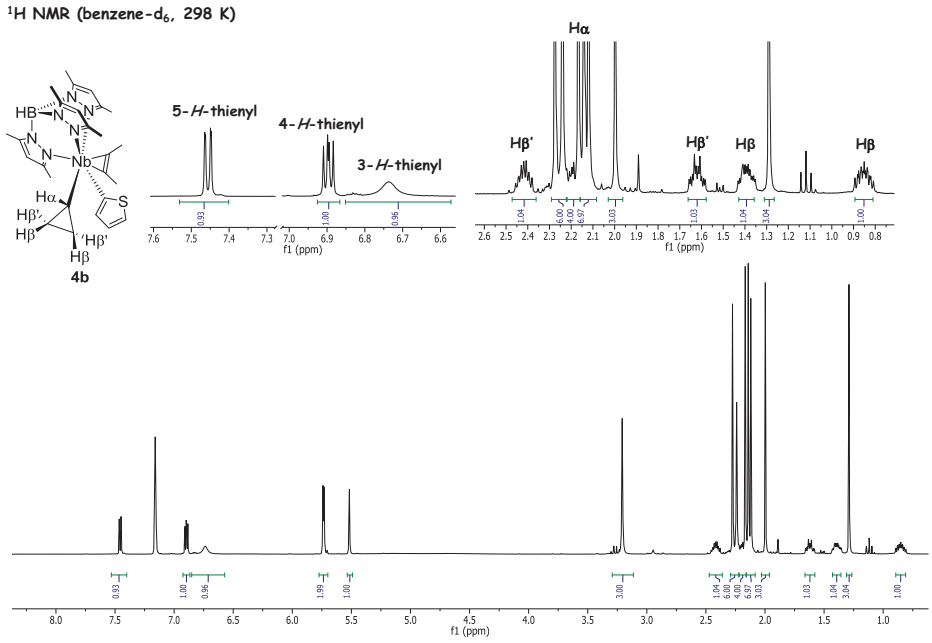

Figure 3.2. *^{1}H NMR of **4b** in benzene-d$_6$ at 298 K.*

3.3.3- Structural description

Yellow single crystals of **4a** suitable for X-ray characterization were obtained by slow evaporation of a pentane solution at –40 °C (Figure 3.3).The complex crystallizes in the space group P 21/n (monoclinic system).

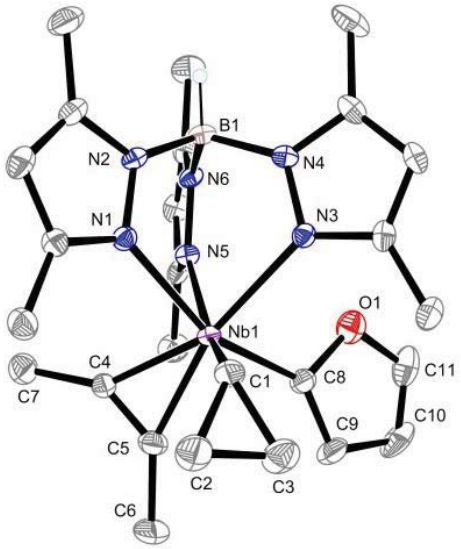

Figure 3.3. *ORTEP plot of the X-Ray structure of complex* ***4a****. Selected bond distances (Å) and angles (°):Nb–C1 2.179(4), Nb–C8 2.214(4), C1–C2 1.513(5), C1–C3 1.528(5), C2–C3 1.467(6), C8–C9 1.343(5), C9–C10 1.438(7), C10–C11 1.319(7), O1–C8 1.417(4), O1–C11 1.355(5), Nb–C8–O1 118.0*

Overall the structure is similar to previously described [Tp^{Me2}NbX(*c*-C_3H_5)(MeCCMe)] structures for which a distorted pseudooctedral coordination around the niobium is observed if the alkyne occupies one coordination site. Salient geometrical features include a planar 2-furyl ring, which approximately lies in the same plane as the *trans* dimethylpyrazolyl ring (N1N2 based), with the oxygen O1 directed *syn* to the Tp^{Me2} ligand. The 2-furyl is η^1-bound to the niobium (Nb1–C8 2.214(4) Å; Nb1–C8–O1 118.0(2)°). There is localized bonding in the furyl ring with short C8–C9 and C10–C11 bonds (1.343(5); 1.319(7) Å, respectively) and a long C9–C10 bond (1.438(7) Å). O1–C11 (1.355(5) Å) is significantly shorter than O1–C8 (1.417(4) Å). The conformation of the cyclopropyl ring is unremarkable (C3–C1–Nb1–C8 = –27°) as is the Nb–C1 bond (2.179(4) Å); there is no statistical difference between both Cα–Cβ bonds [C1–C3 1.528(5); C1–C2 1.513(5) Å]. There appears to be no structurally characterized group 5 furyl complexes. For early transition metals, an *ansa*–molybdenocene dihydride activates furan non selectively at position 2 and 3 by loss of H_2 followed by oxidative addition. The X-ray crystal structure of [$Me_2Si(C_5Me_5)_2MoH(2\text{-}C_4H_3O)$] was reported.[22] [$(C_5Me_5)_2YH]_2$ activates furan, most probably by σ-bond metathesis, to give ultimately the X-ray characterized compound [$(C_5Me_5)_2Y(2\text{-}C_4H_3O)$(thf)], which exhibits very similar bonding parameters within the 2-

furyl ligand as compared to **4a**.[23] (Y–Cα 2.436(9), Y–Cα–O 116.3(7), Cα–Cβ 1.333(15), Cγ–Cδ 1.270(2))

3.4- C–H bond activation of 1–alkyne and alkene.

3.4.1- Synthesis and characterization of [Tp^{Me2}Nb(c-C$_3$H$_5$)(CCPh)-(MeCCMe)] (5)

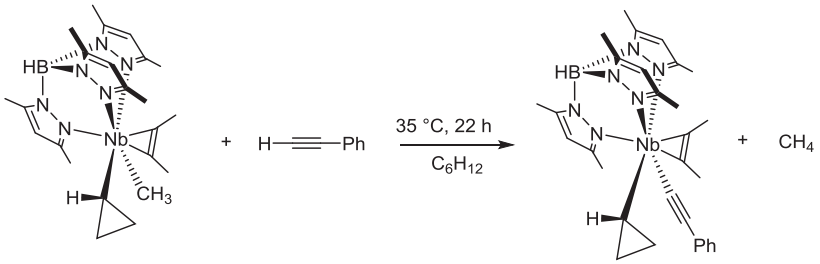

1 **5**

40%

Scheme 3.5**. C–H bond activation of phenylacetylene by **1

[Tp^{Me2}NbMe(*c*-C$_3$H$_5$)(MeCCMe)] reacted with phenylacetylene (50 equivalents) to afford the complex [Tp^{Me2}Nb(*c*-C$_3$H$_5$)(CCPh)(MeCCMe)] (5) as orange crystals in 40% yield (Scheme 3.5), which is stable under Ar in benzene solution at 318 K.

In addition to the signals assigned to the Tp^{Me2} and alkyne ligands, the ^{1}H NMR spectrum showed the three characteristic signals of the phenyl alkynyl ligand at δ 7.47 (*o*-C$_6$H$_5$), 7.02 (*m*-C$_6$H$_5$) and 6.94 (*p*-C$_6$H$_5$) ppm in a 2:2:1 ratio. The cyclopropyl group displays five multiplets at δ 2.25 (*c*-C$_3$*H*$_5$β'), 2.18 (*c*-C$_3$*H*$_5$α), 1.37 (*c*-C$_3$*H*$_5$β'), 1.29 (*c*-C$_3$*H*$_5$β) and 0.71 (*c*-C$_3$*H*$_5$β) ppm (Figure 3.4). In the ^{13}C spectrum, the signals corresponding to the Cα, Cβ and Cβ carbons of the cyclopropyl group are observed at δ 77.9 ($^1J_{CH}$ 146 Hz), 23.2 ($^1J_{CH}$ 159, 163 Hz) and 8.4 ($^1J_{CH}$ 159, 163 Hz) ppm, respectively. Moreover, the characteristic resonances of the Nb*C*αCPh and NbC*C*βPh carbon atoms are observed at δ 149.2 and 125.9 ppm, respectively. No sign of aryl activation was seen.

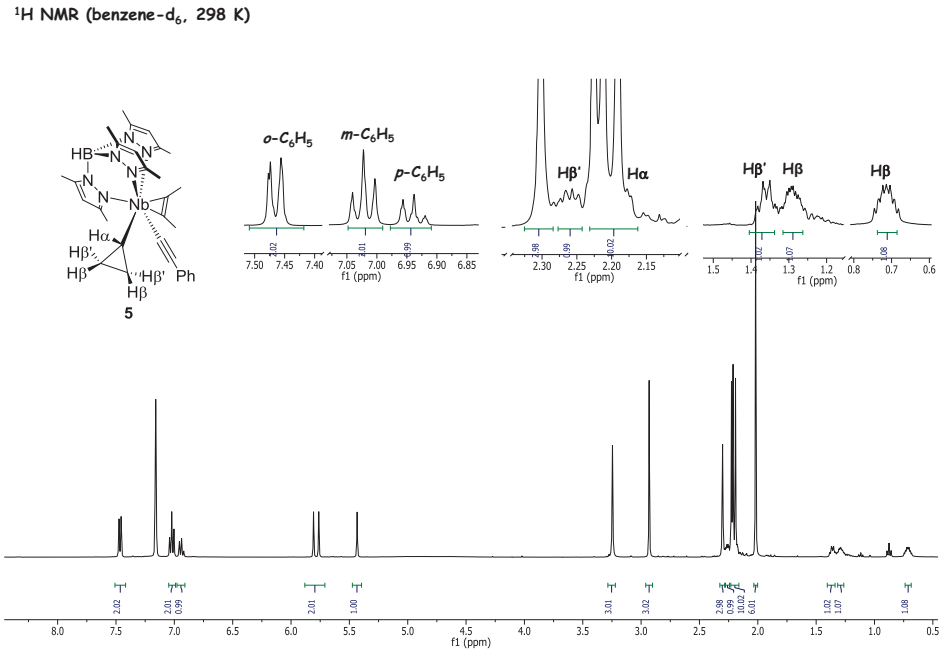

Figure 3.4. *^{1}H NMR of [Tp^{Me2}Nb(CCPh)(c-C$_3$H$_5$)(MeCCMe)] (**5**) in benzene-d$_6$ at 298 K.*

Orange single crystals of **5** suitable for a X-ray crystal structure determination were obtained by slow evaporation of a pentane solution at –40 °C (Figure 3.5).

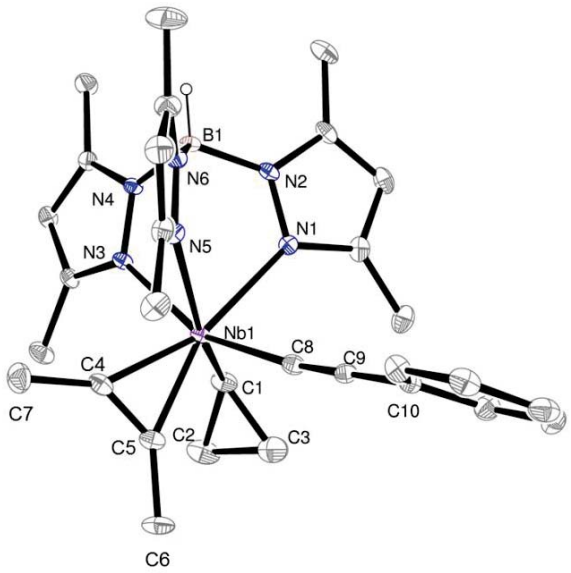

Figure 3.5. *ORTEP plot of the X-Ray structure of complex **5**. Selected bond distances (Å) and angles (°): Nb–C1 2.173(4), Nb–C8 2.197(4), C1–C2 1.490(6), C1–C3 1.528(7), C2–C3 1.479(8), C8–C9 1.206(5), Nb1–C8–C9 172.5(3), C8–C9–C10 179.0(4)°*

The overall structure is similar to that of **1** and **4**. An almost linear (Nb1–C8–C9 172.5(3)°, C8–C9–C10 179.0(4)°) phenyl alkynyl (C8–C9 1.206(5) Å) is η^1-bound to the niobium (Nb1–C8 2.197(4) Å). Remarkably the niobium–cyclopropyl bond is even shorter than the Nb–alkynyl bond. The two Cα–Cβ bonds of the cyclopropyl group (C1–C2, 1.490(6), C1–C3 1.528(7) Å) are barely different. Similar data were reported for two other structurally characterized niobium complexes containing the phenylalkynyl ligand Nb–CCPh ([Cp'$_2$Nb(NPh)(CCPh)]: Nb–Cα–Cβ 177.9(6), Cα–Cβ–Cγ 175.4(8)°; Nb–Cα 2.170(7), Cα–Cβ 1.20(1) Å;[24] Nb–Cα–Cβ 167.5(7), Cα–Cβ–Cγ 179.5(9)°; Nb–Cα 2.173(8), Cα–Cβ 1.190(10) Å).[25]

3.4.2- Synthesis and characterization of [Tp^{Me2}Nb(c-C$_3$H$_5$)(c-1-C$_5$H$_7$)-(MeCCMe)] (6)

1 also activates the weaker non-conjugated C*sp*^{2}–H bond of cyclopentene under similar conditions to give the cyclopentenyl complex [Tp^{Me2}Nb(*c*-C$_3$H$_5$)(*c*-1-C$_5$H$_7$)-(MeCCMe)] (**6**) in 66% yield, which can react with benzene solution at 318 K.

In the ^{1}H NMR spectrum, **6** exhibits a broad singlet at δ 6.29 assigned to NbC=C*H* as well as five multiplets at δ 2.03 (*c*-C$_3$*H*$_5$ β'), 1.76 (*c*-C$_3$*H*$_5$ α), 1.49 (*c*-C$_3$*H*$_5$ β'), 1.35 (*c*-C$_3$*H*$_5$ β) and 0.89 (*c*-C$_3$*H*$_5$ β) ppm corresponding to the diastereotopic protons of the cyclopropyl group (Figure 3.6). In the ^{13}C NMR spectrum, the Cα, Cβ and Cβ carbons of the cyclopropyl group resonate at δ 66.5, 21.1 and 12.3 ppm, respectively. The signals of Nb*C*α=CH and NbC=*C*βH were observed at δ 201.6 and 136.4 ppm, respectively, the latter being a doublet with $^1J_{CH}$ = 160 Hz.

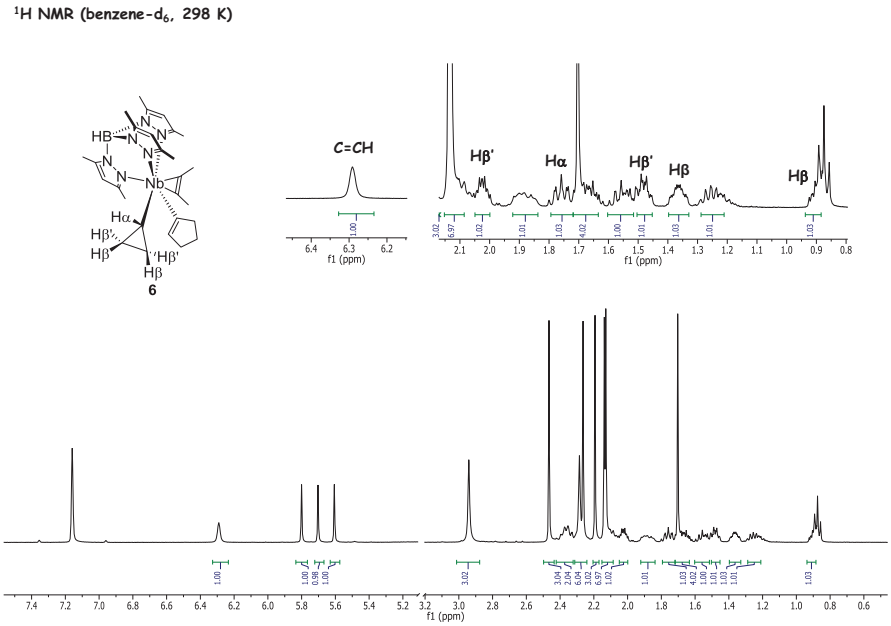

Figure 3.6. *^{1}H NMR of [Tp^{Me2}Nb(c-C$_3$H$_5$)(c-1-C$_5$H$_7$)(MeCCMe)] (6) in benzene-d$_6$ at 298 K.*

Yellow single crystals of **6**, suitable for an X-ray crystal structure determination, were obtained by slow evaporation of a pentane solution at –40 °C (Figure 3.7).

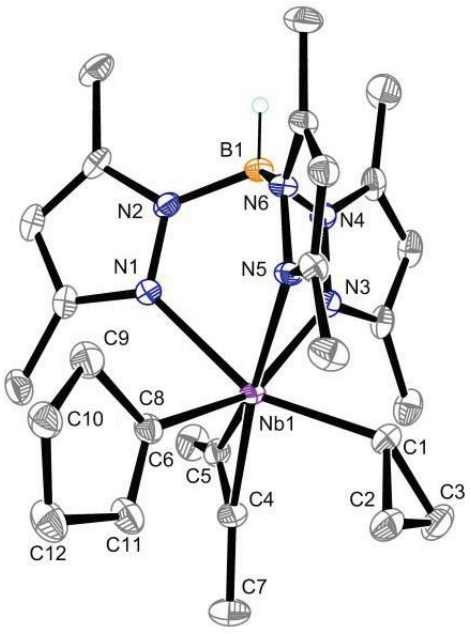

Figure 3.7. *ORTEP plot of the X-Ray structure of complex **6**. Selected bond distances (Å) and angles (°): Nb–C1 2.177(2), Nb–C8 2.230(2), C1–C2 1.501(3), C1–C3 1.537(3), C2–C3 1.480(4), C8–C9 1.509(3), C8–C11 1.351(3), Nb1–C8–C11 126.61(16), Nb1–C8–C9 126.02(15)°*

The η^1-1-cyclopentenyl ligand [C8-C12] sits approximately in the same plane as that of the *trans* dimethylpyrazolyl ring (N3N4 based). The C8–C11 bond length is consistent with that of a carbon–carbon double bond and it is unremarkable as compared to those of other alkenyl niobium complexes [6,26–29] The Nb–C8 bond length of 2.230(2) Å is similar to that described in related six-coordinate $Tp^{Me2}Nb$ vinyl complexes such as [Tp^{Me2}NbCl{NP(iPr$_2$)$_2$}(CPh=CEt$_2$)] 2.252(7) Å, [Tp^{Me2}NbO{CMe=CMeCH(CH$_2$CHCMe$_2$)-CMe$_2$O}] 2.235(4) Å.[6,26] They are slightly shorter than those reported for 18e niobiocene derivatives such as [Cp$_2$Nb(CO){*Z*-C(CO$_2$Me)=CH(CO$_2$Me)}] 2.295(3) Å; [Cp$_2$Nb-(Me$_3$SiCCSiMe$_3$){*E*-C(CO$_2$Me)=CH(CO$_2$Me)}] 2.297(5) Å;)[28,29] but not as short as that revealed in the five-coordinate square pyramidal complex [(BDI)NbBr(NtBu)(*E*-CPh=CHMe)] 2.155(3) Å.[27] The two Cα–Cβ bonds in the cyclopropyl ring are statistically different [C1–C2 1.501(3), C1–C3 1.537(3) Å], pointing at a possible α–CC agostic interaction. There is again a short niobium–cyclopropyl bond Nb1–C1 of 2.177(2) Å.

3.5- CH bond activation of ferrocene

We have been looking for convenient internal standards for kinetic studies on these and related reactions. Among other compounds, ferrocene (FcH), seemed a suitable candidate due to its ease of handling, its stability and inertness and its single ^{1}H NMR signal in a region devoid of reactant or product signals belonging to the [Tp^{Me2}NbR(*c*-C$_3$H$_5$)(MeCCMe)] family. In a control experiment, we were surprised to see that **1** was very competent to activate a CH bond of FcH.

3.5.1- Synthesis and characterization of [Tp^{Me2}Nb(Fc)(c-C$_3$H$_5$)(MeCCMe)](7)

Tp^{Me2}NbMe(*c*-C$_3$H$_5$)(MeCCMe) reacted with ferrocene (2 equivalents) over 6 h at 325 K, affording the dinuclear complex [Tp^{Me2}Nb(Fc)(*c*-C$_3$H$_5$)(MeCCMe)] (**7**) in 42% yield (Scheme 3.6).

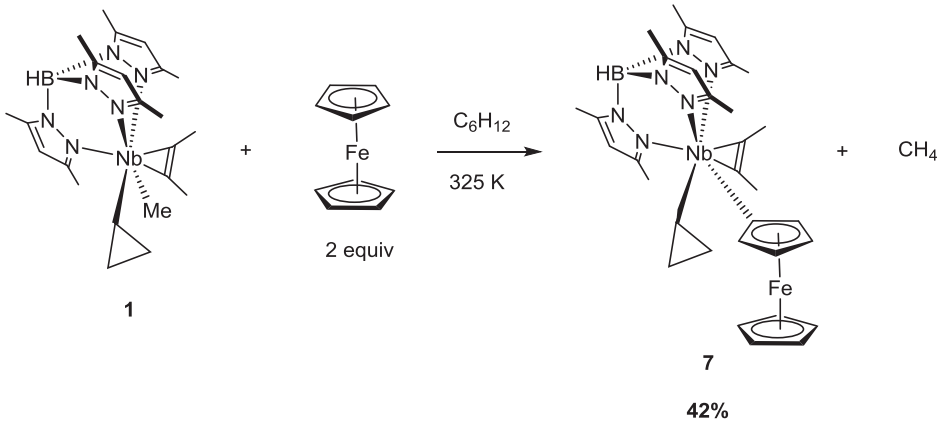

Scheme 3.6. *CH bond activation of ferrocene by* ***1***

Complex **7** was characterized by spectroscopic means and by X-ray crystallography. The metallated cyclopentadienyl moiety of **7** shows three signals in the ^{1}H NMR spectrum at 283 K for the 4 diastereotopic protons at δ 4.32, 3.74 (d, $^{2}J_{HH}$ = 1.4 Hz, 1 H each) and 4.05 (t, $^{2}J_{HH}$ = 1.4 Hz, 2 H each) ppm while the η^{5}-Cp ring gave a single resonance at δ 4.09 ppm (Figure 3.8). The diastereotopic protons of the cyclopropyl group appear as multiplets at δ 2.21 (*c*-C_3H_5 β'), 1.70 (*c*-C_3H_5 α), 1.41 (*c*-C_3H_5 β'), 1.27 and 0.96 (*c*-C_3H_5 β) ppm (Figure 3.6). In the^{13}C NMR spectrum of **7**, the Cα, Cβ and Cβ carbons of the cyclopropyl group give three signals at δ 67.2, 21.7, and 12.5 ppm, respectively. The niobium-bound carbon was not observed, whereas the other four carbons of the metallated ring were found at δ 80.0, 78.3, 68.6 and 68.0 ppm as doublets with $^{1}J_{CH}$ = 172 Hz.

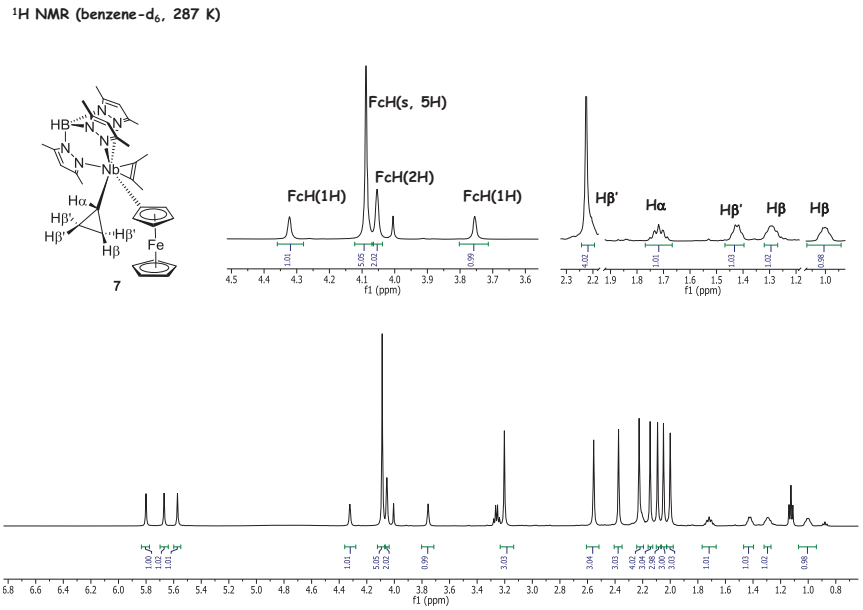

Figure 3.8. *^{1}H NMR of* ***7*** *in benzene-d_6 at 287 K.*

Complex **7** is very stable but it was found to react slowly with benzene. After 14 h at 287 K, the ^{1}H NMR spectra of **7** in benzene-d_6 shows the appearance and growth of the FcH signal together with a mixture of the [$Tp^{Me2}Nb(C_6D_5)$(*c*-C_3H_4D)(MeCCMe)] and compound **7** resonances in a ca. 1.8:1 ratio (Scheme 3.7).

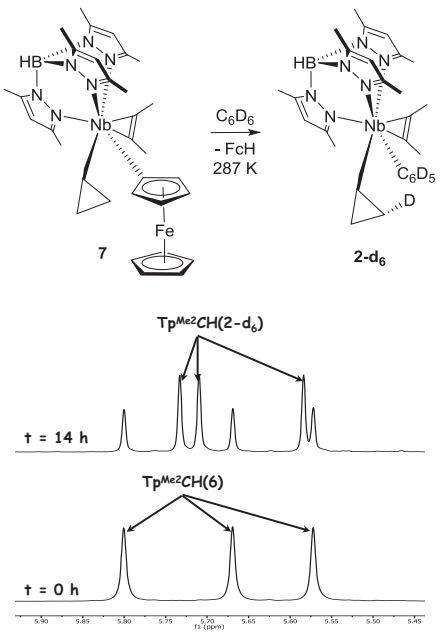

Scheme 3.7. *Reaction of 7 with benzene-d_6 at 287 K.*

Purple single crystals of **7**, suitable for an X-ray crystal structure determination, were obtained by slowly adding pentane into a saturated solution of **7** in cyclohexane and further cooling at –40 °C (Figure 3.9).

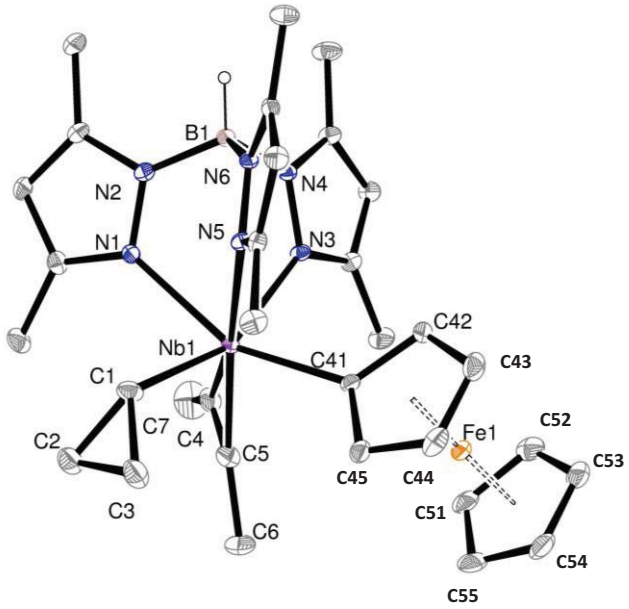

Figure 3.9. *ORTEP plot of the X-Ray structure of complex 7. Selected bond distances (Å) and angles (°): Nb–C1 2.201(5), Nb–C41 2.211(5), C1–C2 1.499(7), C1–C3 1.518(7), C2–C3 1.493(8), Fe1–C41 2.131(4), Fe1–C42 2.069(5), Fe1–C43 2.034(5), Fe1–C44 2.021(5), Fe1–C45 2.034(5), N1Nb1C41C42 –17°*

As shown in Figure 3.9, metric parameters in [Tp^{Me2}NbR(*c*-C_3H_5)(MeCCMe)] exhibit similar features when R = Fc in **7** and R = Ph in **2**.[20] The Nb–C bond with the cyclopropyl ring in **7**, Nb1–C1 (2.201(5) Å), is identical to that in **2** (2.196(4) Å) and the Nb–C bond with the ferrocenyl group in **7,** Nb–C41 (2.211(5) Å), is slightly shorter than the Nb–C_{Ph} bond in **2** (2.254(4) Å) and similar to the Nb–$C_{alkynyl}$ bond in **6** (2.230(2)). A related behavior was noted in titanocene compounds, where the Ti–Fc bond of the [Cp_2TiFc_2] complex (2.19 Å) is shorter than the Ti–Ph bond of the [Cp_2TiPh_2] compound (2.27 Å).[30] The ferrocenyl moiety does not perfectly sit in a wedge between two pyrazolyl rings as observed for **2** and **6** (torsion angle N1Nb1C41C42 = –17°) most probably because of a steric clash with a pendant methyl group of the N3N4-based pyrazolyl ring. On the ferrocenyl side, the niobium–bound carbon C41 is displaced 0.035 Å away from the mean plane formed by the four other carbon atoms of the ring. The C41 to Fe distance (Fe1–C41 2.131(4) Å) is significantly elongated with respect to the other four carbons in the ring (Fe1–C42 2.069(5), Fe1–C43 2.034(5), Fe1–C44 2.021(5), Fe1–C45 2.034(5) Å). Fe–C distances in the other eclipsed ring are in the range 2.033(5) – 2.067(5) Å. The C41–C42 and C41–C45 bonds (1.442(7) and 1.445(7) Å, respectively) are

longer than the C43–C44 and C44–C45 distances (1.403(8) and, 1.415(7), respectively) and the five C–C bonds in the other Cp ring, range 1.405(8) – 1.425(8) Å.

3.6- CH bond activation of pentafluorobenzene

3.6.1- Synthesis and characterization of [Tp^{Me2}Nb(C$_6$F$_5$)(c-C$_3$H$_5$)-(MeCCMe)] (8)

Given the ease with which different types of CH bonds were cleaved by intermediate **A**, we were interested to study whether it might be reactive also towards CF bonds.[31–33] Hexafluorobenzene showed no sign of reaction with **1** under similar conditions such as those described herein for other hydrocarbons; only decomposition of **1** occurred upon heating at higher temperatures. We then suggested that CF bond cleavage might be facilitated, at least entropically, after an initial CH bond cleavage in a mixed hydrofluoroarene. In this vein, we reacted **1** with pentafluorobenzene (Scheme 3.8). [Tp^{Me2}NbMe(*c*-C$_3$H$_5$)(MeCCMe)] reacted with C$_6$F$_5$H (24 equiv) affording, after 72h of stirring at room temperature, the yellow [Tp^{Me2}Nb(C$_6$F$_5$)(*c*-C$_3$H$_5$)(MeCCMe)] (**8**) complex in 60% yield.

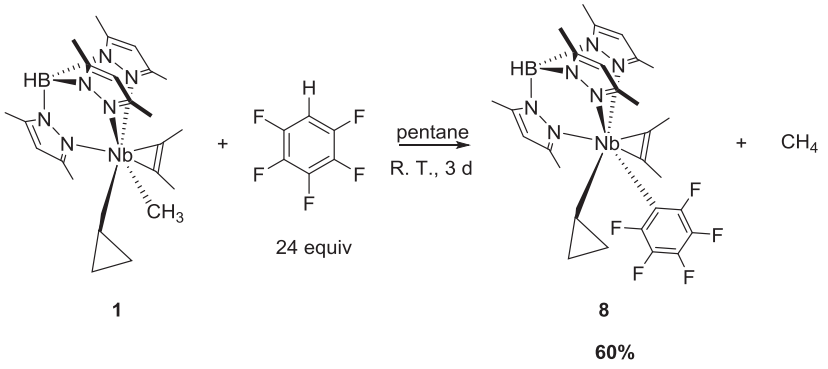

Scheme 3.8. *CH bond activation of pentafluorobenzene by **1**.*

The ^{1}H NMR spectrum of **8** is shown in Figure 3.10. One of the alkyne methyl groups shows through-space coupling with one fluorine appearing as a doublet (J_{HF} = 5.6 Hz) at δ 2.88 ppm. The resonances for the diastereotopic protons of the cyclopropyl group appear as multiplets at δ 2.72(*c*-C$_3$*H*$_5$ α), 2.47(*c*-C$_3$*H*$_5$ β'), 1.65(*c*-C$_3$*H*$_5$ β'), 1.53 (*c*-C$_3$*H*$_5$ β) and 0.24 (*c*-C$_3$*H*$_5$ β) ppm (Figure 3.11). Again, the niobium-bound carbon of C$_6$F$_5$ is not observed in the ^{13}C{^{1}H} NMR spectrum of **8**. The Cα, Cβ and Cβ carbons of the cyclopropyl group resonate at 86.6, 24.9, and 2.1 ppm, respectively. One of the niobium-bound alkyne carbon δ 23.2 ppm (d, J_{CF} = 10.7 Hz) and one of the cyclopropyl Cβ at δ 2.1 ppm (d, J_{CF} = 10.2 Hz) shows

through-space coupling to one fluorine. Five fluorine signals in the δ –100.2 - –163.2 ppm range attributable to the pentafluorophenyl NbC_6F_5 group are observed in the $^{19}F\{^1H\}$ NMR spectrum at room temperature consistent with slow rotation around the Nb–C_6F_5 bond in **8**.

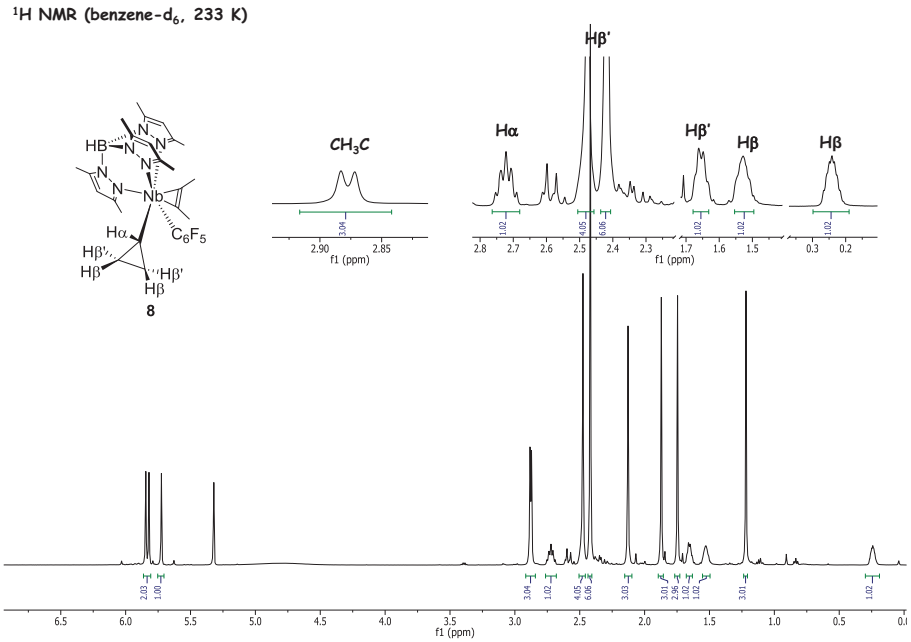

Figure 3.10. *^1H NMR of **8** in benzene-d_6 at 243 K.*

3.6.3- Isomerization of 8. Synthesis and characterization of [Tp^{Me2}Nb(C_6F_5)]–HC(CH_3)–HC=C(CH_3)–(CH_3)C=Nb] (9a, 9b)

Upon gentle heating in benzene at 45°C, **8** underwent an intramolecular cyclopropyl ring opening and 2-butyne coupling to give an inseparable 88:12 mixture of two regioisomers **9a** and **9b**, respectively (Scheme 3.9). This ratio was consistently found when repeating the reaction under identical conditions. The interpretation of spectroscopic data and the identity of **9a** and **9b** was ascertained by a X-ray diffraction analysis on a single crystal (see below). This behavior differs from that of the phenyl derivative **2**, which, in the presence of C_6D_6, undergoes reversible β-H abstraction of the cyclopropyl to form benzene and **A**, which activates the C–D bond of C_6D_6 to form **2**-d_6.[6]

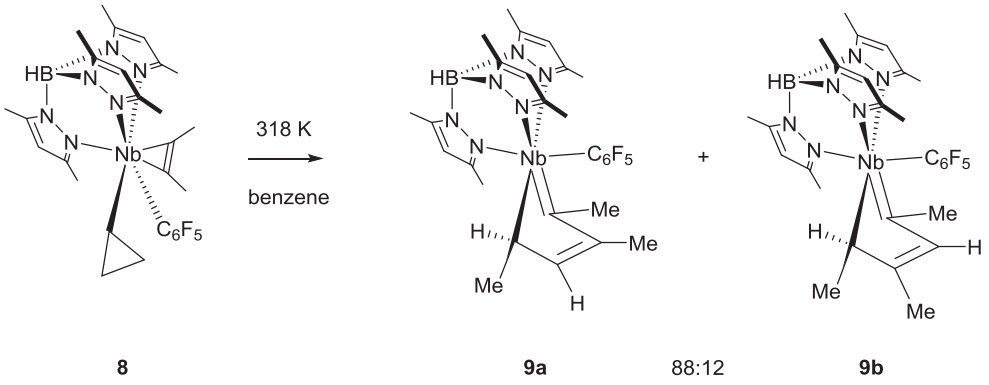

Scheme 3.9. *Isomerization of* ***8*** *to* ***9a*** *and* ***9b***

In the ^{1}H and ^{13}C NMR spectra of **9a** and **9b** in benzene-d_6, each set of the Tp^{Me2}CH hydrogens and carbons appears in a 1:1:1 ratio in accordance with the lack of a plane of symmetry in these niobacycles. In the ^{1}H NMR of **9a**, the major isomer, (Figure 3.11), the characteristic Hγ proton (m, δ 6.09 ppm) is in a *trans*-disposition to the Hδ proton (dd, δ 1.05 ppm). The Hδ proton couples with the Hγ proton ($^{3}J_{HH}$ = 12 Hz) but also to the methyl group (δ 2.40 ppm) bound to the same Cδ atom ($^{3}J_{HH}$ = 6 Hz). The CH_3 attached to Cα and Cβ resonate at δ 2.13 and 2.65 ppm, respectively.

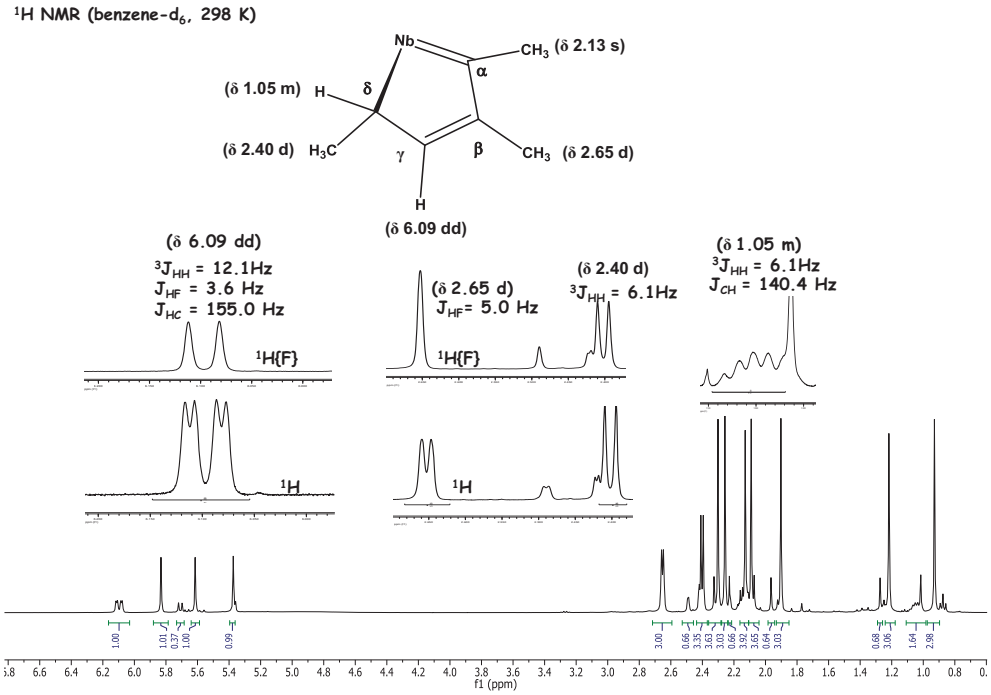

Figure 3.11. *^{1}H NMR of* ***9a*** *in benzene-d_6 at 298 K*

The ^{13}C NMR spectrum shows a deshielded NbCα with an alkylidene character at δ 260.2 ppm as well as the sequence of the three other carbons along the ring, the sp^2 Cβ (δ 120.0 ppm) and Cγ (δ 101.6 ppm, dd, $^1J_{CH}$ = 155 Hz) and the sp^3 Cδ (δ 87.3). The methyl groups attached to the quaternary carbons Cα and Cβ resonate at δ 24.4 and 22.9 ppm, respectively, whereas the methyl group attached to the tertiary carbon Cδ at δ 21.1. These data match perfectly those of the allyl-rearranged product [Tp^{Me2}NbCl(=CPh–CMe=CH–CHMe)].[34]

The ^{19}F NMR spectrum of **9a** in benzene-d_6 shows the characteristic signals of the C_6F_5 ring: two *ortho*-fluorines at δ –115.7 (dt) and –109.5 (br d) ppm, two *meta*-fluorines at δ –163.0 (m) and –164.1 (m) ppm and one *para*-fluorine at δ -158.3 (t) ppm (Figure 3.12). The minor peaks belong to the fluorine signals of the C_6F_5 ring of **9b**: two *ortho*-fluorines at δ –104.7 (dt) and –115.7 (dt) ppm, two *meta*-fluorines at δ –163.4 (m) and –164.3 (m) ppm and one *para*-fluorine at δ -158.4 (t) ppm.

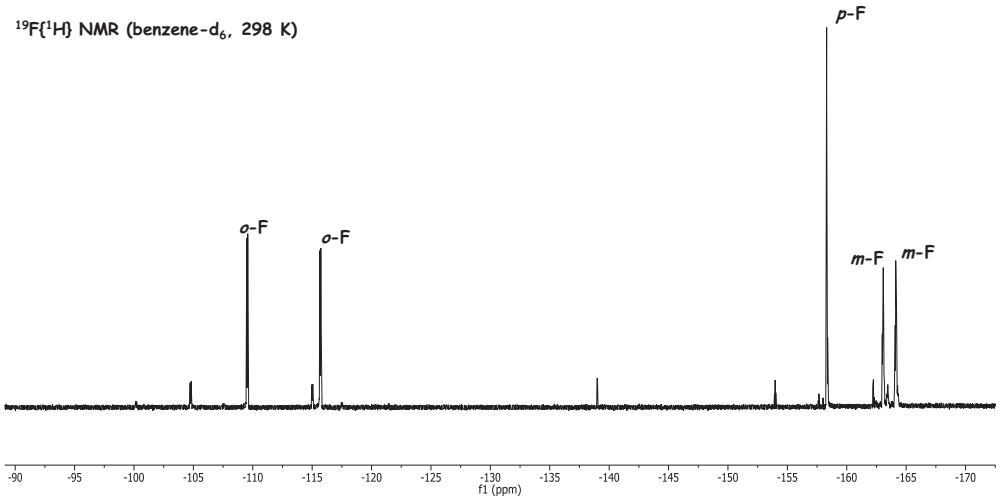

***Figure 3.12**. ^{19}F NMR of a mixture of **9a** and **9b** (molar ratio 88:12) in benzene-d_6 at 298 K.*

The β-Me group as well as the γ-CH group display additional through-space couplings with one fluorine from the C_6F_5 ring that sits on top of the metallacycle, with J_{HF} and J_{CF} of 5, 15 Hz and 4, 6 Hz, respectively. The ^1H-^{19}F HOESY spectrum (Figure 3.13) shows that these protons correlate with the *ortho*-fluorine at δ –115.7 (dt) and δ –109.5 (br d). The latter sharpens to a doublet of triplets upon ^1H decoupling.

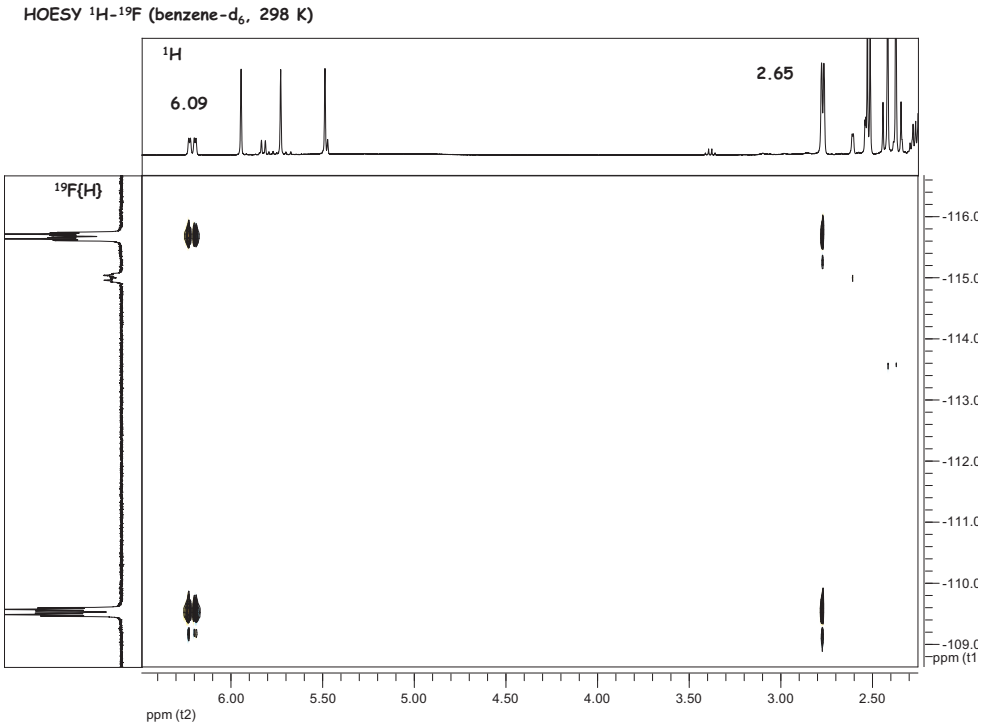

Figure 3.13. *^{1}H-^{19}F HOESY of **9a** in benzene-d_6 at 298 K*

Concerning complex **9b**, definitive assignment of the position of the hydrogens and methyl groups along the metallacycle follows form a comparison of the NMR data with those for **9a**. Scheme 3.10 shows the overall ^{1}H NMR and ^{13}C NMR characterization of **9b**.

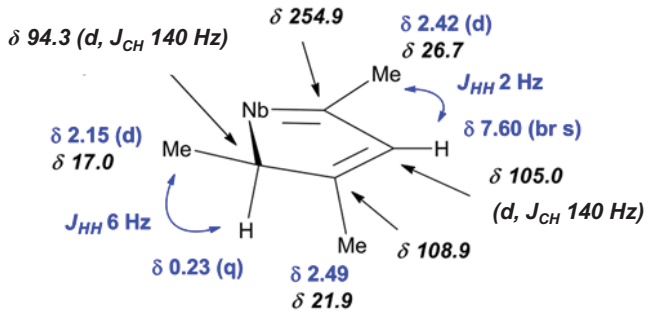

9b

Scheme 3.10. *^{1}H NMR and ^{13}C NMR characterization of **9b**.*

Strikingly, Hβ and Hδ (δ 7.06 and δ 0.23, respectively) are not coupled and are thus isolated from one another. The former couples to the α-Me protons while the latter couples with the δ-Me protons as for **9a**. Additional through-space ^{1}H-^{19}F couplings to C_6F_5 are observed for the Hβ (J_{HF} = 2.6 Hz, J_{CF} = 9.5 Hz) and γ-CH_3 protons in the ^{1}H NMR and ^{1}H-

^{19}F HOESY spectra. Given the low concentration of **9b**, the gated ^{13}C{^{19}F} NMR spectrum did not yield reliable $^{1}J_{CH}$ but all the carbons of the niobiacycle were observed.

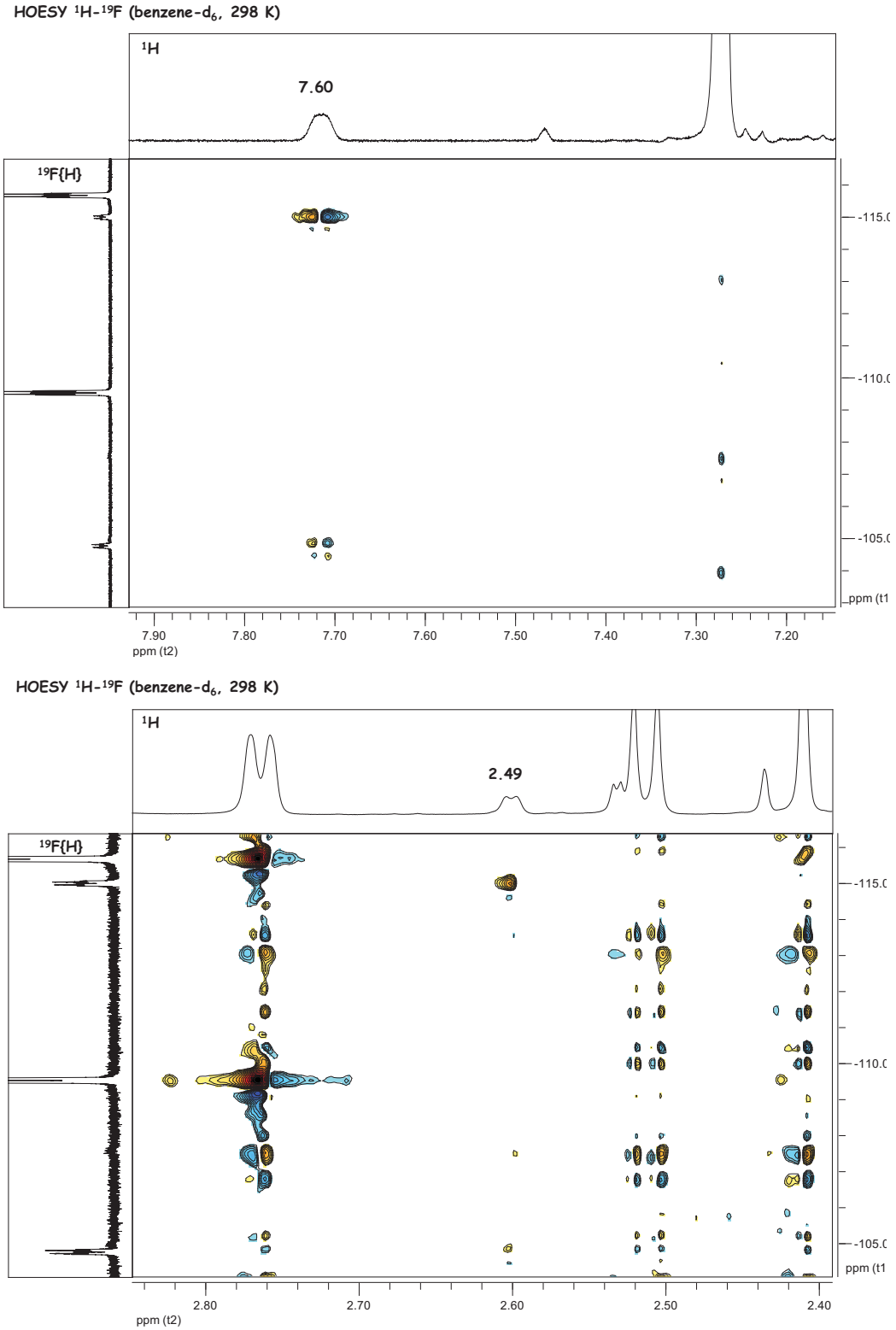

Figure 3.14. *^{1}H-^{19}F HOESY of **9a** in benzene-d_6 at 298 K*

In order to see whether **9a** could be converted to **9b** through intramolecular hydrogen migration between the α and δ positions of **9a** or **9b** under heating, a variable temperature (VT) ^{1}H NMR study has been carried out in the 298 – 343 K temperature range on the mixture of complexes **9a** and **9b** (ratio of 88:12) (Scheme 3.12). No broadening of the peaks of **9b** was noted, especially the signal of the Hβ proton at δ 7.60 (Scheme 3.12), indicating that **9a** and **9b** do not interconvert through intramolecular hydrogen migration. Therefore, **9a** and **9b** must be formed from **8** by different pathways.

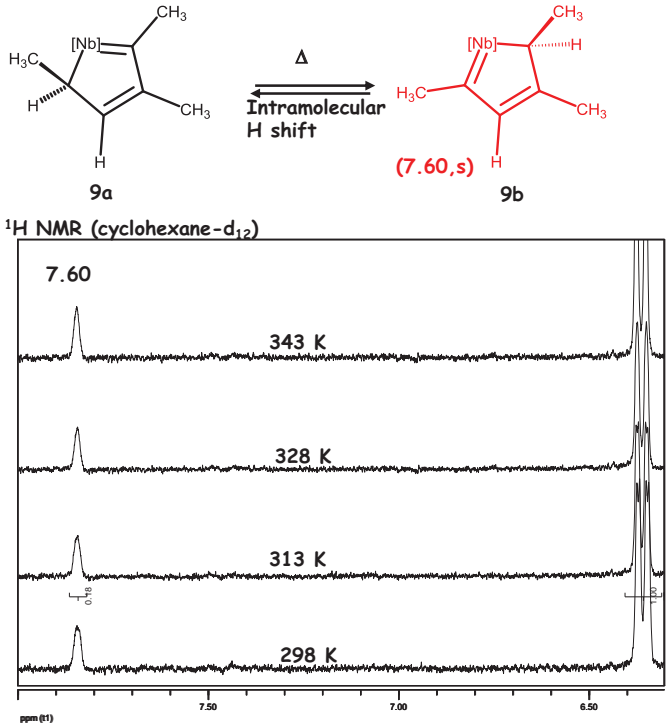

Scheme 3.12. *Low field expansion of the VT ^{1}H NMR spectra of a mixture of **9a** and **9b** (ratio of 88:12).*

Orange single crystals of **9a** and **9b**, suitable for an X-ray crystal structure determination, were obtained by slow evaporation of a pentane solution of **9a** and **b** at –40 °C (Figure 3.15).

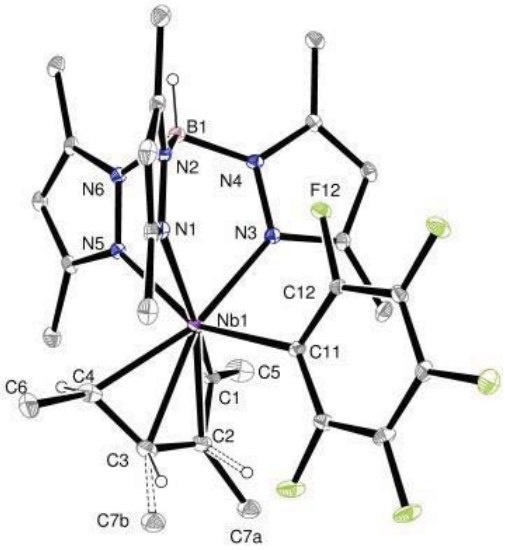

Figure 3.15. *ORTEP plot of the X-Ray structure of complex* ***9a,b****. Selected bond distances (Å) and angles (°): Nb–C1 2.002(5), C1–C2 1.412(6), C1–C5 1.472(6), Nb–C2 2.348(4), C2–C3 1.421(6), Nb–C3 = 2.347(4), C2–C7a 1.493(2) C3–C7b 1.42(4), Nb–C4 2.226(4) C3–C4 1.428(7), C4–C6 1.501(7), Nb–C11 2.344(4), C1–C11 2.345(6), C1C2C3C4 9.9°.*

The noteworthy features are (i) the disordered η^4–trimethylbutadienyl unit and (ii) the presence of pentafluorophenyl ring. The latter is perpendicular (88°) to the planar (C1–C2–C3–C4 10°) four-membered niobacycle and sits above the Cα (C2) and Cβ (C3) carbons and their hydrogen and methyl substituents, justifying the through-space couplings observed with the *ortho* fluorine atoms in the NMR spectra. The observed disorder was successfully modelled in a 88 (**9a**):12 (**9b**) ratio of two occupancies of methyl groups C7a on C2 (H3 on C3) and C7b on C3 (H2 on C2). The disorder does not involve any other atoms in the structure most particularly those of the metallacycle. The ratio observed in the solid state, therefore, matches that observed in solution. The five-membered niobacycle is folded around the C1–C4 axis (113°) so that all four carbons are at bonding distance of the niobium. There is a Nb–C double bond between Nb1 and C1 (Nb1–C1 = 2.002(5) Å) and a Nb–C single bond between Nb1 and C4 (Nb1–C4 = 2.226(4) Å). The C2 and C3 atoms interact symmetrically with the niobium center (Nb1–C2 2.348(4), Nb1–C3 2.347(4) Å). All C–C bonds in the four-carbon chain are identical pointing to a fully delocalized picture (C1–C2 1.412(6), C2–C3 1.421(6), C3–C4 1.428(7) Å). These parameters are similar to those reported for the η^4-butadienyl [Tp^{Me2}NbCl(=CPh–CMe=CH–CHMe)] complex[34] (Nb=Cα 1.993(4), Nb–Cβ 2.334(4), Nb–Cγ 2.370(5), Nb1–Cδ 2.277(5), Cα–Cβ 1.439(7), Cβ–Cγ 1.418(6), Cγ–Cδ 1.392(7)) and are consistent with the limiting structures in Scheme 3.11.

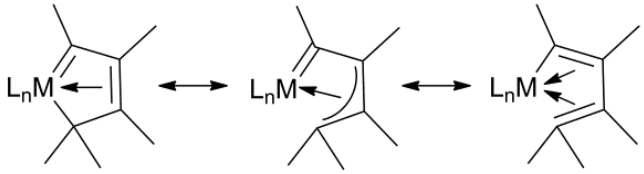

Scheme 3.11. *Limiting structures for* ***9a,b***

3.7- Electrochemistry

Electrochemical studies carried out with Dr Alix Sournia-Saquet at the LCC were conducted to probe the influence of the hydrocarbyl ligand R (Me, *c*-C_5H_7, CCPh, Fc) on the redox properties of [Tp^{Me2}NbR(*c*-C_3H_5)(MeCCMe)] **1**, **5**, **6** and **7** but also the influence of the fragment [Tp^{Me2}Nb(*c*-C_3H_5)(MeCCMe)] on the redox properties of Fc. The cyclic voltammogram (CV) of **7**, including FcH (0.55 V vs SCE) as a reference, is shown in Figure 3.16. It has been carried out in THF, with ca. 0.08 M [*n*-Bu_4N][PF_6] as supporting electrolyte at a Pt disc electrode.

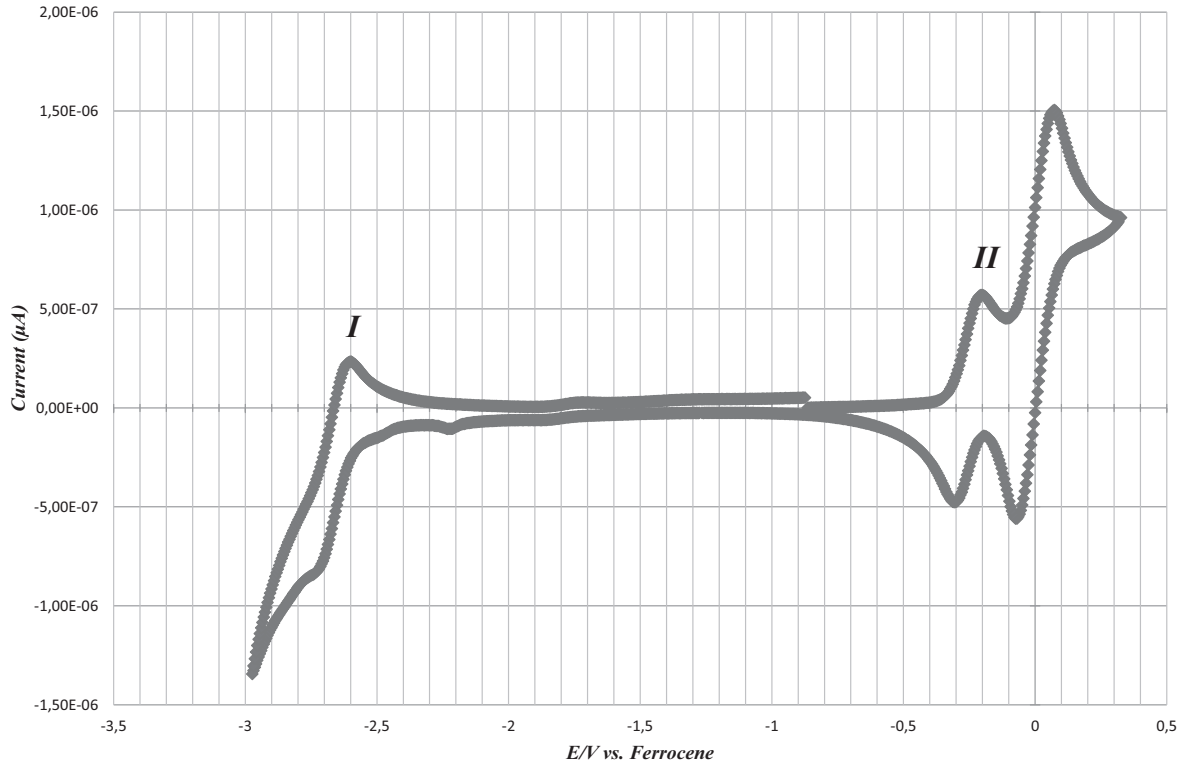

Figure 3.16*. Room-temperature cyclic voltammogram of [$Tp^{Me2}Nb(C_{10}H_9Fe)(c\text{-}C_3H_5)$-MeCCMe)](7)($1\times10^{-3}$ M) with ferrocene as reference (THF, [n-Bu_4N][PF_6], Pt electrode, scan rate 200 mV s^{-1}*

The cyclic voltammogram of **7** exhibits one partially reversible one-electron reduction wave (I) at $E_{1/2}$ = –2.67 V *vs*. Fc/Fc^+, assigned to the reduction of the Nb center, and one reversible one electron oxidation wave (II) at $E_{1/2}$ = –0.26 V *vs*. Fc/Fc^+, assigned to the oxidation of the ferrocenyl group (Scheme 3.13). The energy difference of the two waves is 2.4 eV. Since the color of the solution of **7** is purple, in the UV/vis spectrum we would expect an absorption band at around 520 nm, due to one electron charge transfer from the ferrocenyl group to the Nb center.

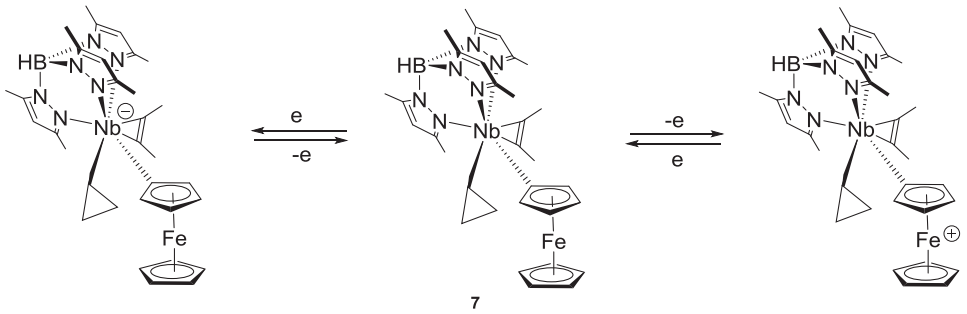

Scheme 3.13. *The 1 e⁻ reduction and oxidation processes for complex 7*

The complexes **1**, **5** and **6** display a partially reversible one-electron wave at negative potentials, again attributed to the niobium-centered reduction. Table 3.1 shows the half wave reduction potentionals ($E_{1/2}$/V) of compounds **1**, **5**, **6**, and **7**.

Table 3.1*. Electrochemical data for the reduction of **1**, **5, 6** and 7 (scan rate = 200 mV)*

complex [a]	$E_{1/2}$/ V [b]	ΔE_p/mV [c]
1	–2.85	83
5	–2.41	92
6	–2.75	103
7	–2.67	98

[a] In THF containing 0.1M [*n*-Bu_4N]PF_6, at a Pt-bead working electrode, except **7** with 0.08 M [*n*-Bu_4N]PF_6. The potential have been measured vs Fc/Fc^+. [b]Defined as the average of the cathodic and anodic peak potentials (±0.02 V). [c]Defined as the separation of the cathodic and anodic peak potentials. [d]Ratio between the anodic and cathodic peak current.

The complexes are more easily reducible in the order **5** ($E_{1/2}$ = –2.41 V) > **7** ($E_{1/2}$ = –2.67 V) > **6** ($E_{1/2}$ = –2.75 V) > **1** ($E_{1/2}$ = –2.85 V), which follows the hybridization of the

niobium-bound carbon *sp* (CCPh) > sp^2 (*c*-C_5H_7) > sp^3 (Me), the more the s character, the more π-accepting character of the group, the easier the reduction of the metal center. The Fc substituent fits in between sp^2 and *sp* hybridized carbons being more electron poor than the cyclopentenyl ligand with $E_{1/2}$ = –2.67 V *vs*. $Fc/Fc^{+\cdot}$ for **7**. The niobium fragment [Tp^{Me2}Nb(*c*-C_3H_5)(MeC≡CMe)] is strongly electron-donating as **7** exhibits a reversible one-electron oxidation process at $E_{1/2}$ = –0.26 V *vs*. Fc/Fc^{+}. The ferrocenyl group in **7** is therefore more easily reducible than ferrocene, its half wave potential being 0.26 V less positive than that of ferrocene. This is 0.04 V less positive than [(C_5H_5)(C_5Me_5)Fe].[35]

These complexes are formally pseudo-octahedral 16e species. Their molecular orbital diagram, shown in Figure 3.17, resembles that of the [$TpNbCl_2$(MeCCMe)] compound.[36,37] In a first approximation we can consider the interaction diagram between the ML_5 fragment [Tp^{Me2}NbR(*c*-C_3H_5)] with the alkyne. The fragment [Tp^{Me2}NbR(*c*-C_3H_5)] has no π-acceptor ligands and display d_{xz}, d_{yz}, d_{x2-y2} and d_{z2} type frontier molecular orbitals, according to an increasing energy order. The remaining d_{xy} orbital forms strong σ-bond interactions with two pyrazolyl nitrogens, cyclopropyl and the R orbital and is consequently not shown. The d_{z2} orbital, involving some niobium p_z character, points toward the alkyne group and displays the correct symmetry to interact with the alkyne-based $\pi_{\parallel}$ orbital. The other occupied alkyne-based $\pi_{\perp}$ orbital interacts with the d_{yz} orbital, affording a linear combination slightly higher in energy than that with the d_{z2} orbital. A further π-interaction occurs between the antibonding alkyne-based $\pi_{\parallel}$* orbital and the d_{xz} orbital, providing as a linear combination the HOMO of the molecular orbital diagram. The LUMO of the system is the d_{x2-y2} orbital which is essentially a nonbonding orbital. The more π-accepting character of the R group, the lower the energy of the LUMO orbital and therefore the easier the reduction of the Nb metal center.

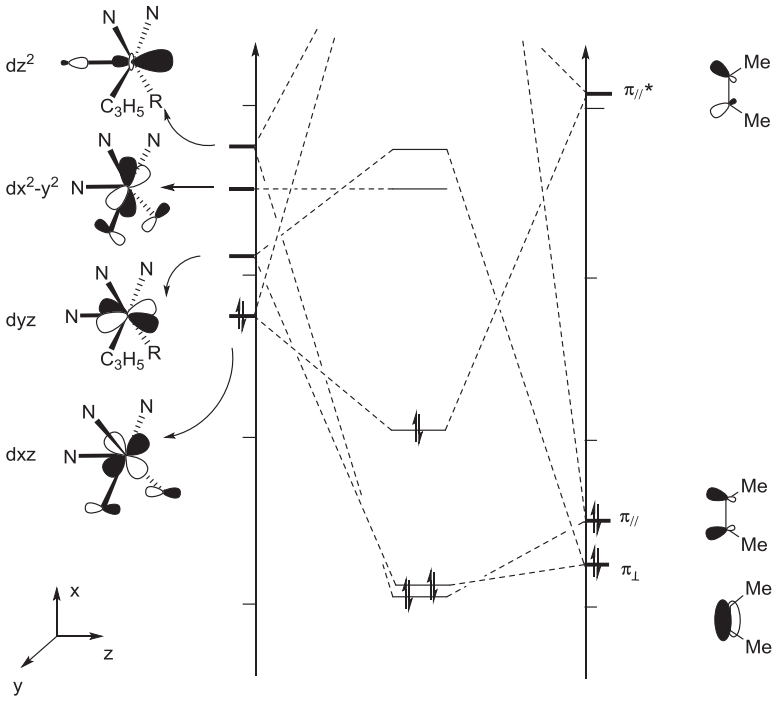

Figure 3.17. *Molecular orbital diagram for the interaction between the [TpNbCl$_2$] fragment and the alkyne.*

3.8- Discussion

3.8.1- Relative Nb-carbon bond strengths

The chemical selectivity in the formation of metal–carbon bonds is governed by kinetic and thermodynamic factors. The greater the metal–carbon bond strengths, the more readily can this bond be formed kinetically and/or thermodynamically. Marks *et al.* used calorimetry to measure various Zr−C and Th−C bond strengths, showing linear correlations between D_{M-C} and D_{C-H} (BDE).[38] Wolczanski *et al.* used exchange reactions to calculate relative Ti−C bond strengths for a series of [(^{t}Bu$_3$SiNH)$_3$Ti(R)] complexes, formed by the 1,2–addition of RH to the [(^{t}Bu$_3$SiNH)$_2$Ti=NSi^{t}Bu$_3$] compound, reporting again a linear correlation between D_{Ti-C} and D_{C-H} (BDE).[39] Jones *et al.* used the same method to calculate relative Rh−C bond strength for the systems [Tp^{Me2}Rh(L)(R)(H)] (L = CNneopentyl, PMe$_3$, P(OMe)$_3$), formed by oxidative addition of RH to the unsaturated Tp^{Me2}Rh(L) complexes. They also observed a linear correlation between D_{M-C} and D_{C-H} (BDE).[40–43] For the [Tp^{Me2}Rh{P(OMe)$_3$}(R)(H)] compounds, two separate linear correlations, obtained by plotting the D_{Rh-C} versus the D_{C-H} (BDE), were found. The slope for α-substituted substrates and for unsubstituted hydrocarbons measured 1.45 and 1.55, respectively, the Rh–C bond energies for α-substituted substrates being higher by ~7 kcal.mol^{-1} than those for

unsubstituted hydrocarbons.[42] Comparison of the analogous [Tp^{Me2}Rh(L)(R)(H)] (L = CNneopentyl, PMe_3, $P(OMe)_3$) systems shows that the slopes of the correlations follow the order CNneopentyl < $PMe_3 \leq PMe_3$, indicating that the Rh–C bond strengths increase with the electron donating power of the ligand. Eisenstein and Perutz carried out DFT calculations on the metal−carbon bond strengths for both the [Tp′Rh(CNneopentyl)(R)(H)] and [Ti(R)(silox)$_2$(NHSi^{t}Bu$_3$)] (silox = OSi^{t}Bu$_3$) systems.[44] The calculated slopes of $D_{M–C}$ versus $D_{C–H}$ (BDE) are in excellent agreement with experiment. Generally, the higher the C–H bond strengths of the activated hydrocarbon, the greater the metal–carbon bond strengths formed. The trend of the metal–carbon bond strengths is as follows: alkynyl > alkenyl ≈ cyclopropyl > arenyl ≈ benzyl > alkyl.

In order to get information on the Nb–R bond strengths in the [Tp^{Me2}Nb(R)(*c*-C_3H_5)(MeC≡CMe)] complexes, the thermodynamic exchange reactions of different [Tp^{Me2}Nb(R)(*c*-C_3H_5)(MeC≡CMe)] compounds with benzene were carried out qualitatively and were monitored by ^{1}H NMR (Scheme 3.14).

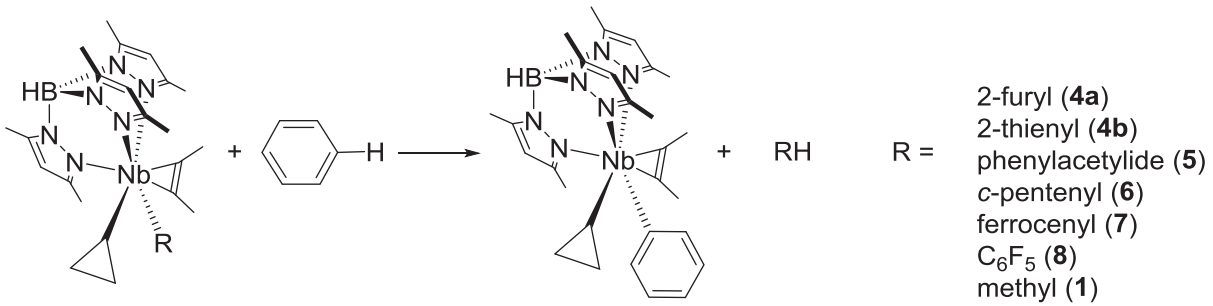

Scheme 3.14. Thermodynamic exchange reactions of [Tp^{Me2}Nb(R)(*c*-C_3H_5)(MeC≡CMe)] with benzene.

At room temperature or at mild heating (318 K), [Tp^{Me2}Nb(*c*-C_3H_5)(2-C_4H_3O)(MeCCMe)] (**4a**), [Tp^{Me2}Nb(*c*-C_3H_5)(2-C_4H_3S)(MeCCMe)] (**4b**), [Tp^{Me2}Nb(*c*-C_3H_5)(CCPh)(MeCCMe)] (**5**) and [Tp^{Me2}Nb(*c*-C_3H_5)(C_6F_5)(MeCCMe)] (**8**) were dissolved in benzene and kept in solution for 1 day. These complexes however were so stable that they did not react with benzene to give the exchange products [Tp^{Me2}Nb(*c*-C_3H_5)Ph(MeCCMe)] (**2**) with the corresponding hydrocarbons (RH), indicating that i) they are thermodynamicallymore stable than [Tp^{Me2}Nb(Ph)(*c*-C_3H_5)(MeC≡CMe)] (**2**) and ii) the Nb–R bond strengths of **4a**, **4b**, **5** and **8** are bigger than that of the Nb–Ph bond in [Tp^{Me2}Nb(Ph)(*c*-C_3H_5)(MeC≡CMe)] (**2**). However, [Tp^{Me2}Nb(*c*-C_3H_5)(2-C_5H_7)(MeCCMe)] (**6**) reacted with benzene at 318 K to form [Tp^{Me2}Nb(Ph)(*c*-C_3H_5)(MeC≡CMe)] and cyclopentene. The

complex [Tp^{Me2}Nb(*c*-C_3H_5)(Fc)(MeCCMe)] (**7**) also reacted with benzene-d_6 to form [Tp^{Me2}Nb(C_6D_5)(*c*-C_3H_5)(MeC≡CMe)] and FcH even at 287 K. Therefore, the formation of the [Tp^{Me2}Nb(R)(*c*-C_3H_5)(MeC≡CMe)] species follows the following trend of thermodynamic stability: [Tp^{Me2}Nb(*c*-C_3H_5)(CCPh)(MeCCMe)] > [Tp^{Me2}Nb(*c*-C_3H_5)(2-C_4H_3O)(MeCCMe)] ≈ [Tp^{Me2}Nb(*c*-C_3H_5)(2-C_4H_3S)(MeCCMe)] ≈ [Tp^{Me2}Nb(*c*-C_3H_5)(C_6F_5)(MeCCMe)] > [Tp^{Me2}Nb-(Ph)(*c*-C_3H_5)(MeC≡CMe)] > [Tp^{Me2}Nb-(*c*-C_3H_5)(2-C_5H_7)(MeCCMe)] > [Tp^{Me2}Nb(*c*-C_3H_5)(Fc)(MeCCMe)] > [Tp^{Me2}Nb(*c*-C_3H_5)- (Me)(MeCCMe)]. This translates to the following Nb–R bond strengths: Nb–alkynyl > Nb–heteroaromatic > Nb–phenyl > Nb–vinyl > Nb–Fc > Nb-Me . In accordance with the literature discussed above, if we plot the Nb–R bond strengths vs. the C–H bond strengths we expect an approximate linear correlation displaying the following hydrocarbon activation trend: phenylacetylene > furan ≈ thiophene ≈ pentafluorobenzene > benzene > cyclopentene > methane (Scheme 3.14). In addition we are able to predict that the C–H bond of FcH should be stronger than that of methane and equal or weaker than that of benzene. Therefore, it can be concluded that the higher the BDE of the hydrocarbon CH bond , the more favorable its activation. Moreover, since the C–H bond activation of an hydrocarbon by the η^2-cyclopropene Nb intermediate involves a proton transfer in a polar four center transition state , it can be predicted that the C–H bond of hydrocarbons with lower pK_a values are easier to be cleaved by the η^2-cyclopropene Nb intermediate. According to the pK_a value reported in Scheme 3.15,[45-49] the C–H bond activation of the corresponding hydrocarbons follows the following thermodynamic preference order: phenylacetylene > furan ≈ thiophene ≈ pentafluorobenzene > benzene > cyclopentene > methane. The C–H bond activation of ferrocene should be thermodynamically more favorable than that of benzene according to their pK_a value (Scheme 3.15).[45-47] However, the Nb–Fc bond reacts with benzene to form Nb–Ph and FcH, indicating that the Nb–Ph bond is stronger than the Nb–Fc one. A possible reason might be related to the steric congestion around the Nb center in the presence of the 2-butyne, cyclopropyl and the large Fc group. It is this steric hindrance around the metal which may drive the Nb–Fc to react with benzene to form a less steric demanding Nb–Ph bond. The regioselectivity for the CH bond activation of electron-deficient arenes is also controlled by the pK_a values when polar transition states are involved. Furan and thiophene are activated at 2-position rather than 3-position because the pK_a values of the CH bond at 2-positions are smaller than those at 3-positions (Scheme 3.15).

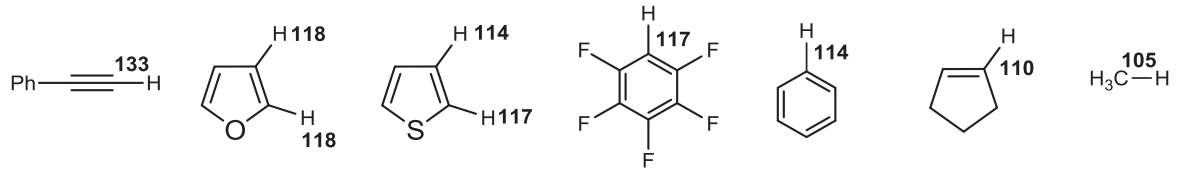

Scheme 3.14. *CH bond dissociation enthalpies, BDE (kcal/mol, 298 K).*[40,43,46,48]

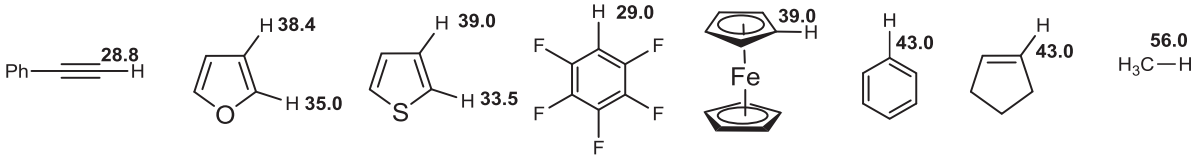

Scheme 3.15*. pK_a values of hydrocarbons (DMSO, 298 K).*[45-47, 49]

3.8.2- Positional disorder and implication for the reaction outcome and mechanism.

A remarkable feature of the disorder observed in the X-ray structure of **9a** and **9b** is that it involves only the Cβ and Cγ carbons and the hydrogen and methyl group directly attached to them. No other atoms in the structure and most strikingly none of the other atoms of the butadienyl ligand are involved in the disorder. This can be judged from the well-defined, small thermal ellipsoids of C1, C4, C5 and C6 for example. Consequently, Nb–C1 (NbCα) and Nb–C4 (NbCδ) bear well-defined double and single bond character, respectively. Thus the disorder cannot result from a statistical distribution of H4 between C1 and C4. A mechanism occurring through the coupling of the 2-butyne ligand with a rearranged cyclopropyl group in **8** leading to **9a** would result in C5, C1, C2, C7a and C3, C4, C6 belonging to the alkyne and cyclopropyl ligands in **8**, respectively. Looking at **9b**, one realizes that a similar route would necessitate C–C bond cleavage in the alkyne ligand, a potentially disfavored event. Alternatively, C6, C4, C3, C7b and C5, C1, C2 might originate from the formerly alkyne and cyclopropyl ligands, respectively, a much more reasonable assumption. However in that case, the mechanism would imply the migration of at least one more hydrogen, namely H4. Recall that in solution, the same 88:12 ratio between **9a** and **9b** is observed and that there is no evidence that **9a** and **9b** interconvert thereby confirming that a fast migration of hydrogen between Cα and Cδ is most probably not at the origin of the observed chemistry. Also, this isomerism has never been observed is the previous examples of η^4-butadienyl complexes.

Dr. Abel Locati and Prof. Feliu Maseras (ICIQ, Tarragona, Spain) have performed some theoretical calculations to give some insights on the mechanism of this rearrangement. Although the whole pathway is still not fully satisfactory some ideas are presented here. The key idea was to account of the formation of two isomers from a common intermediate without invoking the apparently simpler Hα migration between so-called Cα and Cδ. The M06 functional, as implemented in the Gaussian 09 suite of program, was used throughout this study where the SDD pseudopotential and its associated basis set was used to described Nb and a split valence 6-31G(d) basis et was used for all other atoms

The formation of the common intermediate **split_int** from which two reaction pathways split to is shown in Scheme 3.16. The origin of energy is the starting cyclopropyl complex **8**. The first step is the migratory insertion of the cyclopropyl group on to the alkyne to give a high energy intermediate **mig_int** that undergoes cyclopropyl ring opening. This ring opening can be described an intramolecular CC bond activation similar to an oxidative addition. The rather stable intermediate **open_mig** then transfers a β-H to the α-C of the alkyne, now singly bound to Nb to give a more stable intermediate **split_int**. Interestingly, no true hydride complex was computed at this stage.

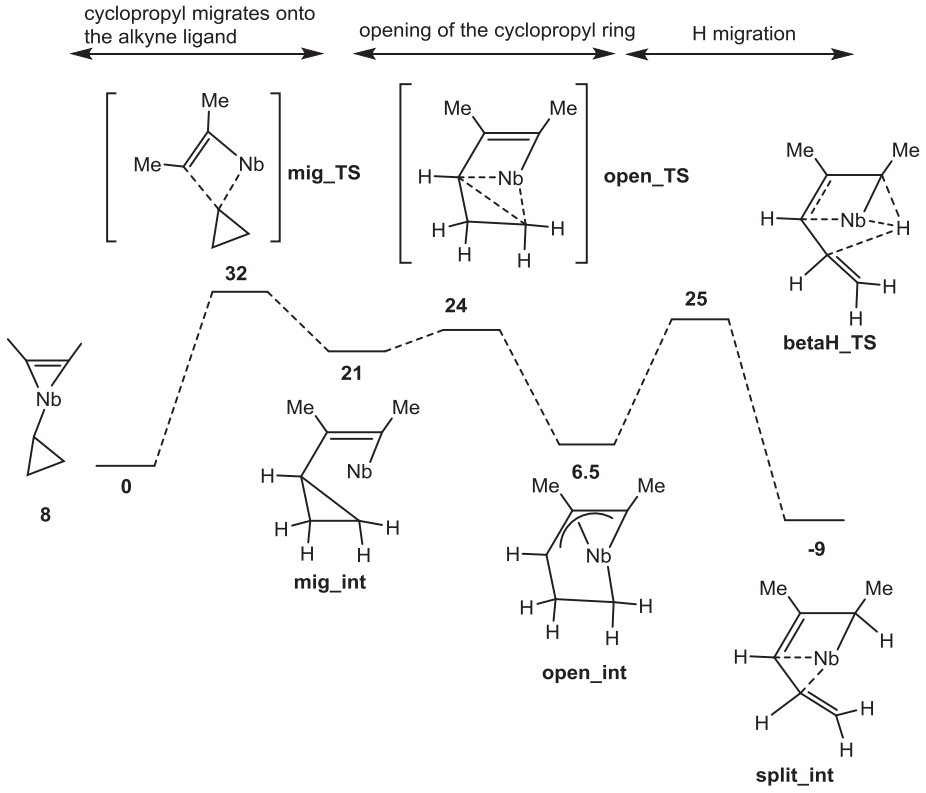

Scheme 3.16. *Computed Gibbs energy profile for the formation of the common intermediate* ***split_int***

From **split_int**, two pathways independently lead to the products (Scheme 3.17). Through a lower energy transition state **alphaH_TS**, the hydrogen on the alkyne can migrate back to the other end of the carbon chain giving the main product **9a_opt**. A slightly higher energy pathway, now proceeding through a true hydride intermediate, eliminates another hydrogen from the formerly cyclopropyl ligand before reinserting it at the end the carbon chain to give **9b_opt**.

The mechanism proposed here locates **9a** as the most stable regioisomer. The apparent flexibility of the carbon backbone after opening of the cyclopropyl ring that was noted during the computational modeling might indicate that some other pathways could also be taken into account to rationalize perfectly the selectivity. Definitely more work is needed here.

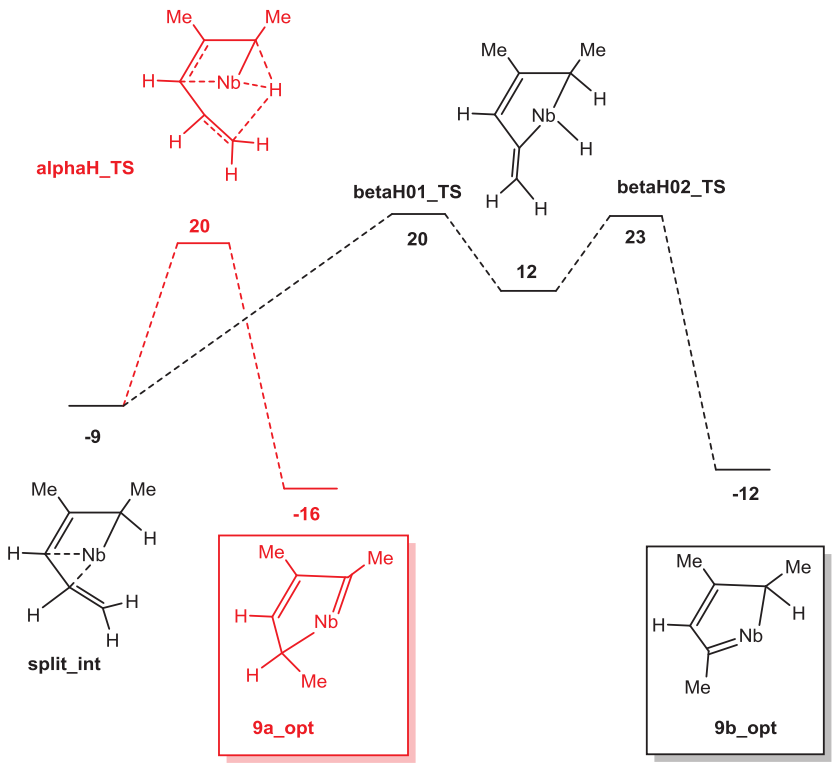

Scheme 3.17. *Computed Gibbs energy profile showing the pathway leading to either* ***9a*** *or* ***9b*** *from a common intermediate* ***split_int.***

3.9- Conclusion

We have investigated the reactivity of complex **1** towards heteroaromatics, unsaturated hydrocarbons, ferrocene (FcH) and pentafluorobenzene, the mechanism involved passing through a β-H abstraction/1,3-CH bond activation pathway. Compound **1** is able to selectively

activate the C–H bond of furan, thiophene, 1-cyclopentene, phenylacetylene, pentafluorobenzene and ferrocene, yielding the corresponding products [Tp^{Me2}NbX(*c*–C_3H_5)(MeCCMe)] (X =2-C_4H_3O (**4a**), 2-C_4H_3S (**4b**), PhC≡C(**5**), 1-C_5H_7 (**6**), Fc(**7**), and C_6F_5 (**8**)) at mild conditions. Complexes **4**–**7** have been isolated and characterized by ^{1}H, ^{13}C NMR spectroscopy and by X-ray diffraction analysis. Electrochemical studies on complexes **1**, **5, 6,** and **7** shows the involvement of the niobium center in a quasi reversible one-electron reduction process. The reducibility of such complexes follows the order: **1** ($E_{1/2}$ = –2.85 V) < **6** ($E_{1/2}$ = –2.75 V) < **7** ($E_{1/2}$ = –2.67 V) < **5** ($E_{1/2}$ = –2.41 V). This trend follows the order of the hybridization of the niobium-bound carbon: sp^3 (Me) < sp^2 (*c*-C_5H_7) < *sp* (CCPh). The reactions between **4a**, **5**, **6**, and **7** with benzene indicate that the Nb–R bond strengths decrease in the order: Nb–alkynyl > Nb–heteraromatic > Nb–phenyl > Nb–vinyl > Nb–Fc bond.

Experimental Section

All experiments were carried out under a dry argon atmosphere using either Schlenck tube or glove box techniques. Diethylether were obtained after refluxing purple solutions of Na/benzophenone under argon. Benzene, toluene, pentane, cyclohexane and dichloromethane were dried by refluxing over CaH_2 under argon. Deuterated NMR solvents were dried over molecular sieves, degassed by freeze-pump-thaw cycles and stored under argon. ^{1}H and ^{13}C NMR spectra were obtained on Bruker Avance 300 (^{1}H, 300.1 MHz ; ^{13}C, 75.5 MHz), Bruker Avance 400 (^{1}H, 400.13 MHz; ^{13}C, 100.6 MHz) and Bruker Avance 500 (^{1}H, 500.33 MHz; ^{13}C, 125.8 MHz) spectrometers. Only pertinent $^{1}J_{CH}$ are quoted in the ^{13}C spectra. Elemental analyses were obtained from the Analytical Service of our laboratory. $Tp^{Me2}NbMe(c\text{-}C_3H_5)(MeCCMe)$ was prepared according to a published procedure.[6,20]

Synthesis of $Tp^{Me2}Nb(c\text{-}C_3H_5)(2\text{-}C_4H_3O)(MeCCMe)$ (4a).

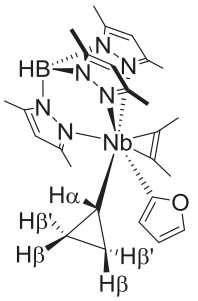

4a

$[Tp^{Me2}NbMe(c\text{-}C_3H_5)(MeCCMe)]$ (0.66 g, 1.32 mmol) was dissolved in pentane (50 mL) and excess furan (0.44 mL, 0.420 g, 6.17 mmol) was added. After 2 days at room temperature, the solvent was evaporated to dryness. Pentane (10 mL) was added and stripped off. The yellow powder was extracted with pentane (50 mL), filtered through a pad of Celite. The solvent was stripped off to leave $[Tp^{Me2}Nb(c\text{-}C_3H_5)(2\text{-}C_4H_3O)(MeCCMe)]$ **2a** as a yellow powder (0.450 g, 0.82 mmol, 62 %), which was stored under Ar at room temperature. Anal. Calcd for $C_{26}H_{36}BN_6NbO$: C, 56.54; H, 6.57; B, 1.96; N, 15.22; Nb, 16.82; O, 2.90. Found: C, 55.66; H, 7.33; N, 16.43.

^{1}H NMR (400 MHz, benzene-d_6, 298 K) δ 7.35 (d, *J* 1.5 Hz, 5-*H*-furyl), 6.49 (d, *J* 3.0 Hz, 4-*H*-furyl), 6.21 (dd, *J* 1.5 Hz and 3.0 Hz, 3-*H*-furyl), 5.79, 5.77, 5.52 (all s, 1 H each, $Tp^{Me2}CH$), 3.16, 2.27 (both s, $CH_3C\equiv$), 2.26, 2.20, 2.19, 2.10, 2.07, 1.34 (all s, 3 H each, $Tp^{Me2}CH_3$), 2.27 (partly obscured m, 1 H, *c*-C_3H_5 β'), 2.03 (m, 1 H, *c*-C_3H_5 α), 1.51 (m, 1 H,

c-C_3H_5 β'), 1.36, 0.76 (m, 1 H each, *c*-C_3H_5 β). **^{13}C NMR (100.6 MHz, benzene-d_6, 298 K)** δ 242.3, 238.7 (Me*C*≡), 210.4 (vbr, 2-*C*-furyl), 153.3, 151.2, 150.9, 143.8, 143.3, 143.2 (Tp^{Me2}*C*CH_3), 142.3 (ddd, *J* 195, 11, 7 Hz, 5-*C*-furyl), 120.5 (dt, *J* 168, 6 Hz, 4-*C*-furyl), 108.2 (ddd, *J* 169, 14, 6 Hz, 3-*C*-furyl), 107.3, 107.0, 106.6 (Tp^{Me2}*C*H), 72.2 (br d, $^1J_{CH}$ 142 Hz, *c*-*C*$_3$H$_5$ *C*α), 22.0, 20.3 (*C*H$_3$C≡), 22.3, 10.3 (both t , $^1J_{CH}$ 160, 162 Hz, *c*-*C*$_3$H$_5$ Cβ, Cβ), 15.2, 14.9, 13.5, 12.7, 12.6, 12.4 (Tp^{Me2}*C*H$_3$).

Synthesis of Tp^{Me2}Nb(*c*-C_3H_5)(2-C_4H_3S)(MeCCMe) (4b).

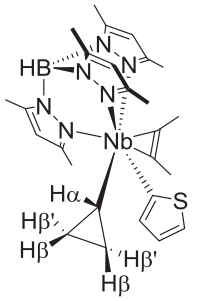

4b

Following an identical procedure as for **2a**, **1** (0.58 g, 1.16 mmol) and thiophene (0.46 mL, 0.500 g, 5.94 mmol) gave **2b** as a yellow powder (0.350 g, 0.62 mmol, 53 %), which was stored under Ar at room temperature. Anal. Calcd for $C_{26}H_{36}BN_6NbS$: C, 54.94; H, 6.38; B, 1.90; N, 14.79; Nb, 16.35; S, 5.64. Found: C, 55.66; H, 7.33; N, 16.43.

^{1}H NMR (300.1 MHz, benzene-d_6, 298 K) δ 7.57 (dd, *J* 4.5, 0.6 Hz, 5-*H*-thienyl), 7.01 (dd, *J* 4.5, 3.3 Hz, 4-*H*-thienyl), 6.85 (br s, 3-*H*-thienyl), 5.85, 5.84, 5.63 (all s, 1 H each, Tp^{Me2}C*H*), 3.32, 2.35 (both s, C*H*$_3$C≡), 2.38, 2.28, 2.25, 2.23, 2.11, 1.40 (all s, 3 H each, Tp^{Me2}C*H*$_3$), 2.52 (m, 1 H, *c*-C_3H_5β'), 2.25 (overlaps, 1 H, *c*-C_3H_5 α), 1.73 (m, 1 H, *c*-C_3H_5β'), 1.50, 0.96 (m, 1 H each, *c*-C_3H_5β).

^{13}C NMR (75.5 MHz, benzene-d_6, 298 K) δ 242.1, 240.6 (Me*C*≡C), 2-*C*-thienyl unobserved, 153.6, 151.6, 151.1, 143.8, 143.3 (Tp^{Me2}*C*CH_3), 136.0 (ddd, *J* 164, 10, 6 Hz, 3-*C*-thienyl Fur *Cβ*), 129.0 (ddd, *J* 169, 9, 8 Hz, 4-*C*-thienyl Fur *Cβ'*), 126.0 (ddd, *J* 163, 8, 5 Hz 5-*C*-thienyl Fur *Cα'*), 107.6, 107.1, 106.8 (Tp^{Me2}*C*H), 74.6 (br d, $^1J_{CH}$ 139 Hz, Nb *c*-*C*$_3$H$_5$ α), 22.4, 12.3 (both t , $^1J_{CH}$ 159, 161 Hz, *c*-*C*$_3$H$_5$ β, β), 22.1, 20.8 (*C*H$_3$C≡), 15.7, 15.2, 14.2, 12.8, 12.7, 12.5 (Tp^{Me2}*C*H$_3$).

Synthesis of $Tp^{Me2}Nb(c\text{-}C_3H_5)(C{\equiv}CPh)(MeC{\equiv}CMe)$ (5).

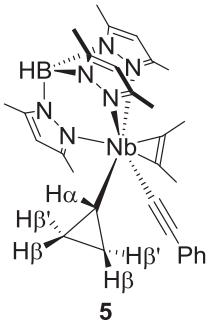

5

1st procedure: [$Tp^{Me2}NbMe(c\text{-}C_3H_5)(MeC{\equiv}CMe)$] (2.00 g, 3.99 mmol) was dissolved in pentane (50 mL) and about 5 equivalents of phenylacetylene (2.15 mL, 2.00 g, 19.58 mmol) were added. After 2 days at room temperature, the orange brown solution is separated by filtration trough a pad of Celite, from an orange yellow sticky solid which was washed 3 times with 10 mL of pentane. The solvent is stripped off, the powder is washed with small among of cold pentane to leave **5** as an orange powder (0.90 g, 1.53 mmol, 38 %), which was stored under Ar at room temperature.

2nd procedure: [$Tp^{Me2}NbMe(c\text{-}C_3H_5)(MeC{\equiv}CMe)$] (0.30 g, 0.60 mmol) was dissolved in C_6H_{12} (4 ml) and phenylacetylene (1.32 mL, 30 mmol) was added. The solution was heated at 35 °C for 22 h. The yellow solution turned to orange and some blocks formed suggesting polymerization due to phenylacetonitrile. After solvent evaporation, the orange blocks was scratched and the orange solid was extracted with pentane (20 mL). The combined solutions were concentrated until some crystals came out and stored at –40 °C overnight to crystallize. Orange crystals of **5** (0.139 g, 0.237 mmol, 40%) were isolated and stored at room temperature under Ar. Anal. Calcd for $C_{30}H_{38}BN_6Nb$: C, 61.45; H, 6.53; B, 1.84; N, 14.33; Nb, 15.84. Found: C, 61.79; H, 6.64; N, 14.01.

^{1}H NMR (400 MHz, benzene-d_6, 298 K) δ 7.47 (d, 2 H, *o*-C_6H_5), 7.02 (t, 2 H, *m*-C_6H_5), 6.94 (t, 1 H, *p*-C_6H_5), 5.81, 5.76, 5.43 (all s, 1 H each, $Tp^{Me2}CH$), 3.25, 2.30 (both s, 3 H each, $CH_3C{\equiv}$), 2.93, 2.22, 2.21, 2.19, 2.03, 2.02 (all s, 3 H each, $Tp^{Me2}CH_3$), 2.25 (m, 1 H, *c*-C_3H_5 β'), 2.18 (overlaps, 1 H, *c*-C_3H_5 α), 1.37 (m, 1 H, *c*-C_3H_5 β'), 1.29, 0.71 (m, 1 H each, *c*-C_3H_5 β).**^{13}C NMR (100.6 MHz, benzene-d_6, 298 K)** δ 239.3, 233.0 (Me*C*≡C), 153.2, 151.4, 150.6, 144.0, 143.4, 143.3 ($Tp^{Me2}CCH_3$), 149.2 (br s, *C*≡C–Ph), 130.9 (*m*-C_6H_5), 128.1 (*o*-C_6H_5), 127.1 (ipso-C_6H_5), 126.2 (*p*-C_6H_5), 125.9 (br s, C≡*C*–Ph), 107.5, 107.1, 106.9 ($Tp^{Me2}CH$), 77.9 (br d, $^1J_{CH}$ 146 Hz, Nb *c*-C_3H_5 α), 23.2, 8.4 (both t , $^1J_{CH}$ 159, 163 Hz, *c*-C_3H_5 β, β), 21.8, 21.1 ($CH_3C{\equiv}$), 16.2, 15.4, 14.7, 12.7, 12.6, 12.3 ($Tp^{Me2}CH_3$).

Synthesis of $Tp^{Me2}Nb(c\text{-}C_3H_5)(c\text{-}C_5H_7)(MeC{\equiv}CMe)$ (6).

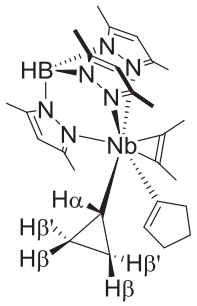

6

$[Tp^{Me2}NbMe(c\text{-}C_3H_5)(MeC{\equiv}CMe)]$ (0.55 g, 1.10 mmol) was dissolved in pentane (50 mL) and about 5 equivalents of cyclopentene (0.50 mL, 0.380 g, 5.50 mmol) were added. After 2 days at room temperature, the yellow brown solution was evaporated to dryness, 10 mL of pentane was added and stripped off. The yellow brown powder is dissolved in 50 mL of pentane and filtrated trough a pad of Celite. The solvent is stripped off, the powder is washed with small among of cold pentane up to leave **6** as a yellow powder (0.120 g, 0.22 mmol, 20 %).

$[Tp^{Me2}NbMe(c\text{-}C_3H_5)(MeC{\equiv}CMe)]$ (0.30 g, 0.60 mmol) was dissolved in cyclopentene (2.5ml). After 22 h at 35 °C when the yellow solution turned to yellow brown, the solvent was evaporated and an oily yellow brown residue was obtained. The residue was dissolved in 20 mL of pentane, filtered through a pad of celite, and washed with pentane (5 mL) × 3 times. The solution was concentrated until a little microcrystalline came out and then filtered to a vial, which was stored at –40 °C overnight to crystallize. A yellow powder of **6** (0.220 g, 0.40 mmol, 66%) was isolated and stored at –40 °C under Ar. Anal. Calcd for $C_{27}H_{40}BN_6Nb$: C, 58.71; H, 7.30; B, 1.96; N, 15.21; Nb, 16.82. Found: C, 58.63; H, 7.66; N, 15.02.

^{1}H NMR (400 MHz, benzene-d_6, 298 K) δ 6.29 (br s, 1H, C=C*H*), 5.80, 5.70, 5.61 (all s, 1 H each, $Tp^{Me2}CH$), 2.94, 2.29 (both s, 3 H each, $CH_3C{\equiv}$), 2.47, 2.26, 2.19, 2.14, 2.13, 1.70 (all s, 3 H each, $Tp^{Me2}CH_3$), 2.36 (m, 2 H, C=CH–CH_2–), 2.09 (m, 1 H, CH_2–C=CH), 2.03 (m, 1 H, *c*-C_3H_5 β'), 1.89 (m, 1 H, CH_2–C=CH), 1.76 (m, 1 H, *c*-C_3H_5 α), 1.65, 1.56 (both m, 1 H each, CH_2–CH_2–C=CH), 1.49 (m, 1 H, *c*-C_3H_5 β'), 1.35, 0.89 (m, 1 H each, *c*-C_3H_5 β).**^{13}C NMR (100.6 MHz, benzene-d_6, 298 K)** δ 240.2, 239.0 (Me*C*≡C), 201.6 (Nb*C*=CH), 152.3, 151.1, 149.8, 143.6, 143.2, 143.1 ($Tp^{Me2}CCH_3$), 136.4 (d, $^1J_{CH}$ 160 Hz, NbC=*C*H), 107.2, 106.9, 106.7 ($Tp^{Me2}CH$), 66.5 (br d, $^1J_{CH}$ 136 Hz, Nb *c*-C_3H_5 α), 43.7 (*C*H_2–

C=CH), 34.6 (C=CH–CH_2), 25.4 (C=CH–CH_2–CH_2), 22.1, 19.1 (CH_3C≡), 21.1, 12.3 (both t , $^1J_{CH}$ 159, 161 Hz, *c*-C_3H_5 β, β), 15.5, 15.2, 14.1, 12.8, 12.6, 12.5 ($Tp^{Me2}CH_3$).

Synthesis of $Tp^{Me2}Nb(C_{10}H_9Fe)(c\text{-}C_3H_5)(MeC{\equiv}CMe)$ (7).

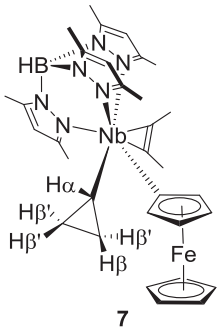

7

[Tp^{Me2}NbMe(*c*-C_3H_5)(MeC≡CMe)] (1) (0.250 g, 0.500 mmol) and Ferrocene (0.186g, 1 mmol) were heated in cyclohexane (10 mL) at 313 K overnight. The colour of the solution changed from bright orange to purple. The solvent was evaporated to dryness. The residue was dissolved in 100 ml of pentane and filtered to another one-necked schlenk bottle under Ar. The resulting solution was cooled at 273 K for 1 overnight. Purple crystals of 7 were obtained (140 mg, 0.21 mmol, 42%) and stored at –40 °C under Ar. Anal. Calcd for $C_{30}H_{42}BN_6Nb$: C, 61.03; H, 7.17; N, 14.23. Found: C, 61.55; H, 7.52; N, 13.92.

^{1}H NMR (500.3 MHz, benzene-d_6, 287 K) δ 5.79, 5.66, 5.57 (all s, 1 H each, Tp^{Me2}-C*H*), 4.32, 3.74 (d, $^2J_{HH}$= 1.2 Hz, 1 H each, Fc*CH*), 4.09 (s, 5 H, Fc*CH*), 4.05 (t, $^2J_{HH}$ = 1.6 Hz, 2 H, Fc*CH*), 4.01 (s, 1 H, Fc*CH*), 3.21, 2.24 (all s, 3 H each, CH_3C≡), 2.54, 2.37, 2.14, 2.10, 2.07, 2.00 (all s, 3 H each, $Tp^{Me2}CH_3$), 2.21 (overlaps, 1 H, *c*-C_3H_5β'), 1.70 (tt, 1 H, *c*-C_3H_5 α), 1.41 (m, 1 H, *c*-C_3H_5β'), 1.27, 0.96 (m, 1 H each, *c*-C_3H_5β). **^{13}C NMR (125.8 MHz, benzene-d_6, 287 K)** δ 241.9, 241.2 (Me*C*≡), 150.6 (*C*ipso), 151.8, 151.1, 150.4, 144.0, 143.8, 143.5 (Tp^{Me2}*C*Me), 130.0 (4-C_6H_4), 128.1, 127.0 (*m*,*o*-C_6H_4), 108.2, 107.3, 107.0 (Tp^{Me2}CH), 76.5 (br t, $^1J_{CH}$ = 117 Hz, Nb*C*H_2Ar), 67.2 (d, $^1J_{CH}$ = 138 Hz, Nb*C*αH), 22.4 ($C_6H_4CH_3$), 21.0, 20.2 (CH_3C≡), 21.7, 12.5 (t, $^1J_{CH}$ = 158, 160 Hz, *C*β, *C*β), 16.5, 15.4, 15.2, 13.0, 12.9, 12.8 ($Tp^{Me2}CH_3$).

Synthesis of $Tp^{Me2}Nb(C_6F_5)(c\text{-}C_3H_5)(MeC{\equiv}CMe)$ (8).

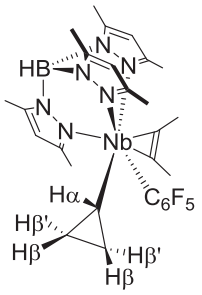

8

$[Tp^{Me2}NbMe(c\text{-}C_3H_5)(MeC{\equiv}CMe)]$ (0.40 g, 0.80 mmol) was dissolved in pentane (6 mL) and C_6F_5H (3.2 g, 19.04 mmol) was added. After 72h of stirring at room temperature, the colour of the solution changed from yellow-brown to dark brown, with the formation of a yellow precipitate. To favor the precipitation, the solvent was partially evaporated and the resulting suspension was cooled to –40 °C for 1 night. The suspension was filtered off and the yellow solid was washed 2 times with cold pentane (5 ml) and dried under vacuum, affording 8 (0.48 mmol, 60 %) and stored at –40 °C under Ar. The complex must be stored below 0°C. Anal. Calcd for $C_{28}H_{33}BF_5N_6Nb$: C, 51.56; H, 5.10; B, 1.66; N, 12.88. Found: C, 51.86; H, 5.78; N, 12.12.

^{1}H NMR (500 MHz, dichloromethane-d_2, 240 K) 5.85, 5.82, 5.72 (all s, 1 H each, $Tp^{Me2}CH$), 2.88 (d, 3 H, J_{HF} = 5.6 Hz, $CH_3C{\equiv}$), 2.13 (s, $CH_3C{\equiv}$), 2.47, 2.42, 2.43, 1.87, 1.75, 1.22 (all s, 3 H each, $Tp^{Me2}CH_3$), 2.72 (tt, 1 H, $c\text{-}C_3H_5$ α), 2.47 (overlaps, 1 H, $c\text{-}C_3H_5$β'), 1.65 (m, 1 H, $c\text{-}C_3H_5$β'), 1.53, 0.24 (m, 1 H each, $c\text{-}C_3H_5$β). **^{13}C{^{1}H} (125.8 MHz, dichloromethane-d_2, 240 K)** 246.0 (s , Me*C*≡) 238.7 (d, J_{CF} = 7.6 Hz, Me*C*≡), 151.0, 150.7, 149.4, 144.6, 143.6, 143.5 ($Tp^{Me2}CCH_3$), 148.9, 146.9 (*o*-C_6F_5), 138.7 (*m*-C_6F_5), 135.9 (*p*-C_6F_5), 106.8, 106.7, 106.5 ($Tp^{Me2}CH$), 86.6 (s, $c\text{-}C_3H_5$ α'), 23.2 (d, J_{CF} = 10.7 Hz, $CH_3C{\equiv}$), 22.4 (s, $CH_3C{\equiv}$), 24.9 (s, $c\text{-}C_3H_5$ β) 2.1 (d, J_{CF} = 9.2 Hz, $c\text{-}C_3H_5$ β), 15.4, 15.1, 14.0, 13.1, 13.0, 12.7 (all s, $Tp^{Me2}CH_3$). **^{19}F NMR (282.4 MHz, benzene-d_6, 298 K)** –100.2, –117.5 (both m, 1 F each, *o*-C_6F_5), –157.6 (m, 1 F, *p*-C_6F_5), –162.5, –163.2 (both m, 1 F each, *m*-C_6F_5).

Synthesis of $Tp^{Me2}Nb(C_6F_5)[–HC(CH_3)–HC=C(CH_3)–(CH_3)C=Nb]$ (9a).

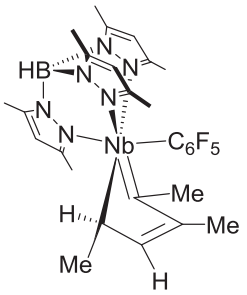

9a

$[Tp^{Me2}Nb(C_6F_5)(c\text{-}C_3H_5)$ (MeC≡CMe)] (0.120 g, 0.18 mmol) was heated in benzene (2 mL) for 24 hours at 45 °C. The colour of the solution changed from yellow to orange. The solvent was evaporated to dryness, and the resulting solid was washed 2 times with cold pentane (2ml) dried under vacuum to leave **9a** and **9b** as an orange solid (0.147 mmol, 80 %) and stored at room temperature under Ar.

^{1}H NMR (400 MHz, benzene-d_6, 298 K): 6.09 (dd, 1 H, J_{HF} = 3.7, J_{HH} = 12.2 Hz (–*H*C=C(CH_3)–), 5.83, 5.61, 5.37 (all s, 1 H each, $Tp^{Me2}CH$), 2.65 (d, 3 H, J_{HF} = 5.0 Hz – HC=C-(*CH*$_3$)), 2.40 (d, 3 H, J_{HH} = 6.1, HC(*CH*$_3$)–), 2.13 (s, 3 H, (*CH*$_3$)C=Nb), 2.30, 2.25, 2.09, 1.90, 1.22, 0.93 (all s, 3 H each, $Tp^{Me2}CH_3$), 1.05 (m, 1 H, –*H*C(CH_3)–). **^{13}C{^{19}F,^{1}H} NMR (125.8 MHz, benzene-d_6, 298 K)** 260.2 (–(CH_3)*C*=Nb), 151.8, 148.7, 148.3, 145.8, 144.8, 143.8 ($Tp^{Me2}CCH_3$), 149.6, 148.5 (*o*-C_6F_5), 138.9 (*m*-C_6F_5), 136.7 (*p*-C_6F_5), 135.9 (br s, *ipso*-C_6F_5), 120.0 (–HC=*C*(CH_3)–), 107.5, 107.4, 106.7 ($Tp^{Me2}CH$), 101.6 (–H*C*=C(CH_3)–), 87.3 (–H*C*(CH_3)–), 24.4 (–(*CH*$_3$)C=Nb), 22.9 (–HC=C(*CH*$_3$)–), 21.1 (–HC=C(*CH*$_3$)–), 16.0, 15.7, 15.1, 13.0, 12.9, 12.7 ($Tp^{Me2}CH_3$). **^{19}F (376.5 MHz, benzene-d_6, 298 K)** –109.5, (dt, 1 F, $^3J_{FF}$ = 18.9, $^4J_{FF}$ = 9.2 Hz, *o*-C_6F_5), –115.7, (dt, 1 F, $^3J_{FF}$ = 29.9, $^4J_{FF}$ = 9.6 Hz, *o*-C_6F_5), –158.3 (m, 1 F, $^3J_{FF}$ = 20.2, *p*-C_6F_5), –163.0, –164.1 (both m, 1 F each, *m*-C_6F_5).

Synthesis of $Tp^{Me2}Nb(C_6F_5)[–HC(CH_3)–(CH_3)C=C(H)–(CH_3)C=Nb]$ (9b).

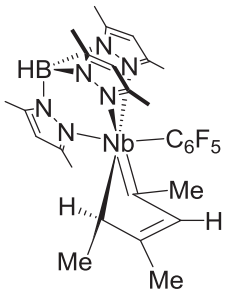

9b

^{1}H NMR (400 MHz, benzene-d_6, 298 K): 6.09 (dd, 1 H, J_{HF} = 3.7, J_{HH} = 12.2 Hz (–*H*C=C(CH_3)–), 5.83, 5.61, 5.37 (all s, 1 H each, Tp^{Me2}C*H*), 2.65 (d, 3 H, J_{HF} = 5.0 Hz –(*CH_3*)C=Nb), 2.42 (d, 3 H,HC(*CH_3*)–), 2.13 (s, 3 H, HC=C(*CH_3*)), 2.30, 2.25, 2.09, 1.90, 1.22, 0.93 (all s, 3 H each, $Tp^{Me2}C$*H_3*), 1.05 (m, 1 H, –*H*C(CH_3)–). **^{13}C{^{19}F,^{1}H} NMR (125.8 MHz, benzene-d_6, 298 K)** 254.9 (–(CH_3)*C*=Nb), 151.8, 148.7, 148.3, 145.7, 144.6, 143.8 (Tp^{Me2}*C*CH_3), 149.6, 148.5 (*o*-*C*$_6F_5$), 138.9 (*m*-*C*$_6F_5$), 136.7 (*p*-*C*$_6F_5$), 135.9 (br s, *ipso*-*C*$_6F_5$), 108.9 (–HC=*C*(CH_3)–), 107.3, 107.2, 106.4 (Tp^{Me2}*C*H), 105.0 (–H*C*=C(CH_3)–), 94.3 (–H*C*(CH_3)–), 26.7 (–HC=C(*CH_3*)–), 21.9 (–(*CH_3*)C=Nb), 17.0(–HC=C(*CH_3*)–), 15.8, 15.6, 15.2, 13.0, 12.9, 12.6 (Tp^{Me2}*C*H_3). **^{19}F (376.5 MHz, benzene-d_6, 298 K)** –104.7, (dt, 1 F, $^3J_{FF}$ = 19.1, $^4J_{FF}$ = 9.2 Hz, *o*-C_6F_5), –115.7, (dt, 1 F, $^3J_{FF}$ = 19.4, $^4J_{FF}$ = 9.6 Hz, *o*-C_6F_5), –158.4 (t, 1 F, $^3J_{FF}$ = 19.9, *p*-C_6F_5), –163.4, –164.3 (both m, 1 F each, *m*-C_6F_5).

Electrochemical experiments

Cyclic voltammetric measurements were carried out with a Autolab PGSTAT100 potentiostat controlled by a GPES 4.09 software. Experiments were performed at room temperature in a homemade airtight three-electrode cell connected to a vacuum/argon line. The reference electrode consisted of a saturated calomel electrode (SCE) separated from the solution by glass frit. The counter electrode was a platinum wire of ca 1cm² apparent surface. The working electrode was a Pt microdisk (0.5mm diameter). The supporting electrolyte (*n*-Bu_4N)[PF_6] (Fluka, 99% electrochemical grade) was dried at 120°C and degassed under argon. THF was freshly distilled prior to use. The solutions of **1**, **4**, and **5** used for the electrochemical studies were typically 10^{-3} M in complex and 0.1 M in supporting electrolyte, except the solution of **7**, which contained 0.08 M supporting electrolyte. All solutions were

prepared in a glove box. Before each measurement, the solutions were degassed by bubbling Ar and the working electrode was polished with a polishing machine. Under the experimental conditions employed throughout this work, the half wave potential ($E_{1/2}$) of the Fc/Fc^+ couple in THF occurs at $E_{1/2}$ = 0.55 V vs SCE. Figure 3.19-21 show the The cyclic voltammogram (CV) of **5**, **6**, and **1**.

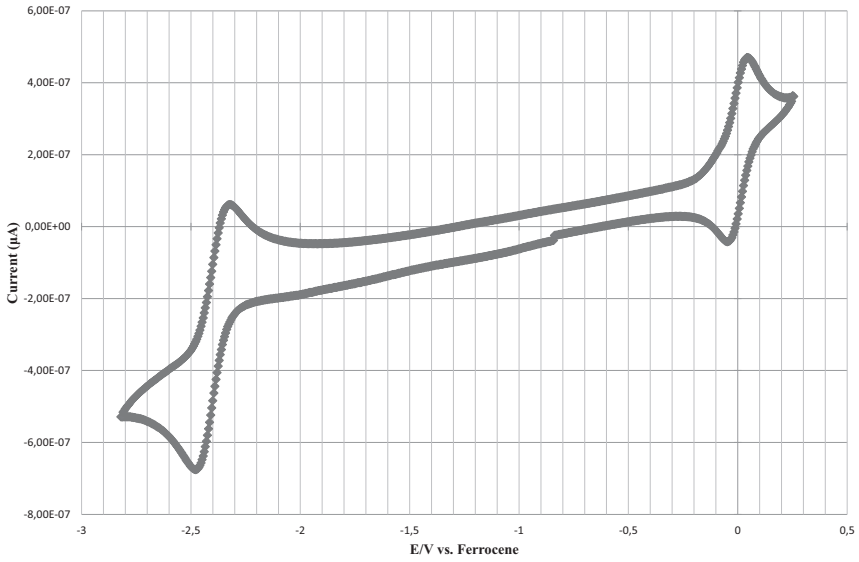

Figure 3.19. *Room-temperature cyclic voltammogram of* $[Tp^{Me2}Nb(c\text{-}C_3H_5)(CCPh)(MeCCMe)]$ (**5**) (1×10^{-3} *M) in THF containing 0.1 M* $[n\text{-}Bu_4N]PF_6$ *(platinum-bead electrode scan rate of 200 mV* s^{-1}*)*

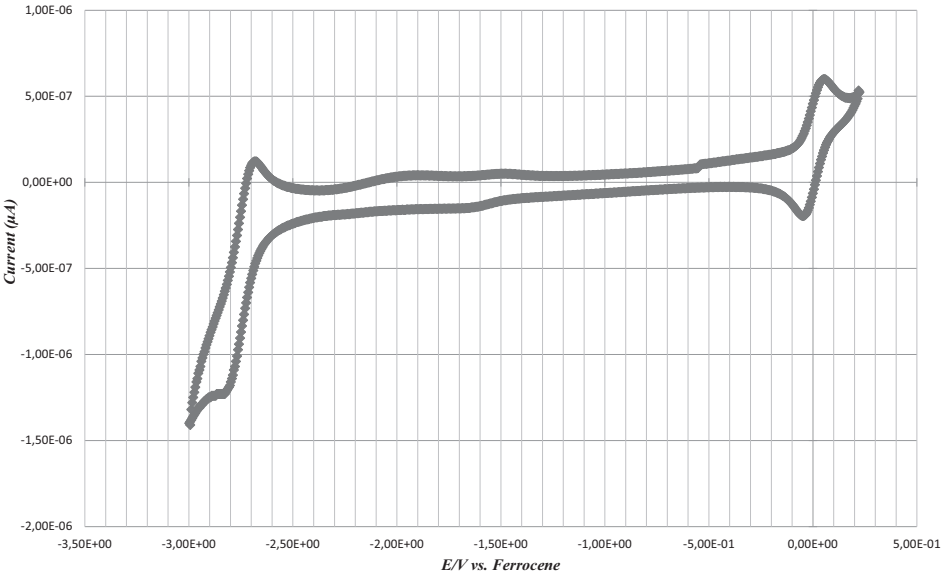

Figure 3.20. *Room-temperature cyclic voltammogram of [Tp^{Me2}Nb(c-C_3H_5)(c-C_5H_7)(MeCCMe)] (**6**) (1×10^{-3} M) in THF containing 0.1 M [n-Bu_4N][PF_6] (platinum-bead electrode, scan rate of 200 mV s^{-1}*

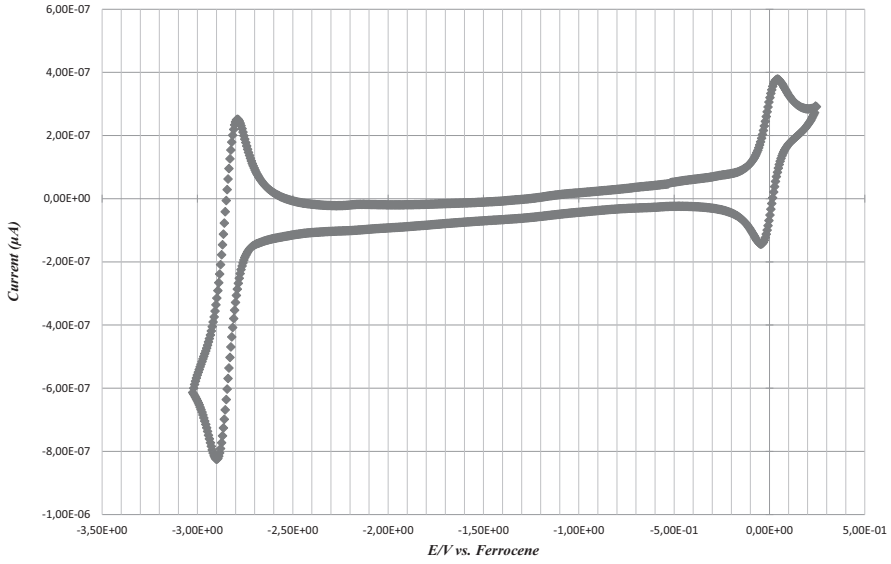

Figure 3.21. *Room-temperature cyclic voltammogram of [Tp^{Me2}NbMe(c-C_3H_5)(MeCCMe)] (**1**) (1×10^{-3} M) in THF containing 0.1 M [n-Bu_4N][PF_6](platinum-bead electrode, scan rate of 200 mV s^{-1})*

References

(1) Erker, G. *J. Organometal. Chem.* **1977**, *134*, 189–202.

(2) Pamplin, C. B.; Legzdins, P. *Acc. Chem. Res.* **2003**, *36*, 223–233.

(3) Wada, K.; Pamplin, C. B.; Legzdins, P.; Patrick, B. O.; Tsyba, I.; Bau, R. *J. Am. Chem. Soc.* **2003**, *125*, 7035–7048.

(4) Zhang, S.; Tamm, M.; Nomura, K. *Organometallics* **2011**, *30*, 2712–2720.

(5) Andino, J. G.; Kilgore, U. J.; Pink, M.; Ozarowski, A.; Krzystek, J.; Telser, J.; Baik, M.-H.; Mindiola, D. J. *Chem. Sci.* **2010**, *1*, 351–356.

(6) Boulho, C.; Oulie, P.; Vendier, L.; Etienne, M.; Pimienta, V.; Locati, A.; Bessac, F.; Maseras, F.; Pantazis, D. A.; McGrady, J. E. *J. Am. Chem. Soc.* **2010**, *132*, 14239–14250.

(7) Debad, J. D.; Legzdins, P.; Lumb, S. A.; Rettig, S. J.; Batchelor, R. J.; Einstein, F. W. B. *Organometallics* **1999**, *18*, 3414–3428.

(8) Debad, J. D.; Legzdins, P.; Lumb, S. A. *J. Am. Chem. Soc.* **1995**, *117*, 3288–3289.

(9) Baillie, R. A.; Man, R. W. Y.; Shree, M. V; Chow, C.; Thibault, M. E.; McNeil, W. S.; Legzdins, P. *Organometallics* **2011**, *30*, 6201–6217.

(10) Baillie, R. A.; Legzdins, P. *Acc. Chem. Res.* **2014**, *47*, 330–340.

(11) Pamplin, C. B.; Legzdins, P. *Acc. Chem. Res.* **2003**, *125*, 15210–15223.

(12) Tsang, J. Y. K.; Buschhaus, M. S. A.; Graham, P. M.; Semiao, C. J.; Semproni, S. P.; Kim, S. J.; Legzdins, P. *J. Am. Chem. Soc.* **2008**, *130*, 3652–3663.

(13) Cavaliere, V. N.; Crestani, M. G.; Pinter, B.; Pink, M.; Chen, C. H.; Baik, M. H.; Mindiola, D. J. *J. Am. Chem. Soc.* **2011**, *133*, 10700–10703.

(14) Cohen, S. a; Cohen, S. a; Bercaw, J. E.; Bercaw, J. E. *Organometallics* **1985**, *4*, 1006–1014.

(15) Kissounko, D.; Epshteyn, A.; Fettinger, J. C.; Sita, L. R. *Organometallics* **2006**, *25*, 531–535.

(16) Buchwald, S. L.; Kreutzer, K. A.; Fisher, R. A. *J. Am. Chem. Soc.* **1990**, *112*, 4600–4601.

(17) Sio, B.; Nb, M.; Hirsekorn, K. F.; Veige, A. S.; Marshak, M. P.; Koldobskaya, Y.; Wolczanski, P. T.; Cundari, T. R.; Lobkovsky, E. B. *J. Am. Chem. Soc.* **2005**, *127*, 4809–4830.

(18) Wang, S. S.; Abboud, K. A.; Boncella, J. M.; April, R. V. *J. Am. Chem. Soc.* **1997**, *119*, 11990–11991.

(19) Boulho, C.; Vendier, L.; Etienne, M.; Locati, A.; Maseras, F.; McGrady, J. E. *Organometallics* **2011**, *30*, 3999–4007.

(20) Oulié, P.; Boulho, C.; Vendier, L.; Coppel, Y.; Etienne, M. *J. Am. Chem. Soc.* **2006**, *128*, 15962–15963.

(21) Hu, Y.; Romero, N.; Dinoi, C.; Vendier, L.; Mallet-ladeira, S.; Mcgrady, J. E.; Locati, A.; Maseras, F.; Etienne, M. *Organometallics* **2014**, *33*, 7270–7278.

(22) Churchill, D. G.; Bridgewater, B. M.; Zhu, G.; Pang, K.; Parkin, G. *Polyhedron* **2006**, *25*, 499–512.

(23) Ringelberg, S. N.; Meetsma, A.; Troyanov, S. I.; Hessen, B.; Teuben, J. H. *Organometallics* **2002**, *21*, 1759–1765.

(24) Antinolo, A.; Fajardo, M.; Lopez-Mardomingo, C.; Lopez-Solera, I.; Otero, A.; Peréz, Y.; Prasher, S. *Organometallics* **2001**, *20*, 3132–3138.

(25) Neshat, A.; Schmidt, J. A. R. *Organometallics* **2010**, *29*, 6219–6229.

(26) Etienne, M.; Mathieu, R.; Donnadieu, B. *J. Am. Chem. Soc.* **1997**, *119*, 3218–3228.

(27) Gianetti, T. L.; Bergman, R. G.; Arnold, J. *Polyhedron* **2014**, *84*, 19–23.

(28) Herberich, G. .; Mayer, H. *J. Organometal. Chem.* **1988**, *347*, 93–100.

(29) Herberich, G. E.; Mayer, H. *Organometallics* **1990**, *9*, 2655–2661.

(30) Kocman, V.; Rucklidge, J. C.; O'Brien, R. J.; Santo, W. *J. Chem. Soc. D Chem. Comm.* **1971**, *21*, 1340.

(31) Andino, J. G.; Fan, H.; Fout, A. R.; Bailey, B. C.; Baik, M. H.; Mindiola, D. J. *J. Organometal. Chem.* **2011**, *696*, 4138–4146.

(32) Fan, H.; Fout, A. R.; Bailey, B. C.; Pink, M.; Baik, M.-H.; Mindiola, D. J. *Dalton Trans.* **2013**, *42*, 4163–4174.

(33) Fout, A. R.; Scott, J.; Miller, D. L.; Bailey, B. C.; Pink, M.; Mindiola, D. J. *Organometallics* **2009**, *28*, 331–347.

(34) Biasotto, F.; Etienne, M.; Dahan, F. *Organometallics* **1995**, *14*, 1870–1874.

(35) Rittinger, S.; Varret, F.; Astruc, D. *Organometallics* **1992**, *11*, 1454–1456.

(36) Etienne, M.; Biasotto, F.; Mathieu, R.; Templeton, J. L. *Organometallics* **1996**, *15*, 1106–1112.

(37) Etienne, M.; Donnadieu, B.; Ferna, J.; Jalo, F.; Otero, A.; Rodrigo-blanco, M. E. *Organometallics* **1996**, *15*, 4597–4603.

(38) Schock, L. E.; Marks, T. J. *J. Am. Chem. Soc.* **1988**, *110*, 7701–7715.

(39) Bennett, J. L.; Wolczanski, P. T. *J. Am. Chem. Soc.* **1997**, *119*, 10696–10719.

(40) Choi, G.; Morris, J.; Brennessel, W. W.; Jones, W. D. *J. Am. Chem. Soc.* **2012**, *134*, 9276–9284.

(41) Evans, M. E.; Li, T.; Vetter, A. J.; Rieth, R. D.; Jones, W. D. *J. Org. Chem.* **2009**, *74*, 6907–6914.

(42) Jiao, Y.; Brennessel, W. W.; Jones, W. D. *Chem. Sci.* **2014**, *5*, 804–812.

(43) Jiao, Y.; Morris, J.; Brennessel, W. W.; Jones, W. D. *J. Am. Chem. Soc.* **2013**, *135*, 16198–16212.

(44) Clot, E.; Megret, C.; Eisenstein, O.; Perutz, R. N. *J. Am. Chem. Soc.* **2006**, *128*, 8350–8357.

(45) Chemistry, O.; Sequoia, E.; Compotrnds, O.; December, R. *J. Organometal. Chem.* **1973**, *57*, 109–119.

(46) Barckholtz, C.; Barckholtz, T. a.; Hadad, C. M. *J. Am. Chem. Soc.* **1999**, *121*, 491–500.

(47) Shen, K.; Fu, Y.; Li, J. N.; Liu, L.; Guo, Q. X. *Tetrahedron* **2007**, *63*, 1568–1576.

(48) Blanksby, S. J.; Ellison, G. B. *Acc. Chem. Res.* **2003**, *36*, 255–263.

(49) Bordwell, F. G.; Drucker, G. E.; Andersen, N. H.; Denniston, A. D. *J. Am. Chem. Soc.***1986***, 108,* 7310-7313.

Appendix

Crystallographic data and ^{13}C NMR spectrum of the $Tp^{Me2}Nb(c\text{-}C_3H_5)(R)(MeCCMe)$ complexes

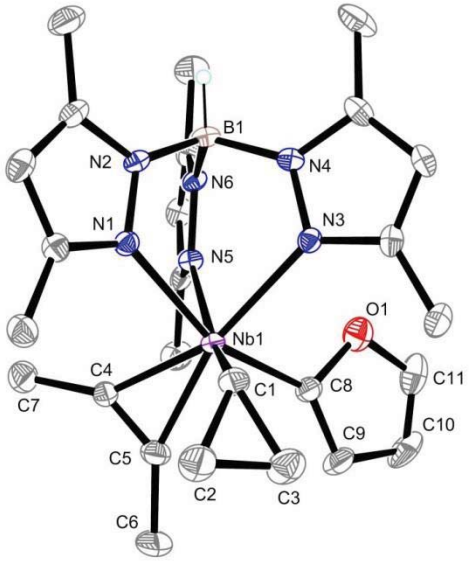

Table 3.2. *Crystal data and structure refinement for* ***4a***

Empirical formula	$C_{26}H_{36}BN_6NbO$, 0.5(C_6H_6)
Formula weight	591.38
Crystal size (mm)	0.15 x 0.1 x 0.02 mm
Crystal system	Monoclinic
space group	P 21/n
a (Å)	13.7378(5)
b (Å)	10.5966(3)
c (Å)	20.1933(6)
α (°)	90
β (°)	93.803(3)
γ (°)	90
V ($Å^3$)	2933.15(16)
Z	4
F	1236
$\rho_{calculated}$ ($g.cm^{-3}$)	1.339
Radiation type	MoKa
Longueur d'onde (Å)	0.71073
Temperature	180 K
Limit of 2θ(°)	2,97-26,37
Nb of the reflections collected	22799
Nb of the reflections independent	6002(0.0725)
Affinement by	F^2
Final R indices [I>2s(I)]	R1 = 0.0484, wR2 = 0.1014
R indices (all data)	R1 = 0.0973, wR2 = 0.1096
G.O.F (S)	1.003
Nb of the reflections used	6002(I>2s(I)])
Nb of the parameters used	351
Δρmin/Δρmax(e. $Å^{-3}$)	0.835/-0.587

Table 3.3. *Bond lengths (Å) for* ***4a***

C(1)-C(2)	1.513(5)	C(31)-C(32)	1.496(5)
C(1)-C(3)	1.528(5)	C(32)-N(3)	1.341(4)
C(1)-Nb(1)	2.179(4)	C(32)-C(33)	1.373(5)
C(2)-C(3)	1.467(6)	C(33)-C(34)	1.364(5)
C(4)-C(5)	1.291(5)	C(34)-N(4)	1.357(4)
C(4)-C(7)	1.488(5)	C(34)-C(35)	1.503(5)
C(4)-Nb(1)	2.057(3)	C(41)-C(42)	1.494(5)
C(5)-C(6)	1.498(5)	C(32)-N(3)	1.341(4)

C(5)-Nb(1)	2.068(4)	C(10)-C(11)	1.319(7)
C(8)-C(9)	1.343(5)	C(42)-N(5)	1.350(4)
C(8)-O(1)	1.417(4)	C(42)-C(43)	1.384(5)
C(10)-C(11)	1.319(7)	C(43)-C(44)	1.370(5)
C(11)-O(1)	1.355(5)	C(44)-N(6)	1.349(4)
C(21)-C(22)	1.495(5)	C(44)-C(45)	1.493(5)
C(22)-N(1)	1.348(4)	C(51)-C(52)	1.360(7)
C(22)-C(23)	1.382(5)	C(51)-C(53)	1.378(6)
C(23)-C(24)	1.360(5)	C(52)-C(53)	1.352(6)
C(24)-N(2)	1.351(4)	C(53)-C(51)	1.378(6)
C(31)-C(32)	1.496(5)	N(1)-N(2)	1.365(4)
C(8)-Nb(1)	2.214(4)	N(1)-Nb(1)	2.302(3)
C(9)-C(10)	1.438(7)	N(2)-B(1)	1.530(5)
C(11)-O(1)	1.355(5)	N(3)-N(4)	1.373(4)
C(21)-C(22)	1.495(5)	N(3)-Nb(1)	2.326(3)
C(22)-N(1)	1.348(4)	N(4)-B(1)	1.539(5)
C(22)-C(23)	1.382(5)	N(5)-N(6)	1.370(4)
C(23)-C(24)	1.360(5)	N(5)-Nb(1)	2.311(3)
C(24)-N(2)	1.351(4)	N(6)-B(1)	1.527(5)
C(24)-C(25)	1.505(5)		

Table 3.4. *Bond angles (°) for* ***4a***

C(2)-C(1)-C(3)	57.7(3)	C(43)-C(44)-C(45)	129.7(3)
C(2)-C(1)-Nb(1)	127.9(3)	C(52)-C(51)-C(53)#1	119.2(4)
C(3)-C(1)-Nb(1)	113.9(3)	C(53)-C(52)-C(51)	120.5(4)
C(3)-C(2)-C(1)	61.7(3)	C(52)-C(53)-C(51)#1	120.2(5)
C(2)-C(3)-C(1)	60.7(3)	C(22)-N(1)-N(2)	106.9(3)
C(5)-C(4)-C(7)	142.8(4)	C(22)-N(1)-Nb(1)	132.1(2)
C(5)-C(4)-Nb(1)	72.3(2)	N(2)-N(1)-Nb(1)	120.9(2)
C(7)-C(4)-Nb(1)	145.0(3)	C(24)-N(2)-N(1)	109.2(3)
C(4)-C(5)-C(6)	135.6(4)	C(24)-N(2)-B(1)	129.8(3)
C(4)-C(5)-Nb(1)	71.3(2)	N(1)-N(2)-B(1)	121.0(3)
C(6)-C(5)-Nb(1)	153.1(3)	C(32)-N(3)-N(4)	105.9(3)
C(2)-C(1)-C(3)	57.7(3)	C(32)-N(3)-Nb(1)	133.7(2)
C(2)-C(1)-Nb(1)	127.9(3)	N(4)-N(3)-Nb(1)	120.1(2)
C(3)-C(1)-Nb(1)	113.9(3)	C(34)-N(4)-N(3)	109.6(3)
C(3)-C(2)-C(1)	61.7(3)	C(34)-N(4)-B(1)	129.3(3)
C(2)-C(3)-C(1)	60.7(3)	N(3)-N(4)-B(1)	120.9(3)
C(5)-C(4)-C(7)	142.8(4)	C(42)-N(5)-N(6)	106.6(3)
C(5)-C(4)-Nb(1)	72.3(2)	C(42)-N(5)-Nb(1)	131.6(2)
C(7)-C(4)-Nb(1)	145.0(3)	N(6)-N(5)-Nb(1)	121.5(2)
C(4)-C(5)-C(6)	135.6(4)	C(44)-N(6)-N(5)	109.8(3)
C(4)-C(5)-Nb(1)	71.3(2)	C(44)-N(6)-B(1)	130.5(3)
C(6)-C(5)-Nb(1)	153.1(3)	N(5)-N(6)-B(1)	119.7(3)
C(9)-C(8)-O(1)	106.8(3)	C(11)-O(1)-C(8)	107.7(3)
C(9)-C(8)-Nb(1)	134.3(3)	C(4)-Nb(1)-C(5)	36.48(14)
O(1)-C(8)-Nb(1)	118.0(2)	C(4)-Nb(1)-C(1)	106.64(15)
C(8)-C(9)-C(10)	108.0(4)	C(5)-Nb(1)-C(1)	90.04(16)
C(11)-C(10)-C(9)	106.9(4)	C(4)-Nb(1)-C(8)	108.88(13)
C(10)-C(11)-O(1)	110.5(4)	C(5)-Nb(1)-C(8)	85.50(14)
N(1)-C(22)-C(23)	109.0(3)	C(1)-Nb(1)-C(8)	110.47(14)
N(1)-C(22)-C(21)	123.3(3)	C(4)-Nb(1)-N(1)	83.24(12)
C(23)-C(22)-C(21)	127.6(3)	C(5)-Nb(1)-N(1)	113.61(13)
C(24)-C(23)-C(22)	106.7(3)	C(1)-Nb(1)-N(1)	83.17(12)
N(2)-C(24)-C(23)	108.2(3)	C(8)-Nb(1)-N(1)	157.09(12)
N(2)-C(24)-C(25)	122.5(4)	C(4)-Nb(1)-N(5)	83.56(13)
C(23)-C(24)-C(25)	129.3(3)	C(5)-Nb(1)-N(5)	108.52(14)
N(3)-C(32)-C(33)	110.2(3)	C(1)-Nb(1)-N(5)	158.03(13)
N(3)-C(32)-C(31)	122.3(3)	C(8)-Nb(1)-N(5)	83.34(12)
C(33)-C(32)-C(31)	127.4(3)	N(1)-Nb(1)-N(5)	78.72(9)
C(34)-C(33)-C(32)	106.8(3)	C(4)-Nb(1)-N(3)	158.99(13)
N(4)-C(34)-C(33)	107.4(3)	C(5)-Nb(1)-N(3)	164.42(13)
N(4)-C(34)-C(35)	122.2(3)	C(1)-Nb(1)-N(3)	83.82(12)
C(33)-C(34)-C(35)	130.4(3)	C(8)-Nb(1)-N(3)	83.28(11)
N(5)-C(42)-C(43)	109.1(3)	N(1)-Nb(1)-N(3)	79.94(9)

N(5)-C(42)-C(41)	123.3(3)	N(5)-Nb(1)-N(3)	80.89(10)
C(43)-C(42)-C(41)	127.6(3)	N(6)-B(1)-N(2)	110.0(3)
C(44)-C(43)-C(42)	106.8(3)	N(6)-B(1)-N(4)	108.9(3)
N(6)-C(44)-C(43)	107.7(3)	N(2)-B(1)-N(4)	110.1(3)

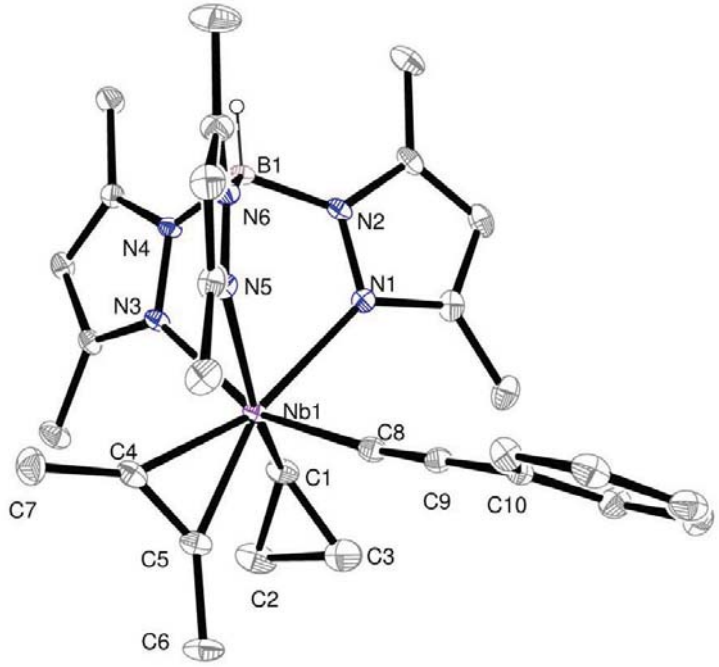

Table 3.5. *Crystal data and structure refinement for* ***5***

Empirical formula	C30 H38 B N6 Nb
Formula weight	586.38
Crystal size (mm)	0.18 x 0.12 x 0.03 mm
Crystal system	Monoclinic,
space group	P121/n1
a (Å)	11.0651(5)
b (Å)	14.9952(7)
c (Å)	17.7145(9)
α (°)	90
β (°)	93.684(2)
γ (°)	90
V ($Å^3$)	2933.2(2)
Z	4
F	1224
$\rho_{calculated}$ ($g.cm^{-3}$)	1.328
Radiation type	MoKa
Longueur d'onde (Å)	0.71073
Temperature	180 K
Limit of 2θ(°)	2.11- 26.37
Nb of the reflections collected	49107
Nb of the reflections independent	5980 (0.0514)
Affinement by	F^2
Final R indices [I>2s(I)]	R1 = 0.0457, wR2 = 0.1066
R indices (all data)	R1 = 0.0701, wR2 = 0.1186
G.O.F (S)	1.071
Nb of the reflections used	5980 (I>2s(I)])
Nb of the parameters used	351
Δρmin/Δρmax(e. $Å^{-3}$)	1.296/ -0.953

Table 3.6. *Bond lengths (Å) for* ***5***

C(4)-C(5)	1.328(6)	C(24)-C(25)	1.485(6)
C(4)-C(7)	1.469(6)	C(31)-C(32)	1.495(5)
C(4)-Nb(1)	2.058(4)	C(32)-N(3)	1.341(5)
C(5)-C(6)	1.483(6)	C(32)-C(33)	1.383(5)
C(5)-Nb(1)	2.071(4)	C(33)-C(34)	1.373(5)
C(1)-C(2)	1.490(6)	C(34)-N(4)	1.352(5)
C(1)-C(3)	1.528(7)	C(34)-C(35)	1.492(5)
C(1)-Nb(1)	2.173(4)	C(41)-C(42)	1.506(6)
C(2)-C(3)	1.479(8)	C(42)-N(5)	1.347(5)
C(8)-C(9)	1.206(5)	C(42)-C(43)	1.368(6)
C(8)-Nb(1)	2.197(4)	C(43)-C(44)	1.379(6)
C(9)-C(10)	1.442(5)	C(44)-N(6)	1.343(5)
C(10)-C(15)	1.383(6)	C(44)-C(45)	1.491(6)
C(10)-C(11)	1.396(5)	N(1)-N(2)	1.371(4)
C(11)-C(12)	1.382(6)	N(1)-Nb(1)	2.369(3)
C(12)-C(13)	1.368(7)	N(2)-B(1)	1.540(5)
C(13)-C(14)	1.373(7)	N(3)-N(4)	1.370(4)
C(14)-C(15)	1.387(6)	N(3)-Nb(1)	2.305(3)
C(21)-C(22)	1.491(6)	N(4)-B(1)	1.536(5)
C(22)-N(1)	1.342(5)	N(5)-N(6)	1.372(4)
C(22)-C(23)	1.383(6)	N(5)-Nb(1)	2.302(3)
C(23)-C(24)	1.368(6)	N(6)-B(1)	1.541(5)
C(24)-N(2)	1.351(5)		

Table 3.7. *Bond angles (°) for* ***5***

C(5)-C(4)-C(7)	137.7(4)	C(22)-N(1)-N(2)	105.8(3)
C(5)-C(4)-Nb(1)	71.8(2)	C(22)-N(1)-Nb(1)	133.5(3)
C(7)-C(4)-Nb(1)	150.5(3)	N(2)-N(1)-Nb(1)	120.7(2)
C(4)-C(5)-C(6)	138.3(4)	C(24)-N(2)-N(1)	110.6(3)
C(4)-C(5)-Nb(1)	70.7(2)	C(24)-N(2)-B(1)	128.9(3)
C(6)-C(5)-Nb(1)	150.8(3)	N(1)-N(2)-B(1)	120.4(3)
C(2)-C(1)-C(3)	58.7(3)	C(32)-N(3)-N(4)	106.5(3)
C(2)-C(1)-Nb(1)	131.0(3)	C(32)-N(3)-Nb(1)	131.7(2)
C(3)-C(1)-Nb(1)	109.9(3)	N(4)-N(3)-Nb(1)	121.5(2)
C(3)-C(2)-C(1)	62.0(3)	C(34)-N(4)-N(3)	109.8(3)
C(2)-C(3)-C(1)	59.4(3)	C(34)-N(4)-B(1)	129.2(3)
C(9)-C(8)-Nb(1)	172.5(3)	N(3)-N(4)-B(1)	121.0(3)
C(8)-C(9)-C(10)	179.0(4)	C(42)-N(5)-N(6)	107.0(3)
C(15)-C(10)-C(11)	118.1(4)	C(42)-N(5)-Nb(1)	130.7(3)
C(15)-C(10)-C(9)	120.6(3)	N(6)-N(5)-Nb(1)	121.9(2)
C(11)-C(10)-C(9)	121.3(4)	C(44)-N(6)-N(5)	109.5(3)
C(12)-C(11)-C(10)	121.0(4)	C(44)-N(6)-B(1)	129.7(3)
C(13)-C(12)-C(11)	119.8(4)	N(5)-N(6)-B(1)	120.8(3)
C(12)-C(13)-C(14)	120.3(4)	N(4)-B(1)-N(2)	109.3(3)
C(13)-C(14)-C(15)	120.1(4)	N(4)-B(1)-N(6)	109.9(3)
C(10)-C(15)-C(14)	120.6(4)	N(2)-B(1)-N(6)	108.4(3)
N(1)-C(22)-C(23)	109.8(4)	C(4)-Nb(1)-C(5)	37.54(16)
N(1)-C(22)-C(21)	123.2(4)	C(4)-Nb(1)-C(1)	108.47(16)
C(23)-C(22)-C(21)	127.0(4)	C(5)-Nb(1)-C(1)	86.90(16)
C(24)-C(23)-C(22)	107.0(4)	C(4)-Nb(1)-C(8)	105.64(15)
N(2)-C(24)-C(23)	106.9(4)	C(5)-Nb(1)-C(8)	85.82(15)
N(2)-C(24)-C(25)	123.7(4)	C(1)-Nb(1)-C(8)	110.82(16)
C(23)-C(24)-C(25)	129.4(4)	C(4)-Nb(1)-N(5)	85.66(14)
N(3)-C(32)-C(33)	109.7(3)	C(5)-Nb(1)-N(5)	115.26(13)
N(3)-C(32)-C(31)	123.7(4)	C(1)-Nb(1)-N(5)	154.79(14)
C(33)-C(32)-C(31)	126.6(4)	C(8)-Nb(1)-N(5)	83.99(12)
C(34)-C(33)-C(32)	106.6(3)	C(4)-Nb(1)-N(3)	85.39(14)
N(4)-C(34)-C(33)	107.4(3)	C(5)-Nb(1)-N(3)	113.28(14)
N(4)-C(34)-C(35)	123.6(3)	C(1)-Nb(1)-N(3)	82.96(14)
C(33)-C(34)-C(35)	129.0(4)	C(8)-Nb(1)-N(3)	157.59(12)
N(5)-C(42)-C(43)	108.9(4)	N(5)-Nb(1)-N(3)	77.36(10)
N(5)-C(42)-C(41)	123.3(4)	C(4)-Nb(1)-N(1)	161.58(14)
C(43)-C(42)-C(41)	127.8(4)	C(5)-Nb(1)-N(1)	160.87(14)
C(42)-C(43)-C(44)	107.4(4)	C(1)-Nb(1)-N(1)	82.23(13)
N(6)-C(44)-C(43)	107.2(4)	C(8)-Nb(1)-N(1)	83.42(12)

N(6)-C(44)-C(45)	123.3(4)	N(5)-Nb(1)-N(1)	79.29(10)
C(43)-C(44)-C(45)	129.5(4)	N(3)-Nb(1)-N(1)	81.03(10)

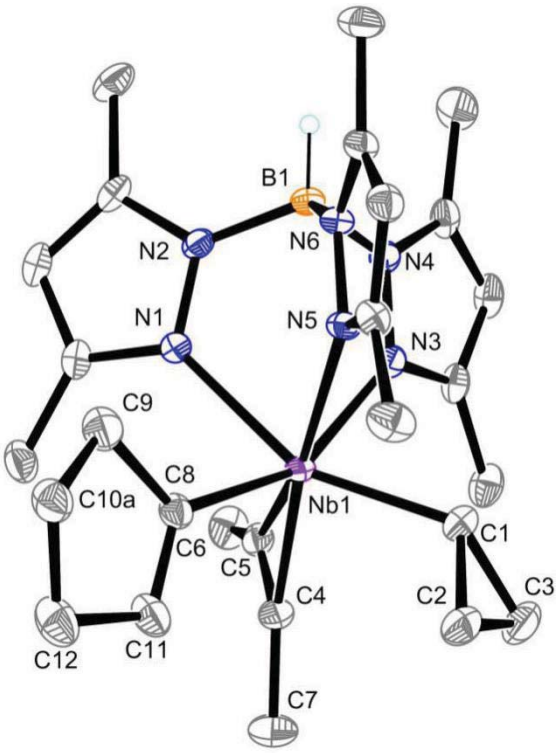

Table 3.8. *Crystal data and structure refinement for* ***6***

Empirical formula	$C_{27}H_{40}BN_6Nb$
Formula weight	552.37
Crystal size (mm)	0.35 x 0.22 x 0.12 mm
Crystal system	Monoclinic
space group	P 21/n
a (Å)	12.0657(2)
b (Å)	16.5205(2)
c (Å)	14.9268(2)
α (°)	90
β (°)	109.051(2)
γ (°)	90
V ($Å^3$)	2812.41(7)
Z	4
F	1160
$\rho_{calculated}$ ($g.cm^{-3}$)	1.305
Radiation type	MoKa
Longueur d'onde (Å)	0.71073
Temperature	180 K
Limit of 2θ(°)	3.11- 26.37
Nb of the reflections collected	29260
Nb of the reflections independent	5744 (0.0211)
Affinement by	F^2
Final R indices [I>2s(I)]	R1 = 0.0266, wR2 = 0.0698
R indices (all data)	R1 = 0.0326, wR2 = 0.072
G.O.F (S)	1.046
Nb of the reflections used	5744 (I>2s(I)])
Nb of the parameters used	327
Δρmin/Δρmax(e. $Å^{-3}$)	0.434/ -0.537

Table 3.8. *Bond lengths (Å) for* ***6***

C(1)-C(3)	1.501(3)	C(24)-C(25)	1.491(3)
C(1)-C(2)	1.537(3)	C(31)-C(32)	1.487(3)
C(1)-Nb(1)	2.177(2)	C(32)-N(3)	1.345(3)
C(2)-C(3)	1.480(4)	C(32)-C(33)	1.394(3)
C(4)-C(5)	1.315(3)	C(33)-C(34)	1.371(3)
C(4)-C(7)	1.493(3)	C(34)-N(4)	1.350(3)
C(4)-Nb(1)	2.073(2)	C(34)-C(35)	1.495(3)
C(5)-C(6)	1.480(3)	C(41)-C(42)	1.494(3)
C(5)-Nb(1)	2.052(2)	C(42)-N(5)	1.343(3)
C(8)-C(11)	1.351(3)	C(42)-C(43)	1.386(3)
C(8)-C(9)	1.509(3)	C(43)-C(44)	1.373(3)
C(8)-Nb(1)	2.230(2)	C(44)-N(6)	1.353(2)
C(9)-C(10B)	1.391(9)	C(44)-C(45)	1.493(3)
C(9)-C(10A)	1.589(4)	N(1)-N(2)	1.371(2)
C(10A)-C(12)	1.468(4)	N(1)-Nb(1)	2.3111(16)
C(10B)-C(12)	1.775(10)	N(2)-B(1)	1.535(3)
C(11)-C(12)	1.510(3)	N(3)-N(4)	1.371(2)
C(21)-C(22)	1.498(3)	N(3)-Nb(1)	2.3219(16)
C(22)-N(1)	1.343(3)	N(4)-B(1)	1.534(3)
C(22)-C(23)	1.388(3)	N(5)-N(6)	1.374(2)
C(23)-C(24)	1.371(3)	N(5)-Nb(1)	2.3563(16)
C(24)-N(2)	1.354(2)	N(6)-B(1)	1.536(3)

Table 3.9. *Bond angles (°) for* ***6***

C(3)-C(1)-C(2)	58.27(15)	N(2)-N(1)-Nb(1)	121.98(12)
C(3)-C(1)-Nb(1)	132.44(18)	C(24)-N(2)-N(1)	109.80(16)
C(2)-C(1)-Nb(1)	112.59(15)	C(24)-N(2)-B(1)	129.74(17)
C(3)-C(2)-C(1)	59.65(15)	N(1)-N(2)-B(1)	120.46(15)
C(2)-C(3)-C(1)	62.08(15)	C(32)-N(3)-N(4)	106.53(16)
C(5)-C(4)-C(7)	136.0(2)	C(32)-N(3)-Nb(1)	131.57(14)
C(5)-C(4)-Nb(1)	70.56(12)	N(4)-N(3)-Nb(1)	121.84(12)
C(7)-C(4)-Nb(1)	153.40(18)	C(34)-N(4)-N(3)	110.05(17)
C(4)-C(5)-C(6)	139.6(2)	C(34)-N(4)-B(1)	129.64(17)
C(4)-C(5)-Nb(1)	72.25(13)	N(3)-N(4)-B(1)	120.17(15)
C(6)-C(5)-Nb(1)	148.18(17)	C(42)-N(5)-N(6)	106.20(15)
C(11)-C(8)-C(9)	107.30(19)	C(42)-N(5)-Nb(1)	133.46(12)
C(11)-C(8)-Nb(1)	126.61(16)	N(6)-N(5)-Nb(1)	120.22(11)
C(9)-C(8)-Nb(1)	126.02(15)	C(44)-N(6)-N(5)	109.61(16)
C(10B)-C(9)-C(8)	112.7(4)	C(44)-N(6)-B(1)	129.20(17)
C(8)-C(9)-C(10A)	103.6(2)	N(5)-N(6)-B(1)	121.19(15)
C(12)-C(10A)-C(9)	104.8(2)	C(5)-Nb(1)-C(4)	37.19(9)
C(9)-C(10B)-C(12)	99.1(5)	C(5)-Nb(1)-C(1)	109.49(8)
C(8)-C(11)-C(12)	114.3(2)	C(4)-Nb(1)-C(1)	88.13(8)
N(1)-C(22)-C(23)	109.05(19)	C(5)-Nb(1)-C(8)	108.34(8)
N(1)-C(22)-C(21)	123.63(19)	C(4)-Nb(1)-C(8)	89.19(8)
C(23)-C(22)-C(21)	127.3(2)	C(1)-Nb(1)-C(8)	110.80(8)
C(24)-C(23)-C(22)	107.05(18)	C(5)-Nb(1)-N(1)	83.91(7)
N(2)-C(24)-C(23)	107.24(18)	C(4)-Nb(1)-N(1)	113.27(7)
N(2)-C(24)-C(25)	123.4(2)	C(1)-Nb(1)-N(1)	155.30(7)
C(23)-C(24)-C(25)	129.4(2)	C(8)-Nb(1)-N(1)	82.87(7)
N(3)-C(32)-C(33)	109.28(19)	C(5)-Nb(1)-N(3)	83.96(7)
N(3)-C(32)-C(31)	123.9(2)	C(4)-Nb(1)-N(3)	111.71(7)
C(33)-C(32)-C(31)	126.8(2)	C(1)-Nb(1)-N(3)	83.20(7)
C(34)-C(33)-C(32)	106.60(18)	C(8)-Nb(1)-N(3)	155.68(7)
N(4)-C(34)-C(33)	107.53(19)	N(1)-Nb(1)-N(3)	77.56(6)
N(4)-C(34)-C(35)	123.3(2)	C(5)-Nb(1)-N(5)	159.30(7)
C(33)-C(34)-C(35)	129.2(2)	C(4)-Nb(1)-N(5)	163.49(7)
N(5)-C(42)-C(43)	110.27(17)	C(1)-Nb(1)-N(5)	81.58(7)
N(5)-C(42)-C(41)	123.74(18)	C(8)-Nb(1)-N(5)	82.51(6)
C(43)-C(42)-C(41)	125.99(19)	N(1)-Nb(1)-N(5)	79.94(6)
C(44)-C(43)-C(42)	105.90(18)	N(3)-Nb(1)-N(5)	79.98(6)
N(6)-C(44)-C(43)	108.02(17)	N(4)-B(1)-N(2)	108.98(17)
N(6)-C(44)-C(45)	122.9(2)	N(4)-B(1)-N(6)	109.77(16)
C(43)-C(44)-C(45)	129.1(2)	N(2)-B(1)-N(6)	109.76(16)

C(22)-N(1)-N(2)	106.86(16)	C(10A)-C(12)-C(11)	102.8(2)
C(22)-N(1)-Nb(1)	131.16(14)	C(11)-C(12)-C(10B)	98.4(3)

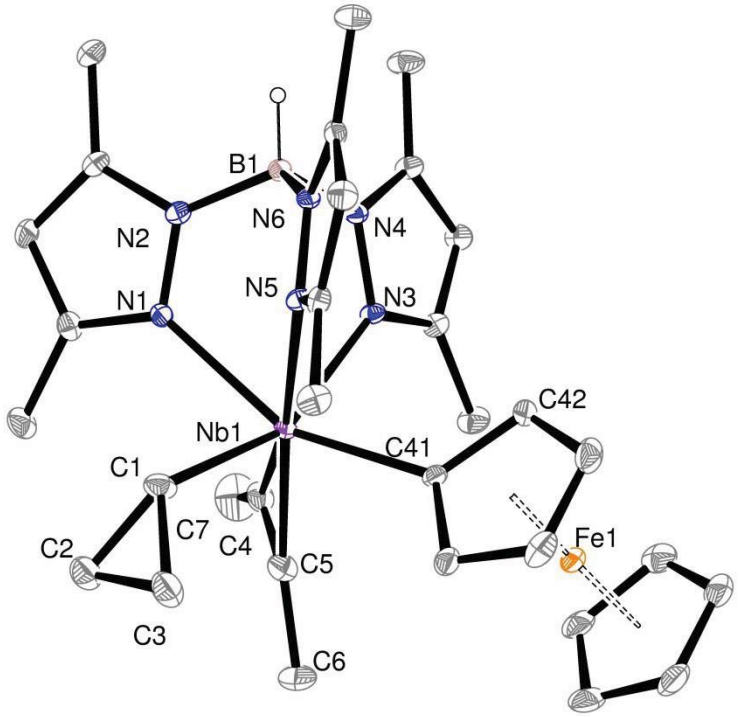

Table 3.10. *Crystal data and structure refinement for* ***7***

Empirical formula	$C_{32}H_{42}BFeN_6Nb$
Formula weight	670.29
Crystal size (mm)	0.15 x 0.02 x 0.02 mm
Crystal system	Monoclinic
space group	P121/c1
a (Å)	11.4037(10)
b (Å)	15.8380(13)
c (Å)	19.2775(16)
α (°)	90
β (°)	105.849(4)
γ (°)	90
V ($Å^3$)	3349.4(5)
Z	4
F	1392
$\rho_{calculated}$ ($g.cm^{-3}$)	1.329
Radiation type	MoKa
Longueur d'onde (Å)	0.71073
Temperature	180 K
Limit of 2θ(°)	1.86 - 24.48
Nb of the reflections collected	38066
Nb of the reflections independent	5529 (0.0892)
Affinement by	F^2
Final R indices [I>2s(I)]	R1 = 0.0494, wR2 = 0.1131
R indices (all data)	R1 = 0.0809, wR2 = 0.1240
G.O.F (S)	1.002
Nb of the reflections used	5529 (I>2s(I)])
Nb of the parameters used	378
Δρmin/Δρmax(e. $Å^{-3}$)	0.656/ -0.643

Table 3.11. *Bond lengths (Å) for* ***7***

C(1)-C(3)	1.499(7)	C(41)-Fe(1)	2.131(4)
C(1)-C(2)	1.518(7)	C(41)-Nb(1)	2.211(5)
C(1)-Nb(1)	2.201(5)	C(42)-C(43)	1.428(7)
C(3)-C(2)	1.493(8)	C(42)-Fe(1)	2.069(5)
C(4)-C(5)	1.362(8)	C(43)-C(44)	1.403(8)
C(4)-C(7)	1.444(8)	C(43)-Fe(1)	2.034(5)
C(4)-Nb(1)	2.062(5)	C(44)-C(45)	1.415(7)
C(5)-C(6)	1.495(7)	C(44)-Fe(1)	2.021(5)
C(5)-Nb(1)	2.055(5)	C(45)-Fe(1)	2.034(5)
C(11)-C(12)	1.489(7)	C(51)-C(55)	1.419(8)
C(12)-N(1)	1.333(6)	C(51)-C(52)	1.425(8)
C(12)-C(13)	1.400(7)	C(51)-Fe(1)	2.067(5)
C(13)-C(14)	1.373(7)	C(52)-C(53)	1.408(8)
C(14)-N(2)	1.363(6)	C(52)-Fe(1)	2.055(5)
C(14)-C(15)	1.491(7)	C(53)-C(54)	1.405(8)
C(21)-C(22)	1.491(6)	C(53)-Fe(1)	2.045(5)
C(22)-N(3)	1.349(6)	C(54)-C(55)	1.411(9)
C(22)-C(23)	1.383(7)	C(54)-Fe(1)	2.033(5)
C(23)-C(24)	1.375(6)	C(55)-Fe(1)	2.050(5)
C(24)-N(4)	1.350(6)	N(1)-N(2)	1.389(5)
C(24)-C(25)	1.472(7)	N(1)-Nb(1)	2.348(4)
C(31)-C(32)	1.482(7)	N(2)-B(1)	1.520(6)
C(32)-N(5)	1.334(6)	N(3)-N(4)	1.382(5)
C(32)-C(33)	1.395(6)	N(3)-Nb(1)	2.323(4)
C(33)-C(34)	1.383(7)	N(4)-B(1)	1.542(6)
C(34)-N(6)	1.358(5)	N(5)-N(6)	1.381(5)
C(34)-C(35)	1.487(7)	N(5)-Nb(1)	2.366(3)
C(41)-C(42)	1.442(7)	N(6)-B(1)	1.531(6)
C(41)-C(45)	1.445(7)		

Table 3.12. *Bond angles (°) for* ***7***

C(2)-C(1)-C(3)	59.3(3)	C(51)-C(52)-Fe(1)	70.3(3)
C(2)-C(1)-Nb(1)	130.0(4)	C(54)-C(53)-C(52)	108.0(6)
C(3)-C(1)-Nb(1)	122.7(4)	C(54)-C(53)-Fe(1)	69.4(3)
C(2)-C(3)-C(1)	59.7(3)	C(52)-C(53)-Fe(1)	70.3(3)
C(3)-C(2)-C(1)	61.0(4)	C(53)-C(54)-C(55)	108.1(6)
C(5)-C(4)-C(7)	135.5(5)	C(53)-C(54)-Fe(1)	70.3(3)
C(5)-C(4)-Nb(1)	70.4(3)	C(55)-C(54)-Fe(1)	70.5(3)
C(7)-C(4)-Nb(1)	154.1(5)	C(54)-C(55)-C(51)	108.7(6)
C(4)-C(5)-C(6)	137.8(5)	C(54)-C(55)-Fe(1)	69.1(3)
C(4)-C(5)-Nb(1)	71.0(3)	C(51)-C(55)-Fe(1)	70.5(3)
C(6)-C(5)-Nb(1)	151.1(4)	C(12)-N(1)-N(2)	106.5(4)
N(1)-C(12)-C(13)	110.1(4)	C(12)-N(1)-Nb(1)	133.5(3)
N(1)-C(12)-C(11)	123.8(4)	N(2)-N(1)-Nb(1)	119.8(3)
C(13)-C(12)-C(11)	126.2(5)	C(14)-N(2)-N(1)	109.4(4)
C(14)-C(13)-C(12)	106.4(4)	C(14)-N(2)-B(1)	128.7(4)
N(2)-C(14)-C(13)	107.7(4)	N(1)-N(2)-B(1)	121.8(4)
N(2)-C(14)-C(15)	122.1(5)	C(22)-N(3)-N(4)	105.1(4)
C(13)-C(14)-C(15)	130.3(5)	C(22)-N(3)-Nb(1)	132.0(3)
N(3)-C(22)-C(23)	110.3(4)	N(4)-N(3)-Nb(1)	122.6(3)
N(3)-C(22)-C(21)	122.5(4)	C(24)-N(4)-N(3)	110.9(3)
C(23)-C(22)-C(21)	127.1(4)	C(24)-N(4)-B(1)	129.8(4)
C(24)-C(23)-C(22)	106.8(4)	N(3)-N(4)-B(1)	119.3(4)
N(4)-C(24)-C(23)	106.9(4)	C(32)-N(5)-N(6)	106.7(3)
N(4)-C(24)-C(25)	123.3(4)	C(32)-N(5)-Nb(1)	133.2(3)
C(23)-C(24)-C(25)	129.8(5)	N(6)-N(5)-Nb(1)	119.1(2)
N(5)-C(32)-C(33)	109.9(4)	C(34)-N(6)-N(5)	109.8(4)
N(5)-C(32)-C(31)	124.0(4)	C(34)-N(6)-B(1)	128.7(4)
C(33)-C(32)-C(31)	126.1(4)	N(5)-N(6)-B(1)	121.1(3)
C(34)-C(33)-C(32)	106.4(4)	N(2)-B(1)-N(6)	110.3(4)
N(6)-C(34)-C(33)	107.1(4)	N(2)-B(1)-N(4)	108.4(4)
N(6)-C(34)-C(35)	122.7(4)	N(6)-B(1)-N(4)	110.0(4)

C(33)-C(34)-C(35)	130.1(4)	C(5)-Nb(1)-C(4)	38.6(2)
C(42)-C(41)-C(45)	104.3(4)	C(5)-Nb(1)-C(1)	86.0(2)
C(42)-C(41)-Fe(1)	67.6(2)	C(4)-Nb(1)-C(1)	104.1(2)
C(45)-C(41)-Fe(1)	66.1(2)	C(5)-Nb(1)-C(41)	85.78(19)
C(42)-C(41)-Nb(1)	128.3(3)	C(4)-Nb(1)-C(41)	110.97(19)
C(45)-C(41)-Nb(1)	121.9(3)	C(1)-Nb(1)-C(41)	109.13(17)
Fe(1)-C(41)-Nb(1)	150.0(2)	C(5)-Nb(1)-N(3)	113.70(18)
C(43)-C(42)-C(41)	109.2(5)	C(4)-Nb(1)-N(3)	85.98(18)
C(43)-C(42)-Fe(1)	68.3(3)	C(1)-Nb(1)-N(3)	156.33(16)
C(41)-C(42)-Fe(1)	72.2(3)	C(41)-Nb(1)-N(3)	86.26(15)
C(43)-C(44)-C(45)	107.4(5)	C(5)-Nb(1)-N(1)	117.84(18)
C(43)-C(44)-FE(1)	70.3(3)	C(4)-Nb(1)-N(1)	86.68(18)
C(45)-C(44)-FE(1)	70.1(3)	C(1)-Nb(1)-N(1)	81.82(16)
C(44)-C(45)-C(41)	110.5(5)	C(41)-Nb(1)-N(1)	155.15(15)
C(44)-C(45)-FE(1)	69.0(3)	N(3)-Nb(1)-N(1)	77.40(13)
C(41)-C(45)-FE(1)	73.4(3)	C(5)-Nb(1)-N(5)	159.11(18)
C(55)-C(51)-C(52)	106.5(6)	C(4)-Nb(1)-N(5)	162.11(18)
C(55)-C(51)-Fe(1)	69.2(3)	C(1)-Nb(1)-N(5)	82.49(16)
C(52)-C(51)-Fe(1)	69.3(3)	C(41)-Nb(1)-N(5)	81.63(14)
C(53)-C(52)-C(51)	108.7(5)	N(3)-Nb(1)-N(5)	82.13(12)
C(53)-C(52)-Fe(1)	69.5(3)	N(1)-Nb(1)-N(5)	77.73(12)
C(44)-Fe(1)-C(54)	102.0(2)	C(54)-Fe(1)-C(51)	68.2(2)
C(44)-Fe(1)-C(43)	40.5(2)	C(43)-Fe(1)-C(51)	162.4(3)
C(54)-Fe(1)-C(43)	117.0(2)	C(45)-Fe(1)-C(51)	125.4(2)
C(44)-Fe(1)-C(45)	40.8(2)	C(53)-Fe(1)-C(51)	68.1(2)
C(54)-Fe(1)-C(45)	121.3(2)	C(55)-Fe(1)-C(51)	40.3(2)
C(43)-Fe(1)-C(45)	67.9(2)	C(52)-Fe(1)-C(51)	40.4(2)
C(44)-Fe(1)-C(53)	118.6(2)	C(54)-Fe(1)-C(42)	154.7(2)
C(54)-Fe(1)-C(53)	40.3(2)	C(43)-Fe(1)-C(42)	40.7(2)
C(43)-Fe(1)-C(53)	104.3(2)	C(45)-Fe(1)-C(42)	67.5(2)
C(45)-Fe(1)-C(53)	156.0(2)	C(53)-Fe(1)-C(42)	122.2(2)
C(44)-Fe(1)-C(55)	119.1(3)	C(55)-Fe(1)-C(42)	164.6(2)
C(54)-Fe(1)-C(55)	40.4(2)	C(52)-Fe(1)-C(42)	111.5(2)
C(43)-Fe(1)-C(55)	153.2(3)	C(51)-Fe(1)-C(42)	128.8(2)
C(45)-Fe(1)-C(55)	108.5(2)	C(44)-Fe(1)-C(41)	68.88(19)
C(53)-Fe(1)-C(55)	67.7(3)	C(54)-Fe(1)-C(41)	160.0(2)
C(44)-Fe(1)-C(52)	156.6(3)	C(43)-Fe(1)-C(41)	68.33(19)
C(54)-Fe(1)-C(52)	67.7(2)	C(45)-Fe(1)-C(41)	40.51(18)
C(43)-Fe(1)-C(52)	123.8(3)	C(53)-Fe(1)-C(41)	159.7(2)
C(45)-Fe(1)-C(52)	162.4(2)	C(55)-Fe(1)-C(41)	127.3(2)
C(53)-Fe(1)-C(52)	40.2(2)	C(52)-Fe(1)-C(41)	127.2(2)
C(55)-Fe(1)-C(52)	67.4(2)	C(51)-Fe(1)-C(41)	113.0(2)
C(44)-Fe(1)-C(51)	157.1(2)	C(42)-Fe(1)-C(41)	40.13(18)

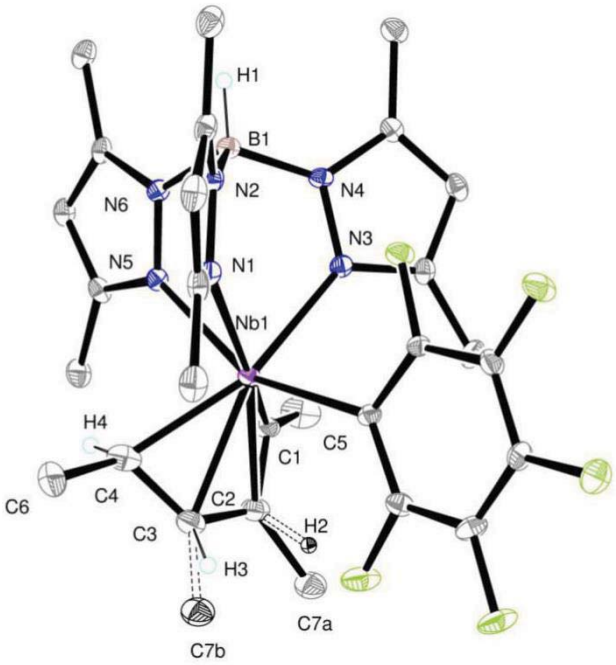

Table 3.13. *Crystal data and structure refinement for* ***9a, b***

Empirical formula	C28H33B1F5N6Nb1
Formula weight	651.32
Crystal size (mm)	0.19 x 0.04 x 0.02 mm
Crystal system	Triclinic,
space group	P-1
a (Å)	a = 8.2780(6)
b (Å)	15.8037(11) A
c (Å)	17.7145(9)
α (°)	76.156(3)
β (°)	81.396(2)
γ (°)	85.430(3)
V ($Å^3$)	1730.2(2)
Z	2
F	668
$\rho_{calculated}$ ($g.cm^{-3}$)	1.252
Radiation type	MoKa
Longueur d'onde (Å)	0.71073
Temperature	180 K
Limit of 2θ(°)	1.34 - 26.37
Nb of the reflections collected	15730
Nb of the reflections independent	6217 (0.0457)
Affinement by	F^2
Final R indices [I>2s(I)]	R1 = 0.0531, wR2 = 0.1199
R indices (all data)	R1 = 0.0839, wR2 = 0.1289
G.O.F (S)	1.012
Nb of the reflections used	6217 (I>2s(I)])
Nb of the parameters used	383
Δρmin/Δρmax(e. $Å^{-3}$)	0.558 / -0.594

Table 3.14. *Bond lengths (Å) for* ***9a, b***

C(1)-C(2)	1.412(6)	C(22)-C(23)	1.398(6)
C(1)-C(5)	1.472(6)	C(23)-C(24)	1.377(6)
C(1)-Nb(1)	2.002(5)	C(24)-N(2)	1.341(5)
C(2)-C(3)	1.421(6)	C(24)-C(25)	1.485(6)
C(2)-C(7A)	1.492(7)	C(31)-C(32)	1.482(6)

C(2)-Nb(1)	2.348(4)	C(32)-N(3)	1.340(5)
C(3)-C(7B)	1.42(4)	C(32)-C(33)	1.386(6)
C(3)-C(4)	1.428(7)	C(33)-C(34)	1.367(6)
C(3)-Nb(1)	2.347(4)	C(34)-N(4)	1.352(5)
C(4)-C(6)	1.501(7)	C(34)-C(35)	1.496(6)
C(4)-Nb(1)	2.226(4)	C(41)-C(42)	1.499(6)
C(11)-C(16)	1.380(6)	C(42)-N(5)	1.348(5)
C(11)-C(12)	1.389(5)	C(42)-C(43)	1.389(6)
C(11)-Nb(1)	2.344(4)	C(43)-C(44)	1.371(6)
C(12)-F(12)	1.348(5)	C(44)-N(6)	1.351(5)
C(12)-C(13)	1.380(6)	C(44)-C(45)	1.499(6)
C(13)-F(13)	1.351(4)	N(1)-N(2)	1.377(5)
C(13)-C(14)	1.364(6)	N(1)-Nb(1)	2.287(3)
C(14)-F(14)	1.350(5)	N(2)-B(1)	1.533(6)
C(14)-C(15)	1.365(6)	N(3)-N(4)	1.370(5)
C(15)-F(15)	1.351(5)	N(3)-Nb(1)	2.258(3)
C(15)-C(16)	1.383(6)	N(4)-B(1)	1.541(6)
C(16)-F(16)	1.356(4)	N(5)-N(6)	1.375(5)
C(21)-C(22)	1.486(6)	N(5)-Nb(1)	2.366(3)
C(22)-N(1)	1.350(5)	N(6)-B(1)	1.538(5)

Table 3.15. *Bond angles (°) for* ***9a, b***

C(2)-C(1)-C(5)	127.0(4)	N(4)-C(34)-C(35)	123.6(4)
C(2)-C(1)-Nb(1)	85.0(3)	C(33)-C(34)-C(35)	128.9(4)
C(5)-C(1)-Nb(1)	145.7(3)	N(5)-C(42)-C(43)	109.8(4)
C(1)-C(2)-C(3)	121.0(4)	N(5)-C(42)-C(41)	124.5(4)
C(1)-C(2)-C(7A)	121.1(4)	C(43)-C(42)-C(41)	125.6(4)
C(3)-C(2)-C(7A)	117.9(4)	C(44)-C(43)-C(42)	106.6(4)
C(1)-C(2)-Nb(1)	58.2(2)	N(6)-C(44)-C(43)	107.4(4)
C(3)-C(2)-Nb(1)	72.4(2)	N(6)-C(44)-C(45)	124.3(4)
C(7A)-C(2)-Nb(1)	144.7(3)	C(43)-C(44)-C(45)	128.2(4)
C(7B)-C(3)-C(2)	108.9(17)	C(22)-N(1)-N(2)	106.3(3)
C(7B)-C(3)-C(4)	125.2(17)	C(22)-N(1)-Nb(1)	129.4(3)
C(2)-C(3)-C(4)	125.8(4)	N(2)-N(1)-Nb(1)	122.5(2)
C(7B)-C(3)-Nb(1)	142.4(16)	C(24)-N(2)-N(1)	110.6(3)
C(2)-C(3)-Nb(1)	72.4(2)	C(24)-N(2)-B(1)	130.1(4)
C(4)-C(3)-Nb(1)	67.2(2)	N(1)-N(2)-B(1)	119.2(3)
C(3)-C(4)-C(6)	120.8(4)	C(32)-N(3)-N(4)	107.2(3)
C(3)-C(4)-Nb(1)	76.5(3)	C(32)-N(3)-Nb(1)	129.3(3)
C(6)-C(4)-Nb(1)	136.4(3)	N(4)-N(3)-Nb(1)	122.8(2)
C(16)-C(11)-C(12)	112.0(4)	C(34)-N(4)-N(3)	109.4(3)
C(16)-C(11)-Nb(1)	127.0(3)	C(34)-N(4)-B(1)	130.1(3)
C(12)-C(11)-Nb(1)	120.8(3)	N(3)-N(4)-B(1)	120.4(3)
F(12)-C(12)-C(13)	113.6(3)	C(42)-N(5)-N(6)	105.8(3)
F(12)-C(12)-C(11)	121.7(3)	C(42)-N(5)-Nb(1)	134.9(3)
C(13)-C(12)-C(11)	124.7(4)	N(6)-N(5)-Nb(1)	119.2(2)
F(13)-C(13)-C(14)	119.2(4)	C(44)-N(6)-N(5)	110.4(3)
F(13)-C(13)-C(12)	120.7(4)	C(44)-N(6)-B(1)	127.9(3)
C(14)-C(13)-C(12)	120.1(4)	N(5)-N(6)-B(1)	121.2(3)
F(14)-C(14)-C(13)	120.6(4)	C(1)-Nb(1)-C(4)	89.84(16)
F(14)-C(14)-C(15)	121.0(4)	C(1)-Nb(1)-N(3)	87.69(14)
C(13)-C(14)-C(15)	118.4(4)	C(4)-Nb(1)-N(3)	160.41(15)
F(15)-C(15)-C(14)	119.3(4)	C(1)-Nb(1)-N(1)	161.11(15)
F(15)-C(15)-C(16)	121.2(4)	C(4)-Nb(1)-N(1)	93.66(14)
C(14)-C(15)-C(16)	119.5(4)	N(3)-Nb(1)-N(1)	82.80(11)
F(16)-C(16)-C(11)	121.4(4)	C(1)-Nb(1)-C(11)	112.07(16)
F(16)-C(16)-C(15)	113.3(4)	C(4)-Nb(1)-C(11)	114.96(15)
C(11)-C(16)-C(15)	125.3(4)	N(3)-Nb(1)-C(11)	83.86(12)
N(1)-C(22)-C(23)	108.9(4)	N(1)-Nb(1)-C(11)	83.17(12)
N(1)-C(22)-C(21)	122.5(4)	C(1)-Nb(1)-C(3)	68.52(17)
C(23)-C(22)-C(21)	128.7(4)	C(4)-Nb(1)-C(3)	36.26(16)
C(24)-C(23)-C(22)	107.0(4)	N(3)-Nb(1)-C(3)	154.03(15)
N(2)-C(24)-C(23)	107.2(4)	N(1)-Nb(1)-C(3)	122.96(14)

N(2)-C(24)-C(25)	122.7(4)	C(11)-Nb(1)-C(3)	95.25(14)
C(23)-C(24)-C(25)	130.1(4)	C(1)-Nb(1)-C(2)	36.80(17)
N(3)-C(32)-C(33)	108.8(4)	C(4)-Nb(1)-C(2)	67.28(16)
N(3)-C(32)-C(31)	124.0(4)	N(3)-Nb(1)-C(2)	118.84(14)
C(33)-C(32)-C(31)	127.1(4)	C(34)-C(33)-C(32)	107.2(4)
N(4)-C(34)-C(33)	107.4(4)	N(1)-Nb(1)-C(2)	158.02(14)
C(11)-Nb(1)-C(2)	94.76(14)	C(11)-Nb(1)-N(5)	154.70(12)
C(3)-Nb(1)-C(2)	35.24(16)	C(3)-Nb(1)-N(5)	109.36(13)
C(1)-Nb(1)-N(5)	83.30(15)	C(2)-Nb(1)-N(5)	108.63(13)
C(4)-Nb(1)-N(5)	83.84(14)	N(2)-B(1)-N(6)	108.8(3)
N(3)-Nb(1)-N(5)	76.57(11)	N(2)-B(1)-N(4)	109.3(3)
N(1)-Nb(1)-N(5)	78.65(11)	N(6)-B(1)-N(4)	109.1(3)

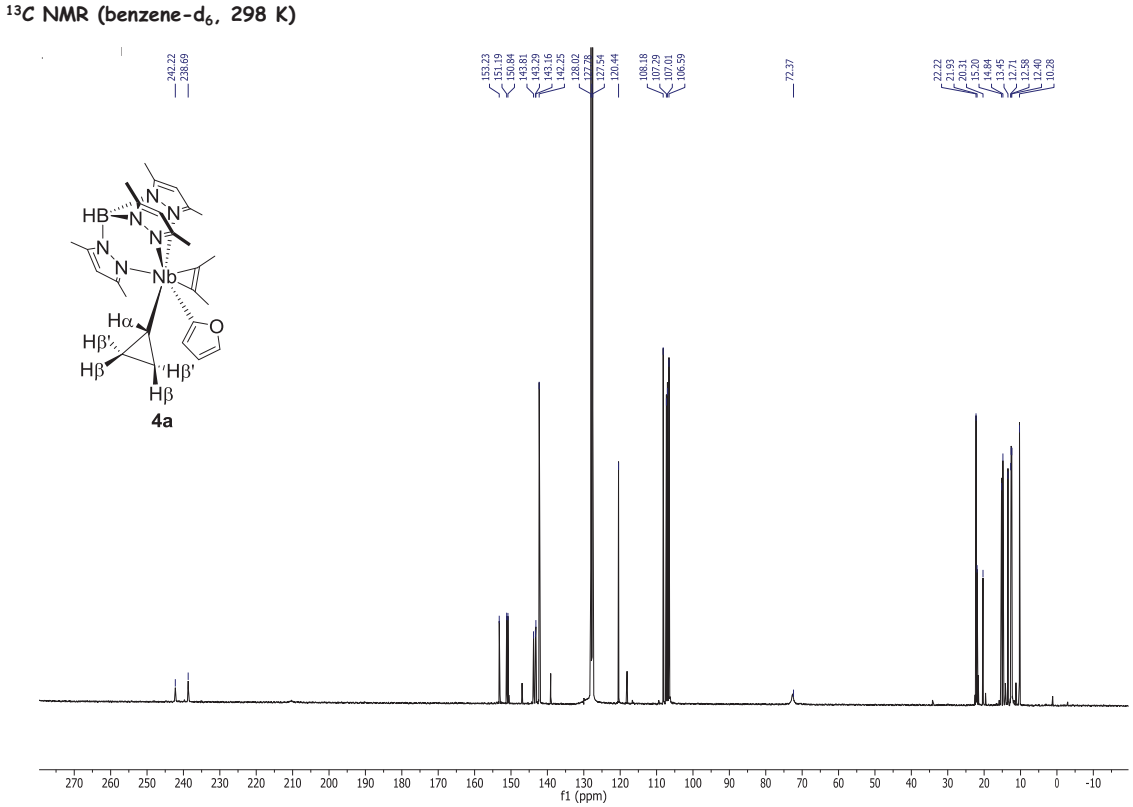

Figure 3.22. *^{13}C NMR of **4a** in benzene-d_6 at 298 K*

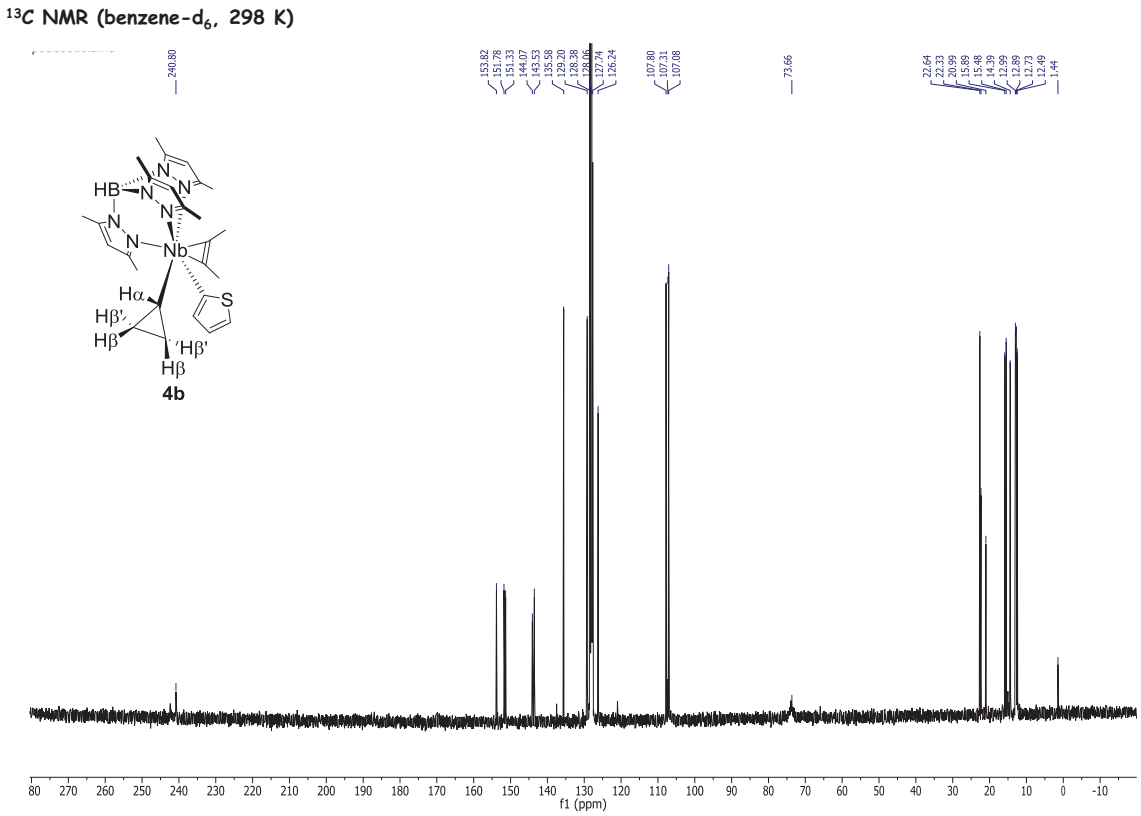

Figure 3.23. *^{13}C NMR of **4b** in benzene-d_6 at 298 K*

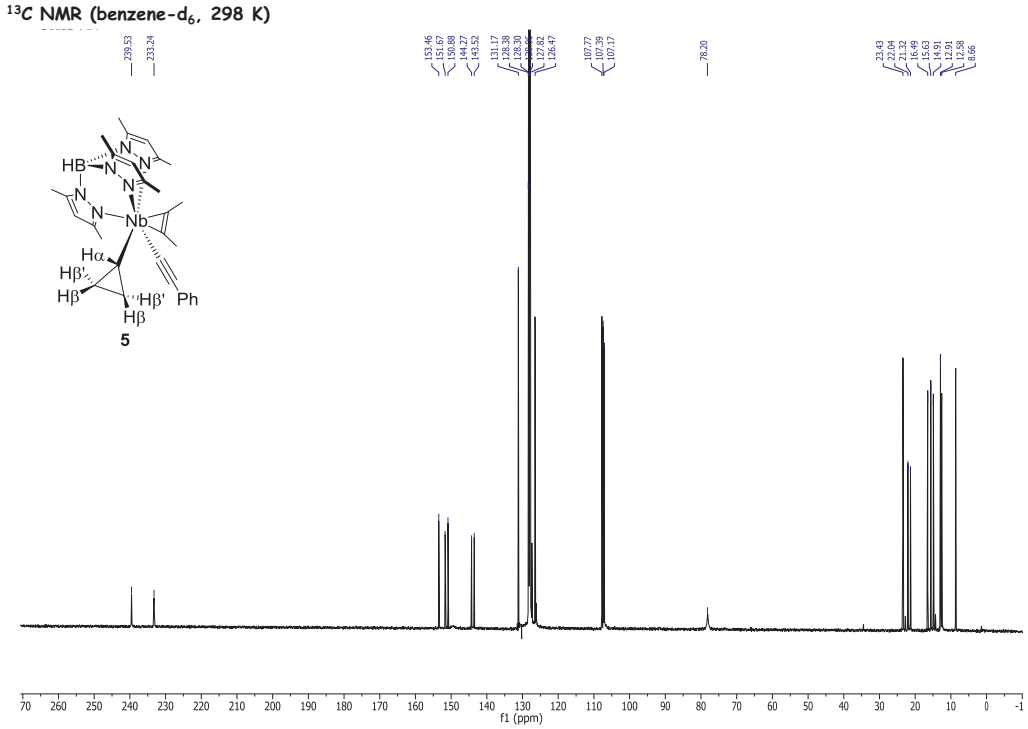

Figure 3.24. *^{13}C NMR of **5** in benzene-d_6 at 298 K*

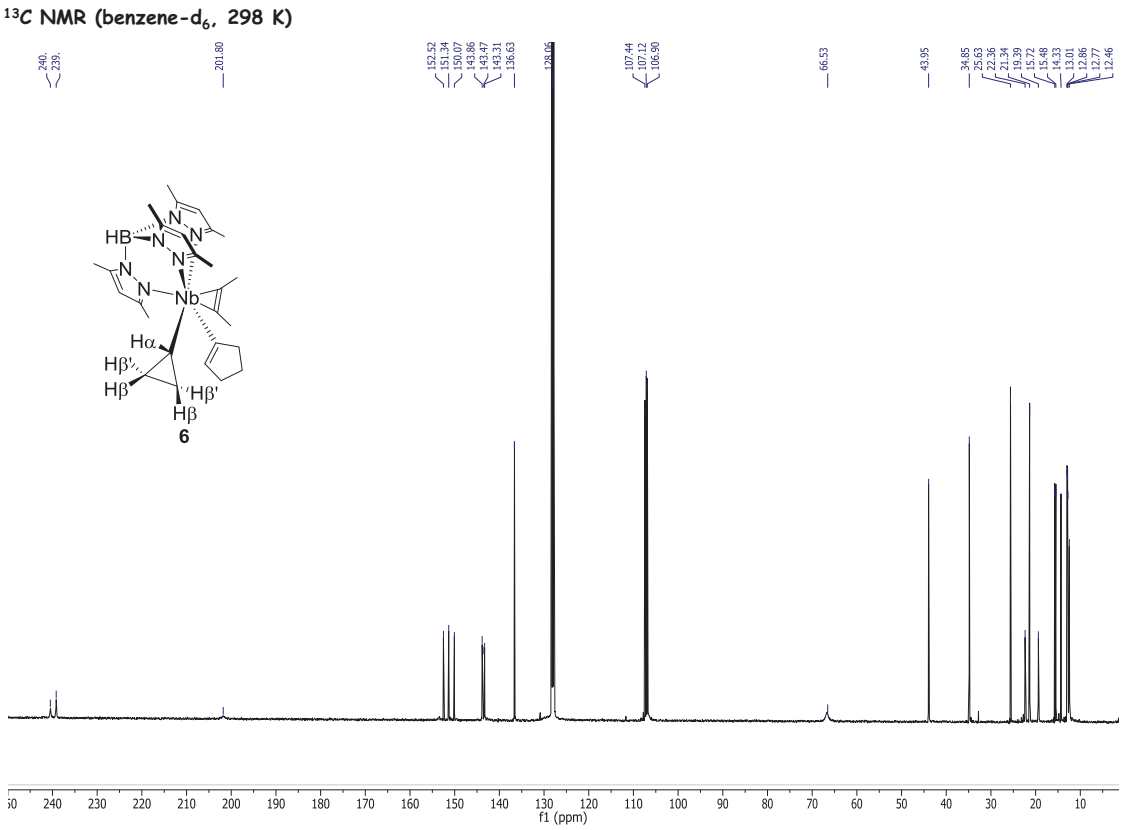

Figure 3.25. *^{13}C NMR of **6** in benzene-d_6 at 298 K*

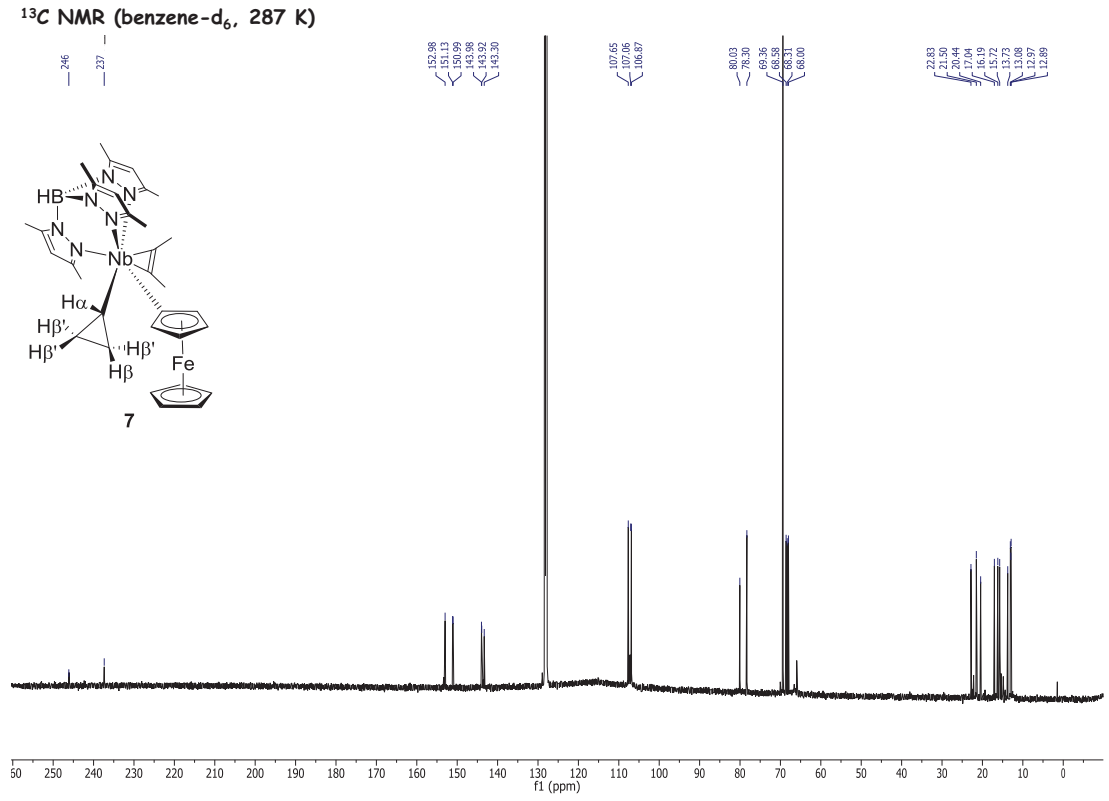

Figure 3.26. *^{13}C NMR of **7** in benzene-d_6 at 287 K*

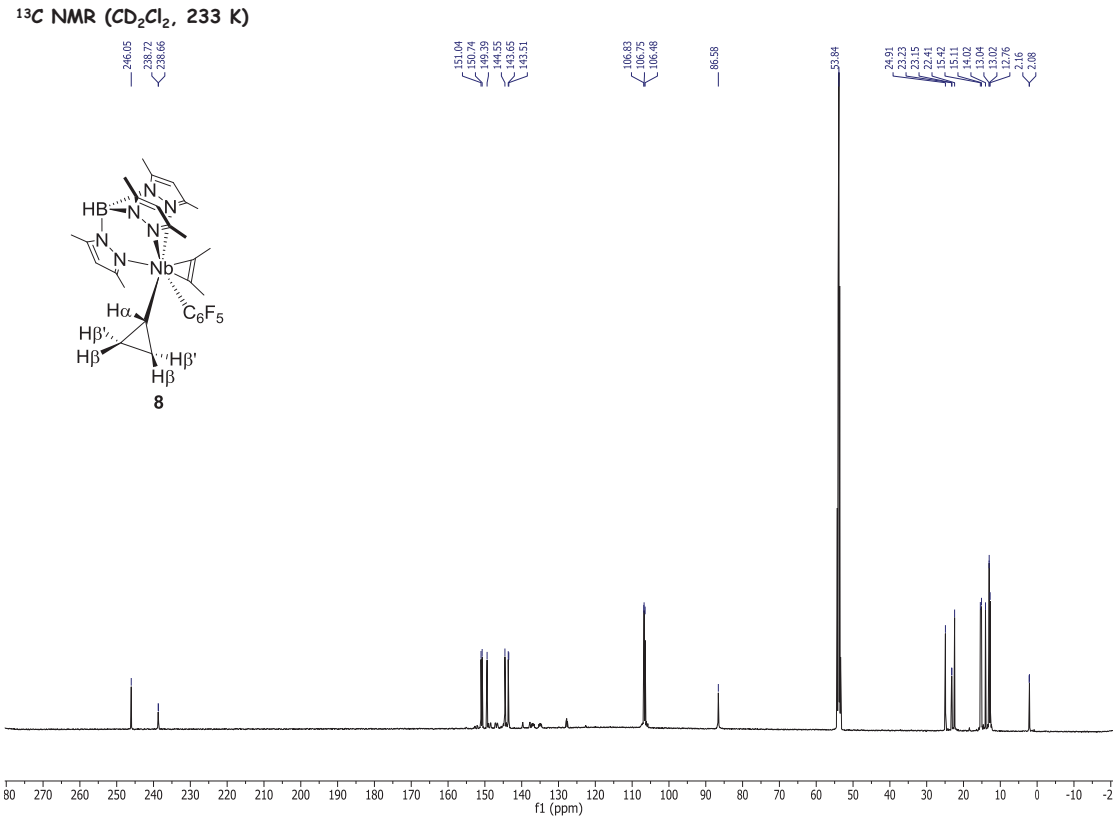

Figure 3.27. *^{13}C NMR of **8** in CD_2Cl_2 at 233 K*

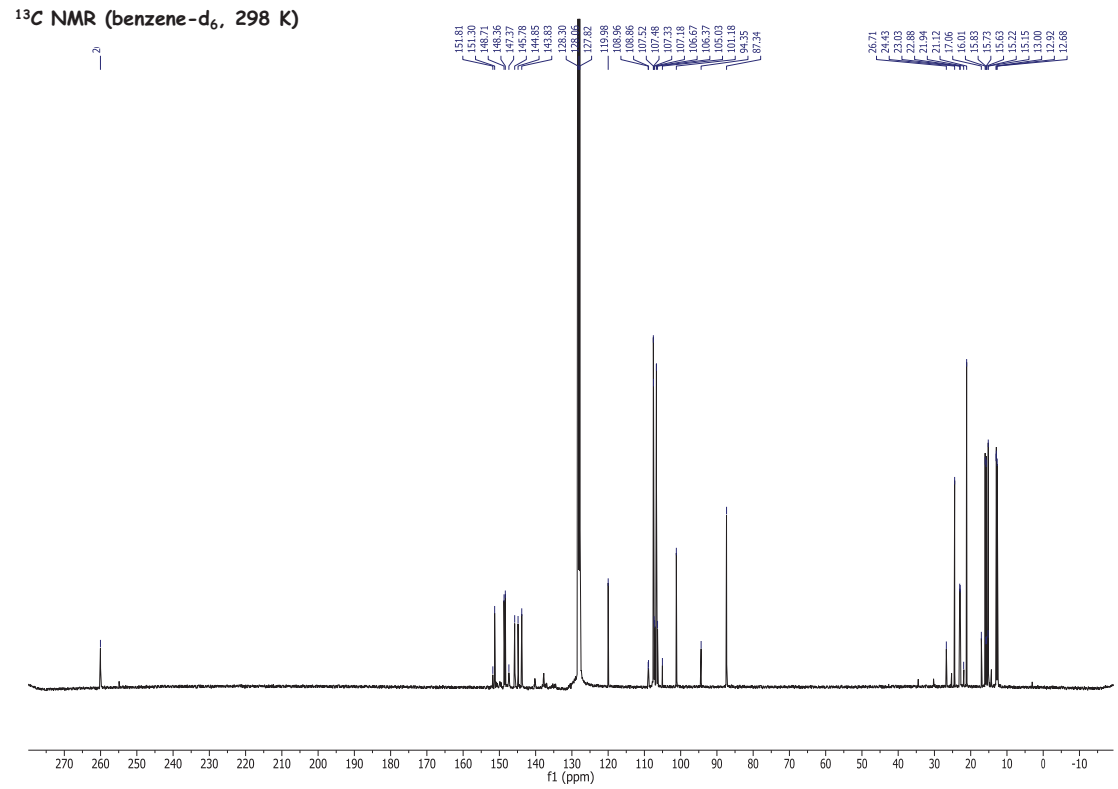

Figure 3.28. *^{13}C NMR of a mixture of **9a** and **9b** (molar ratio 88:12) in benzene-d_6 at 298 K*

Conclusion and perspectives

In the first part of this manuscript, we have proved that the transient η^2-cyclopropene complex [$Tp^{Me2}Nb(\eta^2$-*c*-$C_3H_4)(MeCCMe)$] (**A**), generated by an intramolecular abstraction of a β-H of the cyclopropyl group to form methane from [$Tp^{Me2}NbCH_3$(*c*-C_3H_5)(MeCCMe)] (**1**), could activate the CH bond of methane via a 1,3-addition mechanism under mild conditions. Degenerate reaction of **1** with $^{13}CH_4$ formed the isotopologue product **1-$^{13}CH_3$**. The fact that the degenerate reaction of **1** with CD_4 yields two diastereoisomers in a 3:1 ratio conclusively indicates that two elementary steps are involved in the activation of methane: (i) the generation of the transient η^2-cyclopropene intermediate **A** and, (ii) the activation of the CH bond of methane by **A** in a stereospecific 1,3-addition process. Spin saturation transfer experiments demonstrate that **1** activates the CH bond of methane by β-H abstraction/1,3-addition pathway, a dissociative mechanism. Kinetic study on the reaction of [$Tp^{Me2}Nb$(Mesityl)(*c*-C_3H_5)(MeCCMe)] (**3**) with CH_4 shows that the reaction is 1st order in **3** and zeroth order in CH_4, indicating that the formation of the transient η^2-cyclopropene intermediate **A** is rate-determining. The β-H abstraction step has a very negative activation entropy due to a highly ordered transition state. The rate constants for the CH bond activation of methane by the β-H abstraction/1,3-addition mechanism have the same order of magnitude as those for α-H abstraction/1,2-addition processes in related complexes. DFT studies reveal that the intermediate **A** forms labile σ-adduct complex with methane (σ-CH_4) via a loose van der Waals interaction before the activation of the CH bond of methane. The optimized transition state for the methane CH bond elimination/activation is in a four-center σ-bond metathesis mode with a distinctive involvement of both carbons of the η^2-cyclopropene ligand engaged in the hydrogen transfer.

In the second part of this manuscript, we have shown that the CH bond of heteroaromatics, unsaturated hydrocarbons, pentafluorobenzene and ferrocene (FcH) could be activated by **A** via the same 1,3-CH bond addition mechanism to form [$Tp^{Me2}NbX$(*c*-C_3H_5)(MeCCMe)] [X =2-C_4H_3O (**4a**), 2-C_4H_3S (**4b**), PhC≡C (**5**), 1-C_5H_7 (**6**), Fc(**7**) and C_6F_5 (**8**)] under mild conditions. Electrochemical studies of complexes **1**, **5, 6,** and **7** shows one-electron reversible reduction of the niobium center. The reducibility of complexes follows the order, **1** ($E_{1/2}$ = -2.85 V) < **6** ($E_{1/2}$ = -2.75 V) < **7** ($E_{1/2}$ = -2.67 V) < **5** ($E_{1/2}$ = -2.41 V), which reflects the LUMO energy of the complexes should in the order **1** > **6** > **7** > **5** influenced by the hybridization of the niobium-bound carbon sp^3 (Me) < sp^2 (*c*-C_5H_7) < sp^2*(Fc)* < *sp*

(CCPh). The exchange reactions between **4a**, **5**, **6**, **7** with benzene indicate that the regioselectivity issues are influenced by the thermodynamic preferences for the CH bond activation of hydrocarbons, which is determined by the intrinsic Nb-C bond strengths of the complexes. Besides, the regioselectivity is also affected by the pK_a values of the C-H bond, and steric effects of both the complexes and the hydrocarbons.

A first perspective of this work could be focused on synthesizing other cyclopropyl organometallic precursors of the general formula $L_nMR(c\text{-}C_3H_5)$, (L_n = monoanionic multidentate ligand; R = alkyl group), that would form $L_nM(\eta^2\text{-}c\text{-}C_3H_4)$ intermediates able to activate the strong CH bond of CH_4 and other hydrocarbons. The metals would be those of groups 3 to 6. Various ligands L_n (Cp, Tp, etc.) forcing *cis*-arrangement needed for RH elimination would provide scaffolds whose steric and electronic properties can be tuned conveniently. In connection, a second perspective would be to achieve a full understanding of the whole β-H abstraction/1,3-CH bond addition mechanism in which the C-H bond of methane is cleaved by these $L_nM(\eta^2\text{-}c\text{-}C_3H_4)$ intermediates by isotopic labelling using CD_4 and $^{13}CH_4$, kinetic studies including SST and numerical simulation of concentration profiles. Reaction pathways, including the structure of the intermediates and transition states, will be unveiled by DFT calculations. Attempts at observing these intermediates $L_nM(\eta^2\text{-}c\text{-}C_3H_4)$ directly in the gas phase is planned through the use of intermediates by UV-PES. This spectroscopy allows the determination of ionization potentials of the molecules, real electronic "fingerprints", which can be directly correlated with the molecular orbitals energy levels. Coupled with flash vacuum thermolysis, UV-PES would allow to monitor on-line the thermal degradation of the cyclopropyl complexes.

Finally, coupling these CH bond activation reactions with a reaction that would functionalize methane, ideally catalytically, is the ultimate goal. We must admit that currently, there is no such reaction.

Activation de la liaison CH du méthane par un complexe intermédiaire η^2-cyclopropène de niobium

Activation de la liaison CH du méthane par un complexe intermédiaire η^2-cyclopropène de niobium

Le manuscrit se concentre sur l'activation de la liaison CH de différents hydrocarbures, en particulier le méthane par un η^2-cyclopropène intermédiaire de niobium. Seule l'activation de la liaison CH du méthane est ici résumée.

Chapitre 1: Les processus d'activation de la liaison CH du méthane.

Le méthane est une source d'énergie et de produits chimiques en raison de son abondance sous forme de gaz naturel (80-90%) et de gas de schiste. Les utilisations actuelles du méthane comprennent son oxydation complète en CO_2 et H_2O pour fournir de la chaleur (et d'électricité) et la production de syn gaz (un mélange de CO et H_2) par steam reforming ($CH_4 + H_2O = CO + 3H_2$), un processus endergonic très exigeant énergétiquement, catalysé par des catalyseurs à base de nickel à des températures élevées (*ca* 700 - 1000 ° C) et une pression modérée (< 25 bars), qui est utilisé pour la synthèse de toute une gamme de produits chimiques de base.

La fonctionnalisation catalytique du méthane dans des produits chimiques facilement transportables et à haute valeur ajoutée selon une voie propre, économique et durable reste un objectif à long terme d'un point de vue scientifique, environnementale et économique. Le méthane est en effet très inerte, montrant un potentiel d'ionisation de ~ 12,5 eV, avec une électronégativité de Pauling $\chi_C = 2,55$ et $\chi_H = 2,20$, une valeur de pK_a estimé à ~ 50 - 51 et une enthalpie de dissociation homolytique de la liaison C-H de 440 kJ/mol à 25 ° C. Par conséquent, il est très difficile d'activer la forte liaison CH du méthane directement, par une voie hétérolytique ou homolytique.

Dans le but de bénéficier de la flexibilité des systèmes homogènes, des applications importantes ont été trouvé dans la catalyse par des complexes des métaux de transition. L'utilisation de complexes de métaux de transition, en outre, permet un réglage précis de

divers facteurs, de sorte que la conception moléculaire des catalyseurs et la compréhension détaillée du mécanisme intime des réactions soient possibles. Un résumé des différentes voies de clivage d'une liaison CH par des complexes des métaux de transition est représenté dans le schéma 1.1. Certains complexes de métaux de transition de la gauche et de la droite du tableau périodique sont capables d'activer le méthane par différentes voies mécanistiques, mais seulement quelques-uns d'entre eux ont conduit à des applications catalytiques. Dans les sections suivantes, nous allons décrire par un aperçu général les différents schémas d'activation de la liaison CH selon les lesquels les complexes des métaux de transition peuvent activer le méthane dans des conditions homogènes.

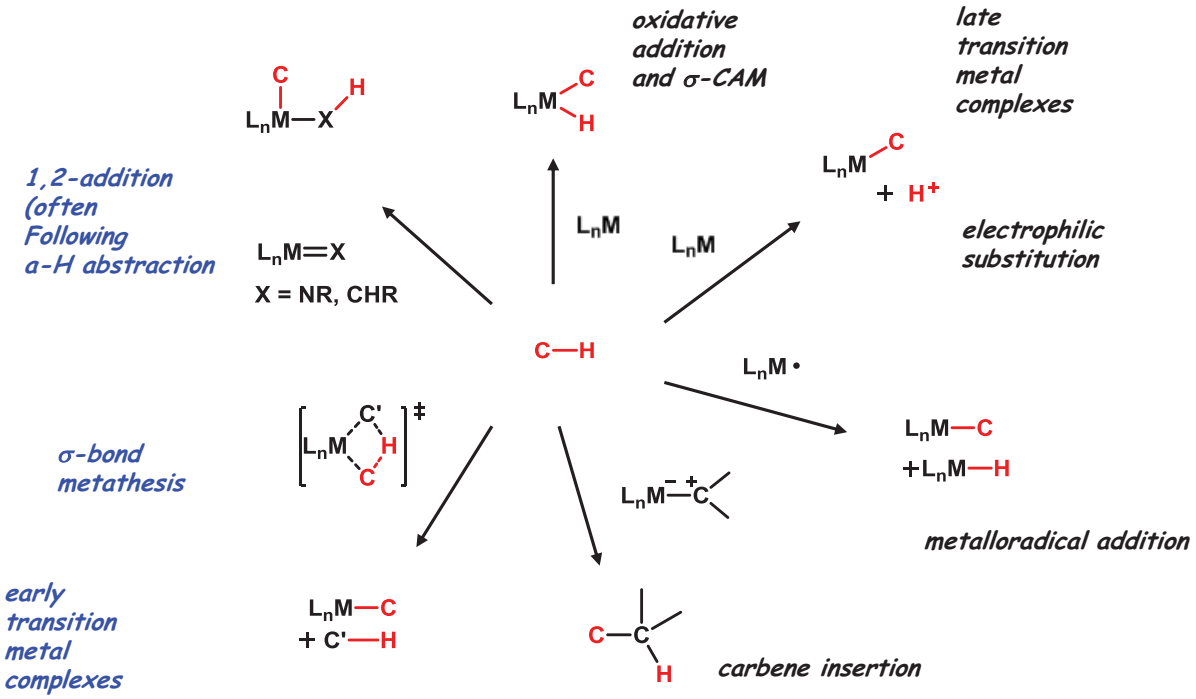

Schéma 1.1. *Les principales voies d'activation de la liaison CH effectué par des complexes des métaux de transition.*

1.1- Activation de la liaison CH du méthane par des complexes de la droite du tableau périodique

Les complexes contenant des métaux de transition de la droite du tableau périodique sont capables d'activer la liaison CH du méthane par différentes voies telles que la substitution électrophile, l'addition oxydante, l'insertion d'un carbène et l'addition d'un radical

métallique. Dans la section qui suit les principales caractéristiques de chaque mécanisme d'activation seront discutées.

1.1.1- Substitution electrophile

Les métaux de la droite du tableau périodique et les lanthanides agissent comme des acides de Lewis, réagissant avec du méthane par une substitution électrophile en milieu polaire (Équation 1.1).

Le schéma 1.2 décrit les systèmes capables d'activer le méthane selon un mécanisme de substitution électrophile. Ces systèmes sont remarquables car ils constituent des rares exemples de fonctionnalisation catalytique du méthane avec des complexes métalliques homogènes, mais avec une faible TOF et TON.

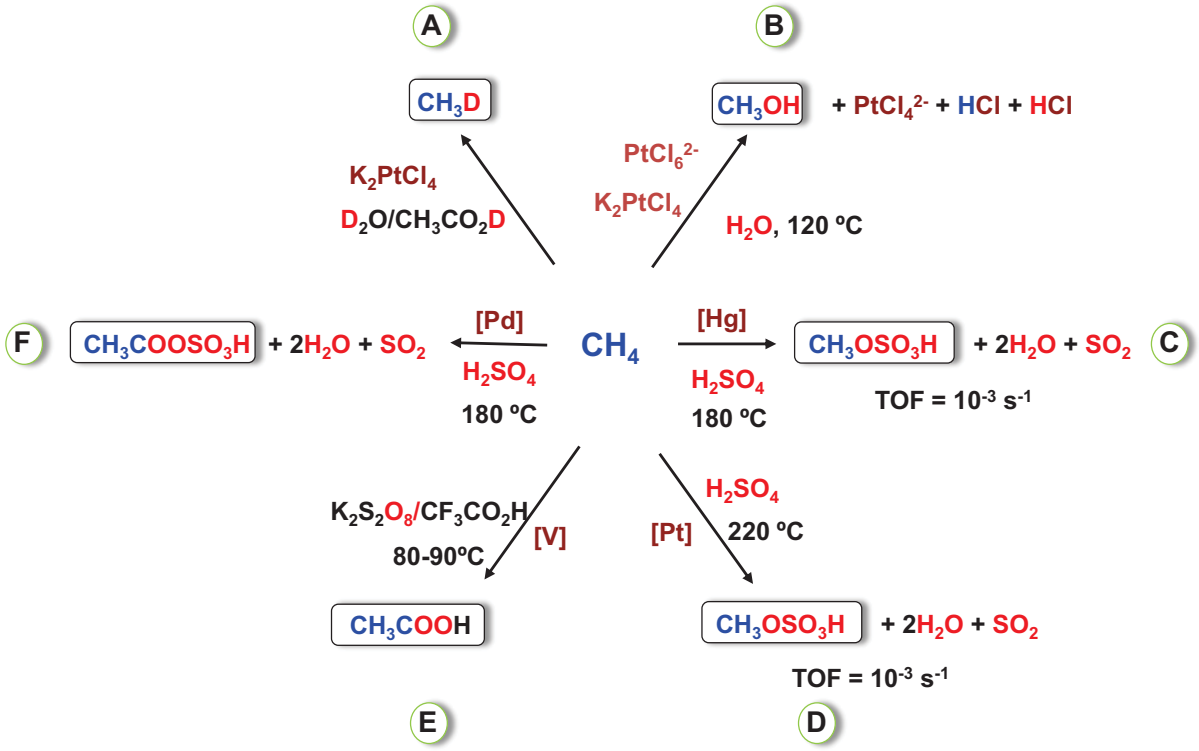

Schéma 1.2. *Fonctionnalisation catalytique de la liaison CH du méthane par la voie de substitution électrophile.*

1.1.2- Addition oxydante

Le mécanisme le plus commun pour l'addition oxydante d'une liaison C-H d'un alcane est l'addition concertée à 3-centre dans laquelle les équivalents de réduction du métal doivent être suffisamment hauts en énergie pour occuper l'orbitale σ* du C-H et former deux nouvelles liaisons (M-C et M-H). D'après l'équation 1.2, par conséquent, l'augmentation de deux unités de l'état d'oxydation du métal est accompagnée par la formation de deux nouvelles liaisons métal-hydrure et métal-méthyle.

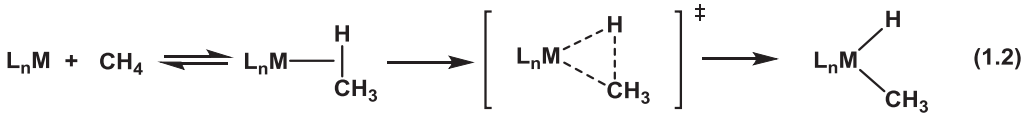

Dans les années 1980, Janowicz et Bergman et Graham ont découvert que des espèces transitoires de cyclopentadienyliridium (I), riches en électrons et à bas degré d'oxydation, pouvaient activer la liaison C-H du méthane (Schéma 1.3 et Schéma 1.4).

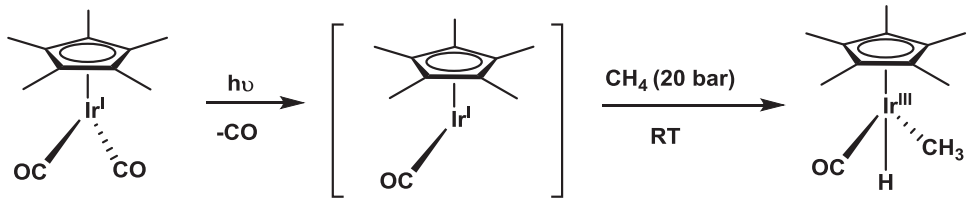

Schéma 1.3. *Addition oxydante du méthane par un complexe insaturé d'Ir(I) photo généré.*

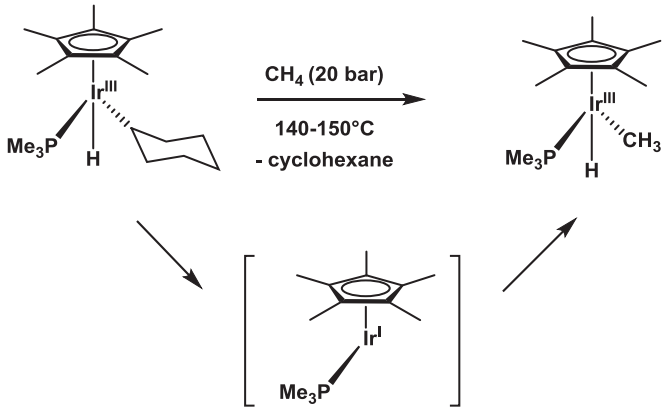

Schéma 1.4. *Addition oxydante du méthane par un complexe insaturé d'Ir(I) thermo généré.*

Les mêmes auteurs ont découvert 10 ans plus tard qu'un complexe cationique d'iridium (III), $[Cp^*Ir(PMe_3)(CH_3)(CH_2Cl_2)][BArF_4]$ est encore plus réactifs vis-à-vis du méthane. Hall

et al. ont calculé une voie d'addition oxydante et d'élimination réductrice impliquant un intermédiaire d'Ir (V) (Schéma 1.5).

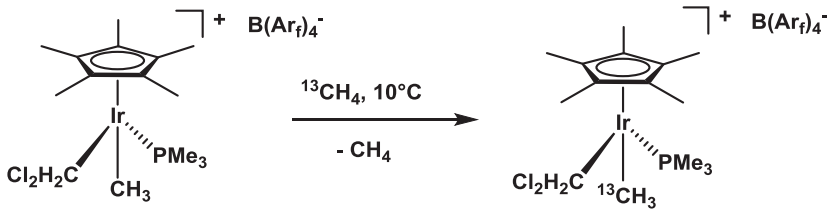

Schéma 1.5. *Activation de la liaison CH du $^{13}CH_4$ par le complexe [Cp*Ir(PMe$_3$)(CH$_3$)(CH$_2$Cl$_2$)][BArF$_4$]*

Jones et Maguire ont profité du couple Re(III)/(V) pour montrer que [CpRe(PPh$_3$)$_2$H$_2$] pouvait catalyser l'échange H/D entre C_6D_6 et CH_4, avec 68 turnovers en 3h, ce qui représente l'un des rares systèmes capables d'activer le méthane par voie catalytique (Schéma 1.6).

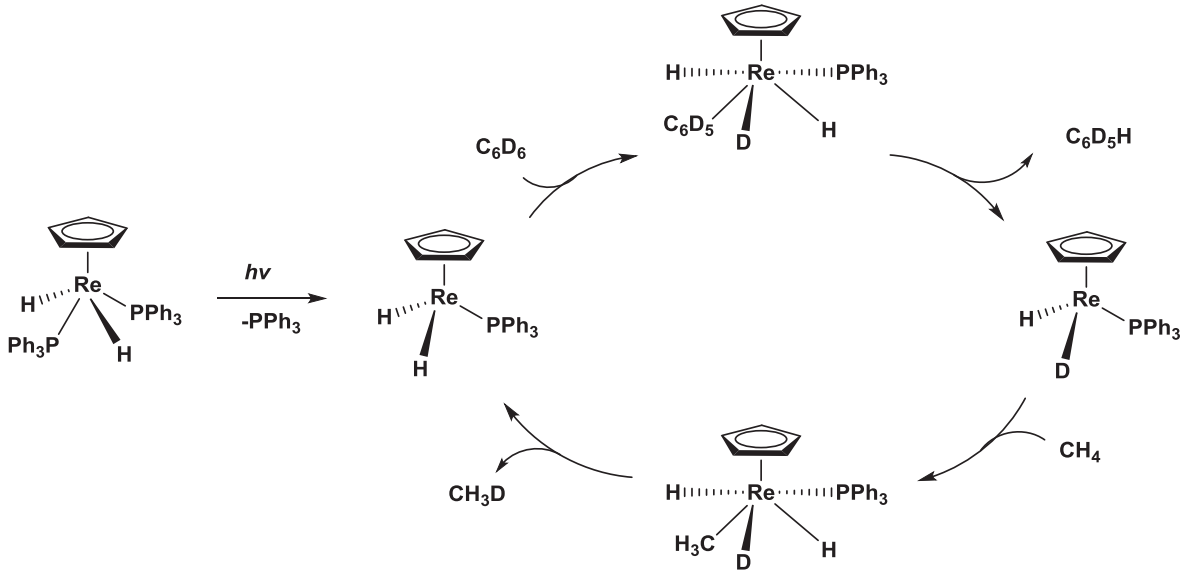

Schéma 1.6. *Mécanisme d'échange H/D entre le CH_4 et le C_6D_6, catalysé par un complexe de cyclopentadienylrhenium(I).*

En présence de certains précurseurs de Re, Rh et Ir, l'addition oxydante, couplée à des réactions de borylation, a montré un grand potentiel pour la fonctionnalisation des alcanes et des arènes vers la formation de liaisons C-C étendues. Cependant, aucune de ces transformations ont été élargis au CH_4, probablement en raison des difficultés rencontrées dans la manipulation de ce gaz ainsi que dans la présence de réactions de compétition avec le

solvant.

1.1.3- Insertion d'un carbene

Une approche différente vers l'activation et la fonctionnalisation de la liaison C-H d'un alcane concerne l'insertion d'un carbone électrophile dans une liaison C-H. Cette stratégie a été réalisée récemment par les groupes de Perez, Etienne et Asensio via l'insertion catalytique d'un carbène dans la liaison CH du méthane. En utilisant un ligand indazolyle borate perfluoré sur un centre métallique d'Ag (I), des pressions élevées de méthane (160 atm), du CO_2 supercritique (250 atm) et du diazoacétate d'éthyle (EDA), le méthane est converti en ethylpropionate par l'insertion du carbène :$CHCO_2Et$ dans une liaison CH du méthane (Schéma 1.7). Des valeurs de TON et TOF de 734 et 1,4 × 10^{-2} s^{-1}, respectivement, ont été atteints, ces derniers étant, au mieux de notre connaissance, les taux de conversion les plus élevés rapportés à ce jour pour la fonctionnalisation du méthane dans des conditions homogènes.

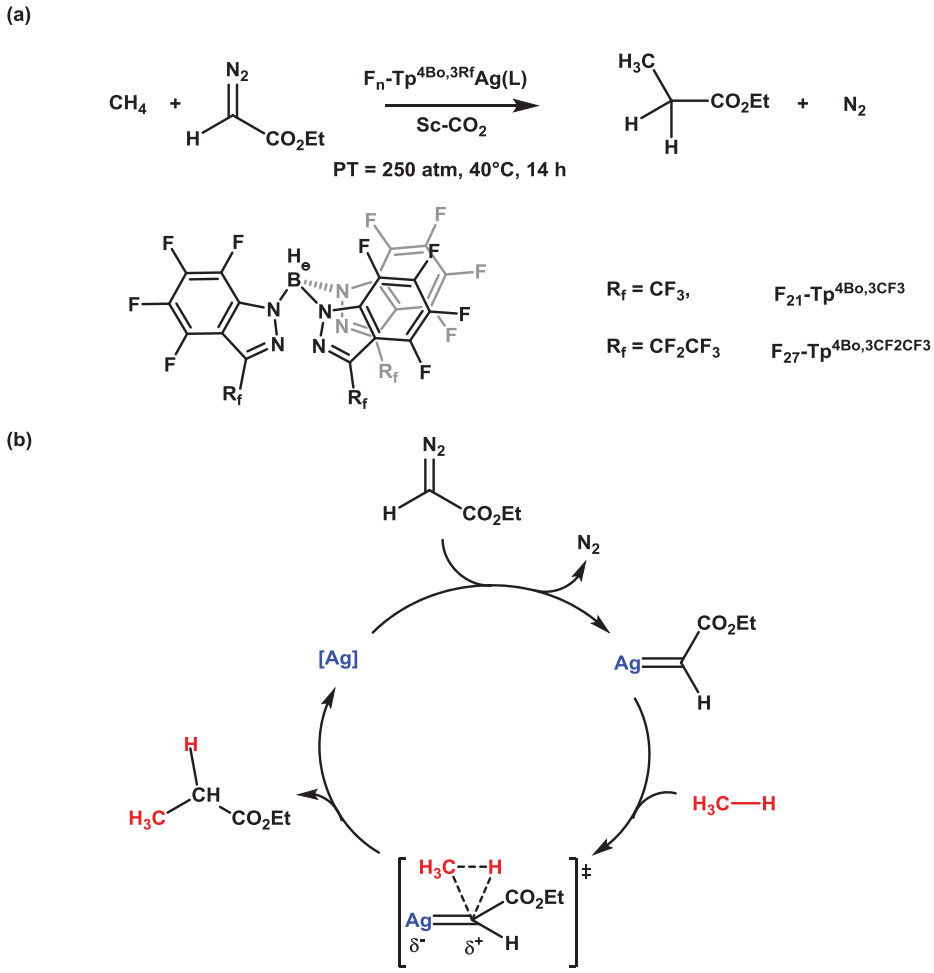

Scheme 1.7. *Fonctionnalisation catalytique du méthane par insertion d'un carbene.*

1.2- Activation de la liaison CH du méthane par des complexes de la gauche du tableau périodique

Des complexes des métaux de transition de la gauche du tableau périodique (et de métaux électropositifs connexes tels que des lanthanides ou des actinides) sont également capables d'activer la liaison C-H du méthane (et plus généralement des hydrocarbures). Dans ce cas, les voies mécanistiques concernées sont la métathèse de liaison σ, l' addition 1,2 (souvent à la suite d'une abstraction d'un H en α) et l'addition 1,3 (souvent à la suite d'une abstraction d'un H en β).

1.2.1- Métathèse des liaisons σ

Certains complexes alkyles et hydrures contenant des métaux de transition d^0 et d^0f^n pauvres en électrons sont capables d'activer des liaisons C-H saturées par métathèse de liaison σ. Le mécanisme de métathèse de liaison σ implique la formation d'un état de transition polaire à quatre centres et à quatre électrons dans lequel la liaison métal-alkyle du complexe initial est rompu pour former une nouvelle liaison métal-alkyle et un alcane libre. La métathèse de liaison σ diffère des autres mécanismes décrits ici en ce que l'activation C-H est l'étape déterminant la vitesse.

Concernant l'activation C-H du méthane, Watson a d'abord constaté que des complexes métallocènes méthyliques d'yttrium et de lutécium activaient la liaison CH du méthane par un état de transition à quatre centres, où l'atome d'hydrogène en cours de transfert est situé à mi-chemin entre les deux groupes méthyles. $^{13}CH_4$ réagit avec $[Cp^*_2M(CH_3)]$ (M = Lu, Y) par un processus d'échange dégénéré pour former $[Cp^*_2M(^{13}CH_3)]$ et CH_4 à 70 ° C (Schéma 1.8).

Des études cinétiques montrent que la vitesse de réaction est du premier ordre en $[Cp^*_2Lu(CH_3)]$ et du premier ordre en CH_4, ce qui implique un état de transition à quatre centres (Figure 1.1).

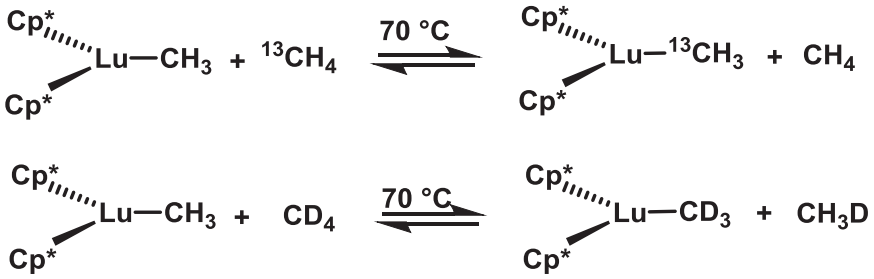

Scheme 1.8. *Réactions dégénérées entre le complexe [$Cp_2Lu(CH_3)$] et le $^{13}CH_4/CD_4$.*

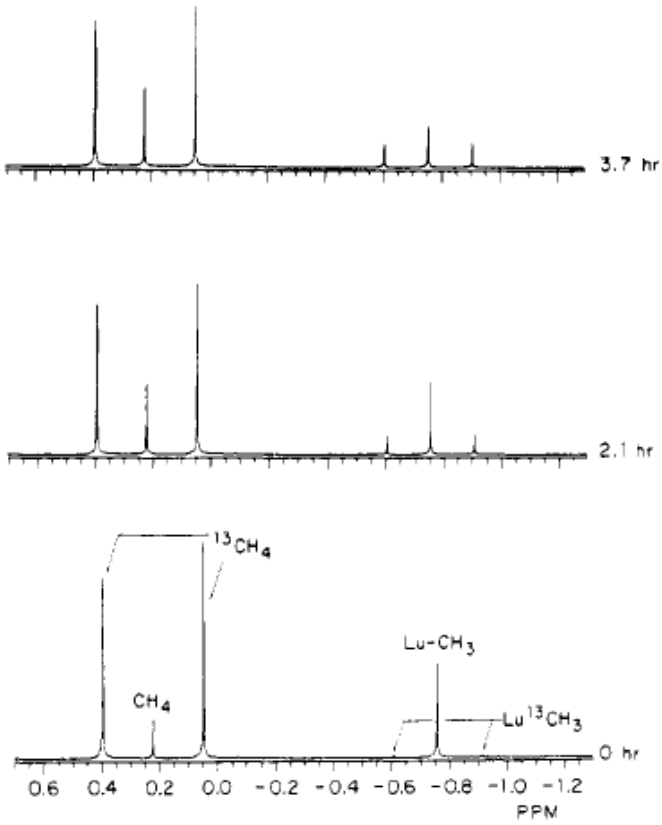

Figure 1.1. *Spectre RMN du ^1H pour la réaction du [$Cp^*_2Lu(CH_3)$] avec $^{13}CH_4$ en fonction du temps à 70 °C.*

Le groupe de Bercaw a étudié des dérivés hydrures ou alkyles du permethylscandocene pour l'activation des liaisons C-H sp^3, sp^2 et sp dans différents hydrocarbures. Le $^{13}CH_4$ réagit avec le composé [$Cp^*_2Sc(CH_3)$] par un processus d'échange dégénérée pour former le derivé [$Cp^*_2Sc(^{13}CH_3)$] et CH_4 à 70 ° C.

Selon plusieurs études expérimentales et computationnelles, l'état de transition (TS) dans le profil réactionnel est obtenu sans passer par un intermédiaire. Le TS pour le clivage de la liaison CH a une forme particulière de cerf-volant avec une disposition presque linéaire entre

les groups CH_3 ... H ... CH_3 (Schéma 1.9). De plus, la distance de la liaison C-H du méthane est beaucoup plus longue dans l'état de transition (1.33Å) que dans le méthane libre (1.09 Â).

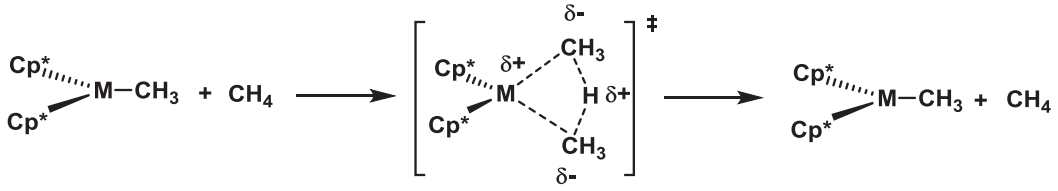

Schéma 1.9. *Métathèse des liaisons σ du méthane (M = Sc, Y, Lu)*

En 2003, Sadow et Tilley ont démontré que les complexes métallocènes alkyles de scandium pouvaient activer le méthane préférentiellement par rapport au benzène à température ambiante. En couplant la métathèse des liaisons σ et l'insertion migratoire, ils ont réalisé le couplage catalytique du méthane et du propène pour donner le 2-méthylpropane. Comme cela est représenté dans le schéma 1.10 (a), [$Cp^*_2ScCH_3$] insère du propène pour donner [$Cp^*_2Sc(CH_2CH(CH_3)_2)$], qui réagit avec CH_4 pour régénérer le complexe méthyle et libérer le 2-méthylpropane avec un faible TON de 4.

Le complexe [$Cp^*_2Sc(CH_3)$] est également un catalyseur pour la réaction de déshydrogénation du méthane et du diphénylsilane par laquelle Ph_2SiH_2 et CH_4 sont convertis en Ph_2MeSiH et H_2 via deux réactions consécutives de métathèse des liaisons σ (Schéma 1.10 (b)).

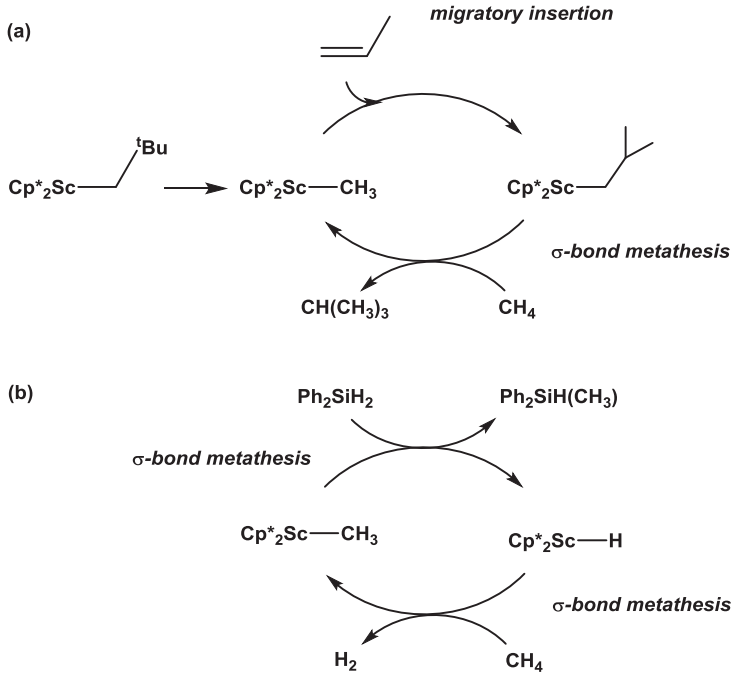

Schéma 1.10. *Métathèse de liaisons σ-du méthane.*

1.2.2- Addition CH 1,2.

L'addition d'une liaison C-H dans une liaison multiple métal-ligand a été désignée comme une addition 1,2 d'une liaison C-H. Bien que ce processus ressemble à la métathèse des liaisons σ, car elle implique un état de transition à 4-centres, le résultat est sensiblement différente. L'addition 1,2 d'une liaison C-H, en effet, implique la formation d'un intermédiaire à haute énergie, contenant une liaison multiple métal-ligand, qui exécute l'étape de clivage de la liaison C-H. Un système remarquable basée sur des métaux du groupe 4, 5 et 6 a été développé par Wolczanski et ses collègues. Le premier exemple décrivant l'activation du méthane (parmi beaucoup d'hydrocarbures) a été décrit avec des complexes alkyles tris (amido) de zirconium du type [(^{t}Bu$_3$SiNH)$_3$ZrR]. Avec R = Cy, le cyclohexane est éliminé au-dessus de 80 °C par une abstraction intramoléculaire CH en α pour donner le complexe transitoire diamidoimido [(^{t}Bu$_3$SiNH)$_2$Zr=NSi^{t}Bu$_3$] non observé, (Schéma 1.11).

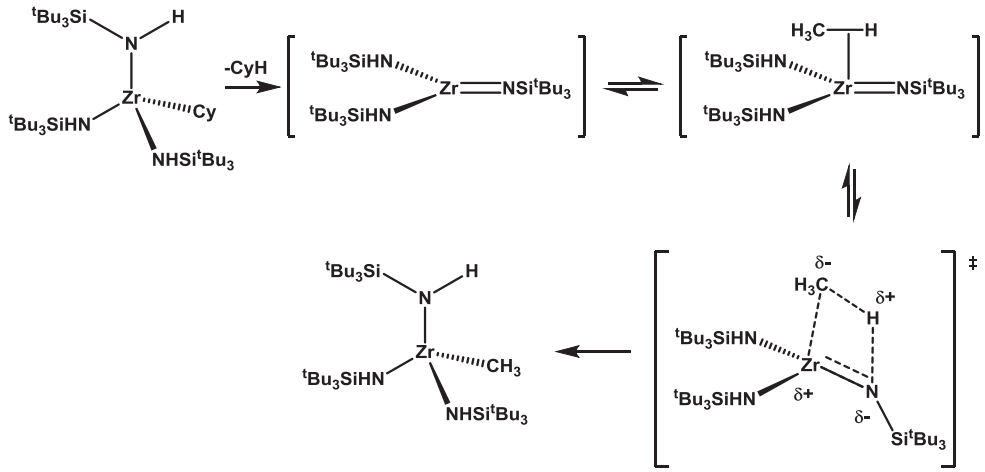

Schéma 1.11. *Activation de la liaison CH du méthane par un intermédiaire imido de Zr.*

Plus récemment, le processus d'abstraction CH en position α/d'addition CH en position 1,2 a été étendu à des liaisons multiples métal carbone par Mindiola (Schéma 1.12). Un composé transitoire alkylidyne de titane [(PNP)Ti≡CR], généré par abstraction d'un H en position α d'un alcane à partir du complexe alkyle alkylidène [(PNP)Ti(=CH^{t}Bu)(CH$_2$^{t}Bu)], casse la liaison CH du méthane selon une voie similaire à celle décrite dessus. Remarquablement le complexe [(PNP)Ti(=CH^{t}Bu)(CH$_3$)] expulse le méthane très lentement à température ambiante ($t_{1/2}$ = 62 h à 25 °C).

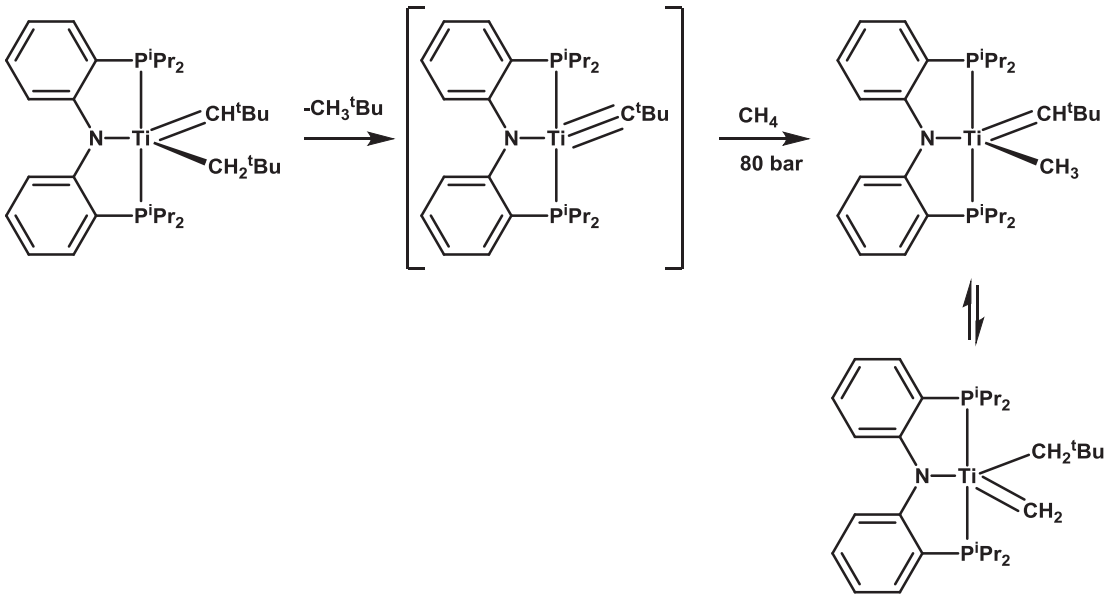

Schéma 1.12*.Activation de la liaison CH du méthane par un intermédiaire alkylidyne de Ti.*

1.2.3- Addition CH 1,3

Par rapport aux nombreux exemples d'abstraction CH réversible en position α / d'addition CH en position 1,2, il existe peu d'exemples d'abstraction CH réversible en position β / d'addition CH en position 1,3, à partir de complexes de dialkyle. Un seul exemple a été décrit pour l'activation du méthane. Erkerhas en premier a démontré qu'un intermédiaire relativement stable de [$Cp_2Zr(\eta^2$-benzyne)] (le benzyne agit comme une bonne base π), généré par une abstraction intramoléculaire réversible d'un H en position β des diarylzirconocenes, est capable de cliver la liaison CH du benzène par une addition 1,3. Dans la plupart des cas, cependant, le complexe η^2–alcène, à la suite d'une perte rapide d'alcène, n'est souvent pas assez stable pour permettre l'activation de la liaison CH dans l'étape suivante (Schéma 1.13).

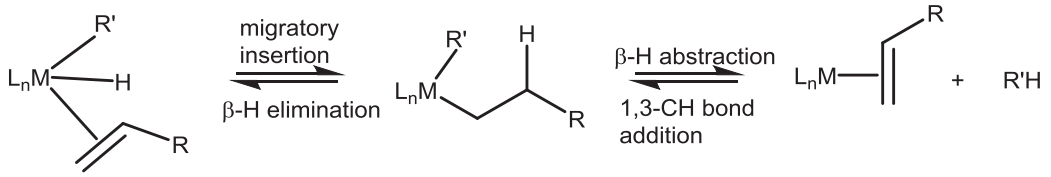

Schéma 1.13. *Abstraction d'un H β et élimination d'un H β dans un complexe alkyle.*

Le seul cas d'activation du méthane suivant cette voie d'addition CH en position 1,3 a été réalisé sur un centre de tungstène dans le groupe de Legzdins (Schéma 1.14). Le complexe insaturé (non observé mais piégé) [Cp*W(NO)(η^2-*trans*-1,3-butadiene)] est généré via une élimination du CMe_4 à partir du précurseur néopentyl-allyle [Cp*W(NO)(CH_2CMe_3)(η^3-$CH_2CHCHMe$)]. Ce complexe peut cliver la liaison C-H du méthane (70 bars), de l'éthane (27 bars) et du n-pentane à température ambiante pour donner les complexes alkyl-allyle correspondants.

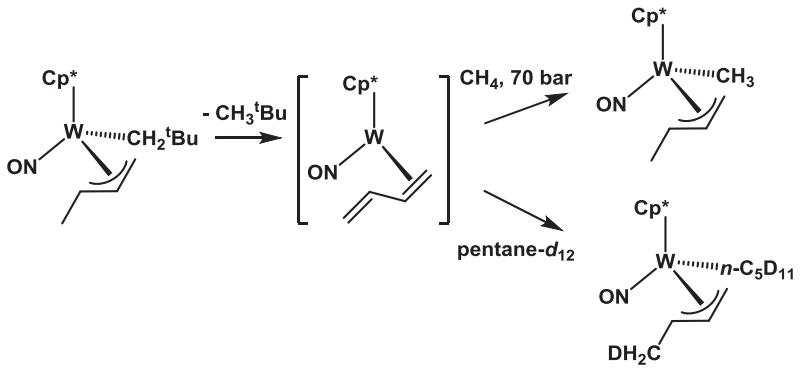

Schéma 1.14. *Activation de la liaison CH du méthane et du pentane-d_{12} par l'intermédiaire [Cp*W(NO)(η^2-butadiene)].*

Notre groupe a également proposé une voie similaire d'addition en position 1,3- pour l'activation de la liaison CH du benzène et de différents alkylaromatiques. Cela implique un intermédiaire transitoire de niobium η^2-cyclopropène, [Tp^{Me2}Nb(c-C_3H_4)(MeCCMe)] (**A**), généré par une abstraction d'un H en position β à partir du complexe méthyle cyclopropyle de Nb [Tp^{Me2}NbCH_3(*c*-C_3H_5)(MeCCMe)] (**1**) (Schéma 1.15). La discussion de cette étude ainsi que nos efforts pour activer la liaison CH du méthane par cette voie et cet intermédiaire seront discutés dans le prochain chapitre.

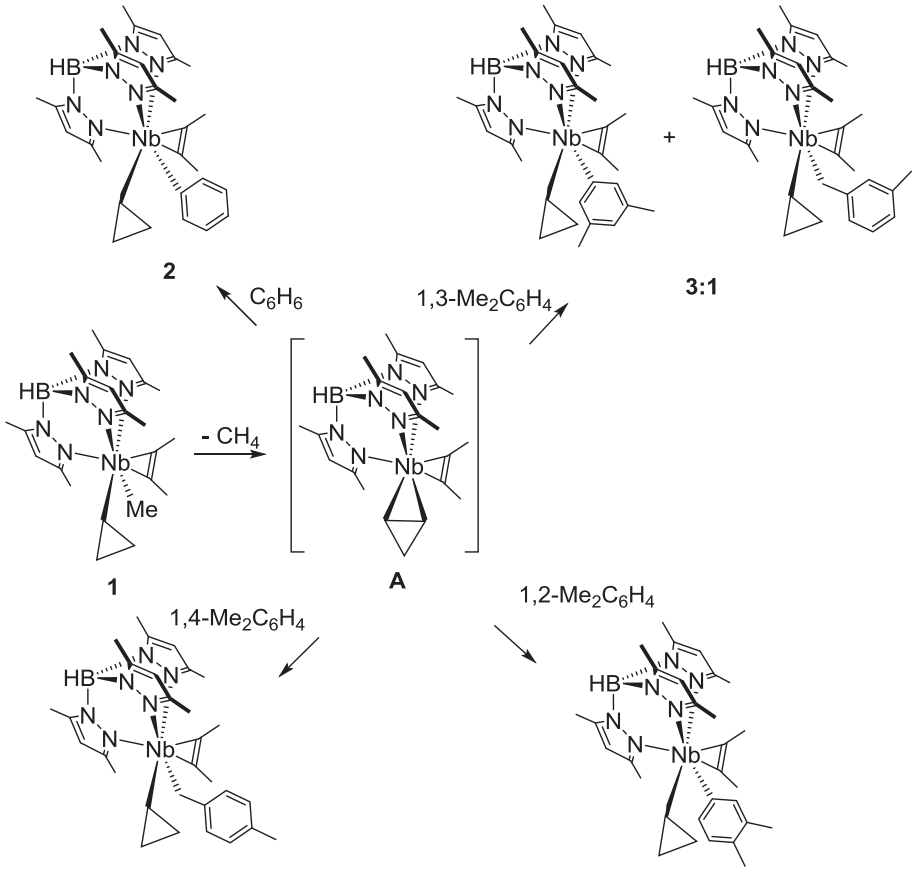

Schéma 1.15. *Activation de la liaison CH du benzène et de différents alkylaromatiques par l'intermédiaire [Tp^{Me2}Nb(c-C_3H_4)(MeCCMe)] (**A**).*

1.3- Conclusions et perspectives

Scientifiquement, la fonctionnalisation du méthane reste un défi majeur en raison de la nécessité de combiner deux étapes indépendantes en une seule réaction: i) le clivage de la liaison CH et ii) la fonctionnalisation du méthane activé. Parmi toutes les voies examinées dans le présent chapitre, trois seulement ont conduit à la fonctionnalisation catalytique du

méthane: i) les routes électrophiles, impliquant des complexes électrophiles homogènes basées principalement sur du Hg, Pt, Pd et V; ii) l'insertion d'un carbène, impliquant des complexes scorpionate perfluorés d'argent très pauvres en électrons et iii) la métathèse des liaisons σ dans des complexes métallocène-alkyles de scandium, par laquelle la hydrométhylation catalytique du propène et la déshydrogénation du diphénylsilane avec du méthane ont été développées. Les autres voies, d'autre part, à savoir i) l'addition oxydante et l'addition radicalaire (idéalement sur des métaux de transition à faible valence), ii) l'addition de la liaison CH en position 1,2- sur une liaison multiple M = X (M = complexes des métaux de transition à haute valence, X = C, NR, etc) et iii) l'addition d'une liaison CH en position 1,3 sur un système M-η^2-alcène (M = complexes de métaux de transition à haute valence) n'a jamais été incorporé dans une fonctionnalisation catalytique du méthane. Bien que ces procédés ne fournissent pas une fonctionnalisation catalytique, ils réalisent le clivage de la liaison CH du méthane, une étape importante vers la conception des réactions catalytiques. Dans les chapitres suivants, nous nous concentrerons donc sur le clivage de la liaison CH du méthane et de différentes molécules insaturées par un intermédiaire η^2-cyclopropène de niobium en utilisant une méthodologie basée sur la synergie entre la synthèse, la caractérisation et études mécanistiques.

Chapitre 2: Activation de la liaison CH du méthane par un complexe transitoire cyclopropene-η^2 de niobium

2.1- Introduction

Des études réalisées auparavant dans notre équipe indiquent que le complexe cyclopropyle de niobium [Tp^{Me2}NbMe(*c*-C_3H_5)(MeCCMe)] (**1**) est capable d'activer la liaison CH du benzène par l'abstraction d'un H en β suivi par une addition en position 1,3 (Schéma 2.1). Le complexe **1** réagit avec du benzène à température ambiante ($t_{1/2}$ *ca.* 7 h) pour donner le composé [Tp^{Me2}NbPh(*c*-C_3H_5)(MeCCMe)] (**2**) et du méthane. Des études cinétiques ont montré que la réaction de conversion de **1** en **2** est du premier ordre par rapport au composé **1** et d'ordre zéro par rapport au benzène avec une constante de vitesse k_{obs} de $2.93 \pm 0.05 \times 10^{-5}$ s^{-1} à 303 K. Les études cinétiques effectués à différentes températures (303-323 K) conduisent aux paramètres d'activation $\Delta H^{\dagger} = 99 \pm 5$ kJ/mol and $\Delta S^{\dagger} = -6 \pm 10$ J/Kmol. La réaction de **1** avec C_6D_6 au lieu de C_6H_6 montre un effet isotopique négligeable avec un rapport k_H/k_D de 1.0 à 303 K. Ces données confirment que l'étape cinétiquement déterminante est l'abstraction intramoléculaire d'un H β du groupe cyclopropyle pour former du méthane, ce qui donne l'intermédiaire transitoire insaturé cyclopropène-η^2/metallacyclobutane [Tp^{Me2}Nb(η^2-*c*-C_3H_4)-(MeCCMe)] **A**. Ceci est suivi par l'addition de la liaison CH du benzène en position 1,3 pour donner le composé **2**. Des études DFT confirment que la formation de **A** passe par un état de transition à quatre centres (**1-TS**) présentant une disposition presque linéaire du système C... H ... C (angles CHC > 166°) avec l'hydrogène positionné symétriquement entre les deux carbones (Schéma 2.1). Ce réarrangement structural est très similaire à ceux décrits par Legzdins et rappelle le processus de métathèse des liaisons σ.

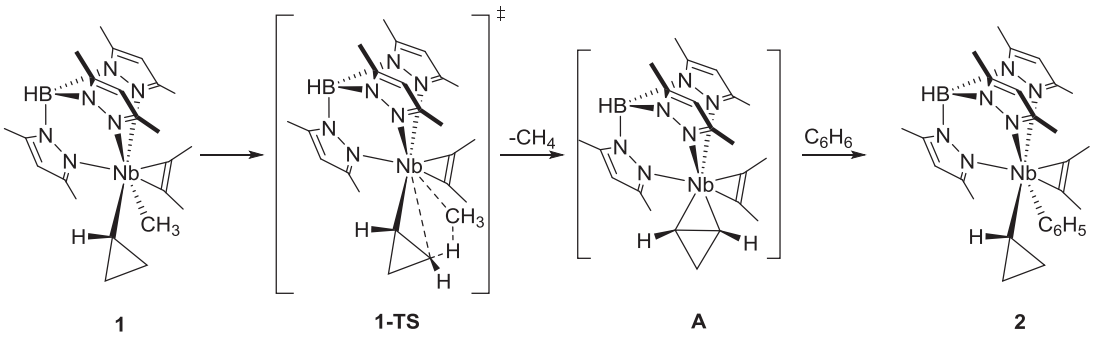

Schéma 2.1. *Activation de la liaison CH du benzène par un complexe transitoire cyclopropene-η² de niobium [Tp^{Me2}Nb(η²-c-C$_3$H$_4$)(MeCCMe)] (**A**).*

Des modélisations cinétiques effectuées par simulation numérique montrent que les réactions d'activation 1,3 de la liaison CH du méthane et du benzène par l'intermédiaire **A** sont des réactions biomoléculaires, et donc du premier ordre par rapport à A et du premier ordre par rapport au méthane et au benzène, respectivement. A 323 K, la constante de vitesse (k_2) pour la réaction de **A** avec le benzène est environ 3 fois plus importante que celle pour la réaction de **A** avec le méthane (k_{-1}) (Schéma 2.2). Par conséquent, **A** réagit *ca* 3 fois plus vite avec le benzène qu'avec le méthane lui-même à 323 K.

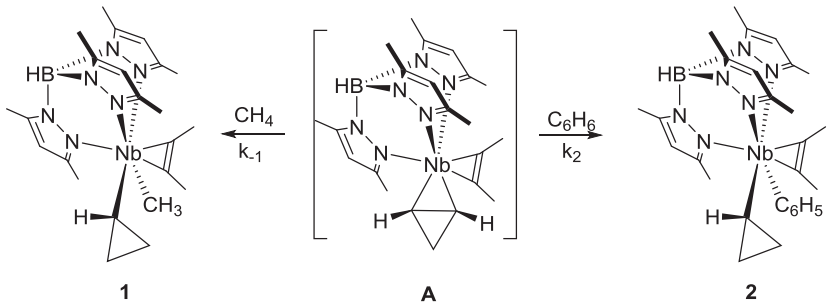

Schéma 2.2. *Reaction de **A** avec le méthane et le benzène.*

Comme le montre la spectroscopie RMN du ^{1}H, ^{2}H et ^{13}C, la réaction du composé **1** avec le C_6D_6 donne deux diastéréoisomères avec l'insertion sélective d'un seul deutérium dans un des deux carbones β sur la même enantioface du cycle cyclopropyle que le niobium, selon un rapport de *ca* 2:1. Ceci établit de façon claire que l'intermédiaire **A** est un complexe cyclopropène-η² insaturé, obtenu à partir de **1** par une abstraction d'un H β pour former du CH_4. La liaison CH/CD du C_6H_6/C_6D_6 s'additionne successivement sur la liaison Nb-C de **A** selon une disposition 1,3 stéréospécifique (Schéma 2.3) pour donner deux diastéréoisomères dans un rapport de 2:1.

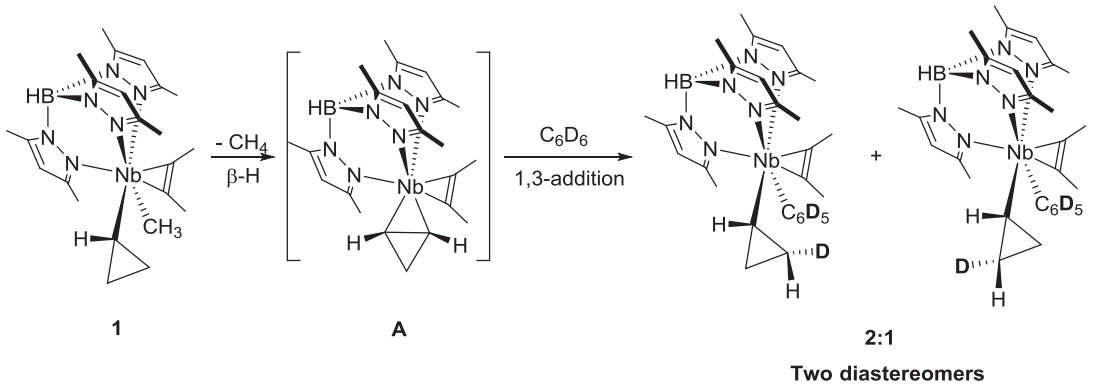

Schéma 2.3. *Activation de la liaison CD du benzene-d_6 par le composé **A**.*

2.2- Objectives du travail

Inspirés par le travail décrit dessus, nous avons cherché à voir si **1** était capable d'activer l'inerte liaison CH du méthane d'une manière similaire que le benzène. Le mécanisme a été d'abord abordé par des expériences de marquage isotopique utilisant du $^{13}CH_4$ et du CD_4 pour voir si **1** pouvait réagir avec du $^{13}CH_4$ et du CD_4 pour former **1-^{13}CH$_3$** et **1-d$_4$**, respectivement (Schéma 2.4). Une étude cinétique sur l'échange dégénéré entre **1** et $^{12}CH_4$ par des expériences de transfert de saturation de spin (SST) a été réalisée pour étudier les étapes élémentaires. Les études cinétiques de la réaction entre le composé [Tp^{Me2}Nb(CH_2-3,5-$Me_2C_6H_3$)- (*c*-C_3H_5)(MeCCMe)] (**3**) et le $^{12}CH_4$ ont révélé que l'abstraction d'un H en position β est l'étape cinétiquement déterminante (RDS), fournissant les constantes de vitesse et les paramètres d'activation qui reflètent la structure de l'état de transition dans l'étape cinétiquement déterminante.

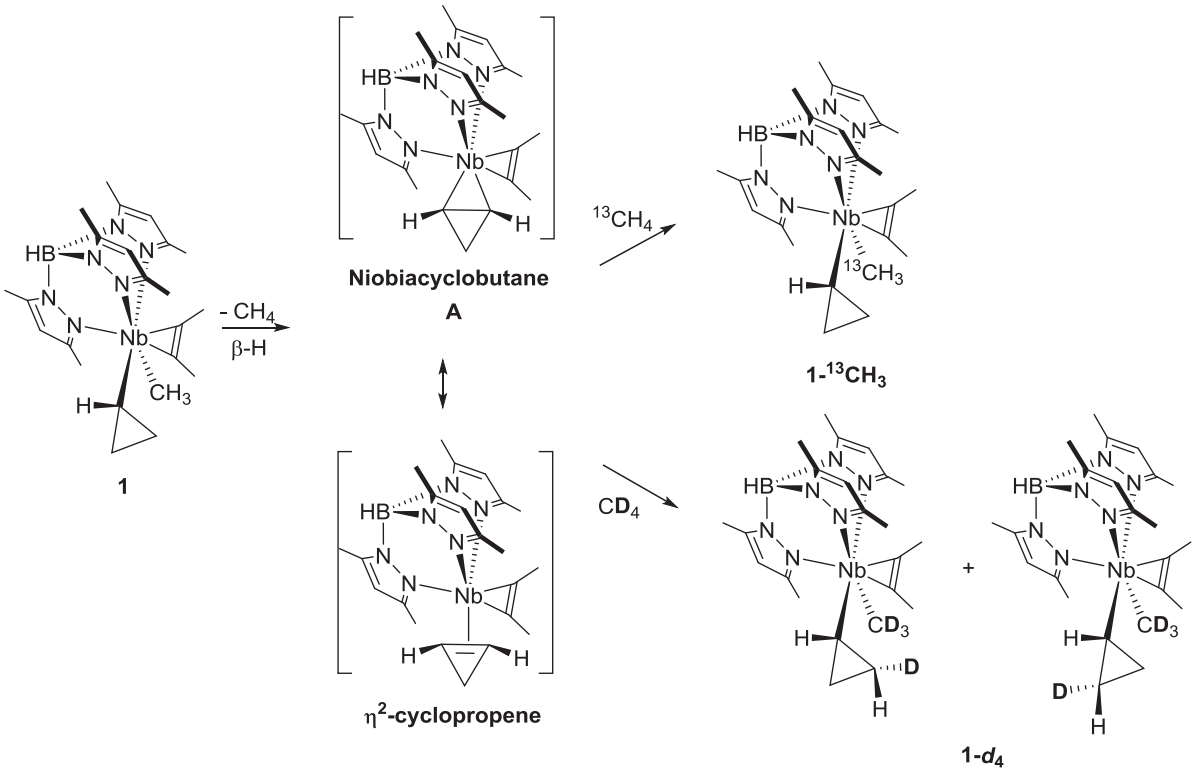

Schéma 2.4. *Activation de la liaison CH du méthane par l'intermédiaire cyclopropene-η²de Nb.*

2.3-Réaction dégénérée entre le compose 1 et le $^{13}CH_4$ et le CD_4

2.3.1-Réaction dégénérée entre le compose 1 et le $^{13}CH_4$

Dans un premier temps, un tube RMN de J Young à moyenne pression a été chargé avec le composé **1** (0.030 g, 0.060 mmol) dans du cyclohexane-d_{12} (0.5 ml) et pressurisé avec du $^{13}CH_4$ jusqu'à environ 3 bar à 173 K pour 1 min. Le tube a été ensuite placé dans le spectromètre RMN avec une sonde fixée à 313 K. 1,2 équivalents de $^{13}CH_4$ ont pu être quantifiés en solution par l'intégration du signal du $^{13}CH_4$ (δ 0.19 (d, $^{1}J_{CH}$ = 125.0 Hz)) par rapport au signal du groupe $Tp^{Me2}CH$ dans le composé **1**. La réaction a ensuite été suivie par RMN du ^{1}H pendant 19 heures, montrant l'activation du $^{13}CH_4$ par le complexe **1** pour former $[Tp^{Me2}Nb^{13}CH_3(c\text{-}C_3H_5)(MeCCMe)]$ **1-$^{13}CH_3$**. Dans les premières 5 heures, le spectre RMN du ^{1}H a montré l'apparition et la croissance de la résonance du $Nb^{13}CH_3$ sous la forme d'un doublet centré à δ = 0.766 avec une $^{1}J_{CH}$ = 119.6 Hz (Figure 2.1). Ce signal a été superposé avec le singulet à δ 0.779 correspondant au groupe $Nb^{12}CH_3$ dans **1** (Figure 2.1).

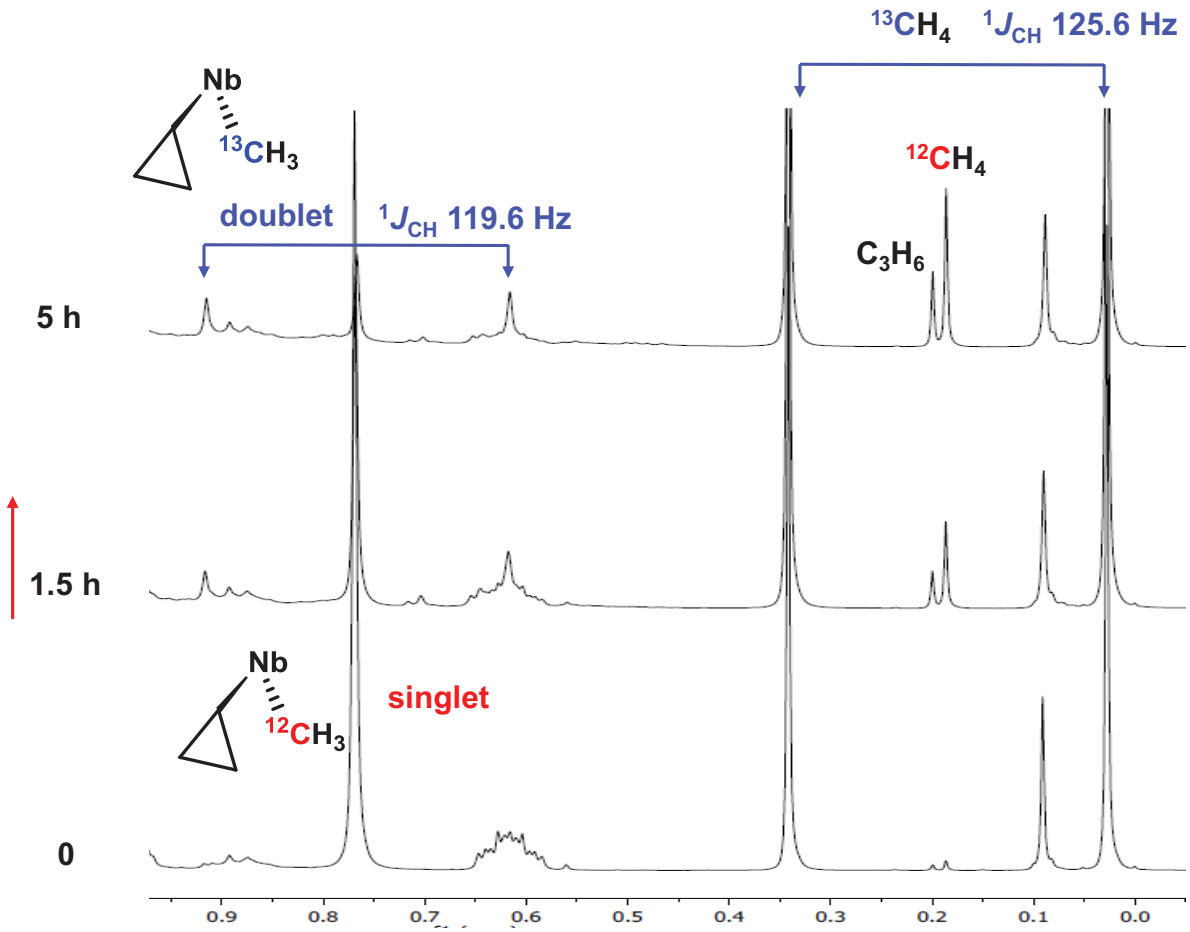

Figure 2.1. *Spectre RMN du ^1H pour la réaction de **1** avec le $^{13}CH_4$ pour former **1-$^{13}CH_3$**.*

Cette expérience préliminaire établit la présence d'un équilibre entre **1** et **1-$^{13}CH_3$** (Schéma 2.5), ce qui confirme que l'intermédiaire **A** réagit facilement avec le méthane.

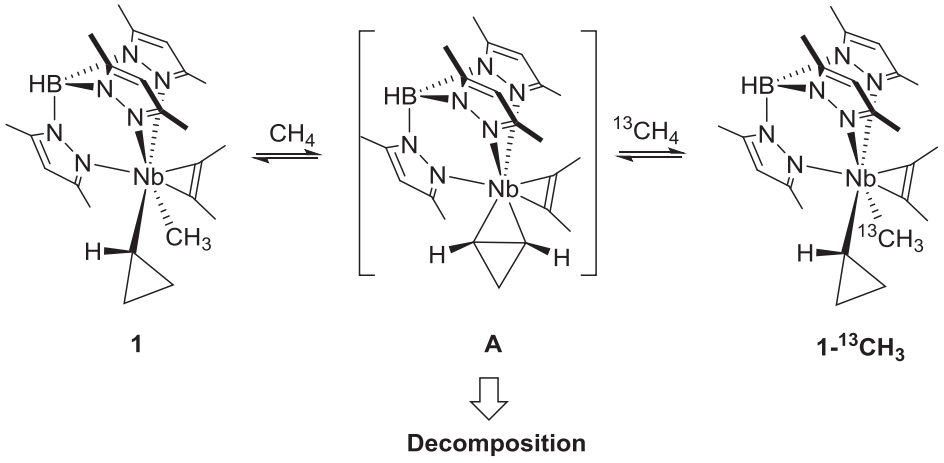

Schéma 2.5*. Réaction de **1** avec le $^{13}CH_4$ pour former **1-$^{13}CH_3$**.*

Pour de plus longues durées de réaction, toutefois, une décomposition de **1** et de **1-^{13}CH$_3$** a été observée à partir de la diminution des signaux du Nb^{12}C*H*$_3$ et Nb^{13}CH$_3$. La pression de ^{13}CH$_4$ n'est pas suffisamment élevée pour empêcher la décomposition de l'intermédiaire **A**, ce qui empêche l'analyse cinétique de la réaction.

2.3.2-Réaction dégénérée de 1 avec le CD_4

2.3.2.1- Caractérisation du [Tp^{Me2}NbMe(c-C_3H_5)(MeCCMe)] par RMN ROESY du ^{1}H

Afin d'évaluer le résultat stéréochimique de la formation de **1-d$_4$** (Schéma 2.4), nous avons réalisé une expérience RMN ROESY du ^{1}H du composé **1**, permettant l'attribution de tous les protons diastéréotopiques du groupe cyclopropyle dans ce complexe **1** (Tableau 2.1). L'interprétation du spectre RMN ROESY du ^{1}H de **1** suit celle de [Tp^{Me2}NbPh(*c*-C_3H_5)(MeC≡CMe)], préalablement décrite. Les protons méthyliques du ligand 2-butyne qui sont lointain du groupe Tp^{Me2} sont déblindés (δ 2.92), alors que ceux qui sont proches du groupe Tp^{Me2} sont blindés (δ 2.24). À 283 K, ils échangent très lentement dans le cyclohexane-d$_{12}$ (Tableau 2.1, Figure 2.2 (a)). Dans le spectre ROESY, on observe clairement une corrélation entre les protons méthyliques lointains et H7, un des hydrogènes β du groupe cyclopropyle. Ceci sert à construire les autres corrélations ROESY (Tableau 2.1, Figure 2.2 (b)).

^{1}H NMR, δ	
H5′ 1.17	
H6′ 1.00	
H6 1.03	
H7′ 0.62	
H7 1.43	

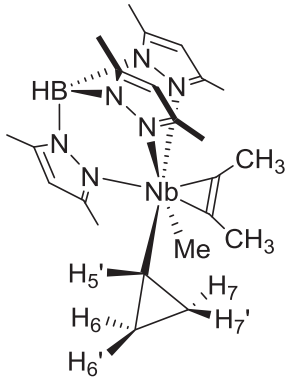

(proximal, δ = 2.24)

(distal, δ = 2.92)

Tableau 2.1.*Protons diastéréotopiques du groupe cyclopropyle dans le compose **1**.*

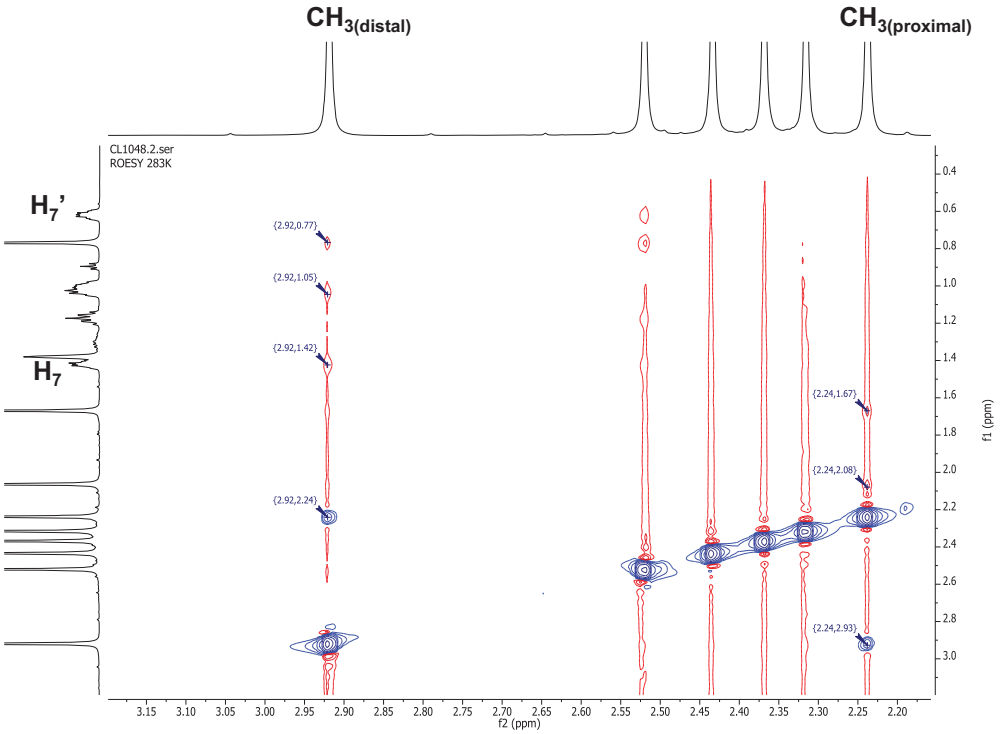

Figure 2.2(a). *Spectre RMN ROESY du composé* ***1****, montrant la corrélation ROESY pour les protons méthyliques du ligand 2-butyne.*

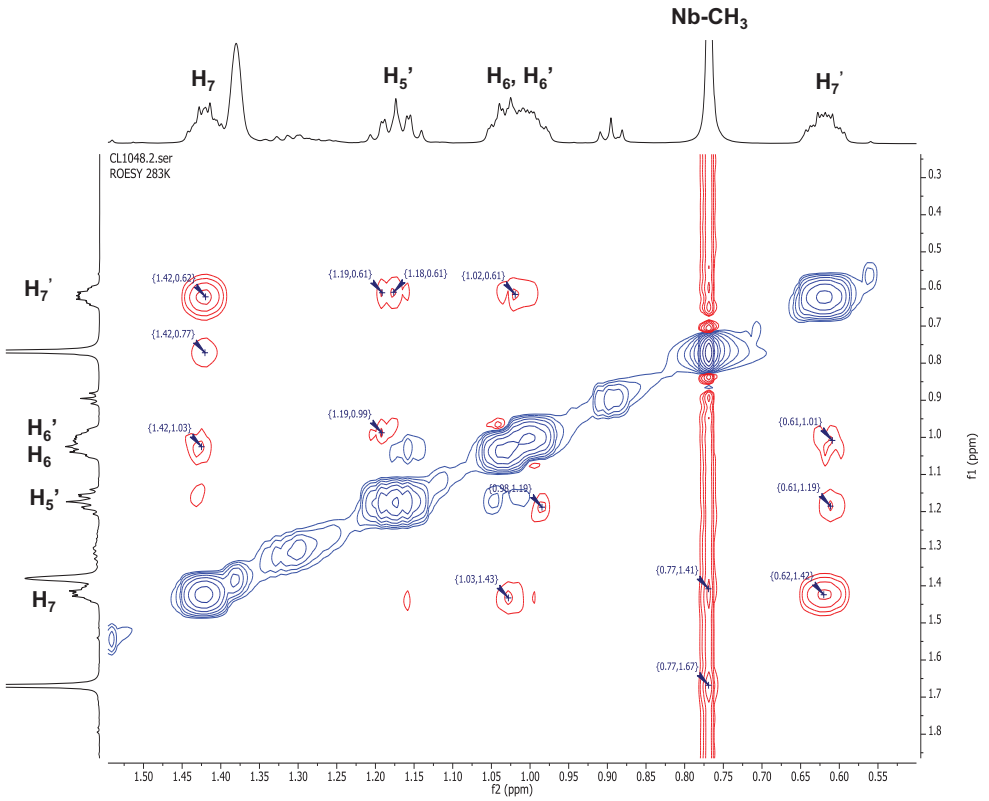

Figure 2.2(b).*Spectre RMN ROESY du* ^{1}H *du composé* ***1*** *(expansion).*

2.3.2.2- Activation de la liaison C-D du CD_4 par le complexe 1.

Un tube RMN de J Young à moyenne pression a été chargé avec le composé **1** (0,030 g, 0,060 mmol) dans du perfluorobenzène (0,5 ml) et pressurisé avec CD_4 jusqu'à environ 8 bar à 157 K pendant 3 minutes. Le tube a ensuite été placé dans le spectromètre RMN équipé d'une sonde cryogénique fixée à 303 K. Le mélange réactionnel a ensuite été étudié par RMN du ^1H et du $^2H\{^1H\}$ pendant 4 heures à 303 K. La comparaison des spectres du ^1H et du $^2H\{^1H\}$ a montré la formation de deux diastéréoisomères de $[Tp^{Me2}NbCD_3$ (*c*-$C_3H_4D)$(MeCCMe)] **1-d$_4$** dans un rapport de 3:1. En plus d'un groupe Nb-CD_3, la présence d'un atome de D soit en position 7 soit en position 6 du cycle cyclopropyle a été observée, respectivement. Fait intéressant, les positions β D6 et D7 sont sur la même enantioface du groupe cyclopropyle que le niobium (Figure 2.3).

Ces résultats confirment que **A** est générée par une étape cinétiquement déterminante à voir l'abstraction intramoléculaire d'un H β du groupe cyclopropyle par le groupe méthyle lié au niobium pour former du méthane à partir de **1**. Ce processus est suivie par son inverse microscopique, à voir l'addition stéréospécifique en position 1,3 de la liaison CH/D du CH_4/CD_4 sur la liaison Nb-C du composé Nb(η^2-*c*-C_3H_4) (Figure 2.3).

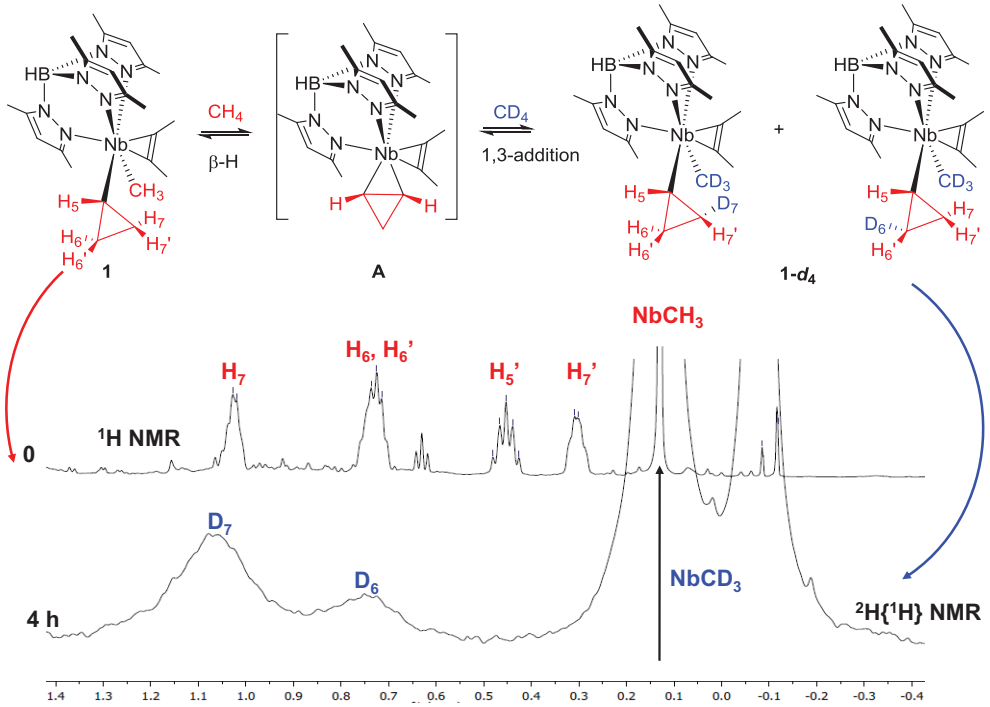

***Figure 2.3**. Spectres RMN du ^1H et du $^2H\{^1H\}$ superposés pour la réaction de **1** avec le CD_4 pour former **1-d$_4$**.*

2.4- Activation de la liaison CH du $^{12}CH_4$ par le composé 1

Afin d'étudier l'activation du méthane d'une façon plus quantitative, nous nous sommes ensuite intéressés à l'étude de la réaction de **1** avec le méthane ($^{12}CH_4$) par des expériences de transfert de saturation de spin (SST). Le schéma 2.6 (a) montre la réaction de **1** avec le méthane, alors que le schéma 2.6 (b) montre les étapes élémentaires impliquées. La réaction directe (constante de vitesse k_1) est l'élimination monomoléculaire du méthane qui donne **A** et du méthane comme indiqué précédemment. La réaction inverse (constante de vitesse k_{-1}) est la réaction bimoléculaire de **A** avec du méthane, qui donne **1** et qui corresponde à l'activation de la liaison CH du méthane.

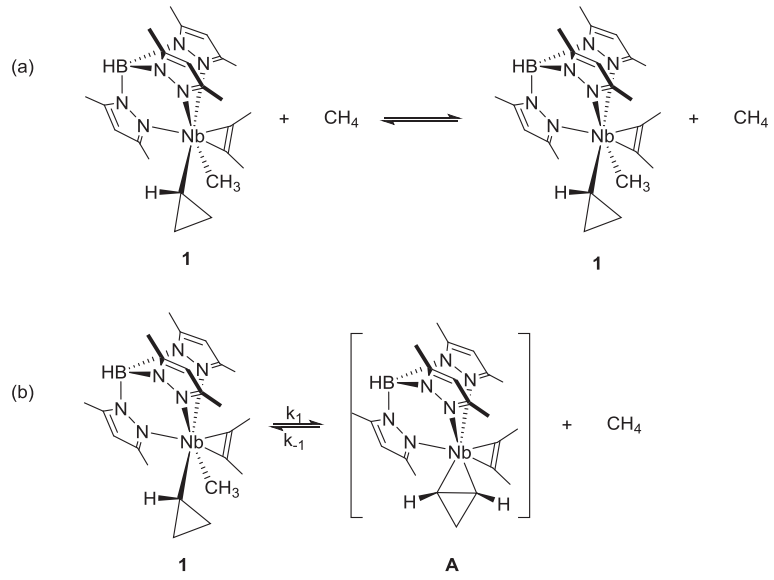

Schéma 2.6. *Réaction dégénérée de **1** avec le méthane (a) et ses étapes élémentaires (b).*

2.4.1- Mécanisme de transfert de saturation de spin (SST)

La procédure concernant les expériences de SST, y compris l'acquisition des données et le traitement cinétique, a été précédemment décrite dans la littérature. Les cinétiques d'échange des deux sites pour la réaction de **1** avec le méthane ($^{12}CH_4$) sont indiqués dans le Schéma 2.7, où [NbMe], [NbMe*], [CH_4] et [CH_4*] sont les populations des états de spin inférieurs et supérieurs du groupe méthyle de **1** et du méthane, respectivement. $M_{(NbMe)}$ = [NbMe] – [NbMe*] et M_{CH4} = [CH_4] – [CH_4*] sont les aimantations net du groupe méthyle de **1** et du méthane, respectivement. **A** est l'intermédiaire cyclopropène-η^2 et C_A est sa concentration.

$T_{1[NbMe]}$ et $T_{1[CH4]}$ sont les temps de relaxation de spin pour le groupe méthyle de **1** et pour le méthane, respectivement. k_1 est la constante de vitesse du premier ordre pour la transformation de **1** en **A** et du méthane, en supposant un mécanisme dissociatif. k_{-1} est la constante de vitesse du second ordre pour la réaction bimoléculaire inverse.

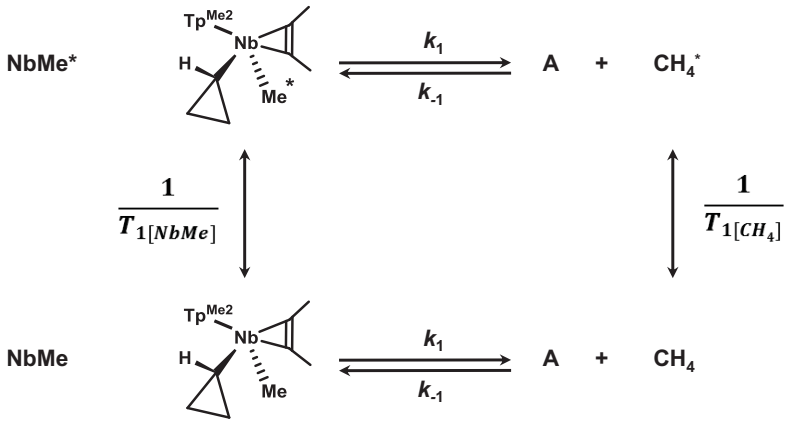

Schéma 2.7. *Cinétiques d'échange des deux sites pour la réaction de **1** avec le methane.*

Si CH_4 est irradié dans une telle manière que $M_{sat(CH4)} = 0$ et que l'état d'équilibre est atteint pour $M_{sat(NbMe)}$ ($dM_{sat(NbMe)}/dt = 0$), alors la constante de vitesse k_1 est donné par l'équation 2.1:

$$k_1 = \frac{1}{T_{1(\mathrm{NbMe})}}\left(\frac{M_{0(\mathrm{NbMe})}}{M_{\mathrm{sat(NbMe)}}} - 1\right) \quad (2.1)$$

Une fois de plus, si NbMe est irradié dans une telle manière que $M_{sat(NbMe)} = 0$ et que l'état d'équilibre est atteint pour $M_{sat(CH4)}$ ($dM_{sat(CH4)}/dt = 0$), alors la constante de vitesse k_{-1obs}, est donnée par l'équation 2.2:

$$k_{-1obs} = k_{-1}C_A = \frac{1}{T_{1(\mathrm{CH4})}}\left(\frac{M_{0(\mathrm{CH4})}}{M_{\mathrm{sat(CH4)}}} - 1\right) \quad (2.2)$$

Il faut noter ici que l'écriture de cette équation nécessite l'assomption de C_A constant. Ceci est parfaitement raisonnable puisque **A** est un intermédiaire très réactif, ce qui justifie la validité de l'approximation de l'état stationnaire.

Les expériences SST ont été effectuées à haute et moyenne pression de CH_4 sur des spectromètres Bruker Avance de 400 et 500 MHz, respectivement.

Concernant les expériences à moyenne pression, une décomposition significative du composé **1** a été observée, ce qui nous a empêché la mesure précise de la constante de vitesse correspondante. Par la suite, donc, seulement les expériences à haute pression de CH_4 seront illustrées.

2.4.2- Etude SST sur la réaction de 1 avec le $^{12}CH_4$ à haute pression.

Afin de favoriser la réaction bimoléculaire du méthane avec **A** par rapport à sa décomposition et afin d'obtenir des résultats quantitatifs, nous avons recouru à des techniques RMN à haute pression (HP) sur un spectromètre de 400 MHz. **1** (0,100 g, 0,200 mmol) a été chargé dans un tube RMN en saphir d'1 cm (diamètre extérieur) et dissous dans un mélange 1:1 de C_6F_6/cyclohexane-d_{12} (2 mL). Le tube RMN à HP a été ensuite mis sous pression avec du méthane à environ 60 bar à température ambiante et agité soigneusement pour assurer une dissolution homogène du méthane. L'étude SST a été effectuée dans un spectromètre RMN de 400 MHz à 351 K avec un rapport [CH_4]:[**1**] de 29. La saturation de la résonance du $NbCH_3$ à δ 0.59 a été suivie par l'observation de la résonance du CH_4 à δ 0.14 (Figure 2.4). L'intégration de la résonance du $NbCH_3$ avant et après la saturation a révélé une diminution de 12%, ce qui donne une constante de vitesse $k_{-1obs} = k_{-1}C_A = (2.67 \pm 0.23) \times 10^{-2}$ s^{-1}, en utilisant l'équation 2.1.

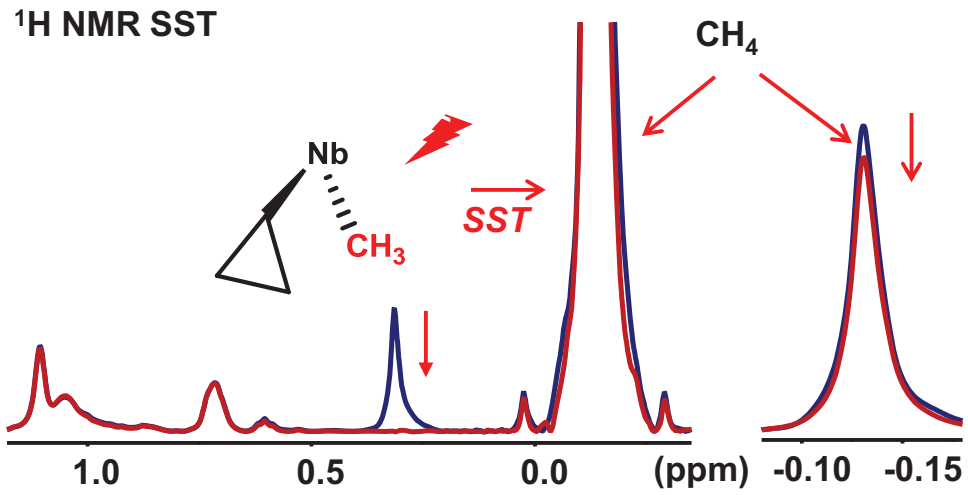

Figure 2.4. *Irradiation du signal du Nb-CH$_3$ et diminution de l'intensité du signal du CH$_4$ (11%), après le transfert de saturation de spin.*

Toutefois, lorsque le signal du méthane à δ 0.14 a été saturé, des changements insignifiants dans l'intensité du signal du méthyle lié au niobium à δ 0.59 dans le complexe **1** ont été observés (Figure 2.5).

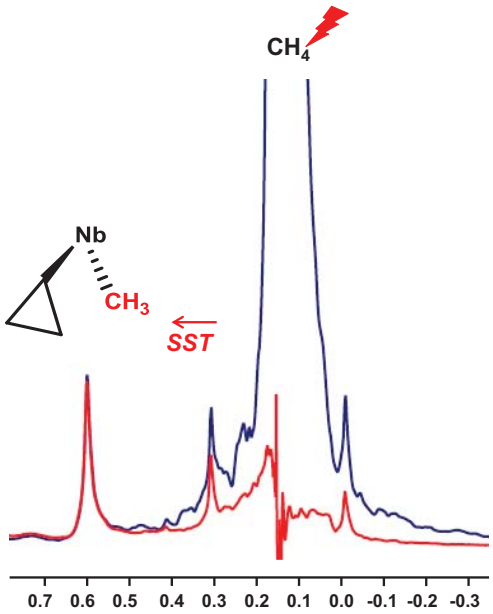

Figure 2.5. *Irradiation du signal du CH$_4$ (δ 0.18 ppm) et très faible diminution de l'intensité du signal du Nb-CH$_3$ après le transfert de saturation de spin.*

Ces expériences SST peuvent être mieux expliquées grâce au schéma cinétique décrit dans le schéma 2.6 (b). La réaction inverse (constante de vitesse k_{-1}) est la réaction bimoléculaire de **A** avec le méthane qui donne **1**, l'activation de la liaison CH du méthane, et k_{-1obs} est égal à $k_{-1}C_A$, en supposant que l'intermédiaire réactif **A** est dans un régime de concentration constante. Malheureusement, cela ne nous permet pas de discuter sur la possibilité de **A** d'activer le méthane puisque nous ne pouvons pas déterminer k_{-1} ici, en connaissant simplement k_{-1obs}. L'impossibilité d'observer un changement d'intensité de la résonance du groupement $NbCH_3$ lorsque nous saturons le signal du méthane malheureusement nous empêche la mesure de k_1 par l'expérience de SST. Cela peut être attribué à la différence de temps de relaxation T1 pour les protons du méthyle lié au niobium [$T_1(NbCH_3)$ =1.34 s] et ceux du méthane [$T_1(CH_4)$ =4.95 s] par rapport à la constante de vitesse k_1. A partir des paramètres d'activation précédemment déterminées pour l'abstraction intramoléculaire du méthane à partir de **1** ($\Delta H^{\dagger}$= 99 ± 5 kJ/mol and $\Delta S^{\dagger}$= -6 ±10 J/K·mol) nous pouvons calculer une valeur de $\Delta G^{\dagger}$ de 101 kJ·mol^{-1} à 351 K, correspondant à une valeur de k_1 de 6.6×10^{-3} s^{-1}. Dans ce cas, seule une variation de moins de 1% de l'intensité du signal du $NbCH_3$ serait attendue lors d'une saturation du signal de CH_4.

2.5- Etude cinétique de la réaction entre le complexe [$Tp^{Me2}Nb(CH_2$-3,5- $C_6H_3Me_2)(c$-$C_3H_5)(MeCCMe)$] (3) et le CH_4

Nous avons néanmoins réalisé une activation productive du méthane. En suivant les études de Jones et Wolczanski, nous avons supposé que la réaction d'une liaison faible Nb-1-mésityle avec une liaison CH forte dans le méthane pourrait engendrer une plus forte liaison Nb-méthyle et une plus faible liaison CH dans le mésitylène. Un excès de méthane devrait rendre la réaction encore plus favorable thermodynamiquement. Ici, nous avons étudié l'activation de la liaison CH du méthane par le complexe de mésityle [$Tp^{Me2}Nb(CH_2$-3,5-$C_6H_3Me_2)$- $(c$-$C_3H_5)(MeCCMe)$] (**3**).

Le composé **3** (0.072 g, 0.12 mmol) a été dissous dans un mélange de cyclohexane-d_{12} (1 ml) et de perfluorobenzène (1 ml) et ensuite transféré dans un tube RMN en saphir à haute pression de 10 mm. Le tube RMN a été pressurisé avec 40 bars de méthane et la réaction a été suivie par spectroscopie RMN du ^{1}H.

A partir du spectre RMN du ^{1}H, il a été constaté que **3** réagit avec CH_4 pour former **1** et du mésitylène (Figure 2.6). Pour mener une étude cinétique complète, la réaction a été étudiée à 290, 303, 314 et 321 K pendant plus de 5 demi-vies, mais pour des raisons pratiques elle a

été traitée au sein de 1.8, 2.3, 2.3 et 3.2 demi-vies, respectivement .L'intégration du signal du CH_4 par rapport au signal du $Tp^{Me2}CH$ dans **3** indique que *ca.* 12-33 équivalents de méthane vs **3** étaient présents en solution. Dans ces conditions de pseudo-premier ordre, la disparition de **3** a été suivie.

La figure 2.7 et le tableau 2.2 montrent les constantes cinétiques obtenues à différentes températures.

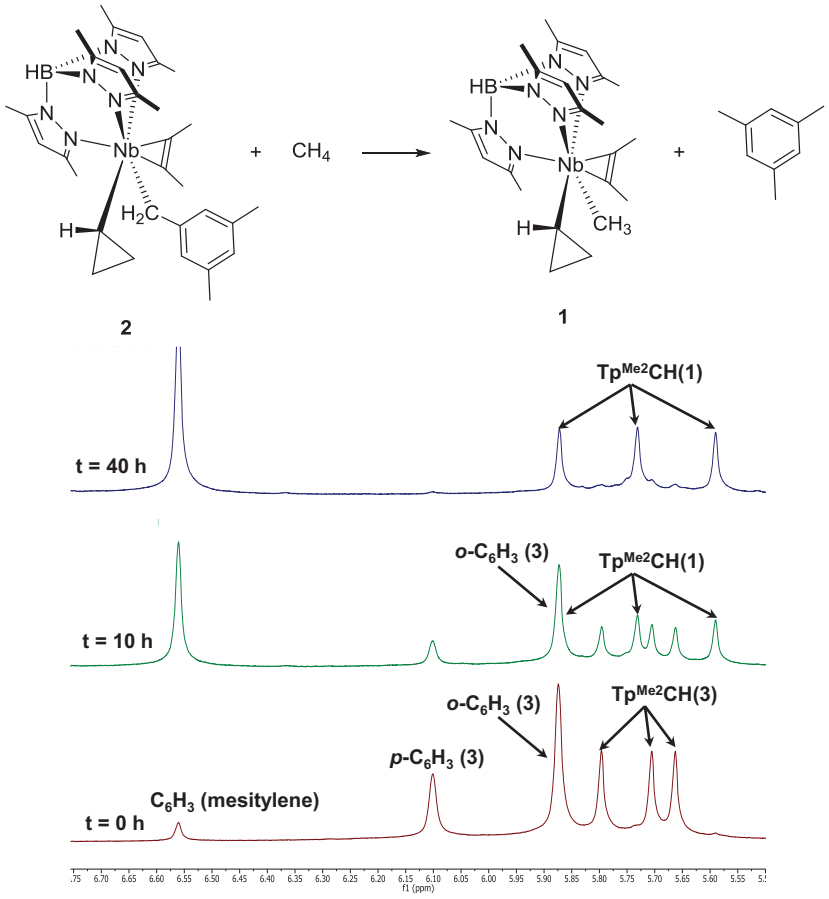

Figure 2.6. *Spectres RMN superposés pour la réaction du composé* ***3*** *avec le méthane pour former* ***1*** *dans du cyclohexane-d_{12} (1 mL) et du perfluorobenzene (1 mL) à 314 K.*

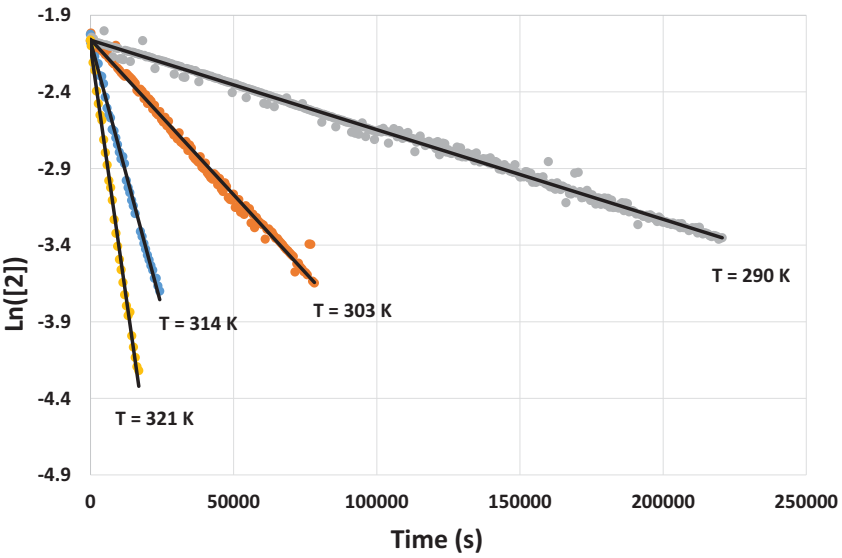

Figure 2.7. *Cinétiques du premier ordre pour l'abstraction du mesitylene dans le composé* ***3*** *en fonction de la température.*

Table 2.2. *Constants de vitesse du premier ordre pour l'abstraction du mesitylene dans* ***3***

T(K)	K($s^{-1} \times 10^{-6}$)	CH_4 equiv.
290	5.85±0.02	12
303	20.3±0.2	29
314	70.2±0.3	27
314	71.9±0.4	33
321	132±2	27

La réaction de **3** avec différentes concentrations de méthane (27 et 33 équivalents) à 314 K donne les mêmes constantes de vitesse (Tableau 2.2), ce qui indique que la réaction est du premier ordre par rapport au complexe **3** et d'ordre zéro par rapport au méthane (Equation 2.3).

$$-\frac{d[2]}{dt} = k_{obs}[2] \quad (2.3)$$

A partir des constantes de vitesse obtenues aux différentes températures (Figure 2.7 et le Tableau 2.2), nous avons pu obtenir les paramètres d'activation en utilisant les équations

d'Arrhenius et d'Eyring. La relation entre le ln*k* et $\frac{1}{T}$ est linéaire, avec la pente représentant $\frac{-E_a}{R}$ (Figure 2.8), qui permet d'obtenir l'énergie d'activation: E_a = 78± 5 kJ/mol.

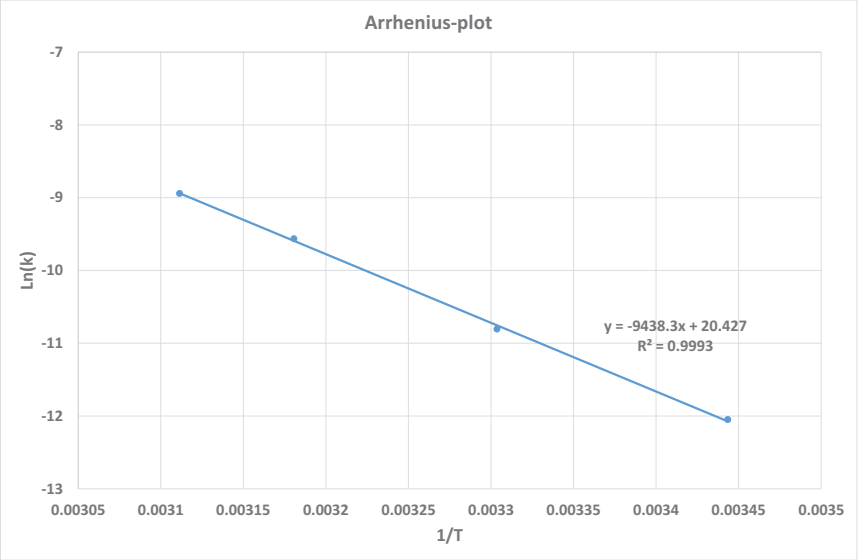

Figure 2.8. *Corrélation d'Arrhenius pour l'abstraction du mesitylene dans* ***3****.*

La relation linéaire entre le $\ln\frac{k}{T}$ et $\frac{1}{T}$ donne par la pente la valeur de $\frac{-\Delta H^{\dagger}}{R}$, tandis que l'intercepte corresponde à $\ln\frac{k_B}{h} + \frac{\Delta S^{\dagger}}{R}$ (Figure 2.9). Par conséquent, nous avons pu obtenir l'enthalpie et l'entropie d'activation, $\Delta H^{\dagger}$= 76 ± 5 kJ/mol and $\Delta S^{\dagger}$= – 84 ±10 J/K.mol, respectivement.

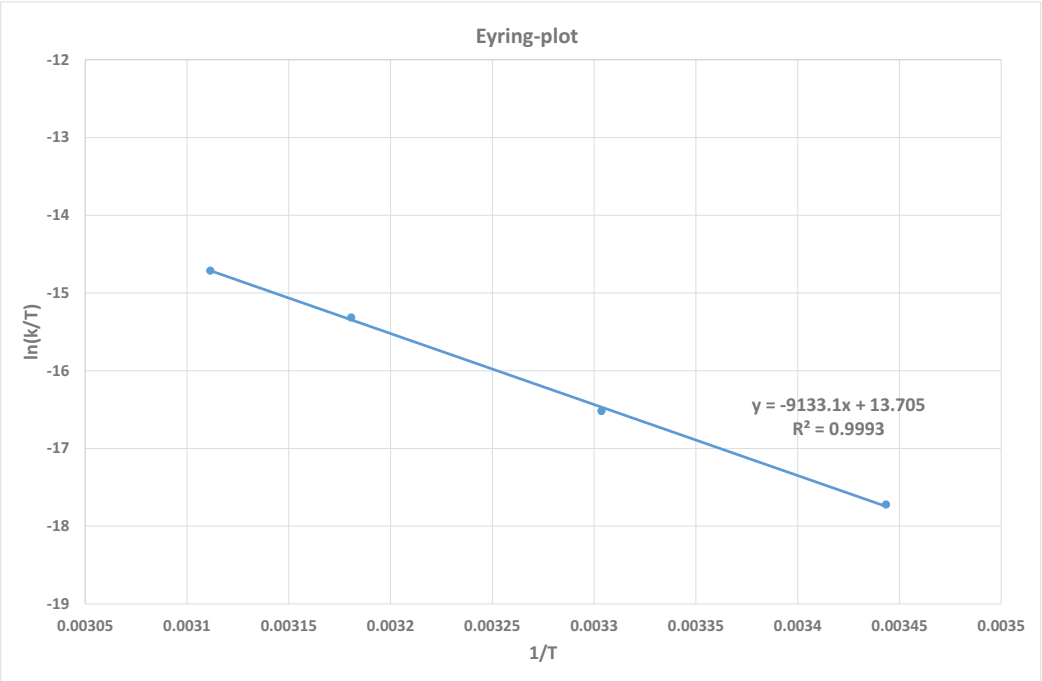

Figure 2.9. *Corrélation d'Eyring pour l'abstraction du mesitylene dans* ***3****.*

Cette analyse cinétique de la disparition de **3** dans une plage de température T = 290-321 K (Figure 2.7) a révélé une dépendance du premier ordre par rapport au complexe **3** et d'ordre zéro par rapport au méthane. Ceci est en accord avec un mécanisme réactionnel qui prévoit la perte intramoléculaire du mésitylène pour former **A**, l'étape cinétiquement déterminante, suivie par une réaction rapide avec CH_4 donnant **1** comme prévu (Schéma 2.8). L'enthalpie d'activation pour l'élimination du mésitylène à partir du composé **3** est inférieure à celle pour l'élimination du méthane à partir de **1**, car la liaison Nb-mésityle est plus faible que la liaison Nb-méthyle. L'entropie d'activation pour l'élimination du mésitylène à partir du composé **3** est nettement plus négatif que celle de l'élimination du méthane à partir de **1** (Schéma 2.8) .On suggère que ceci est le résultat de l'élimination du groupement mésitylène ayant un encombrement stérique plus importante que celui du méthane. Ceci implique donc des changements de conformation plus importants pour atteindre l'état de transition ordonné à quatre centres.

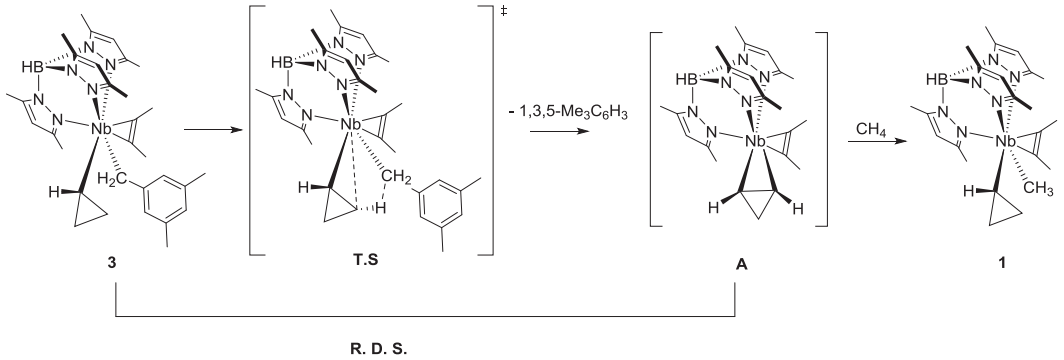

Schéma 2.8. *Activation de la liaison CH du méthane par le composé **3** pour former **1**.*

2.6- Conclusion

Nous avons montré qu'un complexe transitoire insaturé cyclopropène-η^2 de niobium (**A**) est capable de cliver une liaison CH du méthane par l'addition d'une liaison CH en position 1,3 dans des conditions douces. La réaction dégénérée de **1** avec le $^{13}CH_4$ a conduit à la formation du produit isotopologue **1-^{13}CH$_3$**. En présence de CD_4, la formation de deux diastéréoisomères dans un rapport de 3: 1 indique l'implication d'un processus d'addition 1,3 stéréospécifique sur l'intermédiaire cyclopropène-η^2 **A**. Des expériences de transfert de saturation de spin ont démontré que le complexe [Tp^{Me2}NbMe(c-C_3H_5)(MeCCMe)] (**1**) active la liaison CH du méthane par un processus d'abstraction réversible d'un H en position β suivi par une addition en position 1,3. L'étude cinétique de la réaction du composé [Tp^{Me2}Nb(Mesityl)(c-C_3H_5)(MeCCMe)] (**3**) avec du méthane à haute pression montre que la réaction est du 1er ordre par rapport au composé **3** et d'ordre zéro par rapport au CH_4, indiquant que la formation de l'intermédiaire **A** est l'étape cinétiquement déterminante. L'entropie d'activation très négatif, enfin, suggère la formation d'un état de transition ordonné dans l'étape d'abstraction de l'H en position β.

Thèse soutenue par : *Chen Li – Directeurs de thèse: Michel Etienne Chiara Dinoi et Laurent Maron –* ***Date de soutenance:*** *Vendredi 20 novembre 2015 –****Lieu de soutenance:*** *Laboratoire de Chimie de Coordination CNRS (Toulouse, France) –* ***Discipline:*** *Chimie organometallique de coordination*

Résumé

Le chapitre 1 présente un résumé bibliographique des différentes façons de casser une liaison CH d'hydrocarbures, plus particulièrement du méthane, avec des complexes de métaux de transition tant de la gauche que de la droite du système périodique. Pour les métaux de transition de la gauche, notre attention a été principalement axée sur trois mécanismes: i) la métathèse de liaison sigma, ii) l'abstraction d'un hydrogène en position alpha couplée à l'addition-1,2 d'une liaison CH et iii) l'abstraction d'un hydrogène en position beta couplée à l'addition-1,3 d'une liaison CH.

Le chapitre 2 aborde le problème de l'activation d'une liaison CH du méthane par un complexe transitoire eta^2-cyclopropène de niobium. Des études RMN à haute pression en solution, des études de marquage isotopiques ainsi que des analyses cinétiques sur l'échange dégénéré du méthane dans le complexe méthyle [Tp^{Me2}NbCH$_3$(c-C$_3$H$_5$)(MeCCMe)] (**1**) sont décrits. L'activation stœchiométrique du méthane par le complexe mésitylène [Tp^{Me2}Nb(CH$_2$-3,5-C$_6$H$_3$Me$_2$)(c-C$_3$H$_5$)(MeCCMe)] (**2**) pour donner **1** est également réalisée. Les données montrent que ces réactions se déroulent via une abstraction intramoléculaire d'un hydrogène beta du groupe cyclopropyle soit par un groupe méthyle soit par un groupe mésityle à partir du composé **1** ou **2**, respectivement, ce qui donne l'intermédiaire réactif eta^2-cyclopropène [Tp^{Me2}Nb(η^2-c-C$_3$H$_4$)(MeCCMe)] (**A**). Ceci est suivi par sa réaction inverse, l'addition-1,3 d'une liaison CH du méthane pour donner le produit.

Le chapitre 3 explore la réactivité du complexe **1** en vers des hétéroaromatiques, des hydrocarbures insaturés ainsi que le pentafluorobenzène et le ferrocène (FcH) via l'abstraction d'un hydrogène en position beta couplée à l'addition-1,3 d'une liaison CH. Le composé **1** est en mesure d'activer de manière sélective la liaison CH du furane, thiophène, 1-cyclopentène, phénylacétylène, pentafluorobenzène et ferrocène, donnant les produits correspondants [Tp^{Me2}NbX(c-C$_3$H$_5$)(MeCCMe)] (X = 2-C$_4$H$_3$O, 2-C$_4$H$_3$S, 1-C$_5$H$_7$, PhCC, C$_6$F$_5$, Fc) qui ont été isolés et caractérisés par spectroscopie RMN du ^{1}H et ^{13}C, des études électrochimiques ainsi que par des analyses de diffraction des rayons X.

Summary

Chapter 1 reports a literature summary of the different ways of cleaving a hydrocarbon CH bond, most particularly methane, with both early and late transition metal complexes. For early transition metals our attention is focused on three mechanisms: i) the σ-bond metathesis, ii) the α-H abstraction/1,2-CH bond addition and iii) the β-H abstraction/1,3-CH bond addition.

Chapter 2 challenges the problem of the activation of a CH bond of methane by a transient η^2-cyclopropene complex of niobium. High pressure solution NMR, isotopic labelling studies and kinetic analyses of the degenerate exchange of methane in the methyl complex [Tp^{Me2}NbCH$_3$(*c*-C$_3$H$_5$)(MeCCMe)] (**1**) are reported. Stoichiometric methane activation by the mesitylene complex [Tp^{Me2}Nb(CH$_2$-3,5-C$_6$H$_3$Me$_2$)(*c*-C$_3$H$_5$)(MeCCMe)] (**2**) giving **1** is also realized. Evidence is provided that these reactions proceed via an intramolecular abstraction of a β-H of the cyclopropyl group from either methane or mesitylene from **1** or **2**, respectively, yielding the transient unsaturated η^2-cyclopropene intermediate [Tp^{Me2}Nb(η^2-*c*-C$_3$H$_4$)(MeCCMe)] (**A**). This is followed by its mechanistic reverse 1,3-CH bond addition of methane yielding the product.

Chapter 3 explores the reactivity of complex **1** towards heteroaromatics, unsaturated hydrocarbons, pentafluorobenzene and ferrocene (FcH) via the β-H abstraction/1,3-CH bond activation mechanism. Compound **1** is able to selectively activate the C-H bond of furan, thiophene, 1-cyclopentene, phenylacetylene, pentafluorobenzene and ferrocene, yielding the corresponding products [Tp^{Me2}NbX(*c*-C$_3$H$_5$)(MeCCMe)] (X = 2-C$_4$H$_3$O, 2-C$_4$H$_3$S, 1-C$_5$H$_7$, PhC≡C C$_6$F$_5$, Fc) which have been isolated and characterized by ^{1}H, ^{13}C NMR spectroscopy, electrochemical studies and X-ray diffraction analysis.

Key words*: CH activation-Methane-Niobium-Reaction-Mechanism-NMR-Hydrocarbon-Synthesis*